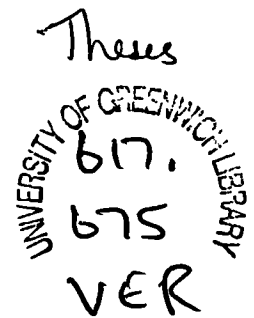


2023 12014

1514141

**Origin and development of internal stresses
during polymerization of composite resins.**

Antheunis Versluis



A thesis submitted in partial fulfillment of the
requirements of the University of Greenwich for the
degree of Doctor of Philosophy

This research program is carried out at the
Minnesota Dental Research Center for Biomaterials
and Biomechanics (University of Minnesota), and the
Centre for Numerical Modelling and Process Analysis
(University of Greenwich).

May, 1994

Acknowledgment

A thesis is the result of several years of intense work, in which a candidate has to prove his ability to do independent quality research, but in which he soon finds out that it is impossible to do so without the support of many others. To all of those who made this work possible I want to express my deepest thanks.

Special thanks I want to express towards Dr. M.C.R.B. Peters, Dr. W.H. Douglas, Dr. R.L. Sakaguchi, and Dr. M. Cross, who offered me the opportunities to start, proceed, and finish my Ph.D.-research.

I also want to thank the members of the examination committee Dr. D.C. Watts and Dr. C.J. Bailey for their critical review and suggestions on this thesis.

Antheunis Versluis

Abstract

This study is focused on the development of polymerization stresses. These are non functional stresses and arise especially when the adhesive composite materials are cured in a cavity, in which the polymerization contraction is restrained by the cavity walls. During masticatory functioning these residual polymerization stresses elevate the overall stress levels. They exercise a cumulative effect, and therefore it is essential to evaluate the internal pre-stressed state of the tooth-composite complex. To study the stress conditions in these complexes, the right tools have to be employed. These consist of dynamic material properties during polymerization, and an appropriate equivalent stress expression for the strength differential effect. The origin of polymerization stresses is a combination of volumetric contraction and development of stiffness during the curing process. Two stages can be distinguished: pre-gel and post-gel. Because stiffness develops after the gel-point, only the post-gel phase plays a role in the development of polymerization stresses. An enhanced strain gage method is developed to determine the dynamic post-gel linear contraction. The development of elastic modulus cannot be measured directly, but has to be assessed indirectly through a polymerization stress evaluation. In an attempt to derive the modulus development, strain and stress data are combined. It turns out that the rate of strain and stress development is greatly dependent on the curing rate, and therefore on the test setup. Two temperature effects (exothermic heating and radiation of the curing light), which play an important role in the volumetric phenomena during the polymerization, are also investigated. Polymerization stress concentrations as a result of different filling techniques are analyzed in a finite element calculation. The numerical analysis suggests that an incremental filling technique raises stresses and cusp displacements. Furthermore, it shows that it is not necessary to model the time-dependent behaviour of the development of mechanical parameters if the worsed case is sought.

Table of contents

Acknowledgment	i
Abstract	ii
1 General introduction	1
1.1 Introduction	1
1.2 Micro structure	2
1.3 Failure mechanisms in restorative composites	4
1.3.1 Yield dominated mechanisms	5
1.3.2 Fracture dominated mechanisms	6
1.3.3 Wear dominated mechanisms	8
1.4 Oral environmental challenge	10
1.4.1 Chemical and physical	11
1.4.2 Biomechanical	11
1.5 Manipulation of composites	12
1.5.1 Placement	13
1.5.2 Curing methods for composites	13
1.6 Statement of the problem	15
1.7 Approach to the problem	17

2	Fracture dominated failure	21
2.1	Fracture toughness in dental composites	22
2.1.1	Introduction	22
2.1.2	Fracture toughness K_{Ic}	22
2.1.3	Fracture toughness specimens and loading	25
2.1.4	Some results of K_{Ic} -experiments	27
2.1.5	Effect of storage and test conditions	30
2.1.6	Effect of micro structure	33
2.1.7	Conclusions	39
2.2	Fatigue in dental composites	41
2.2.1	Introduction	41
2.2.2	Fatigue test specimens	41
2.2.3	Load function	43
2.2.4	Test methodology	45
2.2.5	Test environment	46
2.2.6	Effects of micro structure	47
2.2.7	Conclusions	49
2.3	Discussion	49

3	Yield dominated failure	53
4	Linear polymerization contraction	79
4.1	Introduction	79
4.2	Materials and methods	81
4.3	Results	87
4.4	Discussion	96
4.5	Conclusion	100
5	Polymerization stress development	102
5.1	Introduction	102
5.2	Materials and methods	103
5.3	Results	107
5.4	Discussion and conclusions	114
6	Temperature effects	118
6.1	Introduction	118
6.2	Materials and methods	120
6.3	Results and discussion	124
7	Determination of the elastic modulus	135
7.1	Introduction	135
7.2	Materials	135

7.3	Discussion	137
7.4	Conclusion	150
8	Numerical simulation	152
8.1	Introduction	152
8.2	Materials and methods	153
8.3	Results and discussion	169
	8.3.1 Effect of restoration size	170
	8.3.2 Filling techniques	172
	8.3.3 Coronal surface stresses	185
	8.3.4 Stresses at the tooth-restoration interface	190
8.4	Conclusions	194
9	General Conclusions	196
	References	200

1 General introduction

1.1 Introduction

Since the introduction in the sixties, composite restorative materials have enjoyed an increasingly wide use in dentistry (BOWEN *et al.*, 1985; SMITH, 1985). These composite filling materials are regarded as having certain distinctive advantages over amalgam, the traditional direct filling material. The most significant advantages over amalgam are the ability to bond easily to tooth tissue (current amalgam bonding systems are still in their infancy), preservation of hard tissue, esthetics (so called 'white fillings'), and the absence of heavy metals, with concern about potential toxicity (SMITH, 1982; ASMUSSEN AND MUNKSGAARD, 1985; DOUGLAS, 1985; SODERHOLM, 1985). The presence of mercury in amalgam is becoming more and more an issue, and it is conceivable that legislation constraining the use of mercury amalgam could be introduced in certain countries in the not-too-distant future (BERGLUND, 1993; ELEY AND COX, 1993). As a result the use of restorative composites may be increased even more, and it is imperative that composite restorative materials can be formulated with properties equal to or that exceed those of amalgam in all respects.

However up to the recent past, composites were generally limited to anterior applications, because their mechanical properties still came short of that required for the more exacting posterior use (SUZUKI *et al.*, 1985). Due in part to the amalgam controversy and the steady improvement of the mechanical properties, restorative composites are increasingly used in all areas of the dentition, including high stressed posterior areas (DOGON, 1985). Due to this differential use and the different mechanical and aesthetic service requirements of different areas of the mouth, composite restoratives are formulated with different micro structural configurations (VANHERLE *et al.*, 1985). Structure-property relations have guided these formulations into fairly well-defined

categories of composites (LUTZ AND PHILLIPS, 1983; CRAIG 1985). A brief review of composite micro structure is given here for convenience and by way of introduction.

1.2 Micro structure

(LAMBRECHTS, 1983; LUTZ AND PHILLIPS, 1983; RUYTER, 1985; SODERHOLM, 1985)

A dental restorative composite is a heavily filled paste which consists of a matrix phase, a filler phase and a bonding phase. The matrix phase is a polymeric material. The organic matrix component forms a network, holding the inorganic filler phase. The filler phase exists of glass, quartz, or ceramic particles. The bonding – or coupling – phase takes care of the bonding between filler and matrix material.

Matrix — The matrix phase is build up out of monomers or pre polymers, which are able to form rigid networks when they are brought to polymerization. As a matrix material, usually a Bis-GMA or a urethane dimethacrylate are used. These monomers have a moderately high molecular weight, which will diminish the overall-shrinkage during the polymerization reaction. High viscosity, especially of the Bis-GMA material, necessitates the addition of viscosity regulators. These are monomers with a smaller chain length, which will result in more polymerization shrinkage. Besides the viscosity regulators, other additives are used like inhibitors, catalysers and pigments. Inhibitors, or stabilizers, counteracts spontaneous polymerization reactions, resulting in a better storage time. A catalyst is added to enable the formation of free radicals, which are essential for the polymerization reaction. Some organic or inorganic pigments may be added to the matrix phase to obtain the right color and translucency for a restoration. Dental composites are available in several colors, in order to match the different individual tooth colors.

Fillers — The addition of inorganic fillers to the matrix material will decrease the overall polymerization shrinkage of the composite, the thermal expansion

and the formability, while it increases the modulus, compressive strength and wear. Composites can be divided into three categories, according to their fillers:

- a. Conventional
- b. Microfine
- c. Hybrid.

a. Conventional fillers are obtained by milling of quartz, glass or another ceramic product, such as barium glass, zinc glass, borosilicate glass, lithium aluminium silicate, barium aluminium silicate and strontium aluminium silicate. Quartz (which is rarely used now) has a very high hardness and has good erosion properties. Clinical disadvantages of quartz fillers, however, are radiolucency (fillings are not visible on X-rays) and abrasive properties against the tooth antagonist. The filler sizes of modern conventional filler materials are about 1-5 microns. Conventional composites are composites that only contain fillers obtained by milling. Sometimes they are indicated by small particle composites (if the average filler size is smaller than 5 microns). The filler weight fraction of conventional composites can reach 80%. The volume fraction is always lower than the weight fraction, due to the lower inherent weight of the matrix material relative to the filler materials. Clinical disadvantages of the conventional composites are a high wear rate due to the relatively large inter particle distance. This results in breaking out or plucking out of filler particles. This problem is more serious if the filler size is larger. There are also some cosmetic disadvantages related to these composites, due to their coarse texture, and staining.

b. Microfine fillers are obtained by pyrogenic techniques. The filler sizes are about 0.04-0.15 microns silica particles, sometimes called pyrogenic silica. Addition of these microfine fillers increase the viscosity of the composites considerably. Therefore it is not possible to reach quite as high a filler fraction. The filler fraction can be improved by some techniques, like building the composite out of pre polymerized particles. Another method to improve the filler fraction is to make agglomerates of pyrogenic silicon dioxide of about 1-5 microns. These

agglomerates are entirely inorganic, and can be used in the mentioned pre-polymerized particles. The maximum possible filler weight fraction is about 60%. Microfine composites are mainly used because of their good cosmetic properties. But the strength properties of microfine composites are low and they are prone to chipping.

- c. In hybrid composites the more conventional fillers are combined with the pyrogenic microfine fillers. This reduces the inter particle space, resulting in better wear resistance. A filler weight fraction up to 85% can be achieved. Out of the available composite restorative materials these hybrid composites are most suitable for usage in highly stressed regions.

Bonding — The bonding, or coupling, phase in a composite consists of a silane coupling coating of the filler particles. This silicate coating bonds to the oxides in the inorganic filler particles, and at the same time to organic matrix material. Silanization is most effective for rounded filler particles, because they have less retention.

Due to structure-property relations, the variations in micro structure may be expected to exercise a significant effect on composite properties. When these properties are challenged in the oral environment failure mechanisms may be initiated. Knowledge of these failure mechanisms can be important from a number of points of view. It may assist in better methods of assessment and prediction of composite performance, and when part of the structure-property research loop, knowledge of these failure mechanisms may be used to point the way to improved composite formulations.

1.3 Failure mechanisms in restorative composites

Failure in composite restorations in the mouth is no doubt complex, and comprises an overlap of a number of mechanisms. Nevertheless for the sake of convenience, failure mechanisms may be considered comprehensively under three distinct headings:

1. Yield dominated mechanisms
2. Fracture dominated mechanisms
3. Wear dominated mechanisms

1.3.1 Yield dominated mechanisms

Material strength is generally defined at the yield limit of the particular material, when the material starts to experience plastic flow (NAIDAI, 1950; EWALDS AND WANHILL, 1985). Even brittle materials such as restorative composites will go through some plastic yield, even when this yield is not macroscopically obvious in some failure experiments. Unlike fracture dominated mechanisms, which describes crack propagation, yield is a property that describes properties of the continuous material. Dental restorations have complex three-dimensional geometries, and therefore it may be expected that the stress distribution throughout the restoration is also multiaxial (DE VREE *et al.*, 1984). An appropriate yield criterion for composites should be multiaxial, to incorporate the three-dimensional effects on the limiting mathematical yield surface (DE GROOT *et al.*, 1987). A yield or failure surface is the surface in the (multiaxial) stress space that is built up out of the positions of the limiting values. Dental restorative composites have a brittle nature. Their compressive strength properties are excellent, but the tensile strength is poor (DE GROOT *et al.*, 1988). A yield criterion for restorative composites should take these limits into account. A yield or failure criterion gives a single scalar value, that integrates all the directional stresses, resulting in an equivalent stress (or strain) value. The equivalent stress approach may be highly valuable in combination with finite element stress analysis (ZIENKIEWICZ AND TAYLOR, 1989) for the determination of stress concentrations, locations where the stress level is elevated due to changes in the complex three-dimensional geometry and/or boundary conditions.

Excessive local stress concentrations are sites where localized failure is likely to occur. Such localized failure may present as plastic yield or ultimate rupture as

visualized by the familiar stress-strain curve (CRAIG, 1985). However conditions of cyclic fatigue forces or cyclic contact forces at surprisingly low general stress levels may cause either or both of the two other failure mechanisms to supervene, that is brittle fracture and surface wear.

1.3.2 Fracture dominated mechanisms

(EWALDS AND WANHILL, 1985; BROEK, 1986)

In summary fashion, it may be stated that, it does not necessarily take a catastrophic failure to consider a composite restoration clinically failed. Non-fatal cracks which in case of wear processes, for instance, lead to the volumetric loss of material can also make a replacement of a restoration necessary. As a result the crack resistance of restorative composites is a very significant material property. A crack cleaves a continuous structure, disabling a part of the cracked structure to transfer stresses. This will increase the stresses in other parts of the structure, and localize stresses close to the crack-tip. The discontinuous stress field at the crack-tip results in a local stress singularity. The severity of the stress singularity and the sensitivity of the material to these singularities decides if the crack extends. The crack resistance of a material can be characterized by the fracture toughness factor and by the crack growth rate under cyclic load application. In dental materials the use of fracture properties is twofold: it can be used for material ranking (quality control), and it has potential as a parameter in lifetime estimations.

The two main experimental methods employed in dental materials research to determine these fracture resistance properties are:

- a. Fatigue crack propagation testing
 - b. Fracture toughness testing
- a. *Fatigue crack propagation testing* — Fatigue is a crack propagation process which takes place under cyclic loading. As already noted, because of the cyclic character of the masticatory loading the restorative composite materials will
-

even fail at load levels much lower than the quasi-static material strength, due to fatigue crack propagation. As mentioned earlier, fatigue cracks grow at load magnitudes, which are not high enough to cause quasi-static failure by itself. Cyclic load application causes crack initiation, crack growth and finally failure. The crack initiation period represents the largest amount of fatigue life, and takes place at existing stress concentrations. Stress concentrations are caused by surface damage, geometry of the specimen or inclusions (voids, particles, holes, phase interfaces). The presence of internal flaws and defects decreases the initiation period considerably, because a great amount of the initiation stage is omitted. During this initiation stage local effects (micro scale) control the fatigue crack propagation. If the micro crack becomes a macro crack, the overall stress distribution and bulk material properties become dominant in the fatigue process.

From a literature review conducted for fatigue experiments it can be concluded that the results of the published fatigue experiments (DRAUGHN, 1979; HAHNEL *et al.*, 1986; BENKESER AND SOLTÉSZ, 1988; MCCABE *et al.*, 1990) of various specimens representing different sizes or dimensions can not be compared simply. In order to get comparable test results it is necessary to adopt standard specimen sizes and dimensions and standard test procedures. It is not necessary to adopt the environmental test conditions very close to the *in vivo* case, but the frequency of the cyclic load application is limited to 5 Hz because of the visco-elastic material behaviour (HAHNEL *et al.*, 1986). Therefore a minimal realistic number of fatigue cycles (10^6) is a time-consuming experiment.

- b. *Fracture toughness testing* — The stress intensity factor K describes the magnitude of the stress at the crack tip. Beyond a certain thickness, when the material is predominantly in plane strain and under maximum constraint, the value of the critical stress intensity factor K_c tends to a limiting value: K_{Ic} , *i.e.* the plane strain critical stress intensity factor under mode I loading (opening mode). The required thickness depends on the crack tip plastic zone size and therefore on the material yield strength. The plane strain critical stress intensity factor K_{Ic} can be considered as a material property, characterizing the
-

crack resistance, and is therefore called the plane strain fracture toughness. Knowledge of K_{Ic} , obtained under standard conditions, can be used to predict failure for different combinations of stress, flaw size and geometry. Although the fracture toughness K_{Ic} is an intrinsic material property that should depend only on testing environment and strain rate, a quantitative comparison of fracture toughness results shows that the determined K_{Ic} -values for different investigators (and methods) show more variation than may be expected for such a property.

In the oral environment the resulting fracture behaviour (ROBERTS *et al.*, 1977; LLOYD AND MITCHELL, 1984; DE GROOT *et al.*, 1988) is a complex of interacting factors, whose interrelations are mostly unknown. Although the significance of these influences is widely recognized, low level of standardization makes it often impossible to compare the fracture parameters of different investigators in a qualitative way. Unfortunately, it turns out that even a qualitative comparison is often impossible too.

The brittle character of dental composites is an unfavorable condition in terms of crack sensitivity. For clinical longevity of posterior composite restorations good fracture and wear resistance are important because these restoratives are intended for use in highly-stressed regions. The occurrence of marginal fracture, possibly leading to secondary caries (KUMADA *et al.*, 1991) or fracture of a core buildup (LLOYD AND BUTCHART, 1990) are closely related to the fracture toughness. Because micro cracking may be an important part of the wear process, it is often stated (ROBERTS *et al.*, 1977, 1978; DEVRIES *et al.*, 1981; LEINFELDER, 1981; PILLIAR *et al.*, 1987B) that understanding of the fracture properties can be used in the assessment of the wear process (TRUONG AND TYAS, 1988).

1.3.3 Wear dominated mechanisms

The main function of teeth is the preparation of food for absorption. Oral preparation of food requires particle size reduction by dentition, a process

referred to as comminution. This biophysical process is accompanied by wear of the teeth due to abrasive contacts at the occlusal interfaces.

Excessive loss of occlusal material may lead to reduced masticatory efficiency because of change in anatomic contour. In the wear process the hardness of the contacting surfaces plays an important role (ARCHARD, 1953). Apart from the food bolus itself, three masticatory interfaces may be identified: soft against soft, soft against hard, and hard against hard surface. Because the softest material will suffer the most loss of material in terms of wear, the most favorable situation is generally when the contacting surfaces have the same hardness (GREENWOOD AND WILLIAMSON, 1966). Or, in case of a dental restoration, if the hardness of restorative material is lower or equal to the opposing contact surface which prevents unnecessary loss of irreplaceable biological enamel material.

Within the broad category of tooth to tooth contact, three types of intermaxillary contact may be identified (REEH, 1993):

- a. Swallowing contacts
 - b. Masticatory contacts
 - c. Bruxing contacts
- a. Swallowing contacts, which stabilize the mandible in the process of swallowing, are generally characterized by the absence of any sliding component and therefore are regarded as producing minimal friction and no wear.
 - b. During mastication direct tooth contact occurs. At the beginning of a masticatory sequence the teeth may not touch. Further on in the sequence, when comminuting small food particles to an even finer texture, direct tooth contact may be required. The food is forced along the occlusal grooves, causing wear in these areas where the teeth do not contact each other. Two types of masticatory wear can be distinguished: (1) articular wear which occurs where the teeth contact and (2) non-articular wear that occurs where teeth do not contact, and wear is due to food abrasion.
-

- c. The third kind of intermaxillary contact is a result of bruxing (KYDD AND DALY, 1985; OKESON *et al.*, 1990). Bruxing is a habitual contact which can be demonstrated in only a small proportion of the population. Bruxing contacts can be distinguished from masticatory contacts by a slower cycling rate, a higher occlusal force, a larger contact area, and an alternating motion with the teeth in contact in both directions.

Rubbing between two surfaces involves many encounters between protuberances (GREENWOOD AND WILLIAMSON, 1966). All these encounters contribute to friction, but only a small portion contributes to wear. Friction is therefore dominated by the behaviour of the undamaged contacts and is practically independent of what happens at the small number of encounters contributing to wear (DELONG *et al.*, 1985). This small proportion, however, dominates the wear behaviour. This theory is consistent with the small ranges of friction and the magnitudes of wear found in wear studies. Wear in the oral environment is a complex mechanism, in which chemical and biochemical effects play a role in degrading and eroding, as well as biomechanical effects such as cracking or yielding.

1.4 Oral environmental challenge

The oral environment which is responsible for the unfavorable failure mechanisms described above is surprisingly hostile to dental materials. The oral environmental challenge may be divided into two parts:

- Chemical and physical
- Biomechanical

These two parts to the challenge may be in fact be synergistic (as in a type of corrosion fatigue) and accelerate the degenerative process in restorative materials.

1.4.1 Chemical and physical

The major component of the chemical environment of the oral cavity is water. The oral cavity when closed is essentially at 100% relative humidity. Anterior aspects may be less than this when the mouth is open. The physiological temperature is of course 37°C (DELONG AND DOUGLAS, 1991), but the temperature of the oral surfaces is subject to the thermal cycling of different temperatures of food (SPIERINGS *et al.*, 1987).

The oral surfaces are also bathed in saliva which is a dilute solution of proteins and glycoproteins, which supply various defense mechanisms, including the lubrication between of opposing enamel surfaces (MANDEL, 1980). The oral cavity also has a rich flora of bacteria which form plaques on surfaces. The byproducts of these bacteria can mediate dental diseases such as caries and periodontal disease, and are responsible for a lowering of the oral pH. Below pH 5.5 enamel will start to spontaneously dissolve (JENKINS, 1978). Another function of saliva is to act as a buffering medium, and because of this under ideal conditions the pH of the oral cavity is maintained in the long term in the region of 7 (JENKINS, 1978).

1.4.2 Biomechanical

By biomechanical is meant the stresses which are experienced by the restorative material not only considered alone but as part of the tooth-restorative complex. These stresses can be due to external body forces which are applied during functional mastication due to tooth to tooth contact with or without intervening food. External forces may also be applied during para-functional bruxing (*i.e.* habitual grinding) (OKESON *et al.*, 1990) which refers to tooth to tooth contact only. These are forces external to the restoration and where these stresses are accompanied by a sliding component they will result in wear.

However non functional internal stresses experienced by restoration can arise within the restoration or tooth-restoration complex. Two kinds of internal stress

can be identified. The first is due to the differential coefficient of thermal expansion, leading to a differential volume change in the composite, relative to its hard tissue surroundings. This thermal expansion and contraction may follow the application of heat from any source, such as the curing light at the time of curing the restoration within the tooth or from dietary sources of hot and cold foods which may present a variation of about 50°C on the surface of the tooth and restoration (SPIERINGS *et al.*, 1987; PALMER *et al.*, 1992). Internal stresses may also follow volume contraction due to the polymerization process itself (BOWEN *et al.*, 1983; DAVIDSON *et al.*, 1984). The molar volume of the polymer is much different from that of the monomer, leading to a more efficient packing of the polymer and shrinkage of the volume relative to that of monomeric starting material. This is a near universal phenomenon in which polymerization is accompanied by volume shrinkage, and internal stress within the tooth-composite complex if this contraction is hindered.

These internal stresses are probably semi-permanent stresses, and are superimposed on the functional external loads. Therefore it is the combination of these stresses that will initiate any or all of the failure mechanisms singly or together, mentioned above, and that determine the lifetime of a restoration.

1.5 Manipulation of composites

The most common mode of use of composites is as an intracoronal restoration, that is the composite is placed within a prepared cavity within the crown of the tooth. Thus the composite restoration is surrounded on many sides by the hard tissues of the tooth. This is in contradistinction to an extracoronal restoration, which is typically made of ceramics or gold. Composites are less typically used for extracoronal restorations, that is on the outside of the tooth structure (though not infrequently as veneers). Composites are invariably bonded to the hard tissue structure of the tooth, including both the enamel and the dentine, with the intention that the composite restoration should form a biomechanical continuum with the tooth structure. This bonding procedure requires a number

of preliminary treatment steps to the surface of the tooth to accomplish the bond, before the placement of the composite resin within the crown of the tooth.

1.5.1 Placement

(SUZUKI *et al.*, 1985; LEINFELDER AND LEMONS, 1988)

Amalgam, although lacking in many respects, is looked upon as setting the standard of ease of manipulation as a restoration. An important feature is pressure placement in which the amalgam is packed, and condensed into the cavity. The amalgam is built in incremental placements until the cavity is slightly overfilled. When it has achieved a considerable yield strength, it is carved back to the required occlusal shape of the functional surface of the tooth. At a later stage the surface of the amalgam is finished and polished.

In contrast the placement of a composite is looked upon as being more difficult. Although composites are heavily filled pastes they have a low yield strength in the uncured state. Thus pressure placement is difficult as the placement instrument can penetrate the paste rather than pack or condense it. Composites are also built up in incremental layers, and each layer is cured (polymerized) before the next layer is added. The number of increments is typically 3 or 4, which is less than that of the amalgam buildup. The composite is also overfilled, but cannot be easily carved back because of its unfavorable rheology, and thus it must be cured and cut back to ideal shape, and then finished and polished. This is much more difficult and time consuming process than that for amalgams.

1.5.2 Curing methods for composites

(PHILLIPS, 1982; CRAIG, 1985; RUYTER, 1985)

The curing method for composites which changes them from viscous pastes into rigid solids is typically by vinyl addition, typically multi-functional methacrylic. The polymerization is really part of the manipulative procedure and takes place

within the cavity as the restoration is being formed, and is usually completed mainly within 60 seconds or shorter. Although it is believed that there is a continuing post cure for some time. The polymerization procedure is also intimately linked with the incremental build up procedure, as will be seen later.

For dental restorative composites two polymerization reaction methods are used:

- a. Chemical
- b. Photochemical

Both methods have their own advantages and disadvantages with regard to their applicability, filling technique and possible mechanical properties .

- a. *Chemical* — Chemical curing composites consist of two components, a base and a catalyst. Mixing of these two components will result in a chemical reaction which produces free radicals. These free radicals enable the monomers to cross link, thus forming a rigid network of polymers. Chemical polymerization enables a degree of curing which is independent of the depth of the restoration. However, the chemical polymerization process is slow, and mixing of two components introduces porosity. Porosity decreases the mechanical strength, and enlarges the chance for inhomogeneous material properties. Porosity also may decrease the esthetic appearance over a longer period of time.
 - b. *Photochemical* — Photochemical curing is activated by light of a certain critical wave length. While early composites were activated with ultra-violet light emissions, present photo curing composites are cured using visible blue light (400-500 nm). Photo initiators in the composite material produce free radicals when they are light-cured. These free radicals enable cross linking of the monomer chains into a rigid network of polymers. The degree of curing depends in part on the light intensity of critical wave length of the curing light source. This polymerization method has many advantages over the two-components chemical curing procedure and is widely used. The consistency of the photo curing composite is better, because it is used immediately from the container in
-

manufacturing condition. It has not to be mixed before usage with a second component. Overall photo curing is more convenient to work with than chemical curing composite. A restoration can be finished without the constraints of the time limit of a chemical curing composite. Because the reaction is better controlled, it is easier to apply a restoration in several layers. Some disadvantages for the application of light curing composites are the limited restoration depth and the curing light is harmful for the eyes, which should be protected whenever the curing light is used. The polymerization type and history (*e.g.* light curing and the intensity of the curing light output) have a significant influence on the mechanical longevity of composite restorations.

1.6 Statement of the problem

It is clear that a restorative composite has to fulfill many requirements, with respect to biocompatibility, chemical stability, aesthetics, ease of use, and mechanical properties (JENDRESEN, 1985; VANHERLE *et al.*, 1985). It is equally clear that dental restorative composites are used in a hostile oral environment. A restoration is clinically subjected to endless abrasive and corrosive assaults. One of the factors determining the clinical lifetime of a composite restoration, among others (*e.g.* discoloration and microleakage), is structural disintegration caused by mechanical stresses (SMITH, 1985). During service dental restorations are exposed to continuously varying conditions in temperature, environment and mechanical loading. The load situations vary from low and uniform distributed occlusal loads to extremely high and sudden peak loads. The load range is broad and hardly predictable or reproducible and the resulting stresses are both tensile and compressive. Dental restorative composites can resist high compressive stresses, but are less suitable when subjected to tension (DE GROOT, 1986).

Although one of the advantages of composite materials over amalgam is ability to bond easily to tooth structure, this feature also introduces a new challenge. Because of the bonding, volumetric changes due to polymerization shrinkage are transferred into the tooth. Application of composites in the larger posterior

restorations will increase the problem of stresses induced by volumetric changes due to the larger initial volume of material giving a higher net shrinkage . The subject of this study is focused on the origin and development of internal stresses during polymerization of dental composite restorations, and after. The problem that is investigated in this study can be described in the following four points:

- a. The significant part of polymerization which leads to unfavorable events occurs after the gel point has been passed and is therefore referred to as post-gel shrinkage. This part of the shrinkage process is accompanied by the modulus development which is responsible for the internal stress and its transmission to the boundaries of the restoration and beyond (DAVIDSON AND DE GEE, 1984).
- b. Such stresses will challenge the bond at the hard tissue interface and threaten the marginal integrity of the restoration. This is particularly true during hard tissue bond development at or soon after the placement of the filling (JENSEN AND CHAN, 1985). It may also be a long term residual stress effect (SAKAGUCHI *et al.*, 1991).
- c. Transfer of the internal stresses within the restoration across an intact bond and into the tooth structure may occur. This may also have unfavorable effects either weakening the tooth structure, leading to propagation of enamel cracks or responsible for postoperative sensitivity and pain (JENSEN AND CHAN, 1985), since it is widely believed that the tooth under ideal conditions is a mechanically quiescent structure.
- d. Long term internal stresses residing within the substance of the composite restoration may singly or in combination with the external forces be responsible for the partial or catastrophic failure of the restoration.

Quite clearly then the internal non functional stresses can have effects which may appear to have functional significance, as explained below. It is important therefore to understand the origin, development, and extent of these forces and to probe their significance and the methods of reducing them in the restored dentition.

1.7 Approach to the problem

The mechanical stress environment of the restored tooth is, as may be expected, enormously complex. This introduction has for convenience divided the environment into two broad components. These are the external or body forces which ultimately have their origin in the muscles of mastication, and are mediated to the tooth by mechanical contacts either in function or para-function. Thus another name for such forces might be functional forces. These are applied to the restored tooth over a period of time while it is in service. The second main component of the mechanical environment is the internal or non functional forces, which are mediated to the restored tooth, not by mechanical contact, but by certain changes in physical or chemical environment. Examples of these are forces that attend the volume changes due to thermal expansion and contraction, and in the case of composite resins the contraction due to polymerization.

However, the complexity does not end there, for the failure induced by these forces are equally diverse and, as already shown, can be divided into three main categories: fracture, yield and wear. The matrix of investigation that would be formed by the two main force components, and the three main failure modes is very large indeed. It is evident from the outset as already noted that an area of focal interest will have to be determined in order to make progress within the boundaries of a thesis topic.

In the approach to its focal interest it is not intended in this thesis to ignore other areas which while peripheral to the focal interest might have an important bearing on it. For this reason then, the exposition of this work begins with a consideration of fracture dominated failure in Chapter 2 and in yield dominated failure in Chapter 3. These are not intended to be exhaustive treatments in their own right, but to establish the current state of the art, especially as it relates to composites, and anticipate where the focal interest of internal stress may contribute to these failure mechanisms.

With this perspective established, the remainder of this work focuses on experimental and computational aspects of internal stresses in dental composite resins. The two main changes in composite materials which are responsible for the internal non functional setting stresses are the change in volume and the accompanying modulus of elasticity. To determine these two effects, basically two experimental measuring methods are used:

- Strain gage method
- Load cell method

Two effects during polymerization are responsible for the volumetric changes: polymerization contraction and thermal expansion. The changes in temperature during polymerization are due to both a chemical exotherm and due to radiant heating from the curing light. All of these changes during polymerization and their impact on the stress state in a tooth-restoration complex are considered under the following headings:

- Chapter 4: Linear polymerization contraction
- Chapter 5: Polymerization stress development
- Chapter 6: Temperature effects
- Chapter 7: Determination (development) of elastic modulus
- Chapter 8: Numerical simulation

This approach was determined by the obligation to establish an experimental basis for the work that focused specifically on that part of the contraction which was responsible for stress development, *i.e.* post-gel changes. This emphasis is critical and seems to be missed in the current desire in the clinical community for a "no" or "low" shrinkage composite. It may be entirely possible to substantially reduce the overall shrinkage of a composite by merely reducing the pre-gel shrinkage.

Further in the experimental approach it would be especially useful if the post-gel shrinkage could be determined in real time, rather than as some cumulative number after the passage of time. In this way the work would be kinetically useful, and shed light on the polymerization process itself. This is especially important for the modulus of elasticity in the post-gel phase, which is not a single value but develops from essentially zero to a maximum value somewhere soon after the post-gel period.

Just as the changes in volume and modulus plot the mechanical progress of polymerization, so the exotherm can be thought of as displaying the chemical progress of polymerization. The changes in bond energies during polymerization produce the exotherm. A high temperature rise may be indicative of a high degree of polymerization. It seems that the benefits of a high degree of polymerization are ambivalent, since they couple together increased mechanical performance in the fully cured composite with a high degree of polymerization shrinkage. If the exotherm can be measured with a fast response thermocouple, then it may also have kinetic value and shed light on the polymerization process. Secondly the exotherm may be expected to influence the post-gel shrinkage due to coefficient of thermal expansion. Although this effect could be important, it is likely to be restricted to the period of polymerization and shortly thereafter, since the exotherm will die away as the cured composite reaches equilibrium with its surroundings.

The development of internal stresses in composite resins will also be considered in this work by a study of the coefficient of thermal expansion. This phenomenon affects the volume changes in composites temporarily during the polymerization exotherm and in the radiant heat effects of the curing light. Its most important effect, however, is perhaps during the service life of the composite when the tooth-restoration complex experiences the thermal cycling. This follows from the differential effects of foods of different temperature, which may sequentially bathe the tooth restoration complex. There are two possible effects of thermal cycling. The first will be due structural inhomogeneity of composites and the large differences in coefficient of thermal expansion between

the filler (inorganic) and the resin (organic). This could conceivably lead to stress development at internal interfaces within the composite, and contribute to its degradation. A second effect is expected at the tooth-restoration interface. This is due to the mismatch between the coefficients of thermal expansion for the composite and tooth substance (*i.e.* enamel and dentin), and threaten the integrity of the hard tissue bonding, which has been shown to be important for its contribution to tooth strengthening and the reduction of microleakage.

The assembly of the experimental data that is anticipated in Chapters 4 to 7, should enable a sophisticated model of the tooth-composite complex to be constructed using a finite element approach, with special reference to the development of internal stresses. The power of the experimental approach is its real world significance, but the power of the experimentally-validated finite element model lies in the ability to examine the model at points which are experimentally inaccessible. Further, simulated conditions can be assessed such as different kinds of incremental fillings to determine their alleged benefits, and it may be possible to prescribe the optimal material properties or technique conditions to reduce the adverse effects of polymerization shrinkage.

It is hoped therefore by the approach to the study of the development of internal stresses outlined above, that new light will be shed on this phenomenon, particularly as regards its development, likely importance, and the effectiveness of clinical methods of its control.

2 Fracture dominated failure

Serving in an oral environment, a restoration has to withstand a variety of external and internal stresses. These stresses originate from external dynamic body forces, as well as internal static residual polymerization stresses and internal stresses induced by temperature changes in the oral environment. Cracking of a composite restoration under these constant attacks is the beginning of the end of its functional life. Even when it does not cause a catastrophic failure, crack extension results in a loss in stress bearing material, and therefore causes an increase of the overall stress levels. The moment at which cracking happens, and the rate of mechanical functionality deterioration, depends on the stress levels, the restoration design, and the material properties of a restoration. Fracture dominated failure can be characterized by two phenomena: crack propagation under critical and subcritical stress intensities. The critical and subcritical fracture behaviour of dental composites can be expressed in fracture toughness and fatigue properties respectively.

The critical stress intensity factor K_{Ic} is an inherent material property for crack resistance, that predicts the condition of catastrophic failure (EWALDS AND WANHILL, 1985). Fatigue is a process of incremental crack propagation (sub critical stress intensity), eventually leading to the catastrophic condition of fracture (critical stress intensity). Knowledge of the stress distribution is only important because of the existence of limiting stresses. Limiting stresses depend on local stress intensity values, and their effect on a structure is material dependent. Therefore the determination of crack resistance and fatigue properties is of first importance for the understanding and prediction of the performance of composite restorations. In the next two paragraphs literature reviews are conducted for fracture toughness and fatigue experiments of dental composites. Wear dominated fracture mechanisms are contact problems, in which the internal stress distribution is playing a minor role. For that reason wear mechanisms are not reviewed in the course of this

study, although there may be overlap mechanistically between wear, fracture and yield, as already noted.

2.1 Fracture toughness in dental composites

2.1.1 Introduction

This section is an overview of published K_{Ic} fracture toughness experiments for dental restorative composites. The K_{Ic} -value enables the characterization of the fracture behaviour. There are many ways to perform the experiments, varying the specimen types and the test conditions. Since the specimen type and the test condition might have a significant effect on the value obtained for K_{Ic} , it is important to know the test methods and the influence of several test parameters. Therefore, after a brief introduction of the K_{Ic} -factor and some other fracture mechanics parameters, the main specimen types are introduced and pre-notching methods are evaluated. The results of the fracture toughness experiments are compiled, followed by a discussion of the influence of the storage and test environment and the effects of the micro structure on the fracture behaviour. Some mechanisms that may control the fracture behaviour are considered.

2.1.2 Fracture toughness K_{Ic}

The stress intensity factor K describes the severity of the stress at the crack-tip. The K -factor is given by (EWALDS AND WANHILL, 1985):

$$K = C \sigma \sqrt{\pi a}$$

where: C is the specimen geometry correction factor

σ is the applied stress

a is the crack length

Beyond a certain thickness, when the material is predominantly in plane strain and under maximum constraint, the value of the critical stress intensity factor K_c tends to a limiting constant value: K_{Ic} i.e. the plane strain critical stress intensity factor under mode I loading (opening mode). The required minimum thickness depends on the crack-tip plastic zone size and therefore on the material yield strength. The plane strain critical stress intensity factor K_{Ic} can be considered as a material property, characterizing the crack resistance. The K_{Ic} -value, obtained under standard conditions, can be used to predict failure for different combinations of stress and flaw size and for different geometries.

Another approach to describe the occurrence of fracture follows from Griffith's energy balance approach (EWALDS AND WANHILL, 1985). When a crack grows, the stiffness of the stressed material will decrease, which relaxes some load. Consequently, the elastic energy content drops. Crack propagation takes place if the released elastic energy is sufficient to provide all the energy that is required for crack extension. Therefore the fracture stress for a given crack length depends on both the strain energy release rate G and the modulus of elasticity E . Under plane strain conditions G is given by:

$$G = \frac{\pi a \sigma^2}{E} (1-\nu^2)$$

where: a is the crack length
 σ is the applied stress
 E is the modulus of elasticity
 ν is the Poisson's ratio

The critical strain energy release rate is represented by \bar{G}_{Ic} .

The K_{Ic} -approach has some advantages over the G_{Ic} approach. The G -factor depends on the elastic modulus, while for the K -factor the elastic modulus does not need to be measured separately. Furthermore no assumption has to be made for the K_{Ic} -factor about the strain rate at the crack-tip and the modulus dependency on the strain rate. This indeed is an advantage for viscoelastic

materials. The relationship between the fracture toughness parameter on the one hand and the fracture energy parameter and elastic modulus on the other hand, can be expressed (under plane strain condition) by:

$$K_{Ic}^2 = \frac{E G_{Ic}}{(1 - \nu^2)}$$

Another fracture mechanics parameter, the J integral (EWALDS AND WANHILL, 1985), was introduced for dental composites by DE GROOT *et al.* (1988). In the case of linear elastic material behaviour, the J integral is equal to the strain energy release rate G. The J integral can be calculated by finite element analysis or experimentally determined when the load-deflection (F,u) curves are recorded, using the relation (single-edge notch specimen):

$$J = \frac{2}{B(W-a)} \int F du \quad \text{for} \quad a/W > 0.5$$

where:

- F is the load
- u is the deflection at mid span
- B is the specimen thickness
- W is the specimen width
- a is the notch depth

It is shown that the J_{Ic} -technique is more applicable to small specimens than the K_{Ic} -technique. K_{Ic} is a parameter in the linear elastic fracture mechanics theory, while J_{Ic} can be used in the elastic-plastic fracture mechanics. Therefore, in order to fulfill the plane strain condition, the plastic zone size at the crack-tip must be smaller for the K_{Ic} compared to the J_{Ic} determination.

More information about the fracture mechanics parameters can be found in the publications of EWALDS AND WANHILL (1985) and BROEK (1986).

2.1.3 Fracture toughness specimens and loading

There are several test specimens used to determine the fracture toughness (K_{Ic}) of dental composites. The three major types are:

1. Single-edge notch specimen, **Figure 1A** (ROBERTS *et al.*, 1977; LLOYD, 1982, 1983, 1984; FERRACANE *et al.*, 1987,1988; DE GROOT *et al.*, 1988)
2. Short-rod specimen, **Figure 1B** (PILLIAR *et al.*, 1986, 1987A, 1987B)
3. Double-torsion specimen, **Figure 1C** (GOLDMAN, 1985; COOK AND JOHANNSON, 1987; DAVIS AND WATERS, 1987)

The energetics of fracture of double-torsion specimens are such that the load causing the crack remains constant as the crack deepens. This load is directly related to the fracture toughness, OUTWATER *et al.* (1974). One of the advantages of this method is that the crack length need not be measured. Another advantage is the stable crack growth, permitting many measurements of the fracture energy on one specimen. This experiment can be performed in stroke control mode, because the movement of the crack-tip tends to reduce the load until a cross-head movement increases it again to the critical value.

One of the advantages of chevron-notched fracture toughness specimens is the possibility to omit the pre-cracking stage, NEWMAN (1984). The stress intensity factor K versus crack length characteristic is modified by the chevron shaped slot in such a way that after an initially decreasing stress intensity factor, a minimum value is found. Before this minimum stable and after it unstable crack growth takes place. Besides caused by the specimen dimensions, non-plane strain effects can become a source of error in short-rod testing if the chevron-slots are not sufficiently thin or if the slot bottoms are not sufficiently sharp, BARKER (1984).

To obtain a valid value for the K_{Ic} it is necessary to create a plane strain condition at the onset of fracture. For a plane strain condition at the crack-tip it is required that the thickness has to be large with respect to the size of the

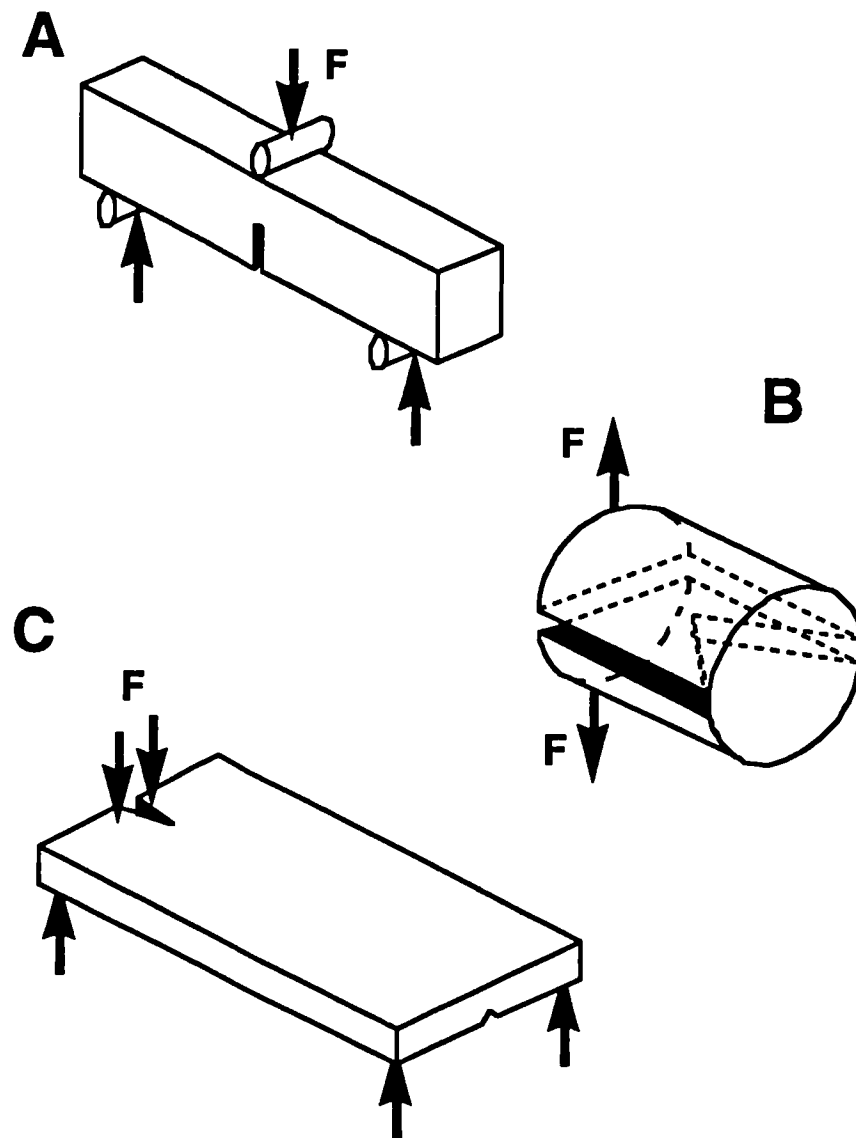


Figure 1. Three fracture toughness specimens:

A. Single-edge notch specimen

B. Short-rod specimen

C. Double-torsion specimen

plastic zone. For the crack size it is also required that the plastic zone size is small compared to the crack length. Pre-notching and pre-cracking is therefore a critical procedure in the preparation of fracture toughness specimens. According to the procedures outlined for metals, fatigue pre-cracking is specified of the existing pre-notch at low stress intensities. For the dental composites, however, this is not practical because of their limited ductility. Pre-notches are either machined or obtained by the insertion of a scalpel blade. Pre-notching by means of insertion of a straight edge scalpel blade might be preferable rather than a machined pre-notch, because it creates a sharp, narrow and smooth pre-notch (LLOYD, 1988). Machining may damage the notch-surfaces, due to pull out of composite material and the friction heating of the composite material. Especially the latter one, temperature rise, might effect the material fracture behaviour.

The cross-head rate has a significant influence on the mode of crack propagation (DAVIS AND WATERS, 1987). When the cross-head rate is increased, the value for crack initiation reduces. If the cross-head rates are ≥ 50 mm/min, the crack propagates in a continuous mode, *i.e.* the K -value for crack initiation is equal to the crack arrest. This phenomenon will be discussed in the paragraph about micro structural effects.

2.1.4 Some results of K_{Ic} -experiments

Because of the great variation in storage and test environments and the variation in batch numbers and specimen production, it is unwise to compare the K_{Ic} -values of different investigations. If the assumption is made that the effect of test environment is small (this assumption is not always correct as will be seen in the next paragraph about environmental influences) and the variation in material composition (which exists for different batch numbers) and specimen production is negligible, some materials can be compared in **Tables I-IV**. The differences in **Tables I-IV** may partly be attributed to differences in pre-notching and possibly to an effect of the specimen type and test environment also. It seems that the K_{Ic} -value obtained using a single-edge

Table I. Comparison for different test methods of some fracture toughness values ($\text{MN m}^{-1.5}$) after 1 day storage in water at 37°C .

	K_{Ic} fracture toughness		
	DE GROOT <i>et al.</i>	LLOYD AND	PILLIAR <i>et al.</i>
	(1988)	ADAMSON (1987)	(1987B)
Occlusin		2.00	1.65
P-30	1.88	1.25	1.15
Specimen	single-edge notch	single-edge notch	mini-short rod

Table II. Comparison for different test methods of some fracture toughness values ($\text{MN m}^{-1.5}$) after 7 days storage in water at 37°C .

	K_{Ic} fracture toughness		
	LLOYD (1982)	PILLIAR <i>et al.</i>	PILLIAR <i>et al.</i>
		(1986)	(1987B)
Adaptic	1.34	1.72	
Concise	1.33	1.83	1.53
Isopast	1.15	1.15	
Specimen	single-edge notch	short rod	mini-short rod

Table III. Comparison for different test methods of some fracture toughness values ($\text{MN m}^{-1.5}$) after 1 month storage in water at 37°C .

	K_{Ic} fracture toughness		
	LLOYD AND ADAMSON (1987)	PILLIAR <i>et al.</i> (1986)	PILLIAR <i>et al.</i> (1987B)
Miradapt	1.03	1.54	
Occlusin	1.79		1.66
P-30	1.13		1.19
Specimen	single-edge notch	short rod	mini-short rod

Table IV. Comparison for different test methods of some fracture toughness values ($\text{MN m}^{-1.5}$) after ~2 months storage in water at 37°C .

	K_{Ic} fracture toughness	
	GOLDMAN (1985)	PILLIAR <i>et al.</i> (1986)
Adaptic	1.63	1.50
Concise	1.84	1.50
Durafil	0.71	0.58
P-10	1.60	1.67
Silar	1.02	0.84
Specimen	double torsion	short rod

notch specimen is higher than the value obtained by a short-rod specimen, which in turn seems to be less than the results obtained with a double-torsion specimen.

LLOYD AND DHURU (1985) and DHURU AND LLOYD (1986) investigated the fracture toughness of repaired dental composites. Because the elastic modulus may not be the same on either side of the repaired interface, the stress distribution at the crack-tip may alter. Other loading modes (II and III) may contribute to the failure stress state. They found that the interface between repairs and additions has a lower fracture toughness than the original material.

2.1.5 Effect of storage and test conditions

Storage and test conditions have a significant effect on the fracture toughness. In **Table V** the storage and test environments are compiled for several publications. Storage conditions consist of: storage time, storage environment, and storage temperature. The test conditions are: test environment, and test temperature.

Storage time is found to have a significant effect on the K_{Ic} value. Until 1 hour storage, no effect is observed for different environments, LLOYD (1982). But after 168 hours a significant increase of the K_{Ic} -value for specimens stored in water is found. This increase is attributed to the plasticizing effect of water. The influence depends on the absorption rate of the material. Obviously a test specimen needs sufficient time to allow water absorption. Besides absorbed water, residual monomers act as plasticizers, LLOYD (1984). In case of extended storage, the K_{Ic} shows a small reduction. This time-dependent behaviour (initial rise to a peak value followed by a small decrease) is explained by the progression of polymerization together with the elution of residual monomer and the absorption of water, LLOYD AND ADAMSON (1987).

PILLIAR *et al.* (1986) find a significant higher K_{Ic} -value for 7-days water-stored samples compared to 1 or 6-months water-stored specimens. Because no reduction of the elastic modulus is observed, the degradative effect of long-term

Table V. Compilation of storage and test environments of some published fracture toughness investigations.

Reference	Storage environment			Test environment	
COOK AND JOHANNSON (1987)	air	5°C	¹⁾		23°C
DAVIS AND WATERS (1987)	air distilled water	RT ²⁾	1 week	air water	23°C
DE GROOT <i>et al.</i> (1988)	tap water	37°C	1 day		23°C
DHURU AND LLOYD (1986)	distilled water	37°C	24 hours	air	RT
FERRACANE <i>et al.</i> (1987)	water	37°C	2 days		
GOLDMAN (1985)	distilled water	37°C	-2 months	wet condition	RT
LLOYD (1982)	air water	37°C	1 hour 168 hours	air water	23°C
	water	37°C	168 hours	water	20, 27, 34, 37, 40°C
LLOYD (1983)	moist air	37°C	7 days		RT
LLOYD (1984)	moist air distilled water 0.1 mol/l saline 0.05 mol/l sucrose solution	37°C	210 days	air	23°C
LLOYD AND ADAMSON (1987)	distilled water	37°C	1 hour 5 hours 1 day 7 days 1 month 3 months	air	RT
LLOYD AND DHURU (1985)	distilled water	37°C	24 hours		
LLOYD AND IANETTA (1982)	air (light pressure)	37°C	0.3-1000 hours	air(?)	RT(?)
	water	37°C	168 hours	air(?)	RT(?)
LLOYD AND MITCHELL (1984)	humid environment	37°C	1 week	air	RT
PILLIAR <i>et al.</i> (1986)	water	37°C	7 days 1 month 6 months	wet condition	RT
PILLIAR <i>et al.</i> (1987B)	distilled water	37°C	7 days	dry condition wet condition	RT
PILLIAR <i>et al.</i> (1987A)	air	RT	14-21 days	wet condition	RT
	distilled water ethanol	37°C	1, 3, 7, or 28 days	wet condition	RT
ROBERTS <i>et al.</i> (1977)		37°C	24 hours		

¹⁾ postcuring at 5, 23, 60, and 100°C in air for 24 hours

²⁾ RT = Room Temperature

water exposure appears to be related to high stress application and possibly related to the fracture process only. This indicates the degradative effect of water on the filler/matrix junctions for dental composites which enables an easier crack propagation.

Addition of salt or sucrose to the water fails to produce any significant alteration to the K_{Ic} -value, LLOYD (1984). Therefore it is concluded that testing may be conducted in distilled water. PILLIAR *et al.* (1987B) report significant increase of the K_{Ic} -value as a result of longer storage time in ethanol, due to chemical softening.

Storage in air at room temperature for different storage times does not have a significantly effect on K_{Ic} , PILLIAR *et al.* (1987B). The small reduction of fracture toughness during storage in air may be attributed to the loss of plasticizer through the evaporation of volatile constituents, LLOYD AND IANNETTA (1982).

The effect of postcuring at different temperatures is studied by COOK AND JOHANNSON (1987). They post-treated their specimens at 5, 23, 60 and 100°C in air for 24 hours, after which they store them in air at 5°C to minimize further postcuring prior to testing. It appears that the K_{Ic} -value rises to a plateau with increasing postcure temperature, caused by additional polymerization which increases the matrix cross link density. It appears that although cross linking may reduce the amount of plastic deformation and hence energy dissipation at the crack-tip, resulting in a reduction in fracture energy, the increase in the elastic modulus as a result of a more dense network is sufficient to lead to a rise in K_{Ic} .

DAVIS AND WATERS (1987) study the 'stick-slip' crack propagation. They discriminate between the critical stress intensity factor for crack arrest K_{Ica} and for crack initiation K_{Ici} . Presence of water increases both K_{Ici} and K_{Ica} , although the main effect is on K_{Ici} . Possible explanations are the influence of water on the nature and strength of the bond between the filler and the matrix, and the plasticizing effect causing crack-tip blunting.

The effect of the test environment on the K_{Ic} -value is investigated by LLOYD (1982), who carried out a set of tests, dry and wet at a constant temperature (23°C). The effect of the test environment appears to be small, except in the case of one product possessing a PMMA matrix (TD 71). For a second set tests are performed in water for different temperatures. From the results of these experiments at varying test temperatures (20 - 40°C) it is concluded (LLOYD, 1982) that temperature dependency does exist but is not very large over the investigated range. SANDS *et al.* (1988) also investigates the influence of the test environment for Occlusin. They report a significant difference between 22°C dry test and 37°C dry test. When tests are performed in water either at 22°C or 37°C no differences can be found due to wet storage. Differences are also found between specimens tested at 22°C and 37°C in water after dry storage. These tests indicate that the test environment may influence the K_{Ic} -value of composites.

2.1.6 Effect of micro structure

In **Table VI** the filler volume fraction, the filler weight fraction and/or average particle size of the same investigated composites are compiled. Microfine composites exhibit generally a lower K_{Ic} -value than fine or coarse particle composites, GOLDMAN (1985). The K_{Ic} -factor generally increases if the filler content increases. The effect of the filler depends on the material properties, the filler content or size, and the filler/matrix bonding.

In a brittle matrix, a rigid filler will increase the fracture toughness, especially if the filler/matrix adhesion is poor. In a ductile matrix, the filler will decrease the fracture toughness, since it inhibits plastic deformation of the matrix. This is more effective if there is filler/matrix adhesion, DAVIS AND WATERS (1987).

Significant correlation is found between fracture energy and filler content. The fracture energy increases if the filler content increases until a certain filler fraction (which depends on particle size, but is generally between 20 and 30% by volume). Beyond this filler fraction it will decrease.

Table VI. Compilation of filler volume fraction, filler weight, and average particle size of some published fracture toughness investigations for dental composites.

References *)	Filler volume (%)								Filler weight (%)			Filler size (μm)	
	[1]	[2]	[3]	[4]	[5]	[6]	[7]	[8]	[9]	[10]	[11]	[10]	[2]
Adaptic		58					62	61					10-20
Aurafill		62											5-10
Clearfil							61				80		
Command	56												
Compocap							62						
Concept									63				
Concise							61	61			78		
Corelite			63										
Delphic				67			67						
Durafil							39	37					
Epolite 100			66										
Estic MF								33					
Experimental									70				
Finesse	20				20		20						
GC Microrest			44										
Heliomolar								46					
Helioait	24						24	26					
Isopast	24						24	24					
Kerr Coreform			57										
Miradapt					62		62	59					
Occlusin					72				86		86		
Orion	28			28			28						
P-10			74			74		68					3-7
P-30		67			73				85	51	86	3.5	
Prisma-fil		53					56	56					1-4
Profile		59	61					72					5-10
Replica								63					
Silar		35		37			37	36					0.04
Silux		38							87			0.04	0.04
Visio-dispers							47	47					
Visio-fil		65											5-10

*) References:

- [1] DHURU AND LLOYD (1986)
- [2] FERRACANE *et al.* (1987)
- [3] LLOYD (1983)
- [4] LLOYD (1984)
- [5] LLOYD AND ADAMSON (1987)
- [6] LLOYD AND DHURU (1985)
- [7] LLOYD AND MITCHELL (1984)
- [8] PILLIAR *et al.* (1986)
- [9] COOK AND JOHANNSSON (1987)
- [10] DE GROOT *et al.* (1988)
- [11] PILLIAR *et al.* (1987B)

DAVIS AND WATERS (1987) study the stick-slip crack propagation. They find that if the filler content increases above 26% by volume, the difference between the crack initiation K_{Ici} -value and the crack arrest K_{Ica} -value decreases. They suggest that it is possible that further increase of the filler content produces continuous crack propagation.

LLOYD AND MITCHELL (1984) use two theories to explain at micro-level the effect of toughening of particulate filled composites with low and with high filler content: crack front bowing and elastic discontinuity.

At low filler content the crack front bowing model is applied (LANGE AND RADFORD, 1971). From observed crack-front/particle interactions and the assumption that the crack-front possesses a line energy, LANGE AND RADFORD (1971) propose that during crack propagation, the crack-front is momentarily pinned by the filler particles, **Figure 2**. This leads to bowing out of the crack-front between the pinning positions, thus increasing the total length. In order to create an increase in crack front length, an increase in strain energy is required which in turn leads to an increase in the materials fracture energy. The fracture energy increases if the spacing between the particles decreases. As the interspacing further decreases, the stress fields from adjacent sections of bowing crack-front overlap, and reduce further energy requirements for propagation. The particle size, which separates the crack-front segments, influences the amount of bowing between the dispersion before the crack-front breaks away. Smaller particles are less effective as pinning positions as larger particles. The matrix strain imposed by the crack has to be accommodated elastically by the particles. If this is not possible particle fracture will take place before the critical (maximum) bowing configuration is reached. This toughening mechanism is effective in filled resins only when the particles are widely spaced. On the basis of filler content, fracture of the microfine filled composites alone may be controlled by this mechanism. Because small particles are less effective, composites containing microfine filler have low fracture energies. The fracture toughness is the square root of the product between the fracture energy and the elastic modulus, which implies that the increase in elastic

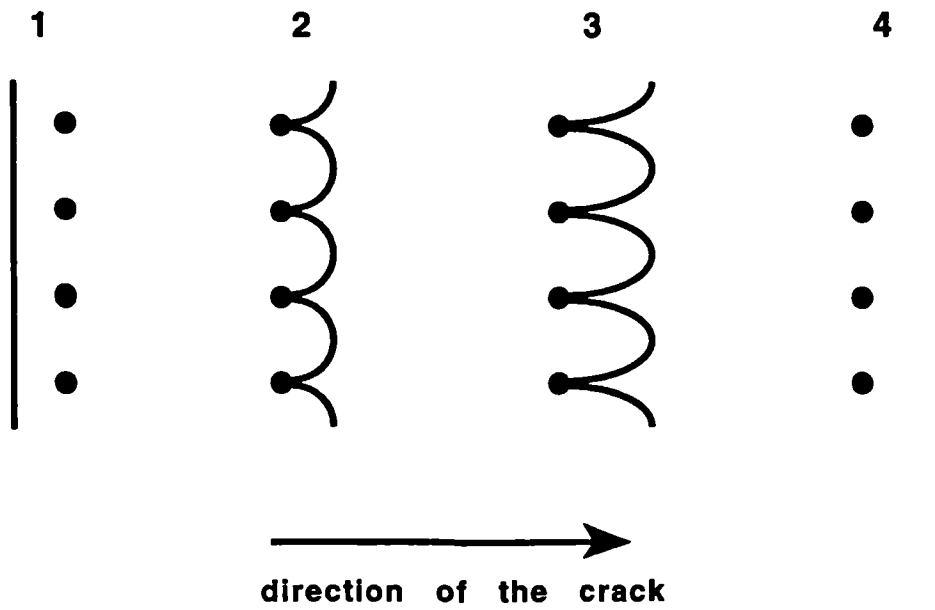


Figure 2. Schematic representation of crack pinning of the crack front by filler particles.

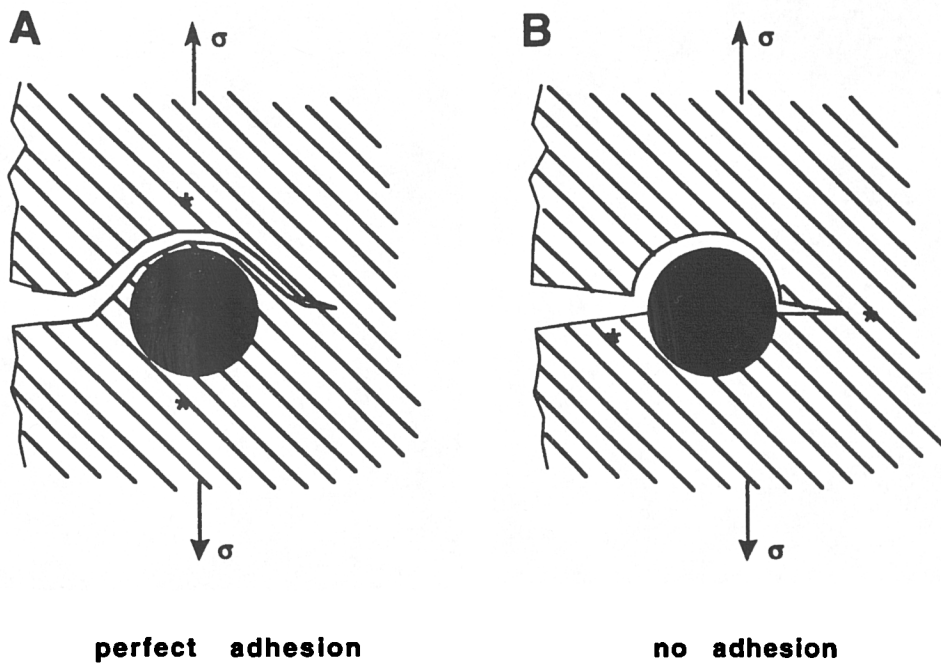


Figure 3. The fracture path through the composite for perfect filler-matrix adhesion and no adhesion. Tensile stress concentrations were located at the positions * when a tensile load σ is applied (LLOYD AND MITCHELL, 1984).

modulus, due to increasing filler content, is less than the decrease in fracture energy, and therefore fracture toughness levels off or begins to decrease.

In the case of heavily filled composites, LLOYD AND MITCHELL (1984) referred to BROUTMAN AND SAHU (1971), who developed a fracture theory based on the elastic inhomogeneity of composites. At the levels of filler contained in products with coarse particles the elastic inhomogeneity of the composite structure together with the degree of adhesion between filler and matrix determine the fracture path. The application of a tensile stress to a matrix containing a particle creates a stress concentration at the interface due to differences in elastic moduli. Two extremes exist for which the distribution of maximum tensile stress concentration are different: perfect adhesion and no adhesion. The two extremes produce two distinct fracture surfaces. When the adhesion is perfect, the crack propagates through the matrix (**Figure 3A**) whereas if the adhesion is lacking the crack propagates through the matrix and around the interface (**Figure 3B**) (LLOYD AND MITCHELL, 1984). Bonding with intermediate strength results in a fracture path which produces a mixture of these two features. Particle fracture is not precluded in this model, although its occurrence implies a lower fracture toughness than might be expected in case of no particle fracture.

These two fracture mechanisms may be able to explain the usually lower K_{Ic} -values for microfilled composites compared to fine particle and coarse particle composites, as is reported in several publications (GOLDMAN, 1985; PILLIAR *et al.*, 1986; FERRACANE *et al.*, 1987).

An additional effect can arise from an increased plastic deformation of the matrix, caused by local plastic deformation which effectively blunts the crack-tip. FERRACANE (1988) states that the phenomenon of crack blunting is prevalent in dental composites, and is most likely the mechanism by which K_{Ic} is increased over that of the neat resin. However, it seems to be more correct to consider the effect of crack blunting as an additional feature of the fracture mechanism.

DAVIS AND WATERS (1987) study the stick-slip crack propagation. They find a clear relation between the stress intensity factor and the yield behaviour for a particulate-filled composite. The yield stress represents a diffuse yielding which surrounds the crack-tip, and blunts it. As result of the blunting effect propagation of the crack requires more energy. The absence of a coupling agent, the presence of water and a low cross-head rate promotes plastic deformation of the matrix. Once the crack has propagated, *i.e.* overcomes the higher fracture resistance due to the blunting effect, the rate of release is greater than that required for a stable crack growth. The crack comes to rest once this excess energy has been used. If there is no significant blunting effect, then the crack propagates in a continuous stable manner. The close relationship between the yield stress and the stress intensity factor for crack initiation clearly shows that blunting of the crack tip has a part to play in increasing the stress intensity factor, particularly when stick-slip behaviour occurs. The relative contributions of crack pinning and crack blunting depends on the test conditions, the cross-head rate and the nature of the filler/matrix interface.

A strong adhesion between filler and matrix improves the strength of a composite. However, it has been reported by FERRACANE *et al.* (1987) that the fracture toughness is reduced if the adhesion is improved. Filler/matrix delamination is more apparent for large particles, implying that the stress concentration around these particles is greater than around the smaller particles. FERRACANE *et al.* (1987) suggest that filler/matrix delamination may be an effective means of crack blunting and toughening. Also LLOYD AND MITCHELL (1984) report that a strong interface reduces the fracture energy during impact loading, *i.e.* for high crack velocities. They argued that a weak bond promotes decohesion of particles at and around the crack-front. Hence the elastic modulus reduces locally, which in turn affects the fracture toughness. A strong interface inhibits this, causing the particles to fracture and thus reduces the fracture toughness. If the crack velocities are low (*e.g.* during fatigue) a strong bond is essential to raise the critical stress intensity because it hinders decohesion, which is favored under these conditions.

It seems that the fracture surfaces are difficult to interpret. It is not always possible to observe whether fracture occurred at the interface or through the matrix, PILLIAR *et al.* (1986). Sometimes opposite observations are reported. For example FERRACANE *et al.* (1987) find rougher surfaces for microfills and very coarse particle composites in comparison with smaller particle composites, whereas PILLIAR *et al.* (1986) observe more irregular fracture surfaces for conventional composites in relation to the microfilled composites. Differences between the fracture paths can also be produced by environmental influences. For P-30 LLOYD AND ADAMSON (1987) observe loss of adhesion between resin and filler, due to water attacking the zinc glass filler, which caused a change in the fracture path from matrix to interface. Noteworthy PILLIAR *et al.* (1987B) do not detect significant differences between the fracture appearance for the air-, water- or ethanol-aged materials, although a significant increase of the K_{Ic} -value is reported as a result of chemical softening in ethanol.

2.1.7 Conclusions

There are several fracture toughness parameters (K_{Ic} , G_{Ic} , J_{Ic}), that all have their own advantages and disadvantages. The K_{Ic} -factor can be considered as a material property that can be used to predict failure of a cracked body for different combinations of stress, flaw size and geometries. The advantage of the K_{Ic} -factor over the G_{Ic} -factor is that the elastic modulus need not to be defined separately. A point of attention is the requirement of plane strain condition at the crack-tip. Therefore a high quality pre-notch is very important.

Pre-notching by means of insertion of a scalpel blade is preferable rather than a machined pre-notch, because a higher quality of the notch-surfaces can be acquired and the surrounding material will not be disturbed. If the pre-notch is assessed carefully, pre-cracking is not necessary for dental composites because low toughness materials (like most dental composites) are less sensitive to the initial notch-radius.

The effect of the storage environment is significant. Therefore the physiological case has to be simulated. The test specimens have to be stored in water (addition of salt or sucrose failed to produce any significant alteration) at 37°C for at least 7 days (in order to facilitate the absorption of water). The test environment may also affect the test results. It can be recommended to perform the tests of water stored composites in water, while the test temperature in that case can be chosen in the range of 20-40°C without significant effect.

A quantitative comparison of fracture toughness results shows that the determined K_{Ic} -values of different investigators show a significant variation for the same material brand. For this reason the determination of the K_{Ic} -factor as an intrinsic material property seems to be unsuccessful as yet. The large variation might be attributed to the many factors which affect the material properties and the results of fracture toughness experiments: different batches, specimen production method, storage conditions and endurance, test conditions and the extent to which the plane strain conditions are fulfilled. It also seems that different specimen types yield different K_{Ic} -values. In order to eliminate most of these effects standardization of the test procedures is most urgent. Only then this factor can be used as a material property for dental composites, as in general engineering where the K_{Ic} -factor has proved to be a very useful material property. Due to non-standardized experiments, the present fracture toughness data are very difficult to use by other investigators, even in a qualitative way.

The K_{Ic} -value generally increases if the filler content increases. The fracture behaviour was explained by the processes of crack pinning (LLOYD AND MITCHELL, 1984), the distribution of stress concentration at the filler/matrix interface due to elastic inhomogeneity, crack tip blunting and strength of the filler/matrix bonding. At low filler content (*e.g.* microfilled composites) the crack pinning effect prevails. For high filler content, when the interparticle spacing is too small for effective crack pinning, the fracture path is controlled by the distribution of stress concentrations due to elastic inhomogeneity of the filler/matrix mixture. A strong interface reduces the fracture resistance during

impact loading, whereas it raises the fracture toughness at low crack velocities, e.g. during fatigue. The interaction of the many micro structural factors is extremely complex. Therefore it seems impossible yet to trace back particular mechanical behaviour to a given micro structure.

2.2 Fatigue in dental composites

2.2.1 Introduction

This section is an overview of published fatigue experiments for dental restorative composites. Clinical life-time of composite restorations is still disappointing in spite of sufficient wear resistance *in vitro*. There is increasing evidence that fatigue is playing an important role in such failures. A restoration is subjected to varying external and semi-permanent internal forces. Fatigue crack growth is a result of the external cyclic mechanical forces, while the internal residual loads elevate the total stress level even further.

Several fatigue experiments are carried out to study the fatigue properties of various types of commercially available composite restorative materials. It seems that there are as many test specimens and test methods as there are publications about fatigue experiments. This section is a review on these various fatigue experiments.

2.2.2 Fatigue test specimens

For dental resin composites generally three test methods are used. These are assumed to represent three types of failure:

1. Volume failure (*i.e.* failure in the material) due to shear stresses (axial compressed cylinder) (DRAUGHN, 1979, 1981, 1985; HAHNEL *et al.*, 1986; MCCABE AND OGDEN, 1987)
 2. Volume failure due to tensile stresses (diametral compressed cylinder) (HAHNEL *et al.*, 1986)
-

3. Surface failure due to tensile stresses (bending specimen) (ASMUSSEN AND JØRGENSEN, 1982; HAHNEL *et al.*, 1986; BRAEM *et al.*, 1988)

Due to the difference in type of failure the results of fatigue experiments for various specimens can not be compared straightforwardly.

HAHNEL *et al.* (1986) compared three different test specimens. The axial compressed cylinder specimen showed an about three times higher fatigue strength compared to the 3-point bending specimen. The latter showed an about two times higher fatigue strength relative to the diametral compressed cylinder. Due to the much higher cyclic loading, internal heating can be expected to play a greater role for the axial compressed specimen. This character makes the axial compressed specimen less suitable for fatigue testing of visco-elastic material. HAHNEL *et al.* (1986) preferred the 3-point bending specimen because it showed the least scatter in fatigue results.

It is advised (LAMBRECHTS, 1983) for the axial compressed cylinder, to use a length/diameter ratio of approximately 2 to avoid a more complicated stress distribution due to the overlapping of the cone formations at both ends of the cylinder. Especially for this type of specimen it is necessary to adopt standard sizes and dimensions to obtain reproducible test results.

The location of cracking can also affect the fatigue results. Different (location dependent) stress situations result in different failure mechanisms. For this reason a bending specimen which is clamped at one end (used by ASMUSSEN AND JØRGENSEN (1982)) may be unwise. The crack can be expected near the clamping, where the situation is extremely complex because of the stress distribution and wear (fretting). Also a bending specimen which is supported at both ends and loaded midside by two opposite load application rollers (used by BRAEM *et al.* (1988)) can be treacherous, because the load application (which represents a complex stress distribution) and the expected crack initiation are located at the same position.

2.2.3 Load function

The function of a simulated chewing load has various parameters:

- a. Sign of the applied load (compression, tension, or both)
 - b. R-value
 - c. Load amplitude
 - d. Load-time curve
 - e. Frequency
- a. *Sign of the applied load* — The sign of the applied load can be kept constant, negative (compression), or varied from negative to positive (compression to tension). The results for the bending specimens of *e.g.* HAHNEL *et al.* (1986), and BRAEM *et al.* (1988) will be different because the stresses of the latter specimen are cycled between compressive and tensile stresses, while the sign of the first will not change (it is kept negative, in compression).
- b. *R-value* — Different R-values ($R = S_{\min}/S_{\max}$, the applied definition of S_{\min} and S_{\max} is given in **Figure 4**) will yield different fatigue results. Sometimes a compressive ground loading is achieved to avoid instability of the specimen attachment when the specimen is loaded in compression ($R > 0$). For dental resin composites the influence of the ground loading is negligible (HAHNEL *et al.*, 1986).
- c. *Load amplitude* — Generally load control mode is used, maintaining a constant load amplitude. If an experiment is performed in displacement (or stroke) control mode (ASMUSSEN AND JØRGENSEN, 1982), in which the maximum deflection (displacement) is kept constant, the applied load will decrease during the fatigue test caused by decreasing stiffness due to fatigue cracking. The results of these two control modes represent very different fatigue information. The decrease of loading during the fatigue testing (displacement control mode) is unlikely to be comparable to what happens *in vivo*.
-

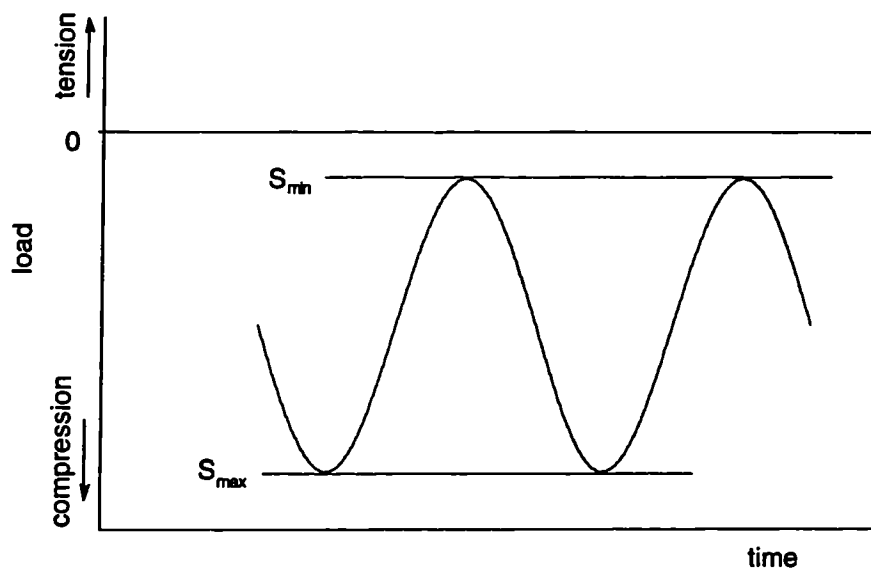


Figure 4. Definition of S_{max} , S_{min} , and hence for $R = S_{min}/S_{max}$.

d. *Load-time curve* — There are three types of load-time figures used:

1. Simulated chewing curve
2. Triangular curve
3. Sinusoidal curve

The influence of these three types of loading is investigated by SOLTÉSZ *et al.* (1985) and HAHNEL *et al.* (1986). It is concluded that if the frequency is kept lower than 10 Hz there are no significant differences in fatigue results.

e. *Frequency* — In order to decrease the testing time, the frequency during fatigue experiments is increased (the *in vivo* frequency is about 2 Hz). The maximum frequency, however, is limited because of the time-dependent material behaviour of the matrix. High frequencies may introduce an extra increase in temperature due to internal damping. Up to 5 Hz the frequency dependency of the fatigue properties is reportedly insignificant (dry or wet environment and temperatures of 22°C or 37°C respectively) (HAHNEL *et al.*, 1986).

A constant amplitude of the strain rate, as applied by MCCABE AND OGDEN (1987), produces a variation in frequency, depending on the load and the modulus of the test material. This is done to avoid a variation in strain rate from one material to another, partly due to visco-elastic nature of the resin matrix. However, this procedure will result in a decrease of frequency during fatigue testing, which is unlikely to mimic the *in vivo* load envelope.

2.2.4 Test methodology

The estimated number of chewing cycles in the oral environment is about $10^6 - 3 \times 10^6$ a year. DRAUGHN (1979, 1981) defined his fatigue limit at 5×10^3 cycles. Besides of the improper use of the term (the definition for fatigue limit is the largest cyclic load level which is still incapable to produce fatigue crack initiation), this maximum number of cycles with respect to the number in service is too short to draw usable conclusions about the fatigue properties.

Although still small with respect to the clinical situation, test cycles $\sim 10^6$ are more realistic and yield more usable results.

Dental composite restorative materials may not show a well defined fatigue limit because of the corrosive effects and chemical disintegration during fatigue life. Moreover, it is known for other materials with high polymer content that they do not show a fatigue limit (HÄHNEL *et al.*, 1986).

Two methods are employed to define the stress-cycles curve: the Wöhler method (HÄHNEL *et al.*, 1986) and the staircase or up-and-down method (DRAUGHN, 1979; MCCABE AND OGDEN, 1987). For the Wöhler method levels of the load amplitude are chosen and for each level the average of the number of cycles until failure is determined. In case of the staircase method the maximum cycling time is chosen and then the load amplitude is determined for which the specimens have a probability of 0.5 to survive this period. The results of these two approaches are different. It is suggested (DRAUGHN, 1979) that the staircase method requires less specimens (~ 15 specimens for an accurate staircase analysis) than the Wöhler approach. The use of the staircase method is useful for materials which do not show a clear relationship between fatigue life and stress (MCCABE *et al.*, 1990). For those materials fatigue behaviour is primarily dependent on the quality of the specimen.

2.2.5 Test environment

The storage time and environment of the specimens has significant influence on the mechanical properties of dental composite resins. For K_{Ic} -experiments it is advised to store the specimens for at least one week in water at 37°C before testing (paragraph 2.1.5). This may be a good advice for fatigue specimens too in order to stabilize the mechanical properties before testing.

An obvious decrease in fatigue strength is found for increasing test temperatures (DRAUGHN, 1985; HÄHNEL *et al.*, 1986). It is suggested that the environmental influence is due to the temperature only. Because no corrosive effects or chemical disintegrations are observed, it is stated that the fracture

mechanism is the same for dry and wet fatigue testing. However, the maximum testing time is no longer than 8 days. *In vivo*, when it takes much longer to reach a certain number of load cycles, the environment may still affect the fracture mechanism.

Test results of HAHNEL *et al.* (1986) point out that it is not necessary to adopt the *in vitro* test conditions very close to the physiological case if the testing time is short with respect to clinical life-time.

2.2.6 Effects of micro structure

The micro structure of a composite restorative material can be described for this occasion by:

- a. Material properties of matrix and filler material
 - b. Filler particle size and shape
 - c. Filler fraction and distribution
- a. *Material properties of matrix and filler material* — Material properties like degree of cure, porosity, visco-elasticity and elastic modulus affect the fatigue behaviour of dental composite materials. A low degree of polymerization or porosity reduces fatigue strength (MCCABE AND OGDEN, 1987). Pores are sources of stress concentrations. Stress raising effects can also be expected for void inclusions.

Visco-elastic material behaviour of the matrix material can cause internal heating of a specimen during fatigue testing, due to internal damping. A higher matrix content results in more internal heating. Significant internal heating is unlikely to happen *in vivo*, because of the low frequencies (≤ 2 Hz) and the many time-delays between the load cycles. To avoid internal heating during fatigue testing it is suggested (HAHNEL *et al.*, 1986) to keep the frequency low (≤ 5 Hz).

Higher fatigue strength is found for glass/silicate filled materials compared to quartz filled materials (DRAUGHN, 1981). This suggests that the fatigue properties are better if the elastic modulus mismatch between the matrix and filler material is lower.

- b. *Filler particle size and shape* — The highest fatigue strength is found for small rounded filler particles, the lowest for large sharp filler particles, and intermediate fatigue strength for intermediate sizes and sharpnesses (DRAUGHN, 1981). The particles act as stress raisers. Stress concentrations are likely at the particle-matrix interface because of the elastic modulus mismatch, or the filler particle in the matrix material acts, more or less, as an internal flaw if the bonding between the filler particles and matrix is poor. In case of a large and sharp particle, the stress concentration will be more severe. For small and rounded particles the stress concentrations will be relatively moderate.
- c. *Filler fraction and distribution* — The filler fraction and distribution will influence the fatigue behaviour. Volume fraction of the particles is found to have a significant effect on the fatigue life (DRAUGHN, 1981). High volume fractions of filler particles reduced the fatigue strength. This may be explained by the existence of many micro cracks (*i.e.* particles), which will accelerate the fatigue weakening of the specimen and therefore lower the fatigue strength.

The type of the failure process depends on the magnitude of the cyclic stress. Fractographic observations (MONTES-G AND DRAUGHN, 1987) show that: (a) at *high* crack velocities the failure mode was dominated by the properties of the filler and matrix material and (b) at *low* crack velocities the strength and stability of the filler-matrix interface was the controlling factor. Environmental conditions are found to be critical factors in low stress fatigue testing (MONTES-G AND DRAUGHN, 1987). For sub-critical stress intensity factors crack velocities are much higher for materials exposed to water.

2.2.7 Conclusions

The published results of fatigue experiments for various specimens or specimens representing different sizes or dimensions cannot be compared simply. In order to get comparable test results it is necessary to adopt standard specimen sizes and dimensions and standard test procedures.

Bending specimens reportedly yield the most reproducible results, and are therefore preferable. Fatigue testing should be done under load control mode, while at least up to 10^6 cycles have to be considered in order to get meaningful fatigue properties. If the frequency is kept ≈ 5 Hz, a sinusoidal load-time curve is appropriate and internal heating is avoided. It is not necessary to adopt the environmental test conditions very close to the *in vivo* case.

2.3 Discussion

As is mentioned earlier, fracture toughness and fatigue characterize critical and sub critical stress intensity crack behaviour. Together with wear (both phenomena have been associated with the erosion of composite restorations) mechanical lifetime of dental composite restorations is mostly covered by these failure processes. However, the material fracture parameters are typically determined *in vitro*, leaving the question about how they relate *in vivo*. Soderholm (in: ANUSAVICE AND DE RIJK, 1990) emphasized the limited value of the prediction of clinical success from *in vitro* experiments, because the material handling of the dentist has a significant effect on the material properties.

The fracture toughness has been related to *in vitro* wear resistance of restorative materials (ROBERTS *et al.*, 1977, 1978; PILLIAR *et al.*, 1987B; DEVRIES *et al.*, 1981). It is also suggested that inadequate fracture resistance or fracture toughness is related to clinical phenomena as the incidence of chip fractures (LAMBRECHTS *et al.*, 1982) and the relatively low wear resistance of conventional dental composites (LEINFELDER, 1981). Clinical observations of *in*

in vivo catastrophic fracture of composite restorations are rare and the common mode of failure is a gradual loss of substance over an extended period of time. It is apparent that the stresses to which these restorations are subjected are generally below those which cause rapid failure and the failure process must involve slow property deterioration and slow crack propagation. The use of fracture toughness as a predictor of *in vivo* wear resistance of dental composites has been suggested (TRUONG AND TYAS, 1988; TYAS, 1990) but the relationship between fracture toughness and wear appears as-yet-undetermined (ROSENFELD, 1981).

The suggested link between the K_{Ic} fracture toughness factor and wear may be questioned. Wear is a gradual surface damage process, while the K_{Ic} is a characteristic plane strain material property, describing catastrophic rupture. Firstly the stress condition at the surface is plane stress. Secondly the definition of the stress intensity factor is derived under assumption of an elastic material behaviour. If the plastic zone size at the crack tip is small in relation to the crack length, the mechanical behaviour at the crack tip may be considered elastic. This proposition seems invalid for wear damage. Thirdly, environmental effects are likely to play a much more significant role in wear damage propagation process because of the different time-scale and pumping action of the repetitive wear contact loads.

Although it is not clear yet how the fracture toughness behaviour *in vitro* corresponds with the *in vivo* situation, the fracture toughness is very useful in several approaches. One application is materials ranking, where new materials can be compared with existing. A very powerful use would also be the application of the fracture toughness factor in an integral material performance theory, as is proposed among others by TRUONG AND TYAS (1988). If the link with clinical behaviour is known, this factor may be used for design of restorations and requirements for materials.

Mechanical fatigue is a complex process. Up to this moment only the fatigue behaviour under constant amplitude loading is investigated for composite resins. *In vivo*, however, the amplitude of the fatigue loading varies. The

fatigue behaviour under variable amplitude loading might be very different due to interaction of peak loads. A next step in fatigue testing should therefore be variable amplitude load application. In order to enable the simulation of the distribution and magnitude of a clinical fatigue loading in experiments, the *in vivo* load spectrum has to be known. A carefully determined and well documented sequence of load levels can be applied in order to resolve the influence of peak loads and load sequences. This information brings lifetime estimation under actual fatigue loading a step closer.

Constant amplitude experiments can still offer most valuable information about sub critical crack propagation properties. This information can be used for materials ranking. It can also be used for crack propagation relations, based on the law introduced by Paris, in which the fatigue crack growth rate is a function of the stress intensity factor. Furthermore, the constant amplitude fatigue data is used for integrated theories of wear processes (TRUONG AND TYAS, 1988). Fatigue is a long term degradation process, and therefore very susceptible to environmental influences. Other than wear, which is a long term contact problem, fatigue is controlled by stresses in the material. These stresses consist not only of the external applied mandibular forces, but are also elevated by residual shrinkage stresses, which are significant considering reported enamel and restoration fractures (ROBERTS *et al.*, 1977; LAMBRECHTS *et al.*, 1985; EICK AND WELCH, 1986; LAI AND JOHNSON, 1993).

The failure condition, in fatigue as well as in the catastrophic rupture, depends on the overall stress state. The stress state is not only determined by external forces, but also by the residual stresses, which are mainly due to polymerization shrinkage and thermal expansion. These internal stresses can elevate the total stress state in the tooth-restoration complex significantly, and therefore may cause fracture or fatigue crack propagation at lower external load levels. Obviously failure assessment in a tooth-composite system requires knowledge of the pre stressed state of the complex, and it is therefore essential to determine the development of residual polymerization stresses.

Since cracks are initiated at stress concentrations, it is also important to know the stress distribution in a tooth-restoration structure. Finite element analysis is a useful tool to assess the stress distribution in these complex-shaped structures. Dental restorative composites exhibit a strong strength differential effect, because the strength in compression is much higher than their tensile strength. This effect should be taken into account when the stress concentration locations are calculated. Therefore a proper failure criterion is also essential.

3 Yield dominated failure

The mechanical integrity of a structure depends on the resulting stress state in the structure due to a loading condition, and the strength of the materials involved. When a structure is loaded (mechanical, external or internal, shrinkage or temperature) the structure deforms. This results in stress distribution through the structure, depending on geometry and material properties. The ability of a structure to sustain the load depends on the strength of the materials of which it is made. Solid materials show elastic and/or plastic deformation when loaded. If the stress exceeds a certain stress level at a certain location, the material will fail.

This mechanical failure of a structure is generally examined by two types of criteria: failure criteria and fracture criteria (NADAI, 1950). A failure criterion describes the ultimate strength behaviour of a continuous material, while a fracture criterion describes the discontinuity of crack extension behaviour. Therefore the difference between both is that for a fracture criterion a crack must prevail. A failure criterion is a general expression for the amount of stress a material can bear. A fracture criterion is structure dependent, *i.e.* this criterion depends on the geometry of the structure. Furthermore, a fracture criterion is controlled by stress intensities, which are singular stress fields existing at crack tips (EWALDS AND WANHILL, 1985). A failure criterion is a material property (VON MISES, 1928). A failure criterion is more appropriate for the examination of uncracked structures, and is of interest at stress concentration locations in a structure (where crack initiation takes place). A failure criterion is especially useful as a design parameter. This failure property plays also a role in the crack resistance of fracture criteria, but due to the singularity at a crack tip it is hard to assess analytically. Therefore fracture criteria are usually expressed in other terms, like stress intensity factors or crack resistance as a material property (EWALDS AND WANHILL, 1985), and are empirically adjusted such that the material failure strength is integrated in the fracture formulation.

Sometimes instead of failure criteria yield criteria are used. These criteria determine the yield point. This makes sense for a lot of engineering materials, such as metals, for which the onset of plastic deformation usually is considered as the ultimate strength limit. For the brittle dental composite materials, however, macroscopic plasticity is hardly observable before catastrophic failure. Therefore in this study the criterion will be referred to as a failure criterion.

A suitable failure criterion is important for the examination of the durability of a structure. At the present stage of computerized stress analysis, the use of an inadequate material model is one of the limiting factors. Failure is the final and most catastrophic incident of a structure. In order to prevent such unfortunate events, usually a safety factor is added to the theoretical strength of a material to anticipate for imperfections in the material like small flaws and damage which always exist and weaken a material (GERE AND TIMOSHENKO, 1990).

The strength of an uncracked structure is limited by the strength of the materials it is made of. The strength limits are exceeded first at points where the stress is concentrated. The existence of those elevated stress locations depend on the geometry of the structure. These stress concentration points are typically located in shape transitions, thickness transitions, and material transitions. Using a failure criterion enables the investigator to check the stress state at those points in order to determine if the material strength limit is exceeded when a certain load is applied. An in essentially similar exercise, is the definition of equivalent stresses. In this approach the applied load can be chosen arbitrary, if it is only used to obtain a stress distribution in the structure. The stresses are expressed in terms of a failure criterion, and yield therefore a direct indication of the locations of troublesome stress concentrations and the significance relative to each other. The equivalent stress integrates all the components of the stresses in each point into only one, axis-orientation independent, scalar expression. Knowledge of the exact strength limit is not required for this approach, only the general shape or form of the failure criterion. Especially for dental restorative composites, where the exact

strength limits for the same material are hardly consistent from batch to batch, this equivalent stress approach is very useful.

The determination of material strength is usually obtained by uniaxial load experiments. For example, diametric tension, axial compression and tension, and three or four-point bending experiments. Besides of the question if the axial compression strength test yields the pretended uniaxial compressive strength, these tests are supposed to determine a material property in one direction. In other words, the stress fields are generally uniaxial. In most applications, however, stress fields are seldom uniaxial. Especially in complicated geometries such as dental structures, the stress fields are generally multiaxial. This means that stresses exists in more than one direction and magnitude. Whereas the stresses in uniaxial stress fields can be treated as scalar type parameters, in multiaxial stress fields the stresses (and strains) are vector type parameters. For uniaxial stress states, a failure criterion is represented by two points, a limit in tension and a limit in compression. For a biaxial stress state the failure criterion can be displayed by a curve in a 2-dimensional plane. And a three-dimensional stress state is described by a surface, the failure surface. The uniaxial and biaxial stress states are special cases of the general three-dimensional stress state. In case of the uniaxial stress state the two (tension and compression) strength limit values are the intersections of the one-dimensional line of the uniaxial stress state and the failure surface. In case of the biaxial stress state the limiting curve is the intersection of the two-dimensional plane with the three-dimensional failure surface.

A stress state is defined with reference to a coordinate-system with components. It is possible to deduce the appropriate components for the stress state in terms of any other coordinate-system. Because the values of the stress components depend on the coordinate-system used to describe the stress state at a point there is a range of possible values. The failure phenomenon however which is governed by the stress state, is not a function of the components defined with respect to some arbitrary coordinate-system (NADAI, 1950; WILLIAMS, 1973). Such phenomenon must be described in terms of functions of the stress

components which are independent of the coordinate system used. These functions must therefore be invariant with respect to the coordinate-system. The functions are the invariants (I_1 , I_2 and I_3) of the stress system at a point. A failure criterion must be a function of these (three) invariants.

In this particular case the investigated material is dental restorative composite. This composite consists of a polymeric matrix (heavily) filled with particulate fillers (glass, quarts). The fillers are randomly distributed. The dimensions of the fillers are such ($< 0.1 \mu\text{m}$), that on macro scale the composite can be considered as a homogeneous isotropic material. Macro scale is defined as the scale of the structures these composites are used for, *i.e.* the size of dental restorations. Homogeneous properties means that the consistence of the material is constant. Isotropic properties means that the material has the same properties in all directions. Considering these assumptions, a general conclusion can be made concerning the shape of the failure criterion. Because of the isotropy assumption the failure surface must be a symmetrical function of all three principal stresses. The principal stresses (σ_1 , σ_2 and σ_3) are the limiting values of the normal stress components (WILLIAMS, 1973). The invariants (which are symmetrical functions of the principal stresses) can be expressed in terms of the principal stresses (WILLIAMS, 1973). Therefore, a failure criterion can be written as:

$$f(I_1, I_2, I_3, \text{Material Properties}) = 0.$$

where: $I_1 = \sigma_1 + \sigma_2 + \sigma_3$

$$I_2 = \sigma_1\sigma_2 + \sigma_2\sigma_3 + \sigma_3\sigma_1$$

$$I_3 = \sigma_1\sigma_2\sigma_3$$

For phenomena which take place at constant volume, the stresses are usually analyzed in terms of deviatoric stresses (WILLIAMS, 1973). The deviatoric stresses are the difference between the actual stress system and the mean or hydrostatic stress. A failure criterion can be expressed in terms of the hydrostatic stress and the deviatoric stress invariants, J_1 , J_2 , J_3 :

$$f(I_1, J_2, J_3, \text{Material Properties}) = 0.$$

where:

$$J_1 = 0$$

$$J_2 = \frac{1}{6} [(\sigma_1 - \sigma_2)^2 + (\sigma_2 - \sigma_3)^2 + (\sigma_3 - \sigma_1)^2]$$

$$J_3 = \frac{1}{3} (\sigma_1^3 + \sigma_2^3 + \sigma_3^3)$$

deviatoric stress tensor s_{ij} :

$$s_{ij} = \sigma_{ij} - \frac{1}{3} \delta_{ij} \sigma_{kk}$$

where: σ_{ij} is the stress tensor

$$\sigma_{kk} = \frac{1}{3} (\sigma_1 + \sigma_2 + \sigma_3) \text{ is the mean stress}$$

$$\delta_{ij} = \begin{matrix} 1 & \text{if} & i=j \\ 0 & \text{if} & i \neq j \end{matrix}$$

The mathematical parameters for an isotropic failure criterion are now established. Failure criteria in many forms and combinations are derived in these mathematical parameters. They can be expressed in the cartesian coordinate system of the principal stresses $f(\sigma_1, \sigma_2, \sigma_3, \text{Material Parameters})=0$ or in the Haigh-Westergaard cylindrical coordinate system $f(h, r, \cos 3\theta, \text{Material Parameters})=0$, related to the cartesian coordinate system by the following equations: $h=I_1/\sqrt{3}$, $r=\sqrt{2J_2}$, and $\cos 3\theta=J_3/3/2 \sqrt{3} J_3/J_2^{3/2}$. The influence of the three invariants is reflected in the shape of the failure surface. The first invariant of the stress tensor (I_1) represents the dependency on the hydrostatic stress. The second invariant of the deviatoric stress tensor (J_2) results in a axisymmetric volumetric shape along the hydrostatic axis, while the third invariant of the deviatoric stress tensor (J_3) results in curved meridians, for example **Figure 7** (Gudehus criterion for $\sigma_c/\sigma_t = 2$ in a deviatoric plane, where σ_c is the ultimate strength in compression and σ_t the ultimate strength in tension).

A brief overview and some examples of failure theories will be given hereafter.

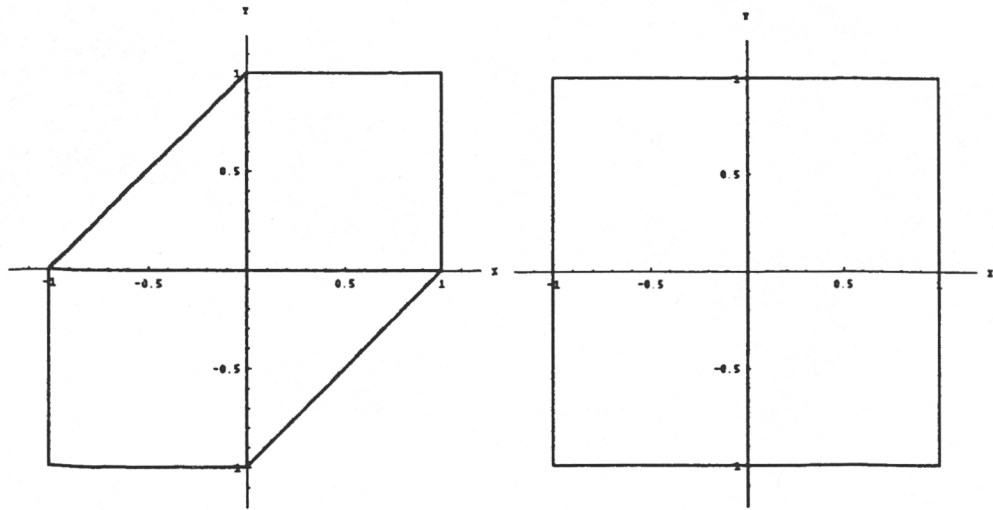


Figure 5. Maximum shear (Tresca) and maximum stress criteria (plane stress, $|\sigma_{\text{failure}}|=1$)

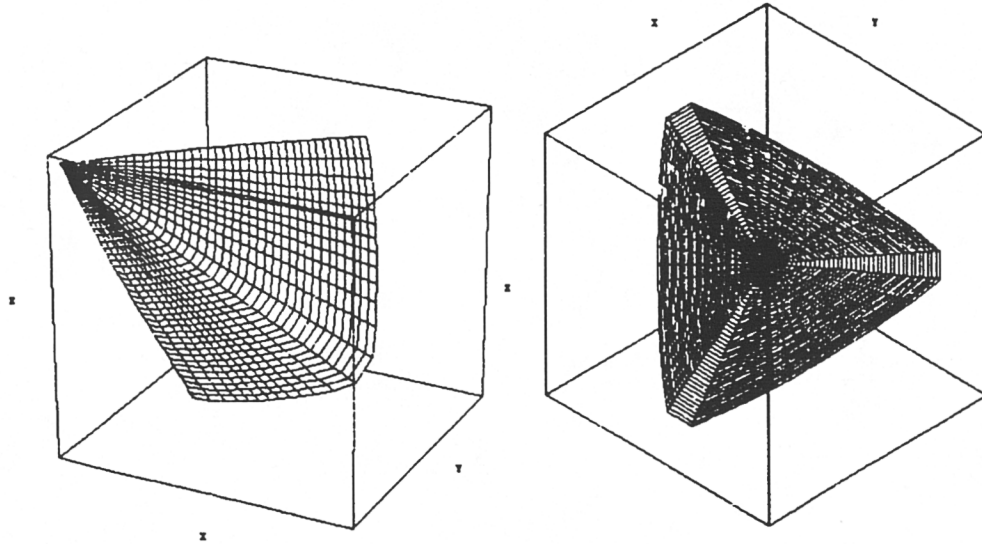


Figure 6. Ottosen failure surface for $\sigma_c/\sigma_t = 10$, side and top view.

In 1776 Coulomb expressed the view that fracture of a solid would occur if the maximum shear strain at some point surpassed a critical value characterizing the mechanical strength of the material (IRWIN, 1958). Since then a number of failure theories have been introduced (NADAI, 1950). Out of these approaches, numerous expressions for failure criteria are developed, several of them claiming to be the general expression to which all other formulations fit. Others are more specifically fitted to the experimental available data for one specific type of material. The most simple expressions are the maximum shear (Tresca) and the maximum stress theories. These criteria were generally used in engineering, where the maximum shear is recommended for ductile materials, while for brittle materials the maximum stress is often used (MARIN, 1957). These two criteria are quite crude and too inaccurate in view of the modern state in computational stress analysis. In the maximum shear criterion the intermediate principal stress plays no role, which is generally thought to be incorrect (MILLS AND ZIMMERMAN, 1970). In the maximum stress criterion only the maximum principal stress is considered. In **Figure 5** the angular shapes of both criteria are shown for plane stress ($\sigma_3=0$).

Angular shapes represent singular points, which is physically unlikely. However, there is not a general consensus for the ultimate shape of a general failure criterion. There is little discussion about the proper form of a failure criterion for isotropic ductile materials like metals, which show almost no differential effect for strength in tension and compression. The generally used criterion in that field is the well-known Von Mises yield criterion, sometimes called Huber-Mises-Hencky criterion. This criterion is based on the theory of constant elastic strain energy of distortion (Huber, Hencky) or the constant octahedral shearing stress. In 1925 Von Mises already-acknowledged the effect of the first invariant of the stress tensor in his yield expression, which dates back to 1913. He suggested that the yield criterion also had to be some ("*schwach veränderliche*") function of $(\sigma_x + \sigma_y + \sigma_z)/3$ (VON MISES, 1928). However, at the same time Schleicher independently worked this idea out further (SCHLEICHER, 1925). In 1967 Stassi-D'Alia presented a modified Von Mises criterion (STASSI-D'ALIA, 1967), which is occasionally referred to as the

Schleicher-Stassi criterion, and was claimed to be the general failure criterion for all types of materials. This modified Von Mises criterion takes into account the strength differential effect (this is not equivalent to the Bauschinger effect, which is a result of work-hardening or strain-hardening), and means that the strength in simple (*i.e.* uniaxial) tension and compression are not equal. Other names in connection with this modification of the Von Mises criterion are MELDAHL (1944) and TSCHOEGL (1971). In the fields of soil mechanics DRÜCKER AND PRAGER (1952) proposed a yield function which is a proper generalization of the Mohr-Coulomb hypothesis ($|\tau_{\max}| = c \cos\phi - (\sigma_x + \sigma_y)/2 \sin\phi$, which will not be discussed here; see NADAI, 1950; or for a simple description MODÉER, 1979). Arguing that the octahedral shearing stress is a function of the mean normal stress (hydrostatic stress), Nadai came to a same expression as Drücker and Prager (NADAI, 1950). This criterion is sometimes referred to as the Nadai-Bauwens-Sternstein criterion (THEOCARIS, 1986). It seems that the name used for a failure criterion depends on the field it is used in. In the fields dealing with soil and concrete mechanics, where the Coulomb-Mohr theory was dominant, the common name is Drücker-Prager criterion. Whereas if this criterion is used in other fields, especially where ductile materials are involved, other names are used. Probably this can be explained by the different backgrounds, which nevertheless resulted in the same failure expression.

Besides these two main approaches, there are numerous other expressions for a failure criterion established, usually based on extensive curve fitting. In the field of brittle materials with inherent strength differential effect the discussions and opinions about the proper shape are confusing. The fields involved here are mainly the polymers (RAGHAVA *et al.*, 1973), concrete (NEWMAN, 1965; MILLS AND ZIMMERMAN, 1970; NEWMAN AND NEWMAN, 1971; OTTOSEN, 1977; LADE, 1982), rock (JAEGER, 1967; SHEORY *et al.*, 1989) and soil (DRÜCKER AND PRAGER, 1952; GREEN AND BISHOP, 1969; GUDEHUS, 1973) mechanics. Dental composite materials also belong among them. Excellent reviews on isotropic failure criteria and theories can be found in NADAI(1950), MARIN (1957), JAEGER (1967, rocks) and NEWMAN (1965, concrete). Some

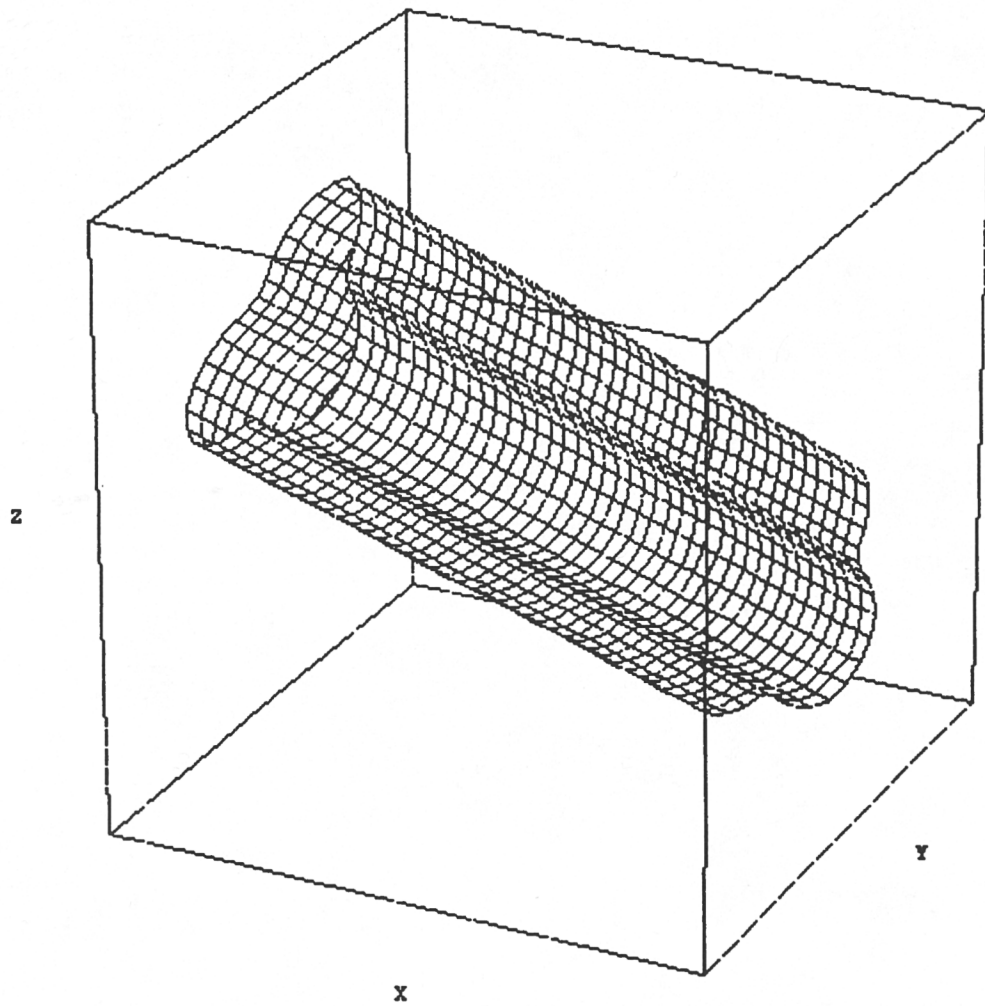


Figure 7. Gudehus failure surface for $\sigma_c/\sigma_t = \frac{1}{2}\sqrt{3}$ ($r_0=2$, the failure surface will be convex if $r_0>4$).

anisotropic failure criteria can be found in HILL (1948), MARIN (1957), TSAI AND WU (1971), WU (1974) and, THEOCARIS AND PHILIPPIDIS (1987).

To demonstrate the appearance of some failure formulations, some examples are shown below.

- a. *Ottosen* — The failure criterion for concrete from OTTOSEN (1977) (**Figure 6**), which contains all three invariants:

$$f_{\text{Ottosen}}(I_1, J_2, J_3, \text{Mat Param}) = A \frac{J_2}{\sigma_c^2} + \lambda \frac{\sqrt{J_2}}{\sigma_c} + B \frac{I_1}{\sigma_c} - 1 = 0$$

where: $\lambda = \lambda(\cos\theta) = \lambda(J) > 0$

$$J = \frac{3\sqrt{3}}{2} \frac{J_2}{J_2^{3/2}}$$

$$\lambda = K_1 \cos\left[\frac{1}{3} \arccos(K_2 \cos 3\theta)\right] \quad \text{for} \quad \cos 3\theta \geq 0$$

$$\lambda = K_1 \cos\left[\frac{\pi}{3} - \frac{1}{3} \arccos(-K_2 \cos 3\theta)\right] \quad \text{for} \quad \cos 3\theta \leq 0$$

σ_c is the uniaxial compressive strength

The characteristics of the failure surface are given by four parameters (A, B, K_1 and K_2).

- b. *Gudehus* — GUDEHUS (1973) criterion (**Figure 7**) is a function of J_2 and J_3 :

$$f_{\text{Gudehus}}(J_2, J_3, \text{Mat Param}) = r_0 - J - 2 J_2$$

where: $J = \frac{3\sqrt{3}}{2} \frac{J_2}{J_2^{3/2}}$

$$\frac{\sigma_t}{\sigma_c} = 2 \sqrt{\frac{-3 + 3r_0}{3 + 3r_0}}$$

σ_t is the uniaxial tensile strength

σ_c is the uniaxial compressive strength

- c. *Lade* — Lade's failure criterion for concrete consists of only three parameters (LADE, 1982), and is only a function of the first and the third invariant (I_1 and I_3):

$$f_{\text{Lade}}(I_1, I_3, \text{Mat Param}) = \left\{ \frac{I_1^3}{I_3} - 27 \right\} \left\{ \frac{I_1}{p_a} \right\}^m = \eta_1$$

where: p_a is the atmospheric pressure

- d. *Guennouni* — Guennouni proposed a two-dimensional yield criterion of heterogeneous materials with rigid-plastic constituents (GUENNOUNI, 1987), expressed with two invariants, by means of a homogenization technique:

$$f_{\text{Guennouni}}(I_1, J_2, \text{Mat Param}) = \left(\frac{I_1}{A} \right)^2 + \left(\frac{J_2}{B} \right)^2 - F^2 - 1$$

where: $A = -\log f(1 - 1.92 f + 5.57 f^2 - 6.04 f^3)$

$$B = \sqrt{3} (1 - 1.33 f^{0.6}) \quad \text{if} \quad f \leq 0.1236$$

$$2.06 e^{-4.9 f} - 4.4 \cdot 10^{-2} \quad \text{if} \quad f > 0.1236$$

- e. *Drücker-Prager* — The Drücker-Prager criterion (Figure 8) is a function of I_1 and J_2 :

$$f_{\text{Drücker-Prager}}(I_1, J_2, \text{Mat Param}) = A I_1 + B \sqrt{J_2} - C = 0$$

- f. *Von Mises* — The well-known Von Mises criterion (Figure 9) is a function of only the second deviatoric stress tensor J_2 :

$$f_{\text{Von Mises}}(J_2, \text{Mat Param}) = J_2 - A = 0$$

For anisotropic materials, this relation can be modified (MARIN, 1957) to:

$$2\sigma^2 = [a(\sigma_1 - \sigma_2)]^2 + [b(\sigma_2 - \sigma_3)]^2 + [c(\sigma_3 - \sigma_1)]^2$$

The Von Mises criterion applies only for materials that exhibit the same strength in tensile as in compressive stresses, like most metals do. For brittle materials however, which are very strong in compression but vulnerable in tension, this criterion is not appropriate. A modification is added to this

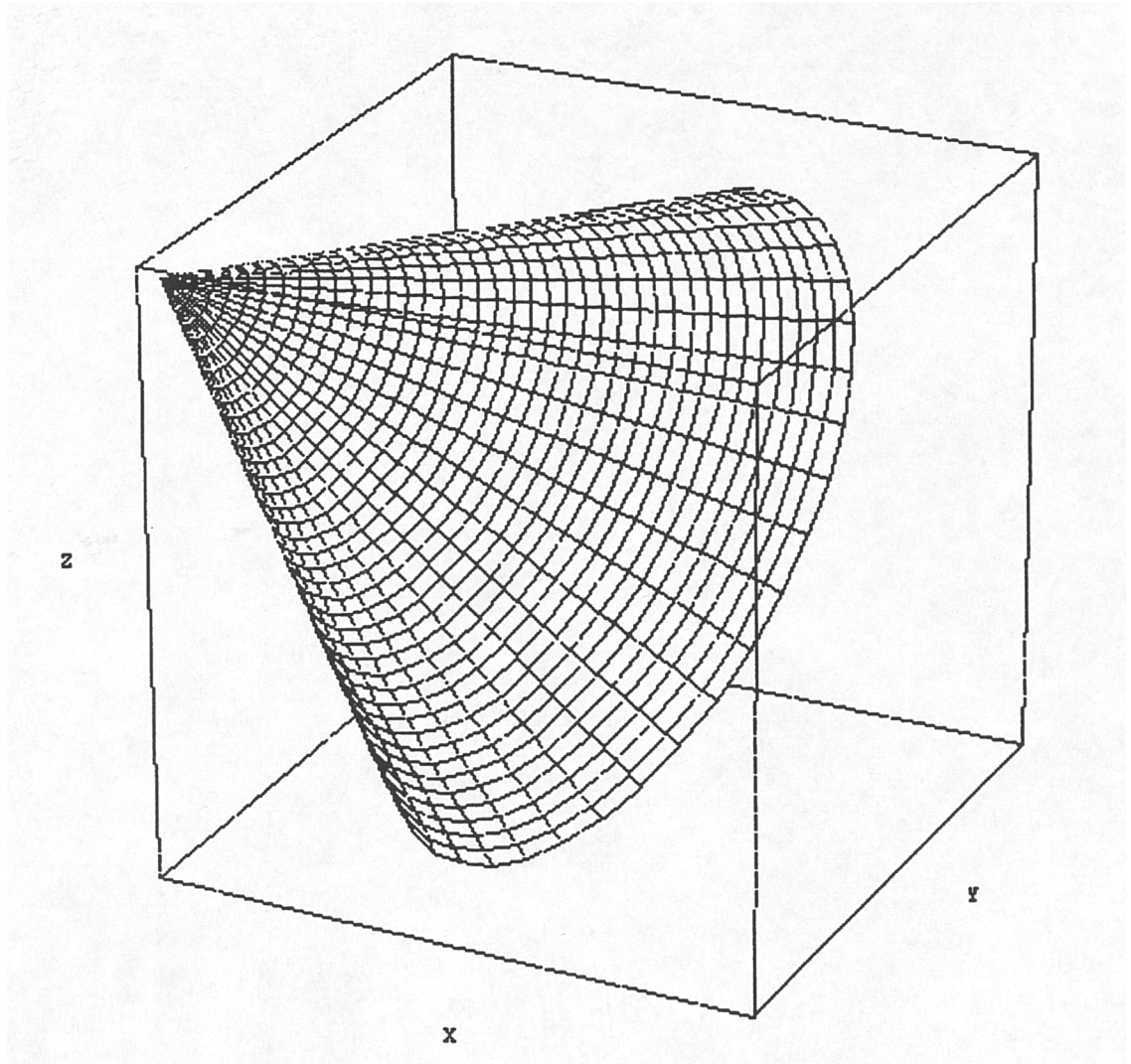


Figure 8. Drucker-Prager failure surface for $\sigma_c/\sigma_t = 10$.

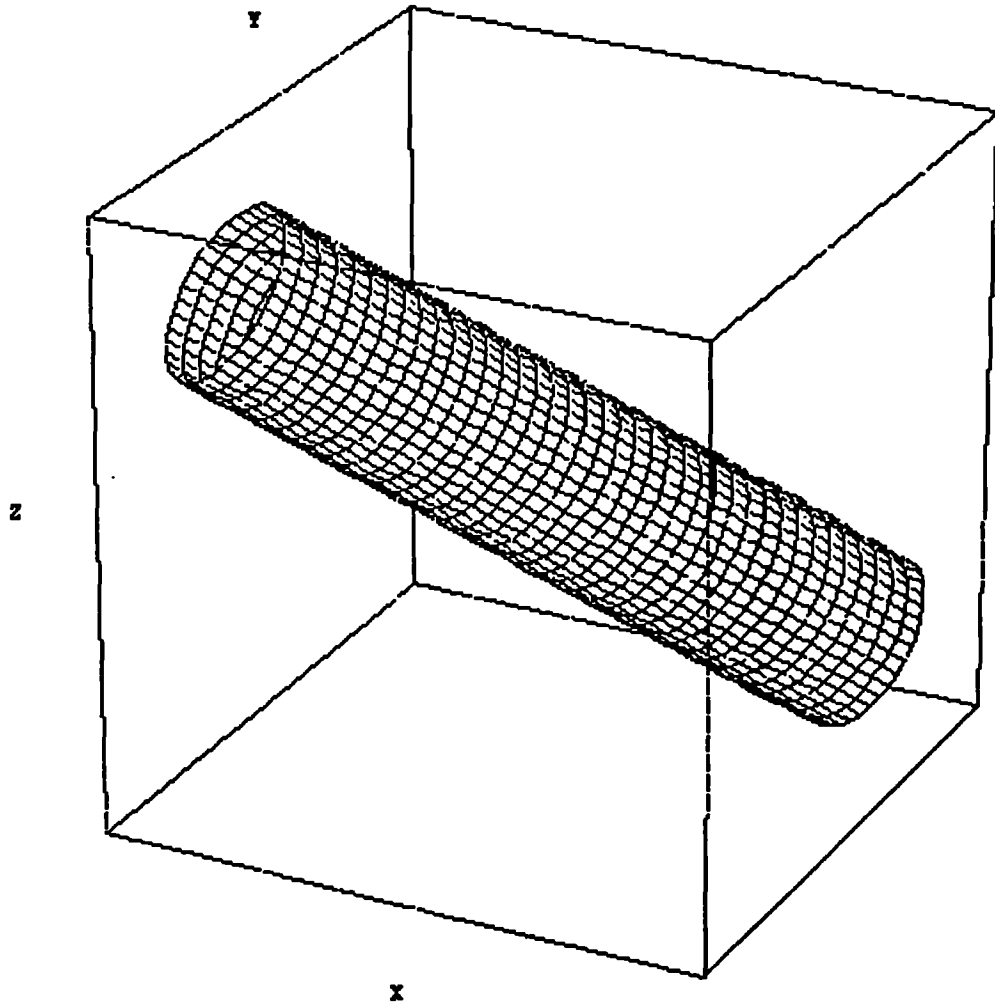


Figure 9. Von Mises failure surface.

criterion (Stassi-D'Alia, Schleicher), to incorporate this strength differential effect, therefore the Modified Von Mises criterion (**Figure 10**) becomes:

$$f_{\text{Modified Von Mises}}(I_1, J_2, \text{Mat Param}) = A I_1 + B J_2 - 1 = 0$$

The constants in this relation can be derived in the following way:

$$\text{simple tension} \quad A \sigma_t + 2 B \sigma_t^2 = 1$$

$$\text{simple compression} \quad -A \sigma_c + 2 B \sigma_c^2 = 1$$

$$\text{therefore} \quad A = \frac{\sigma_c - \sigma_t}{\sigma_t \sigma_c} \text{ and}$$

$$B = \frac{1}{2 \sigma_t \sigma_c}$$

where: σ_t tensile strength limit in simple tension

σ_c compressive strength limit in simple compression

There exists some disagreement about the shape of the failure surface. First about the question if convexity is required, or if concave failure surfaces (*e.g.* **Figure 11**) are possible too. According to the theory of stability of materials (DRUCKER, 1951), the failure surface for materials which are not strain-rate sensitive must be convex (BILLINGTON, 1986). Although convexity is generally accepted as one of the requirements for a failure criterion (OTTOSEN, 1977), NEWMAN AND NEWMAN (1971) point out there are experimental findings that point to the existence of concave surfaces for some stress states.

Another shape factor in discussion is the curvature of the meridians in the planes parallel to the deviatoric plane. In general it is assumed that the failure surface has to be a quadratic surface (HASHIN, -1983; THEOCARIS AND PHILIPPIDIS, 1987; THEOCARIS, 1988), where the axisymmetric-axis is the hydrostatic axis. Here the meridians in the deviatoric and its parallel planes are circular. Theocaris argues that a failure surface should be a quadratic surface since the criterion is based on the balances of elastic energies and eventually of plastic work, which are expressed in terms of squares of the

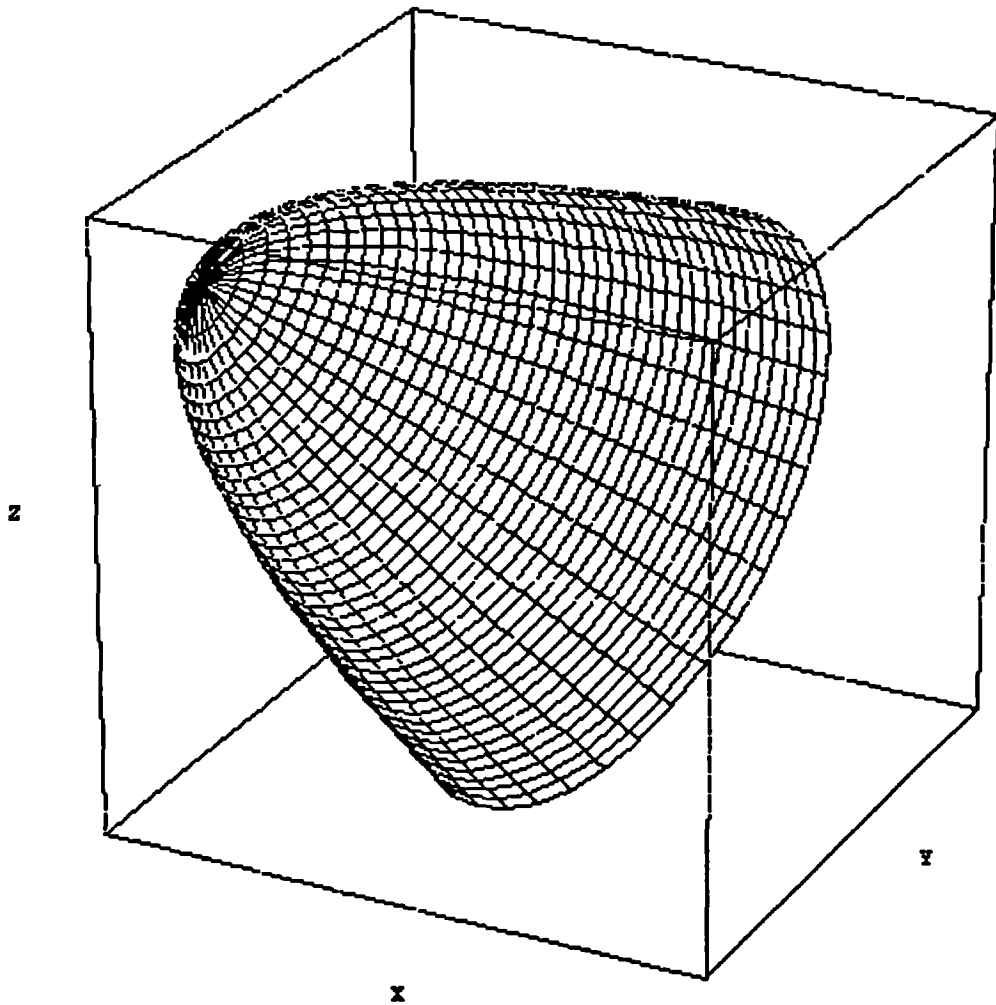


Figure 10. Modified Von Mises failure surface for $\sigma_c/\sigma_t = 10$.

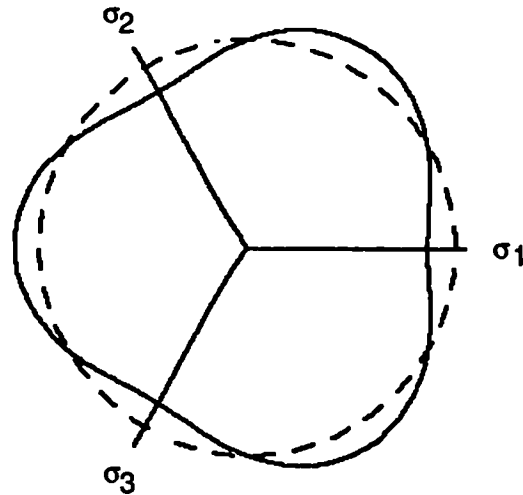


Figure 11. Curved meridian in a deviatoric plane (Gudehus criterion for $\sigma_c/\sigma_t = \frac{1}{2}\sqrt{\frac{5}{3}}$, or $r_0=4$) versus circular meridian (dashed).

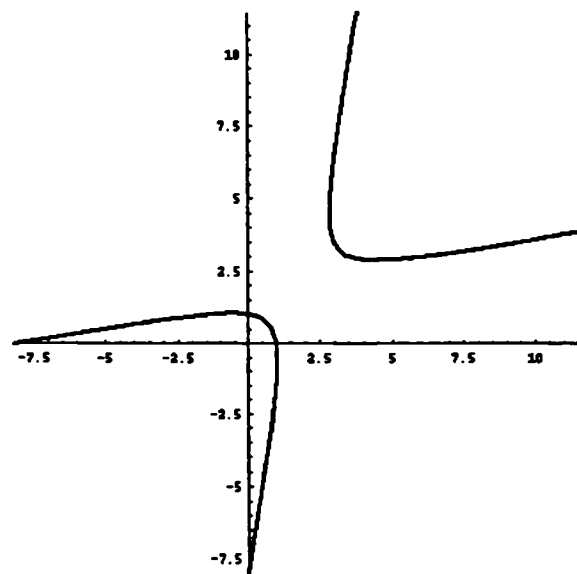


Figure 12. Intersections of the Drucker-Prager criterion ($\sigma_c/\sigma_t = 8$) with principle planes result in hyperbolas.

components of stresses. Hashin emphasizes that this is an assumption of convenience and more associated with the constraints of curve fitting, although the quadratic nature of stress energy has led to attempts of physical interpretation of the quadratic surface approximation (HASHIN, 1983). But according to other publications the meridians have to be smoothly curved as a function of the amount of the hydrostatic stress (OTTOSEN, 1977). An example of curved meridians is shown in **Figure 11** (Gudehus criterion in a plane parallel to the deviatoric plane). Curved meridians imply the inclusion of the third invariant of the deviatoric stress tensor in the expression for the failure criterion. This conclusion has led to several complicated empirical expressions (GUDEHUS, 1973; OTTOSEN, 1977; LADE, 1982; PODGÓRSKI, 1985; GUENNOUNI, 1987), based on extensive curve fitting and which are impractical for general usage. Some of them are so flexible that most other criteria are particular cases of it (PODGÓRSKI, 1985).

The third general shape factor is an open or a closed failure surface. Von Mises failure surface has two open ends, for both hydrostatic tension and compression. When a strength differential effect exists, where the tensile strength is smaller than the strength in compression, the surface must be closed in the direction of hydrostatic tension. Since all materials sustain an unlimited amount of hydrostatic compression the failure surface should be open in the direction of the negative hydrostatic axis (THEOCARIS, 1988). As a result, if a quadratic failure surface is assumed, two types of shapes are possible: a paraboloidal (*e.g.* modified Von Mises) and a conical (*e.g.* Drücker-Prager) surface. According to THEOCARIS (1988) the conic surface presents some inconsistencies, especially at its angular apex, which is a singular point and physically unlikely. Moreover, along its intersections by the principal planes for $R > 3$ ($R = \sigma_c / \sigma_t$) these intersections are hyperbolas (**Figure 12**), non-conforming to experimental evidence.

For dental restorative composites a failure criterion has to fulfill some requirements, which will further resolve an appropriate shape and formulation for an adequate failure criterion. Dental composites have a brittle failure

behaviour. The ultimate strength is limited in the positive direction (tension) of the hydrostatic-axis. The compressive strength is higher (about 5 to 10 times) than the tensile strength. The existence of this strength differential effect implies the dependency of the ultimate strength on the hydrostatic stress, and therefore requires that a failure criterion contains the first invariant (I_1). This conclusion excludes the Von Mises criterion as not appropriate for dental restorative composite materials. From a practical standpoint, the inclusion of the third order stress invariant (J_3) is inconvenient. It causes equations containing third order stress terms, which are hard to solve, especially for the equivalent stress approach. Because there is no evidence of stress dependent curved meridians in the deviatoric plane for dental composites, the third deviatoric invariant is not considered. The failure surface is assumed to contain an axisymmetric volume along the hydrostatic-axis (J_2). Two failure criteria appear to fulfill these criteria the best: Drücker-Prager and modified Von Mises. One represents a cone (Drücker-Prager), the other a paraboloid (modified Von Mises). In **Figure 13** the failure surfaces Von Mises, modified Von Mises and Drücker-Prager are displayed for a strength differential effect $\sigma_c/\sigma_t=2$.

THEOCARIS (1986, 1988) strongly supports the choice of modified Von Mises rather than Drücker-Prager, based on the suggestion of a physical meaning of its mathematical expression. The modified Von Mises criterion depends on equal terms of the distortional component of the strain energy T_d , as well as on a term which implies a dilatational type of strain energy T_v .

$$T_d = \frac{1}{12G} [(\sigma_1 - \sigma_2)^2 + (\sigma_2 - \sigma_3)^2 + (\sigma_3 - \sigma_1)^2]$$

$$T_v = \frac{(\sigma_1 + \sigma_2 + \sigma_3)^2}{18K}$$

where: G is the modulus of rigidity or shear modulus

K is the bulk modulus

Therefore it takes into consideration both components of the elastic strain energy of the deformed material. On the contrary the $\sqrt{J_2}$ -term does not represent any kind of distortional energy component and therefore creates some

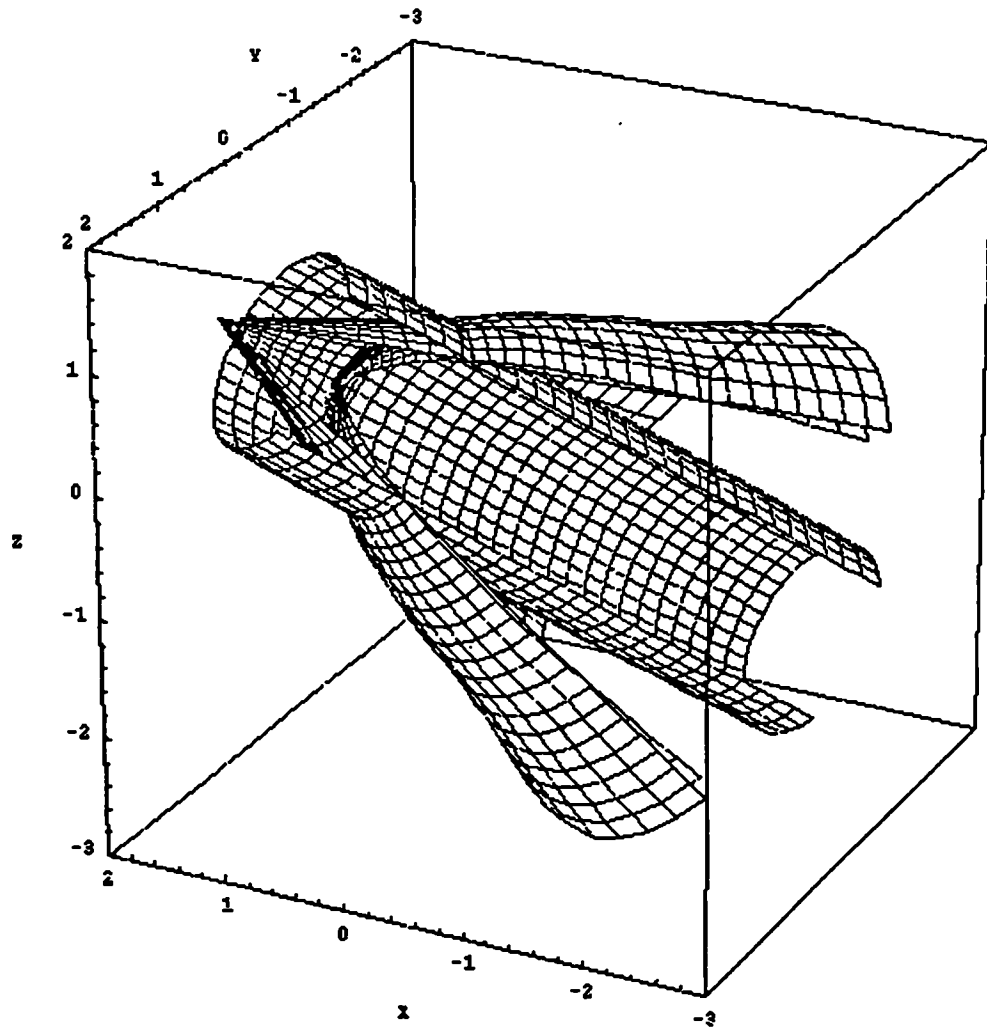


Figure 13. Combination plot of the Von Mises (cylinder), the Modified Von Mises (paraboloid) and the Drucker-Prager (cone) failure surfaces ($\sigma_c/\sigma_t = 2$).

kind of confusion in energy terms included in the criterion. Furthermore there are some questions about the physical likeliness of the conical Drücker-Prager failure surface, as described earlier. Theocaris concluded that the failure expression according to modified Von Mises is more sound. THEOCARIS (1986) reports a large amount of experimental evidence to support the validity of the modified Von Mises criterion for the whole spectrum of ductile and brittle materials. Also STASSI-D'ALIA (1967) reports excellent agreement for a variety of materials. RAGHAVA *et al.* (1973) report that it appears that modified Von Mises more properly reflect the differences in the increase of the yield strength under increasing hydrostatic pressure than a criterion based upon the octahedral shear stress (Drücker-Prager). However, due to a lack of triaxial and even biaxial failure data, there is not enough evidence to support one of the two failure criteria for dental restorative composite materials. Both expressions are convenient expressions, which proved to predict reliable failure stresses. For small strength differential effects ($\sigma_c/\sigma_t \leq 1.5$) the difference between modified Von Mises and Drücker-Prager are minimal, as illustrated in **Figure 14** for plane stress conditions.

For higher strength differential effects the differences between them increase, as shown in **Figure 15** for $\sigma_c/\sigma_t=8$ (plane stress), which is a more realistic number for dental composite materials.

However, in view of the large deviation in material properties of dental composites, even for the same material from the same batch, it is questionable if it possible to distinguish between both failure criteria. Probably the differences are negligible with respect to the other sources of variation in material properties. Therefore in this study both failure criteria will be used, where the modified Von Mises gets the most emphasis because of the more sound mathematical expression.

In order to demonstrate the difference between three criteria (Von Mises, modified Von Mises and Drücker-Prager) for a dental application, a finite-element calculation is performed. A plane strain cross section of a molar is considered, which contains a polymerizing MOD composite restoration, **Figure**

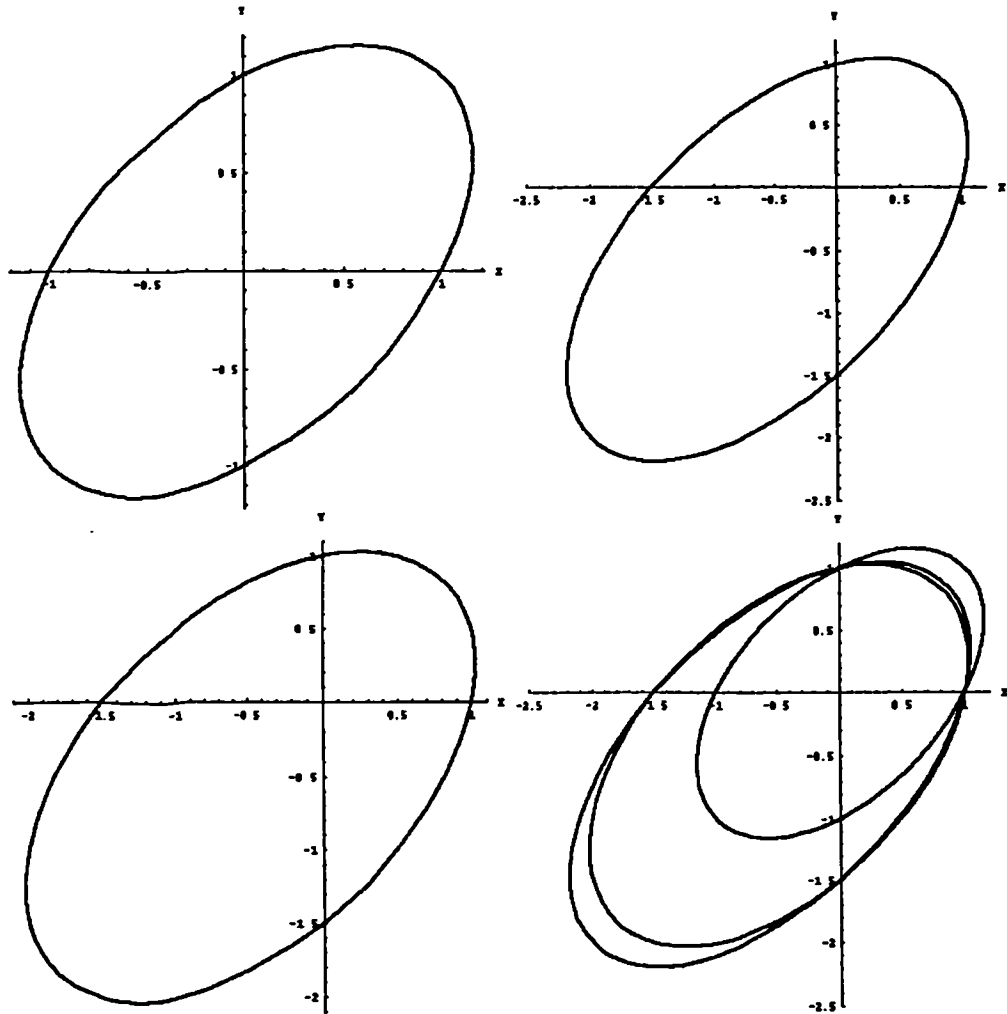


Figure 14. Comparison of three failure criteria (plane stress, $\sigma_c/\sigma_t=1.5$).

Upper left: Von Mises

Lower left: Modified Von Mises

Upper right: Drucker-Prager

Lower right: Combination of all three criteria

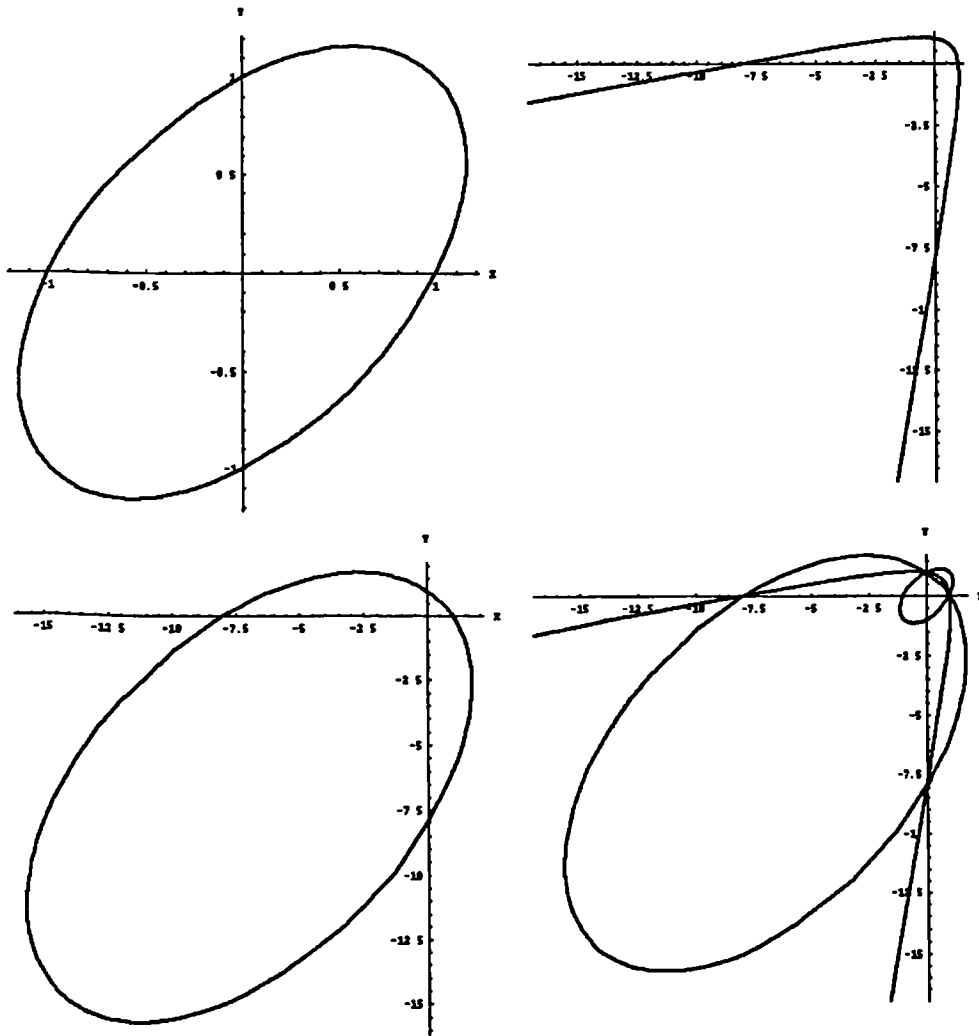


Figure 15. Comparison of three failure criteria (plane stress, $\sigma_c/\sigma_t=8$).

Upper left: Von Mises

Lower left: Modified Von Mises

Upper right: Drucker-Prager

Lower right: Combination of all three criteria

16. The total linear polymerization shrinkage of the composite restoration is set at $\alpha = 0.0022$. The applied elastic moduli are 50 GPa for enamel, 12 GPa for dentin and 20 GPa for the composite restoration. The Poisson's ratios are 0.30 for enamel, 0.10 for dentin and 0.24 for the composite restoration. The choice of these values are discussed in Chapter 8 (Table XXIII). The strength differential effect ratio is $R = \sigma_c/\sigma_t = 8$ for the composite (DE GROOT *et al.*, 1987). The molar is fixed in all directions on both roots, at the three lowest outer nodes. The calculated equivalent stresses are displayed in Figures 17A-C. The σ_{VM} equivalent Von Mises stress expression is:

$$\sigma_{VM} = \sqrt{3J_2}$$

The equivalent stress σ_{MVM} for modified Von Mises and σ_{DP} for Drucker-Prager are:

$$\sigma_{MVM} = \frac{(R-1)I_1 + \sqrt{(R-1)^2 I_1^2 + 12RJ_2}}{2R}$$

$$\sigma_{DP} = \frac{(R-1)I_1 + (R+1)\sqrt{3J_2}}{2R}$$

where: $R = \frac{\sigma_c}{\sigma_t}$

σ_t is the uniaxial tensile strength

σ_c is the uniaxial compressive strength

The results show a significant difference between the Von Mises criterion and the two criteria which include the strength differential effect. According to the Von Mises criterion the highest stress concentration is found in the central groove, while the equivalent stress distributions calculated according to modified Von Mises and Drucker-Prager criteria show the lowest stresses at that location. The lowest Von Mises equivalent stresses are found at the bottom corners of the restoration, whereas these locations are highly stressed if the two other criteria are applied. In all three cases the two upper edges of the restoration display severe stress concentrations. In this example the influence of the incorporation of the strength differential effect is made very clear: in the

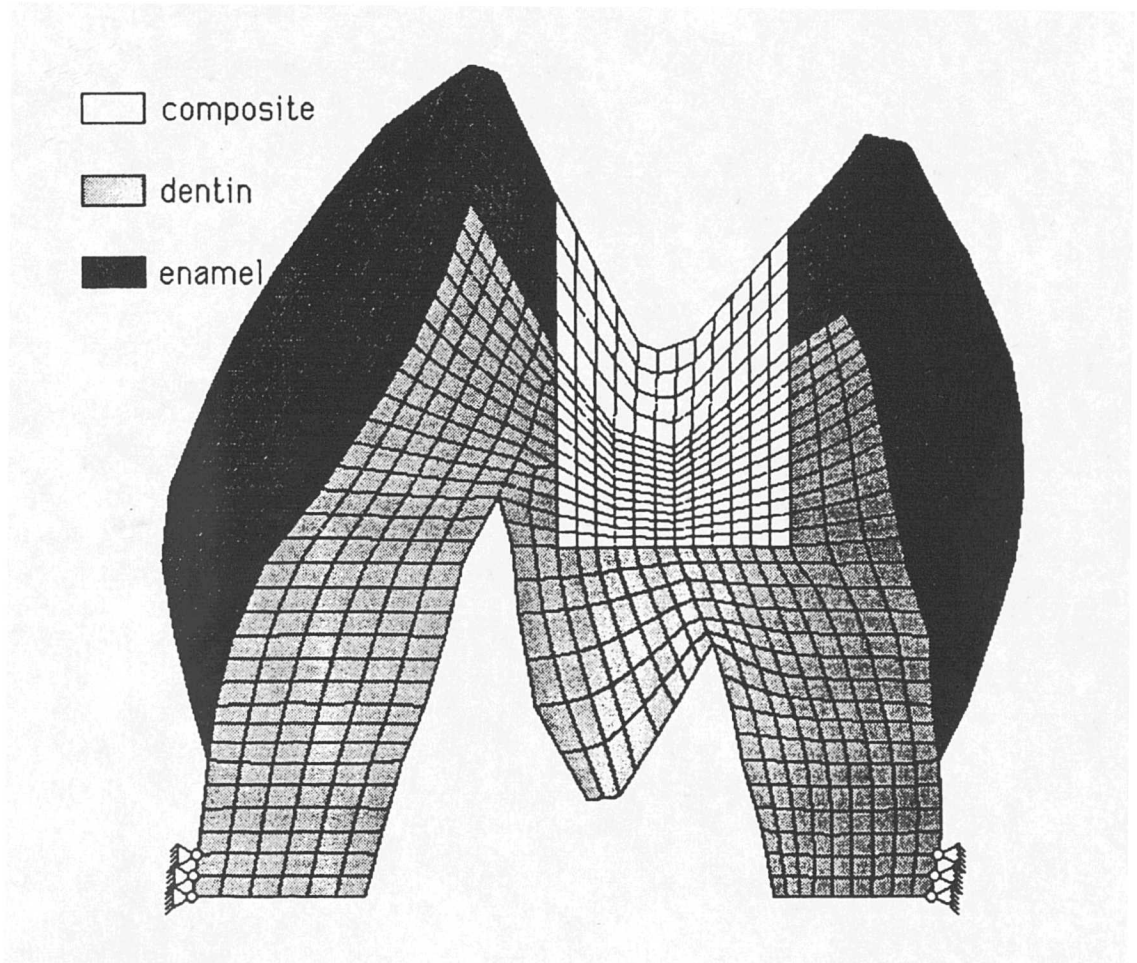


Figure 16. Cross section of a molar with MOD restoration, displaying mesh, materials, and boundary conditions.

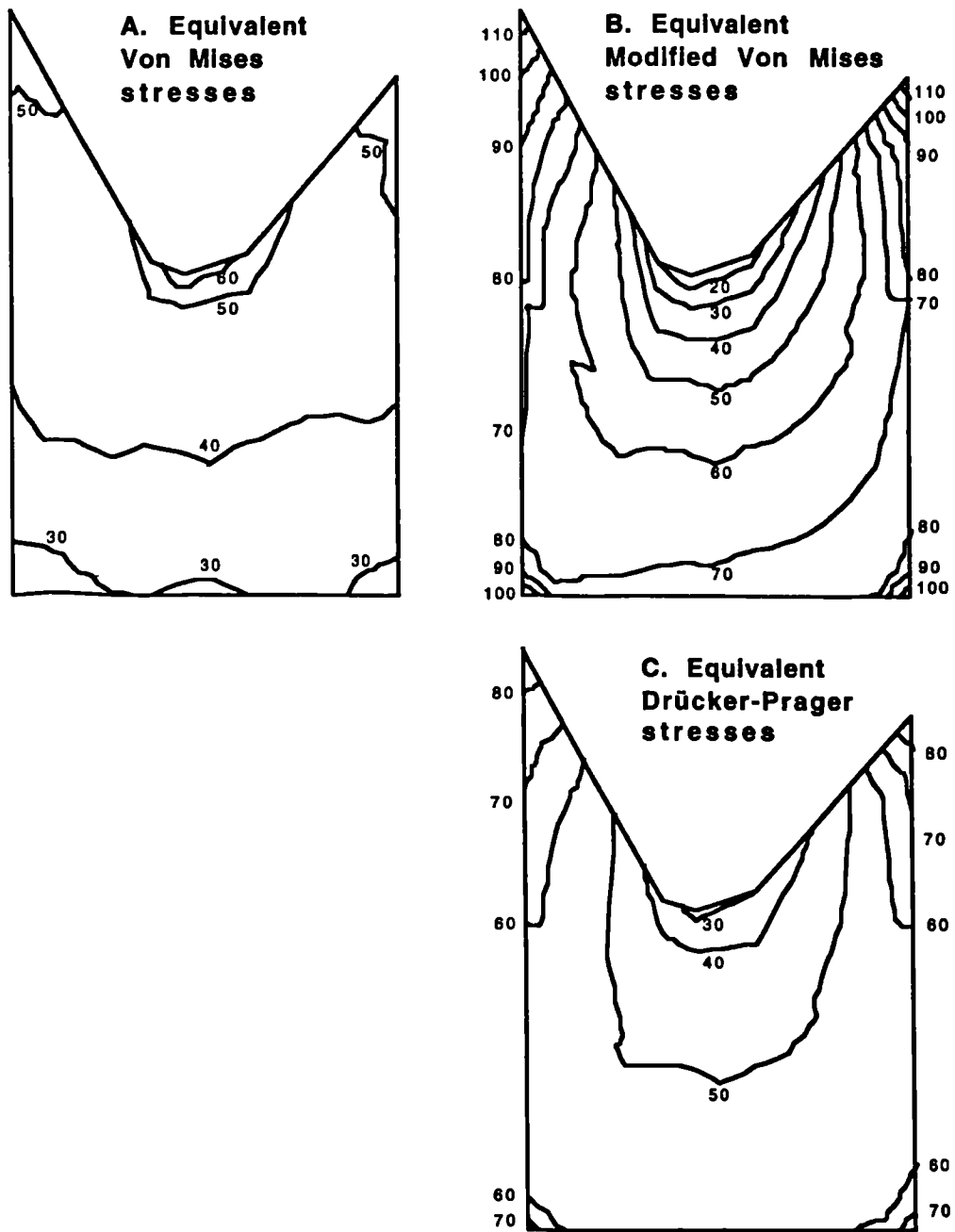


Figure 17. Equivalent stress distributions (MPa), calculated according to the failure criteria of Von Mises (A), Modified Von Mises (B) and Drucker-Prager (C).

central groove high compressive stresses exist, and in the upper corners high tensile stresses. Von Mises' yield criterion does not distinguish between compressive and tensile stresses, and therefore calculates high stress concentrations at both locations. Modified Von Mises and Drucker-Prager criteria weight the effect of the compressive and tensile strength values to determine the sites of stress concentrations, taking into account the vulnerability of composite materials to tensile stresses.

Figure 17 shows the stress distribution in the restoration due to the development of internally applied stresses. Pre-existing internal stresses will be superimposed to the external functional stresses, which will raise the overall stress levels. It is now intended to attempt a more complete picture of the residual stress state within the composite and tooth-composite complex by turning the attention to the development of internal stresses within the composite.

4 Linear polymerization contraction

4.1 Introduction

During the polymerization reaction, dental restorative composite materials manifest volumetric contraction (FEILZER *et al.*, 1990; WATTS AND CASH, 1991; SAKAGUCHI *et al.*, 1992). During the polymerization process of composites the development of contraction stresses can be divided into two phases: the pre-gel and the post-gel phase. In the pre-gel polymerization phase, the composite is able to flow which relieves stress within the structure (DAVIDSON AND DE GEE, 1984). At the gel-point and beyond, the shrinking composite material has to sustain shrinkage stresses, due to the development of stiffness; the flow is unable to compensate for all the contraction stresses. Therefore internal shrinkage stresses will be developed. These conditions often result in heavily pre-stressed restorations which frequently leads to deformation and even fracture (DAVIDSON *et al.*, 1984; FEILZER *et al.*, 1987). Shrinkage takes place during both phases, but only during post-gel, when a modulus is developed, the shrinkage stress will be build up. Therefore only post-gel shrinkage is important.

The clinical significance (SAKAGUCHI *et al.*, 1992) of shrinkage stresses in a restoration is the potential for defects in the composite-tooth bond. This leads to bond failure and micro leakage with possible postoperative sensitivity (EICK AND WEICH, 1986). If the composite-tooth bond is able to withstand the deformation, stresses induced by the contracting composite can cause deformation of the surrounding tooth structure (DONLY *et al.*, 1987; MORIN *et al.*, 1988; SHETH *et al.*, 1988). The resulting coronal deformation may result in postoperative sensitivity and micro cracks in the cervical enamel (BOWEN *et al.*, 1983), which predisposes the tooth to fracture. Careful composite placement can minimize the effects of the polymerization contraction (LUTZ *et al.*, 1986), however coronal deformation is still evident. Stress relaxation through water absorption is

evident in mature composites (FEILZER *et al.*, 1990) but this occurs over a long period of time, well after post-gel polymerization is complete. Therefore the tooth-restoration complex is in a pre-stressed state even before functional occlusal stresses result in further coronal deformation (SAKAGUCHI *et al.*, 1991).

Polymerization shrinkage is usually measured using a dilatometer (DE GEE *et al.*, 1981; PENN, 1986) or fluid weight displacement method (PUCKETT AND SMITH, 1992). In these methods the total volumetric change can be determined by measuring the displacement of fluids or their weight. However, these methods include both pre- and post-gel shrinkage, while with regard to the shrinkage stresses only the post-gel shrinkage is significant. WATTS AND CASH (1991) measured the post-gel shrinkage in a setup in which a disc-shaped specimen was sandwiched between two glass plates. In this study strain gages are used for the determination of post-gel shrinkage. The strain gage method has been described previously (SAKAGUCHI AND DOUGLAS, 1989; SAKAGUCHI *et al.*, 1991), but is further developed in this study. Strain gages can be used if there is strain, *i.e.* after the gel point when the modulus of elasticity is established. Two basic assumptions are made when the strain gage method is used. One assumption is that the bonding between the composite and the strain gage is sufficiently present after the gel point. The second assumption is that the strain gage will only measure shrinkage strains after the gel point, *i.e.* post-gel shrinkage. These assumptions are verified below and the strain output is analyzed.

The aim of this chapter is to determine post-gel polymerization contraction of restorative composites. This information is essential for an integrated polymerization stress-strain development study. Direct results of these polymerization strain measurements are used for a better understanding of the processes during the polymerization reaction, and quality control of present and future dental composite materials.

4.2 Materials and Methods

Figure 18 shows the whole setup for the shrinkage strain measurements. For this study the method described in SAKAGUCHI *et al.* (1991) is modified with respect to the strain gage type, the applied light intensity characteristics, the determination of the start of the reaction, and the data collection.

- a. *Strain gage* — In this study shrinkage is measured, using a stacked strain gage (CEA-06-032WT-120, Micro Measurements Group, Raleigh, NC, USA), **Figure 19**. A stacked strain gage measures shrinkage strains in two perpendicular directions. The strain should be the same for both directions because of the homogeneous isotropic material properties on macro scale. Assuming that there is no modulus before the gel-point, strain gages are only measuring post-gel shrinkage. The composite is placed on top of the strain gage, where the actual measuring surface is about 1 mm^2 . The samples are 1.5 mm high, and cover an area of about 16 mm^2 . The used strain gages are self-temperature compensating, and show a flat temperature response in the temperature range (20-40°C) of these experiments, therefore a strain output correction is not required for the gage factor and the apparent strain.
 - b. *Curing light source* — Only light curing composites are investigated, because this type of composite materials offer a more controllable start of the polymerization process. The curing light probe is positioned 2 mm above the sample. After the curing light source is turned on, it takes some time until the curing light reaches its full light intensity (SAKAGUCHI *et al.*, 1992). This stage of immature light intensity is omitted by means of a shield, that covers the composite sample until the full curing light intensity is reached. The effect of the shield on the light intensity output is shown in **Figure 20**. The full intensity of the used curing light source (Visilux^{1M2}, 3M) is 400 mw/cm^2 . The point at which the composite material is subjected to the curing light is registered by a light sensitive cell. The output of the light cell is recorded along with the strain readings, and provides the exact starting point of the polymerization.
-

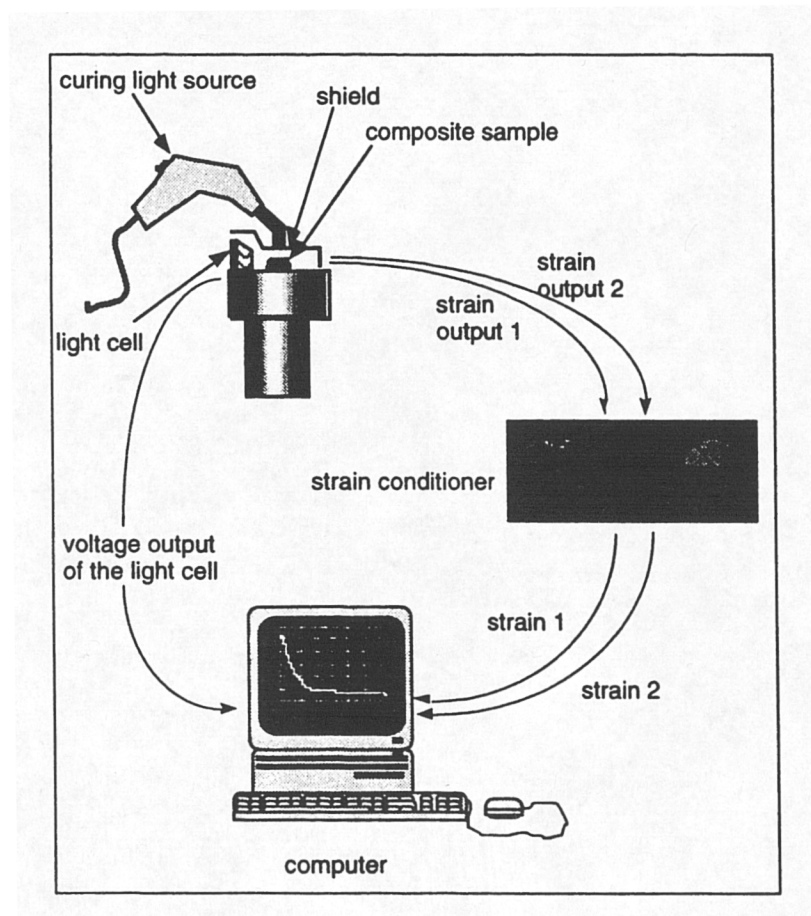


Figure 18. Strain measurement setup.

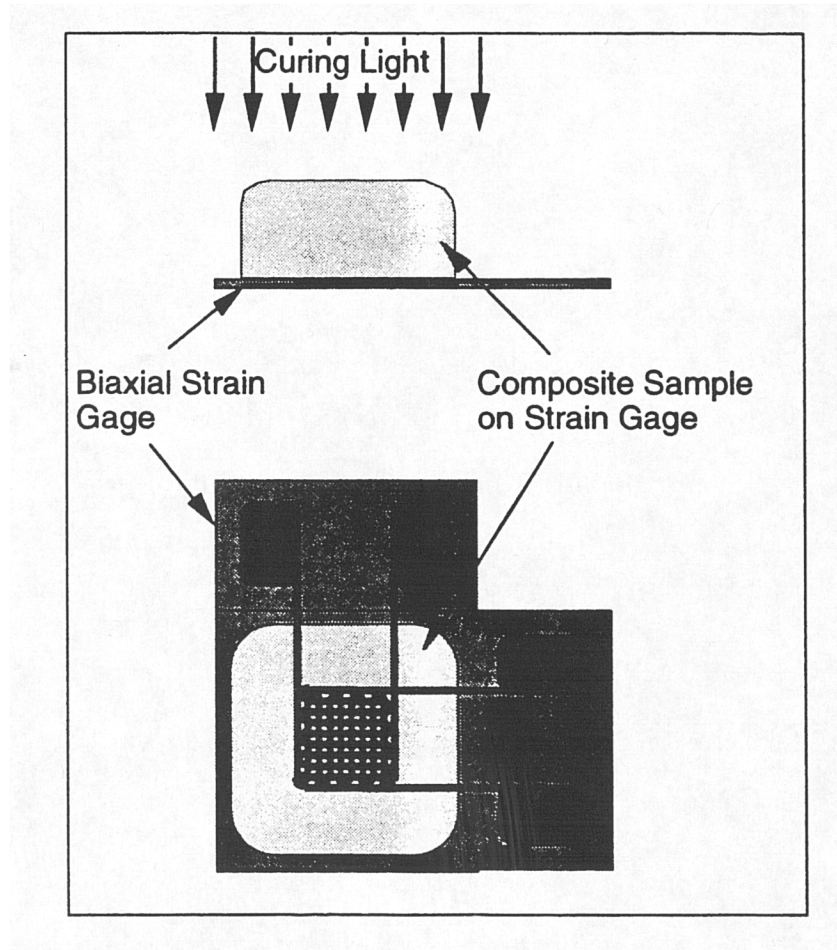


Figure 19. Biaxial strain gage and composite sample.

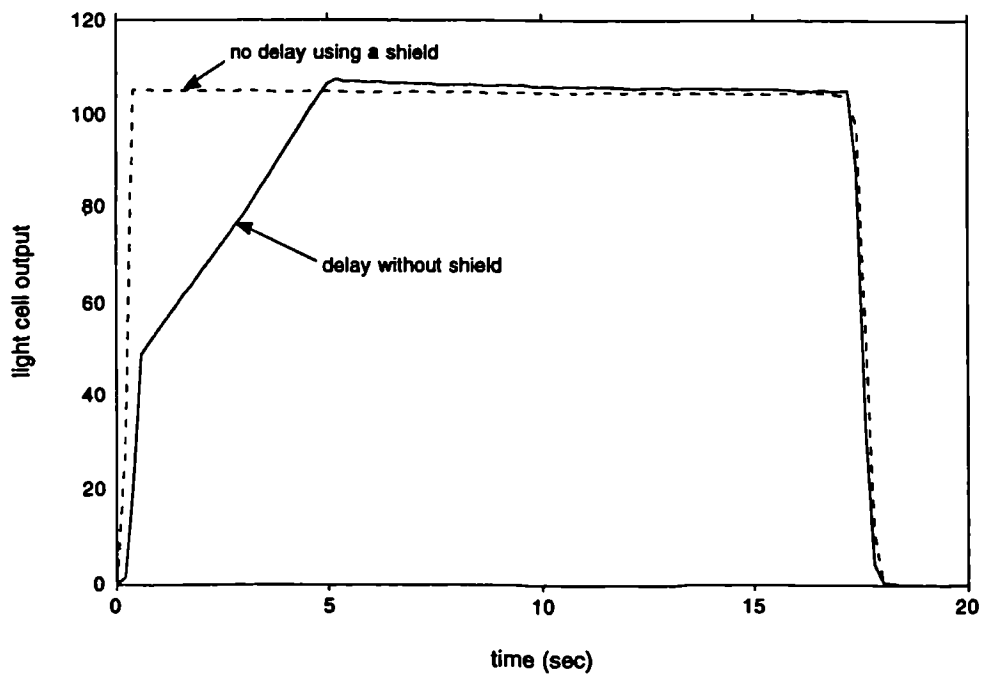


Figure 20. Light intensity output curve both if the delay is omitted (using a shield) and when not omitted (without shield).

- c. *Data collection* — The output of the strain gage is conditioned in a strain conditioner (2101A Series, Micro Measurements Group, Raleigh, NC, USA), using a quarter bridge circuit with an internal dummy gage setup. The conditioned strain readings and output of the curing light cell are acquired through an analog-digital converter and stored on a desk-top computer, as a function of time.
- d. *Materials* — The composite materials used are commonly available and applied restorative composites. The investigated materials are listed in **Table VII**. All the composite materials are light cured for 60 seconds, and the strain output is recorded for 5 minutes. The sample size $n \geq 10$. The output strains for both — perpendicular — directions are averaged. This time-dependent strain value represents the linear shrinkage strain. The well-known relation between the linear contraction coefficient α and the volumetric contraction coefficient ϕ is (GIECK AND GIECK, 1990):

$$\phi = 3 \alpha$$

- e. *Analysis of the strain gage method* — To investigate the strain gage output, some additional experiments are carried out. The whole curing procedure — 60 seconds light curing and 4 minutes monitoring — is performed for (1) a bare strain gage, (2) an uncured conventional composite Z100™ (3M, St Paul, MN), (3) a cured conventional Z100, (4) a cured conventional Z100 positioned loose on the strain gage, (5) a cured conventional Z100 composite sample bonded (M-bond™200 adhesive, Micro Measurements Group Inc.) to the strain gage, (6) an uncured Z100 sample without photo initiator, (7) a cured Z100 sample without photo initiator, and (h) a cured Z100 without photo initiator positioned unbonded on the strain gage. The Z100 resin without photo initiator is forced to polymerize by light curing over a long period (half day).

In order to compare the shrinkage rate, some experiments are carried out for conventional Z100 with two different curing light intensities (both curing light sources are Visilux™2, 3M), with a light intensity of 400 and 500 mw/cm²

Table VII. Materials investigated in this post-gel shrinkage and polymerization temperature study.

Material	Manufacturer	Shade	Batch no.
APH	Caulk	U	061289
BisFil-M	Bisco	B1	029251
Conquest	Jeneric/	A2	150322
	Pentron	A2	2909921
		B1	2019511
		Opaque	2019201
Durafill	Kulzer	C	026
Heliomolar	Vivadent	YB	466401
Herculite XR	Kerr	U	9_2118
Herculite XRV	Kerr	A2	1_3236 893
P50	3M	Y	9CD4D
Silux Plus	3M	DY	9CA1
Tetric	Vivadent	Dentin	440148
Z100	3M	A4	P920402

respectively, and are monitored for 5 hours. The drift of the strain gage output over an extended period is less than $\pm 15 \mu\text{strain}$.

For the conventional Z100 and also for the Z100 without photo initiator, all the successive runs are for the same sample.

4.3 Results

The results of the post-gel strain measurements for the linear and calculated volumetric shrinkage 290 seconds after the start of the polymerization reaction are listed in **Table VIII**. In **Figure 21** a typical strain *versus* time curve is shown.

Figures 22-31 show the results of different polymerization runs (each standard run consists of 60 seconds light curing), that are performed to analyze the different polymerization parameters and to verify some assumptions.

Figure 22 shows the strain output for the bare strain gage, compared with the strain output when a cured conventional Z100 sample lies loose on the strain gage. The loose sample covers the strain gage from the light source.

In **Figure 23** the strain development for the conventional Z100 sample is shown for the curing reaction, the cured material and the loose sample respectively.

The effect of the thermal expansion (due to the curing light) can be subtracted from the total polymerization curve. In **Figure 24** the curing curve without the thermal expansion is plotted.

In **Figure 25** the contribution to the thermal expansion strain output of the strain gage is shown. The thermal expansion of a cured composite sample is eliminated, and compared to the strain output where the sample is laid on the strain gage without any bonding.

Figure 26 shows five successive (standard) curing runs for the cured conventional Z100 sample, where $t_1 < t_2 < t_3 < t_4 < t_5$.

Table VIII. Linear (μ strain) and volumetric (Vol%) post-gel polymerization shrinkage.

Material	Batch no.	Linear shrinkage (μ strain)	Volumetric shrinkage (Vol%)
APH	061289	1342 \pm 105	0.40
BisFil-M	029251	2451 \pm 325	0.74
Conquest	150322	2304 \pm 278	0.69
	2909921	2766 \pm 187	0.83
	2019511	2896 \pm 217	0.87
	2019201	2211 \pm 215	0.66
Durafill	026	1375 \pm 70	0.41
Heliomolar	466401	1547 \pm 27	0.46
Herculite XR	9_2118	1673 \pm 183	0.50
Herculite XRV	1_3236 893	1449 \pm 166	0.43
P50	9CD4D	2196 \pm 86	0.66
Silux Plus	9CA1	1403 \pm 58	0.42
Tetric	440148	1138 \pm 138	0.34
Z100	P920402	2864 \pm 77	0.86

Note: 1 Vol% = $3 \times 10^{-6} \times 100\%$ μ strain

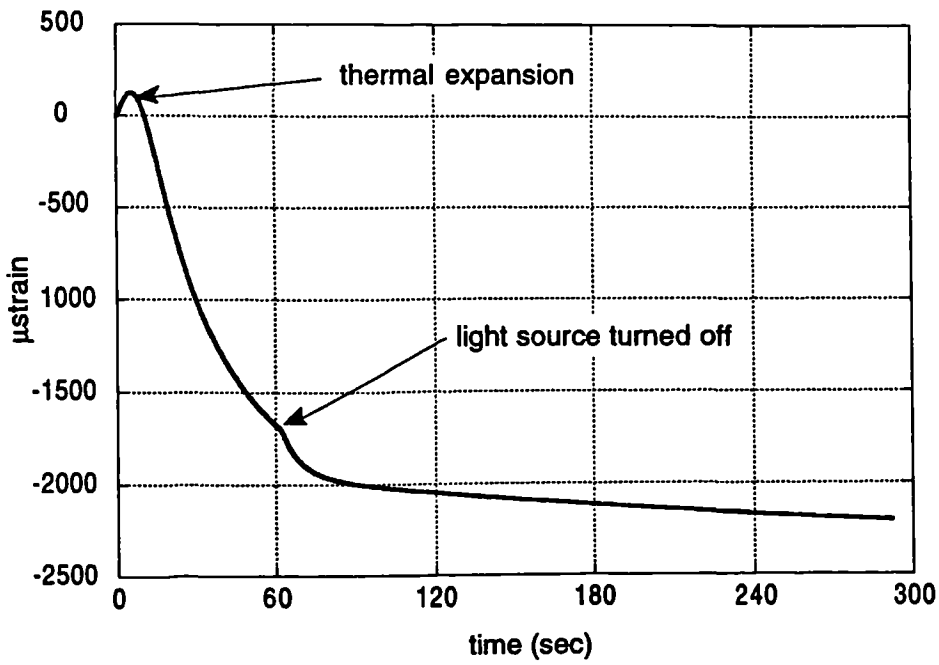


Figure 21. Linear polymerization shrinkage strain versus time for a typical composite.

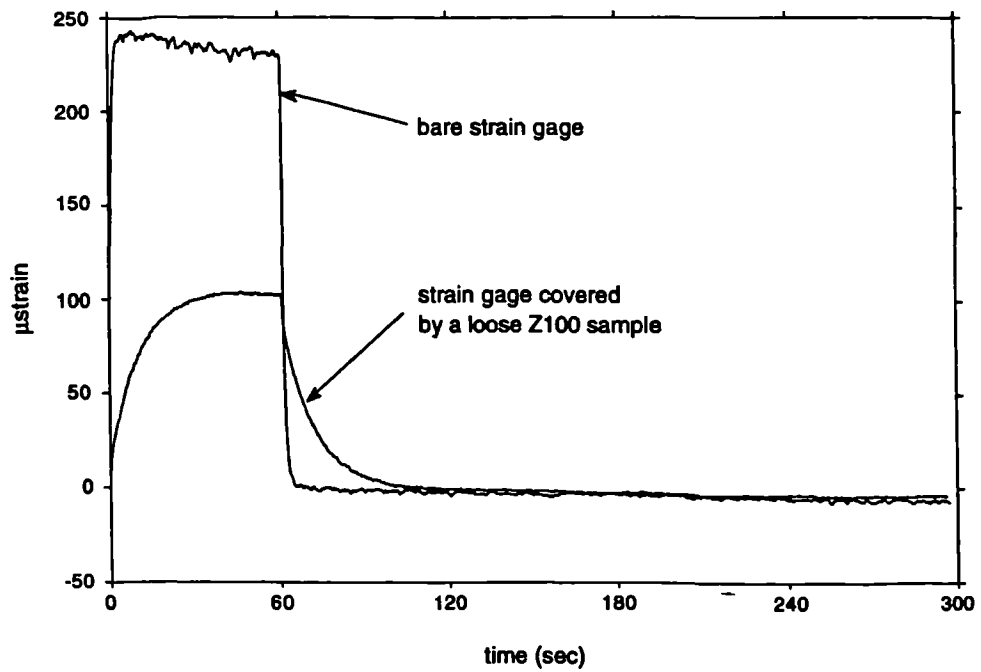


Figure 22. Strain output for a bare strain gage compared with the strain output for a cured conventional Z100 sample, positioned unbonded on the strain gage.

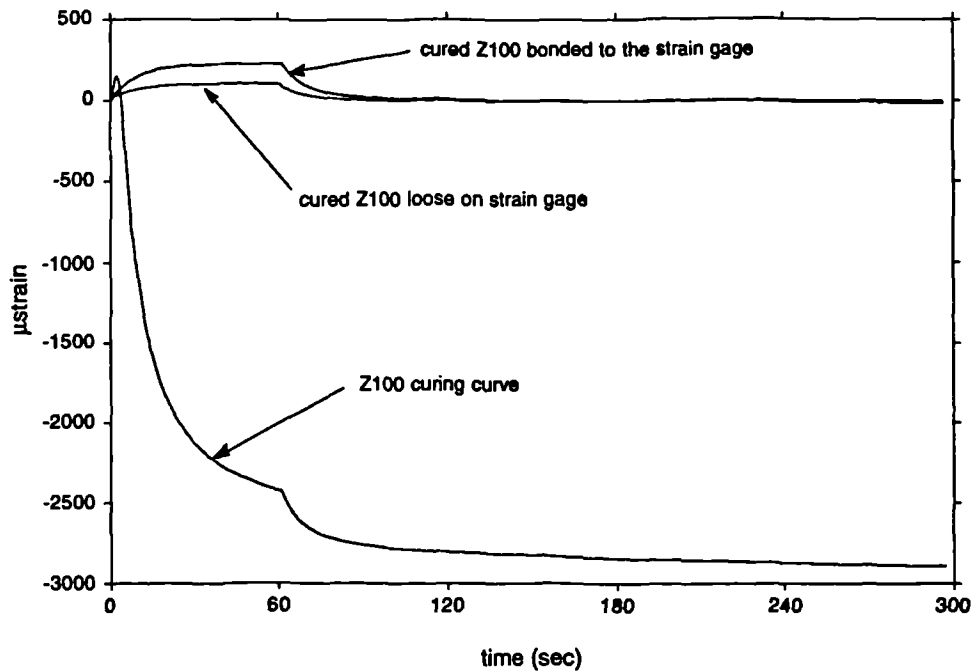


Figure 23. Strain development of conventional Z100 for the curing, the cured, and the unbonded cured sample.

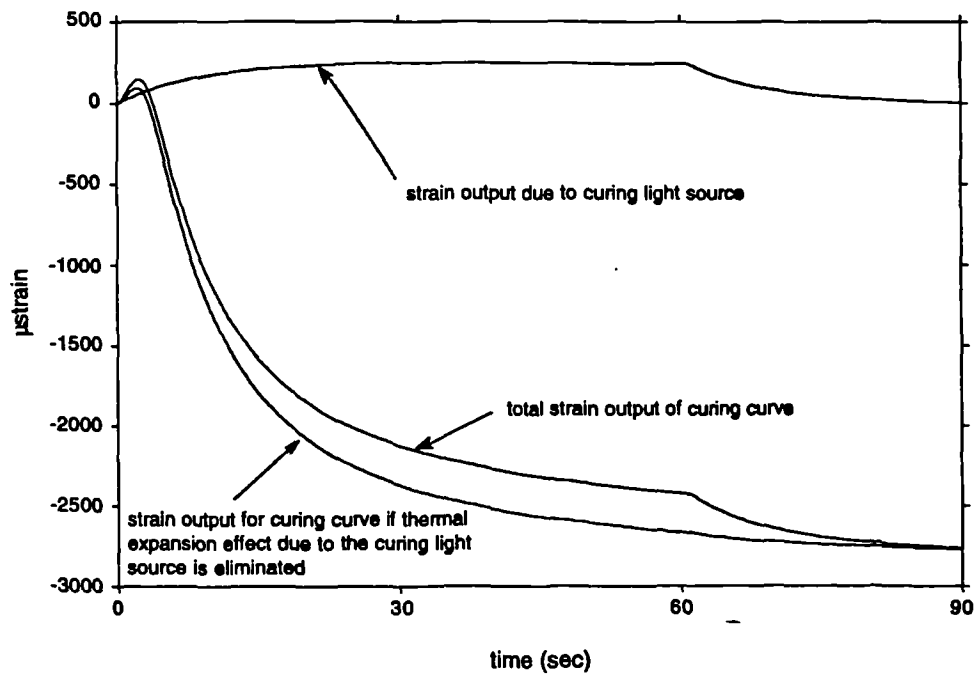


Figure 24. Curing curve without the effect of thermal expansion due to the curing light source, obtained by subtracting the strain output of the cured sample.

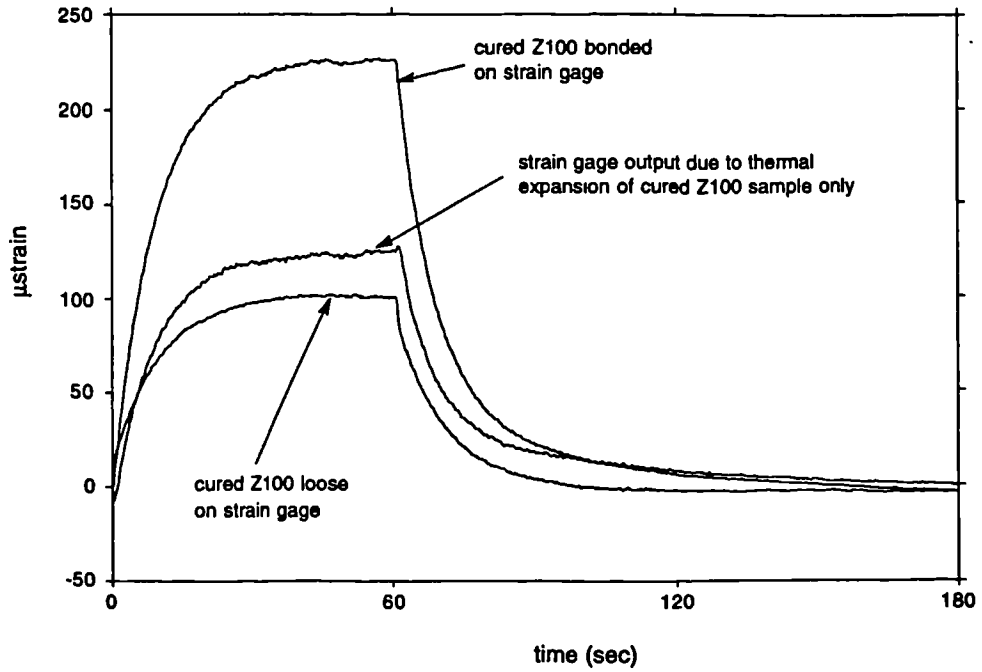


Figure 25. Contribution to the strain output (thermal expansion due to the curing light source) of the strain gage.

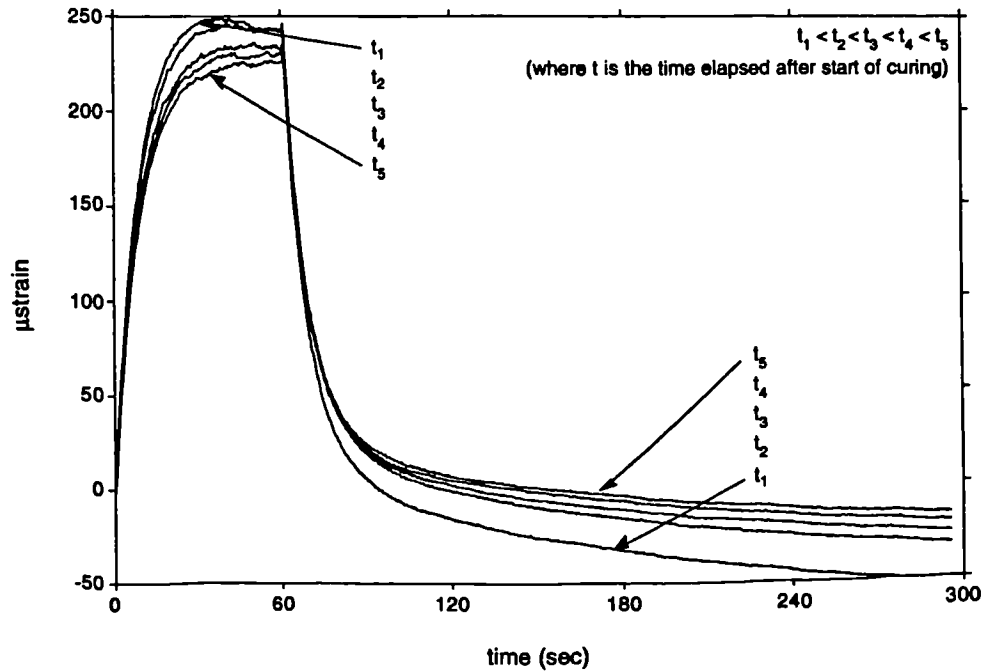


Figure 26. Five successive curing runs for a cured conventional Z100 sample, where $t_{i+1} = t_i + 6$ (min), and the start of the initial curing run is t_0 .

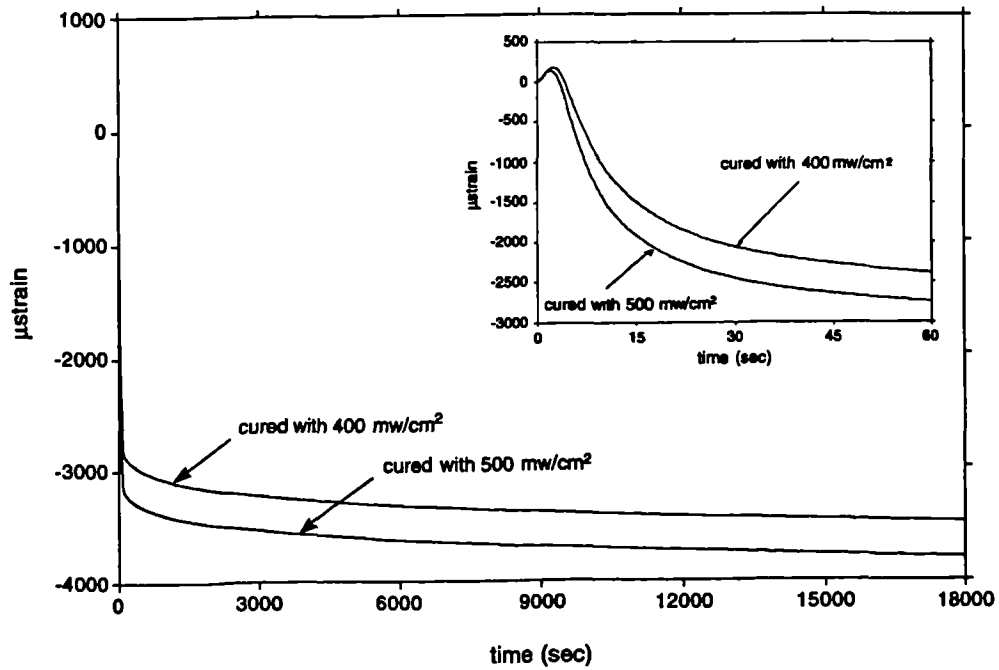


Figure 27. Shrinkage curves for Z100 samples which are cured with two different curing light intensities, monitored for 5 hours.

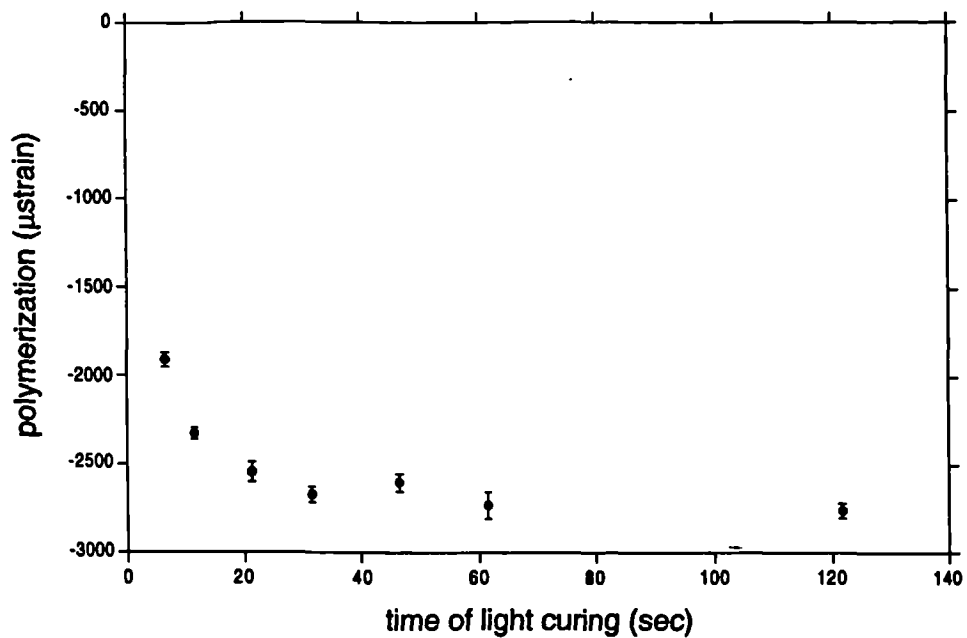


Figure 28. Effect of the time of light curing on the final shrinkage value (5 minutes after start of polymerization).

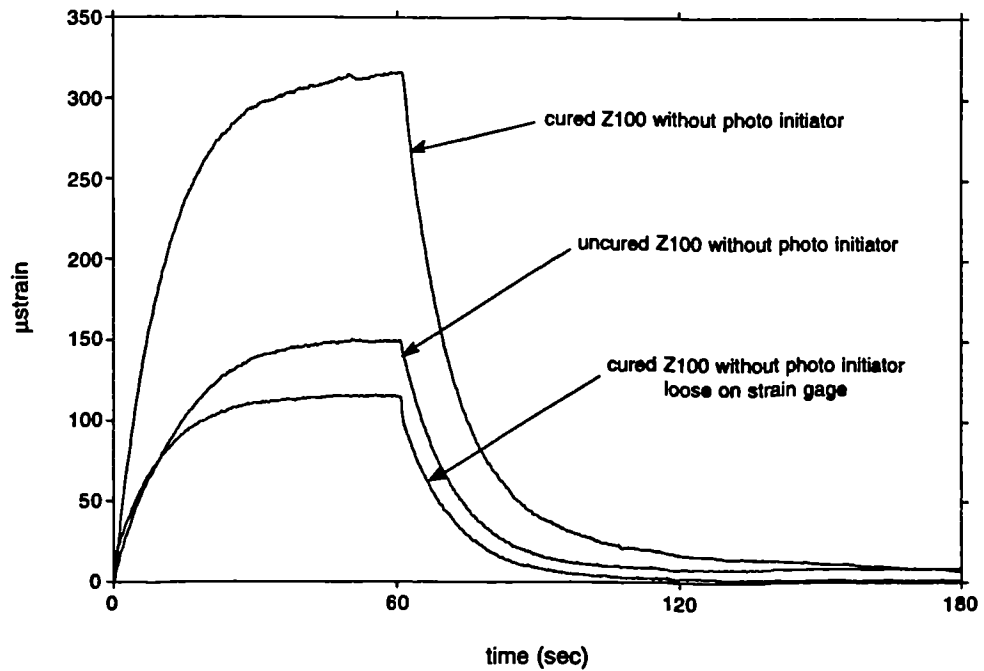


Figure 29. Strain response on a light curing run of a Z100 compound sample without a photo initiator if it is uncured, cured and loose.

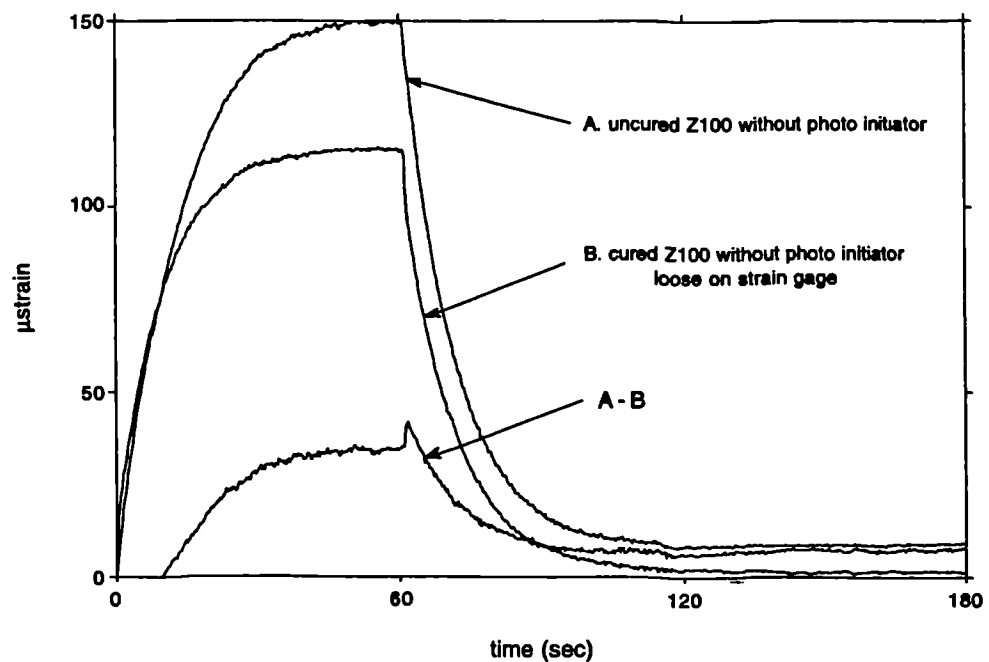


Figure 30. Strain output for a gel-phase compared to the case if there is no bonding.

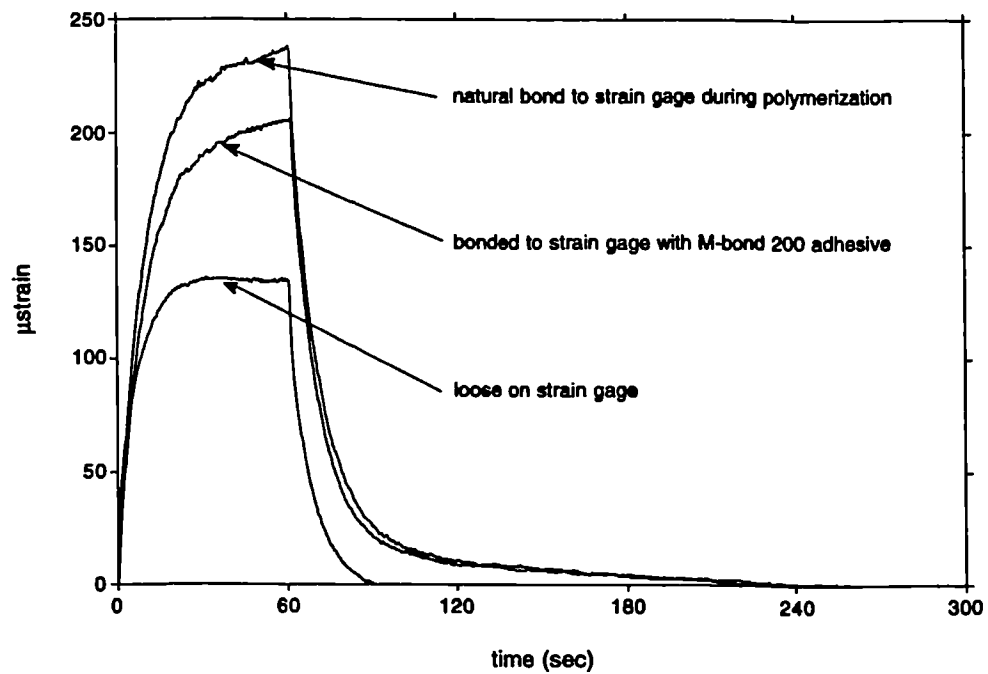


Figure 31. Comparison of the natural bonding of conventional Z100 composite (which is cured on the strain gage) with the same sample if it is bonded to the strain gage with M-bond and subjected to a thermal load by the curing light source.

Table IX. Scheffe's S multiple comparison test on the shrinkage results (p<0.01).

Scheffe's S
Effect: material
Dependent: microstrain
Significance level: .01

	Count	Mean	
Conquest B1	12	-2895.683	
Z100	11	-2863.509	
Conquest A2 (#2909921	12	-2765.808	
Bisfil	11	-2550.945	
Conquest A2 (#150322)	11	-2303.945	
Conquest Opaque	12	-2211.117	
P50	11	-2196.373	
Herculite XR	10	-1673.340	
Heliomolar	10	-1546.750	
Herculite XRV	11	-1449.255	
Silux Plus	10	-1402.690	
Durafill	10	-1375.020	
APH	10	-1341.710	
Tetric	11	-1138.074	

Figure 27 shows the strain development for two different curing light intensities, monitored for a period of 5 hours.

Figure 28 shows the influence of the duration of light curing on the shrinkage value 300 seconds after the start of the polymerization reaction.

Figure 29 shows the strain response of the Z100 compound without the photo initiator for the uncured, the cured, and the loose sample.

In **Figure 30** the strain output for the gel-phase is compared to the no-bonding case.

Finally in **Figure 31** the natural bonding of conventional Z100 composite (which is cured at the strain gage) is compared with the same sample when it is bonded to the strain gage with M-bond 200 adhesive and subjected to a thermal load due to the curing light source during a standard curing run.

4.4 Discussion

In this study the development of polymerization *versus* time is determined in terms of shrinkage and temperature rise. The typical shrinkage behaviour from the starting point of the polymerization reaction is shown in **Figure 21**. The figure shows how the composite expands in the first seconds. This is thermal expansion due to the temperature rise of the exotherm reaction and the curing light source. When the light is turned off — after 60 seconds — the expansion diminishes. In **Table VIII** the shrinkage strains after 290 seconds are listed for some commercially available materials. These linear shrinkage results are analyzed using the Scheffe's S multiple comparison procedure ($p < 0.01$). The results are shown in **Table IX**. The materials are ranked for their polymerization shrinkage from high to low, while bars group the materials that are not significantly different ($p < 0.01$).

The curing light source produces thermal expansion of the strain gage. The amount of thermal expansion depends on the light intensity that reaches the strain gage. This is illustrated in **Figure 22**, where the output of a bare strain

gage is compared with a strain gage that is covered by an unbonded composite sample. The strain output of the bare strain gage is about two times more than when it is covered by a sample. The heat transfer to the strain gage is achieved through the composite sample, and depends therefore on the translucency of the composite and the heat transfer characteristics of the composite. The temperature rise and drop after light shut off is gradual, because of the isolating effect of the covering sample. If the composite is bonded to the strain gage, the strain output will be mainly the result the thermal expansion properties of the composite.

Strain output is caused by at least three phenomena: polymerization shrinkage (S_c), thermal expansion of composite and strain gage due to the heat generated by the exotherm polymerization reaction (T_c and T_g respectively) and thermal expansion of composite and strain gage due to the high intensity curing light source (L_c and L_g respectively). The curing curve in **Figure 23** is the total strain output, which can be written as: $S_c + (T_c + T_g) + (L_c + L_g)$. To get the strain output ($L_c + L_g$) and L_g separately, a standard curing run is performed with the same cured composite bonded and unbonded on the strain gage, **Figure 23**. A standard run takes 5 minutes, and starts with 60 seconds light curing. The run with the cured composite sample does not contain the contribution of the polymerization shrinkage, depending on the amount of polymerization reached. Therefore the strain output shows the sum of the strain gage and the composite thermal expansion. The thermal expansion for the strain gage is determined by placing the same composite sample loose on the strain gage — in the same position as it had when it was bonded — and repeating the standard curing procedure. This provides the thermal expansion due to the curing light source for the strain gage only. This is achieved because the composite lies loose on the strain gage and shields the light from the light source in the same way as it did in the bonded position. Subtraction of the strain output due to the thermal expansion because of the curing light source ($L_c + L_g$) from the strain output of the total polymerization curing run ($S_c + (T_c + T_g) + (L_c + L_g)$), eliminates the strain output due to the curing light ($S_c + (T_c + T_g)$), **Figure 24**.

A closer look at the contribution to the thermal expansion strain output is obtained by **Figure 25**, which compares the thermal strain output due to the curing light for the bonded ($L_c + L_g$) and the not bonded (L_g) cured Z100 sample. The difference between them is the amount of the thermal expansion due the curing light heating of the composite sample only (L_c). This is only true if the strain output is a summation of the two contributions. It is likely that the influence of the strain gage thermal expansion diminishes during the polymerization reaction because the composite/strain gage elastic modulus ratio increases.

To investigate the saturation of curing, a standard curing run is carried out on a cured Z100 sample. This curing procedure is repeated five times for the same sample, **Figure 26**. The start time of the first run was 6 minutes after the start of the initial polymerization run, the additional runs are every time 6 minutes after start of the preceding one ($t_{i+1} = t_i + 6 \text{ min}$). This reveals additional curing. The strain curves are still declining after each curing run, but the rate is steadily diminishing. To further analyze the saturation of curing, curing runs are performed with two light sources with different light intensity, 400 and 500 mw/cm^2 , and are monitored for a period of 5 hours. The 500 mw/cm^2 light source results in the highest polymerization rate, compared to the 400 mw/cm^2 light source, see the enlargement in **Figure 27**. This figure also shows that the amount of the polymerization shrinkage after a fixed time depends on the light intensity of the curing light used. A higher curing light intensity shifts the peak of the polymerization reaction to an earlier point, the curve moves to the left. The polymerization contraction rate is also higher for about the first 15 seconds. The gain in polymerization shrinkage obtained during the first time of the reaction process is not recovered after 5 hours. The time *versus* strain curves for both curing light intensities remain parallel after the first 15 seconds. A reason for this behaviour can be the restrained mobility of the monomer chains and the free radicals after the solidification of the material. When the material is solidified in the first 15 seconds, the advantage of the higher number of free radicals produced by the higher light intensity is eliminated due to restricted mobility. Usually the appropriate light intensity work range for a curing light

source is considered to be between 300 and 500 mw/cm^2 . The results shown here indicate that this causes different polymerization shrinkage. Lower light intensities result in lower shrinkage values. Besides the intensity capacity of the curing light, other parameters effect the curing intensity, such as the distance of the light outlet probe to the composite and the translucency of the composite material.

The duration of the light curing will influence the shrinkage value, **Figure 28**. From this figure it can be concluded that light curing over more than 20 seconds has little effect on the polymerization shrinkage (500 mw/cm^2). When the composite is light cured for less than 20 seconds, the polymerization shrinkage is significantly lowered. If polymerization shrinkage is linearly corresponding to the degree of cure, this means that the highest possible degree for this curing light capacity is not reached before 20 seconds curing. This result and the observation made before about the polymerization shrinkage for different curing light intensities, indicate that high light intensity curing light sources are more important than extended light curing.

One of the basic assumptions when strain gages are used for shrinkage measurements, is the assumption that pre-gel shrinkage does not produce strain output. This assumption is verified with a Z100 resin without photo initiator, provided by 3M (St. Paul, USA). This resin is subjected to the same standard curing runs as the conventional Z100 resin. In **Figure 29** the thermal expansion due to the curing light source strain output for this (very slowly polymerizing resin) is compared for an uncured, a bonded cured and an unbonded cured sample. Although the cured resin has about two times higher strain output, the uncured composite has some strain output despite of the gel-state. This can be partly attributed to the thermal expansion of the strain gage. The strain output for a gel is further analyzed in **Figure 30**. Here the strain output due to the curing light for the uncured gel (A) is compared with the cured gel loose on the strain gage (B). Subtracting both effects (A-B) shows that the strain output starts after some delay after the curing light is turned on. This indicates that a large part of the strain reading is due to thermal

expansion of the strain gage. There will also be a minimal thermal expansion effect due to the exotherm polymerization reaction of the slowly curing gel, which will cause some strain output from the strain gage. And finally, even without the photo initiator, the Z100 sample will start polymerizing because free radicals are produced by the temperature rise when the sample is light cured. The occurrence and homogeneous appearance of the gel point cannot be determined in this experiment. Overall the assumption that shrinkage measurements by means of strain gages yield post-gel shrinkage seems reasonable.

Before the gel point a bonding of the composite to the strain gage is not necessary, because only post-gel shrinkage strain output is desired. The argumentation in the preceding paragraph showed that this requirement is satisfactory fulfilled. However, after the gel point a good bonding to the strain gage is required for accurate strain reading results. This requirement is verified here by comparing the strain output of the thermal expansion due to the curing light of a conventional Z100 sample, which is cured on the strain gage, with the same sample when it is bonded to the strain gage according to the manufacturers specifications. **Figure 31** shows the result of this comparison. The strain output for the samples which are bonded with M-bond 200 adhesive are between 10 and 15% lower than the naturally bonded Z100 samples. This can indicate some distortion of the strain gage because of a less than perfect natural bonding of the Z100 sample, but it can also be because of different thermal properties of the M-bond, which forms a layer between the composite sample and the strain gage. It is found that the quality of the bonding layer has a significant influence on the strain output, and generally increases the standard deviation (see Chapter 6, on the determination of the coefficient of thermal expansion).

4.5 Conclusion

The application of strain gages to measure the shrinkage strains, offers a simple method for the determination of significant material shrinkage data. The

strain gage method yields consistent shrinkage values and displays low standard deviation values. The resolution of the strain gage method is sub-micron; the signal is stable and almost without noise.

Strain gages seem to give a reasonable method for the determination of post-gel linear shrinkage of dental restorative composite materials. Strain gage readings during the light curing and the polymerization reaction contain a significant amount of thermal expansion of both the strain gage itself and the composite sample. This effect has no significant influence on the amount of shrinkage which is read out well after the start of the polymerization reaction, because the system is cooled down at that time. The polymerization shrinkage goes on for a long time before saturation is reached. This period seems independent of the intensity of the applied light curing. Curing with a lower light intensity, however, results in lower shrinkage. As a result the distance of the light probe to the sample, the sample height, the translucency and the light intensity are significant parameters in the determination of the linear shrinkage by means of strain gages.

The results of shrinkage measurements gain in value if they can be related to the environment where they cause shrinkage stresses, *i.e.* to the complex geometries of dental restorations and to filling procedures. This analysis shows that the curing light intensity plays an important role in the amount and rate of shrinkage. The most promising approach to gain an insight into the shrinkage stresses in these complicated structures and on the effect of different filling techniques on the resulting stresses, is a finite element analysis. In the finite element analysis the distance to the curing light source and resulting curing light intensity can be simulated. Also the temperature rise, the radiation through the composite, and the stress relief due to water absorption can be modeled. But, before a finite element analysis is possible, knowledge of the development of polymerization shrinkage stress (in order to calculate the elastic modulus) is required.

5 Polymerization stress development

5.1 Introduction

As is discussed in Chapter 4, after the gel-point and during the polymerization reaction, when the elastic modulus develops, shrinkage stresses are produced if the contracting composite is restrained (by geometry and/or surrounding cavity walls). Stress distributions in complicated tooth-restoration complexes can be assessed by the finite element method. The resulting strain, which is determined in that chapter, is coupled to those stresses by the well-known Hookes law for linear elastic material behaviour. Only strain ϵ , *i.e.* in essence displacement, can be measured directly. However, usually the most interesting factor is the stress σ . Notwithstanding their unique relation, in engineering stress terms are usually preferred for mechanical analysis rather than strain. Partly this may be attributed to the historical role and application of the stress parameter. Moreover a stress distribution reveals critical distributions more conveniently because material properties are integrated in the resulting stresses. Unfortunately, the stress parameter can only be measured indirectly, because it is a function of the strain and the elastic modulus E . During polymerization the strain (*i.e.* shrinkage) is not constant, and neither is the elastic modulus. The elastic modulus is an essential parameter to analyze stress distribution in dental structures of complex shapes by finite-element analysis. Determination of the elastic modulus has to be achieved by combining time-dependent stress and strain measurements. Shrinkage stress measurements of dental restorative composites are infrequently reported in literature. Some publications on polymerization stress development are BOWEN (1967), HEGDAHL AND GJERDET (1977), and BOWEN *et al.* (1983). FEILZER *et al.* (1987, 1993) performed axial stress development experiments, using cylindrical specimens in a stroke controlled test setup. However, it is questionable if the feedback control was really capable of correcting for sub-micron displacements. In this section a test setup is developed to measure axial stress development, featuring a more

straightforward test setup than that reported by FEILZER *et al.* (1987). The results are corrected for the finite compliance of the load cell.

5.2 Materials and methods

The test setup comprises a stiff steel frame, which holds a high-precision low-compliance semi-conductor load cell (Model 41/8619-01, Sensotec Incorporated, Columbus, OH), and two steel rods between which the composite sample is placed, **Figure 32**. The mountings consist of a steel rod with a composite head, attached at one end of the rod, **Figure 33**. The composite mounting heads are made of Z100™ (3M, St. Paul, MN). The purpose of this composite head is to get a good connection between the sample and the steel parts. Bonding between the sample and the precured composite mounting-head is achieved using an air-thinned layer of bonding agent (Multi-Purpose Adhesive, Scotchbond™, 3M, St. Paul, MN). The bonding layer is precured for 10 seconds. It is assumed that the influence of the bonding layer on the test results is negligible. Some of the precured composite mounting-heads are connected to the steel mounting rod, using only mechanical retention. The other precured composite mounting-heads are also chemically connected to the steel mounting rod by a porcelain bond (Light Cure Dental Adhesive, Scotchbond2™, Scotchprime™, 3M, St. Paul, MN). Here it is assumed that the whole frame is extremely stiff, compared to the composite material. As a first approximation the deflection of the composite mounting heads is also not considered. To be able to distinguish the white composite sample from the two composite mounting heads and to measure the cylinder length afterwards, the composite of the mountings is colored by mixing it with some methylene blue.

A Targa non-contact dimensional gaging system with a non-contact capacitance transducer (Model PX305HA, Lion Precision, Minneapolis, MN) is used to measure the load-cell compliance during the polymerization for correction of the axial shrinkage stress output. The target of the capacitance transducer is a grounded gold-coated brass plate.

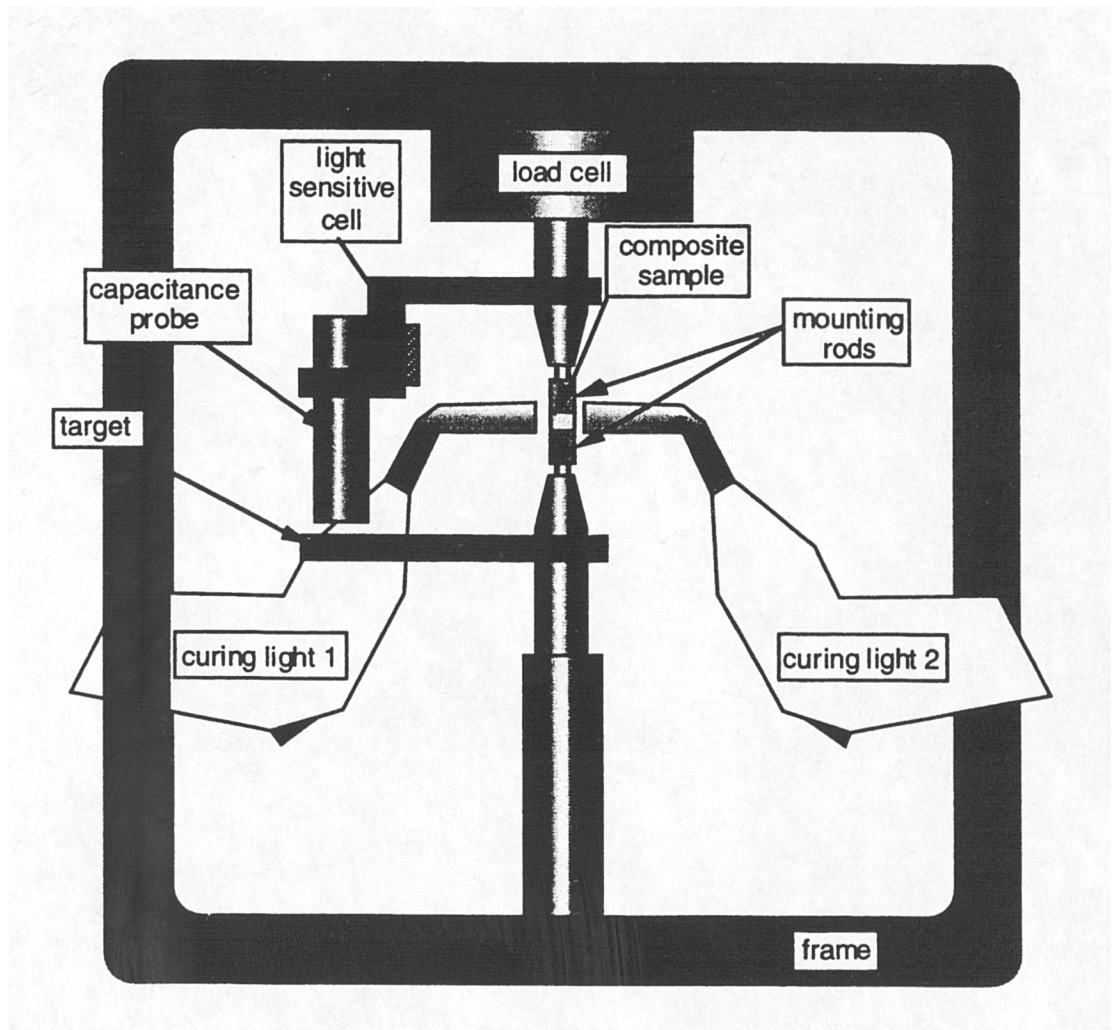


Figure 32. Experimental setup for polymerization stress measurements.

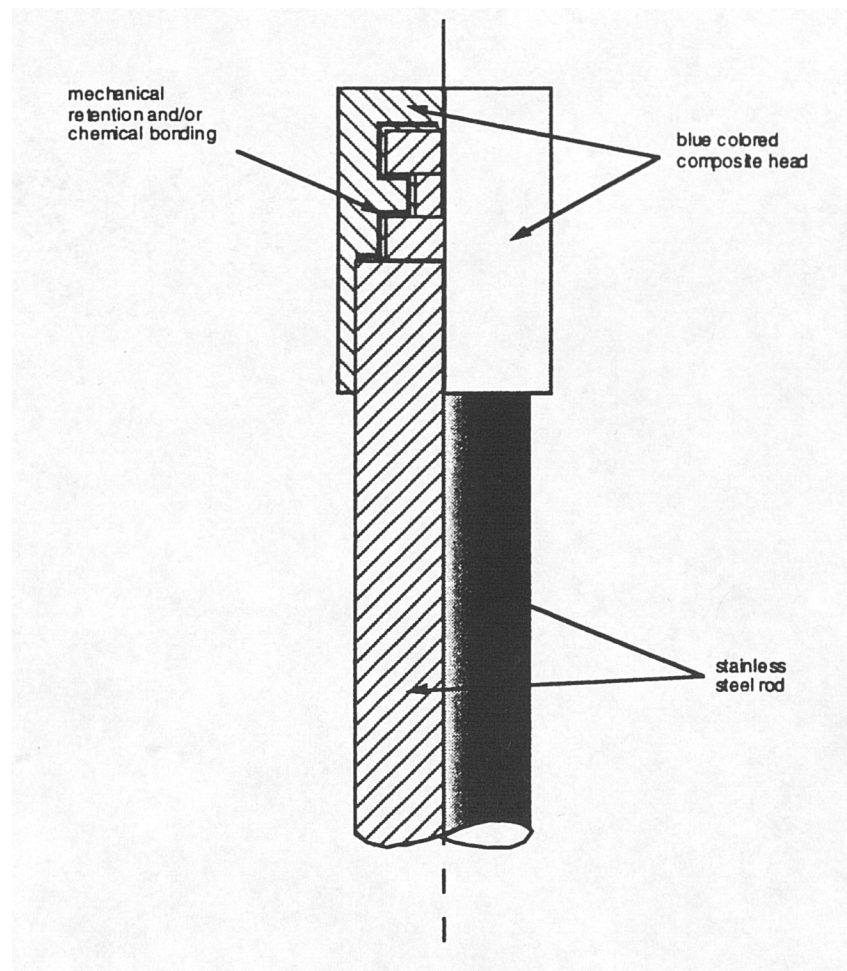


Figure 33. Mounting rod.

Table X. Materials used for shrinkage stress experiments.

Material	Manufacturer	Shade	Batch no.
Z100	3M	A3	5702U(3BJ)
Herculite XR	Kerr	U	24240
Silux Plus	3M	U	5904A3(2BF)

The experiments are carried out in a dark room in order to prevent premature curing of the light sensitive materials. The curing light is shielded until the full light intensity is reached. This is done to improve the repeatability of the experiment. As explained in Chapter 4, there is an initial delay in curing source light intensity. The cylindrical specimen is simultaneously cured from two sides, the outlet of the light probes at 1 mm distance from the specimen. The exact start and end of the light cure is recorded by a light sensitive cell. The specimens in this experiment have a larger cross section than in Chapter 4. In order to make sure that the samples are thoroughly cured, the curing time is extended to 2 minutes (was 1 minute in Chapter 4). The effect of a longer exposure (1 minute *versus* 2 minutes) to the curing light does not alter the polymerization shrinkage, according to the findings in Chapter 4. Two runs are carried out for each specimen, first the *curing* run and second an additional run with the *cured* material in the same position.

The conditioned stress and displacement readings and the voltage output of the light sensitive cell are acquired through an analog-digital converter and stored on a desk-top computer, along with time.

Three different visible light curing composite materials are tested, two hybrids (Z100TM, 3M; Herculite XRTM, Kerr) and one microfilled (Silux PlusTM, 3M) composite, **Table X**. Five samples for each material are tested with only mechanical retained composite mountings, and 10 samples for each material are tested with mountings that are also chemically connected. The cylindrical specimens are shaped according to the diameter of the mountings (\varnothing 4.14 mm), with a typical length of 2-3 mm. The exact dimensions of each specimen are measured after each experiment.

Besides the polymerization stress development experiments, also the linear shrinkage is determined for these three materials. Material properties of dental restorative composites can vary significantly from batch to batch. Therefore the linear shrinkage is determined for the same batch materials as the composites used for the stress development measurements. The test method is discussed in

detail earlier in Chapter 4. The linear shrinkage data will be used in the next section, where the integration of all polymerization parameters is analyzed.

5.3 Results

As illustrated in **Figure 34**, tests carried out using the mountings which are only mechanically retained, tend to result in lower polymerization forces and relaxation. For the both mechanically and chemically connected mountings, however, the polymerization stress increases slightly, or stays constant after light curing. Therefore only the results of the latter will be considered further.

In **Figure 35** the average stress *versus* time curve is shown for all three composites. The thermal expansion effect of the curing light source turns out to temporarily relieve more than 40% of the final shrinkage stress. The axial polymerization stress is calculated using the expression:

$$\sigma = \frac{F}{K A}$$

where: σ is the axial polymerization stress

F is the axial polymerization force

K is the geometric constraint correction factor

A is the cross sectional surface area

The geometric constraint factor can be defined and calculated as follows. The expression for axial stress:

$$\sigma = E\varepsilon$$

which is true for infinitely long rods, *i.e.* only uniaxially stressed. For finite rods, as the cylindrical specimens used in this polymerization stress experiment, the fixed ends of the cylinder restrain the radial component of the strain. This restriction at both fixed ends increases the axial stress in the cylinder. Therefore the actual expression for the axial stress becomes:

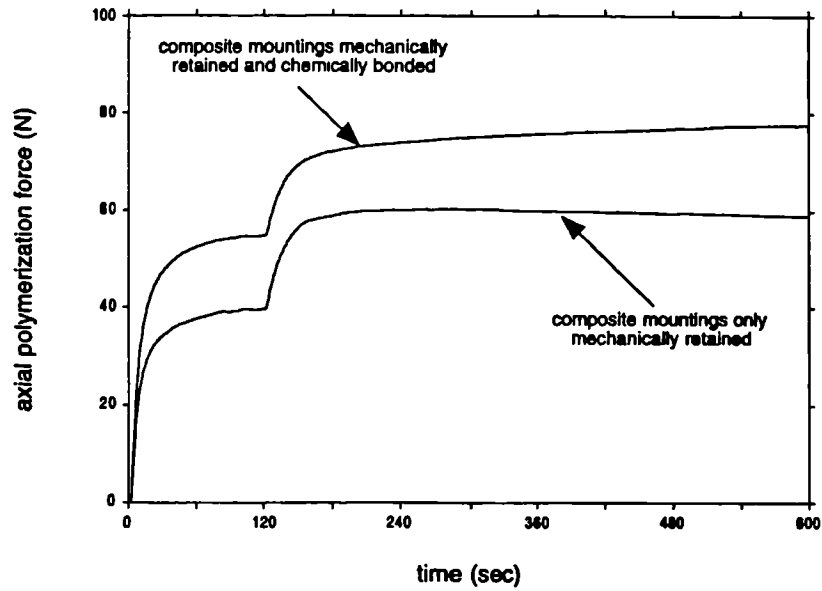


Figure 34. Comparison of polymerization force results for tests carried out with composite mountings which are only mechanically retained and tests carried out with mountings which are both mechanically and chemically connected.

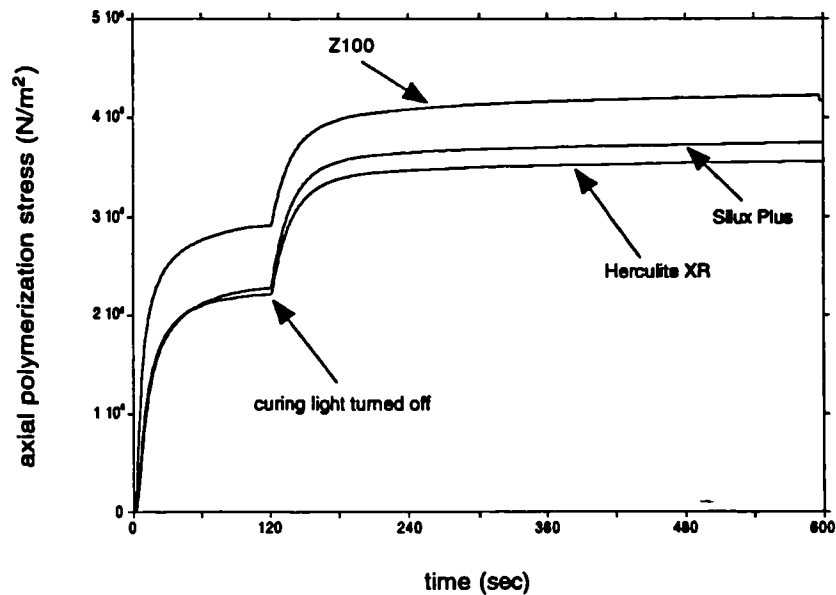


Figure 35. Polymerization shrinkage stress development for Z100, Herculite and Silux Plus.

$$\sigma = K E \epsilon$$

where K is the geometric constraint factor, which is a function of the length-radius ratio. The relationship between the axial stress and the length-radius ratio is examined by means of a finite element simulation. A rod is modeled in a 2-D axisymmetric mesh. The rod is clamped at one side, while the displacement is fixed in cross sections at several intervals over the length of the rod. The rod is shrunk by a temperature decrease. Incrementally a fixed cross section is released while the reaction force is calculated at the clamped side of the bar. Each incremental situation represents an increased rod length. An infinitely long rod is simulated by unrestricted radial displacement at both ends of the rod. The result of the geometric constraint for different length-radius ratios is displayed in **Figure 36**. If the length-radius ratio L/R is lower than 2, the geometric constraint factor K can be estimated by:

$$K = 1.0 + 1.44 e^{-\frac{10}{9} \frac{L}{R}} \quad \text{if} \quad \frac{L}{R} < 2$$

The results of the averaged polymerization stress measurements for all three materials are collected for several time intervals (5, 10, 15, 20, 30, 60, 90, 120, 180, 300, 600 seconds) in **Table XI**. Some of the specimens showed the same gradual relaxation of stress as described before for the tests with only mechanically retained mountings. These specimens are excluded, because this behaviour is attributed to a bad chemical bonding. Therefore the sample size for Z100 is 8, for Herculite is 7, and for Silux Plus remains at 10 valid samples. In **Table XII** the time given for the three composites to reach a certain percentage (0, 10, 20, 30, 40, 50, 60, 70, 80, 90, 100, 110, 120, 130, 140, 150, and 160%) of the polymerization stress at the end of the light curing (120 seconds).

The first part of the development of polymerization stress is enlarged in **Figure 37**. This figure shows the appearance of pre and post-gel. The gel-point for Z100 happens after 1.5 seconds, and for Silux Plus and Herculite XR after about 2 seconds.

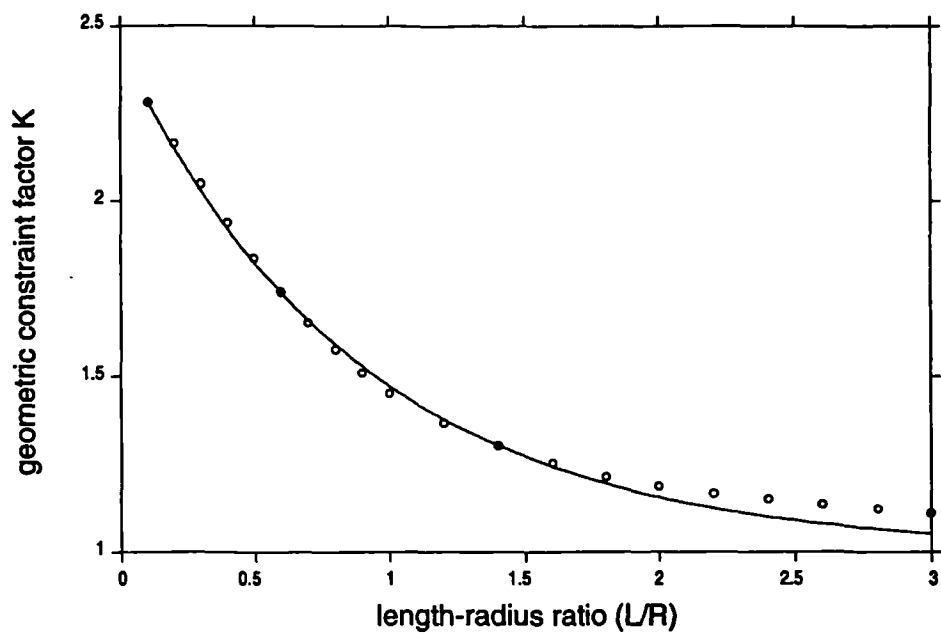


Figure 36. Geometric constraint factor K as function of the length-radius ratio L/R for a cylindrical specimen.

Table XI. Development of polymerization stress for three materials: Z100 (n=8), Herculite XR (n=7), and Silux Plus (n=10).

Time (sec)	Axial polymerization stress (MPa)		
	Z100	Herculite XR	Silux Plus
0	0	0	0
5	0.79 ± 0.08	0.30 ± 0.03	0.20 ± 0.03
10	1.65 ± 0.11	0.94 ± 0.05	0.82 ± 0.11
15	2.04 ± 0.13	1.32 ± 0.07	1.24 ± 0.16
20	2.26 ± 0.15	1.55 ± 0.09	1.50 ± 0.20
30	2.49 ± 0.16	1.82 ± 0.12	1.79 ± 0.26
60	2.76 ± 0.18	2.10 ± 0.16	2.11 ± 0.31
90	2.87 ± 0.19	2.18 ± 0.17	2.23 ± 0.31
120	2.91 ± 0.19	2.22 ± 0.18	2.28 ± 0.32
180	3.98 ± 0.18	3.38 ± 0.26	3.55 ± 0.36
300	4.14 ± 0.19	3.50 ± 0.29	3.69 ± 0.36
600	4.22 ± 0.21	3.56 ± 0.29	3.75 ± 0.38

Table XII. Percentage of polymerization stress at the end of light curing (120 seconds) for Z100, Herculite XR and Silux Plus.

Percentage of polymerization stress at end of light curing (%)	Time (sec)		
	Z100	Herculite XR	Silux Plus
0	0.0	0.0	0.0
10	3.2	4.4	5.4
20	4.2	5.9	7.0
30	5.4	7.6	8.9
40	6.5	9.4	11.0
50	8.5	11.9	13.5
60	11.0	15.0	17.3
70	15.0	20.0	22.5
80	22.5	27.5	31.5
90	39.5	43.0	50.5
100	120.0	120.0	120.0
110	126.8	125.0	124.5
120	134.5	129.5	128.5
130	149.5	135.5	133.5
140	230.0	145.0	141.7
150		166.0	156.5
160		480.5	239.5

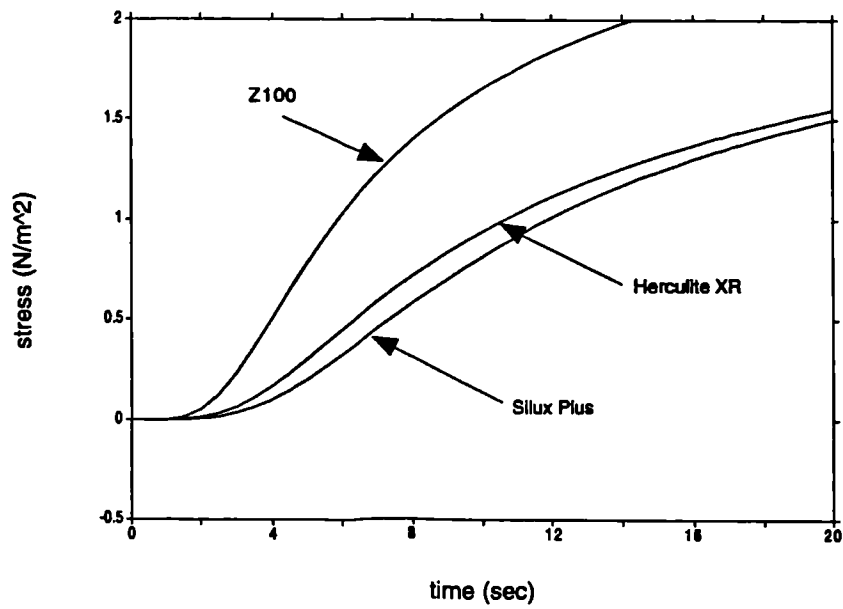


Figure 37. First 20 seconds polymerization stress development for Z100, Herculite XR and Silux Plus.

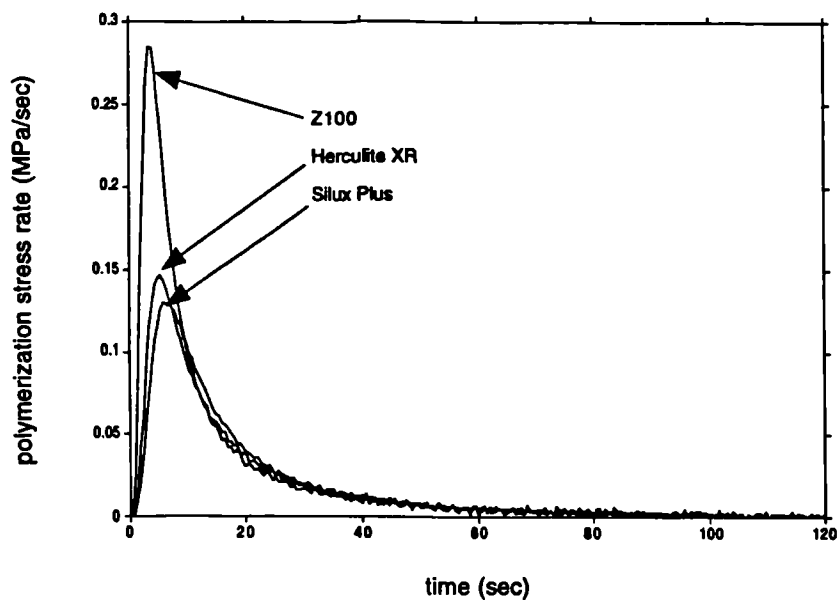


Figure 38. Polymerization stress rate in the first 120 seconds for Z100, Herculite XR and Silux Plus.

The shrinkage rate for the three materials is displayed in **Figure 38**. Except for the first 20 seconds, the polymerization stress rate for all three materials is almost identical. The peak rate and time of occurrence after the start of the polymerization reaction, is listed in **Table XIII**.

5.4 Discussion and conclusions

When a dental restorative composite paste is light cured, free radicals are created. These free radicals start cross linking monomers into polymer molecules. At one point in this process the gel will develop such an amount of cross linking, that the composite is no longer able to compensate density differences by flow. The composite becomes immobile and as a result starts to develop polymerization stresses. This gelation-point may not be sharply defined, because it depends on the homogeneity of the polymerization process. The elastic modulus of the solidified composite develops after the gel-point. In **Figure 37** the occurrence of the gel-point appears within 2 seconds after the start of polymerization (Z100: 1.5 seconds; Herculite XR: 2 seconds; and Silux Plus: 2.5 seconds).

When the gel-point is passed, and the polymerization stress starts to buildup, several observations can be made.

Although Silux Plus (microfine composite) exhibited less post-gel shrinkage (Chapter 4) and generally has a lower elastic modulus than hybrid composites, Silux Plus turns out to yield almost the same high polymerization stress as Herculite XR, which is a hybrid composite (**Table XI**). Shrinkage strain measurements carried out for the same batch numbers as the three investigated materials, point out that for this Silux Plus batch the shrinkage is much higher than the linear shrinkage reported earlier for this microfine material. It is not clear if the Silux Plus used for the polymerization stress experiments, can be considered as a typical microfine composite. Therefore no comparisons and conclusions will be made out of these data about polymerization stress development of microfine and hybrid composites.

Table XIII. Stress development peak rate and occurrence of peak rate after start of polymerization reaction.

Material	Polymerization stress development	
	peak rate	time of peak rate
	(MPa/sec)	(sec)
Z100	0.285	3.5
Herculite XR	0.145	5.5
Silux Plus	0.130	6.5

In **Table XIII** the peak rate and time of the peak after the start of the polymerization reaction is listed for Z100, Herculite XR and Silux Plus respectively. The peak rate for Z100 is twice as high and is reached almost twice as fast after the start of the polymerization reaction as the two other composites. Comparison of these times with the exotherm peak times, shows that the peak of the stress development rate practically coincides with the occurrence of the exotherm peak, which indicates the top activity of the polymerization reaction process. After 20 seconds the polymerization stress rate for all three materials is identical, suggesting that the polymerization reaction is practically over. Regarding the extremely steep rate, especially for Z100, it turns out that the main polymerization reaction takes place within the first 10 seconds. All additional curing can be considered as post-curing. A possible reason for this phenomenon is that the amount of free radicals initiated by the curing light decreases. Furthermore the mobility of these free radicals and the opportunity of establishing cross linking will decrease when the composite solidifies more. Looking at the percentage of the polymerization stress in **Table XII**, 50% of the polymerization stress at the end of light curing (120 seconds) is reached in 8.5, 11.9, and 13.5 seconds for Z100, Herculite XR, and Silux Plus respectively. And 90% is reached after 39.5, 43.0, and 50.5 seconds respectively. Note that the main part of the increase of the polymerization stress after 120 seconds (100% level) is due to the termination of thermal expansion, because the curing light is shut off after 120 seconds.

The thermal expansion effect of the curing light compensates for the polymerization contraction in part as long as the curing light is turned on. This decreases the polymerization stress as much as 40-60% (Z100: 45%; Herculite XR: 61%; Silux Plus: 65%). For Z100, which has a lower coefficient of thermal expansion than Herculite XR and Silux Plus, the effect of the curing light source is lower. The coefficients of thermal expansion for the three materials are 22.5, 32.6, and 41.1 $10^{-6}/^{\circ}\text{C}$, for Z100, Herculite XR, and Silux Plus respectively (Chapter 6).

Aim of this chapter is to gain insight into the development of shrinkage stresses, which are induced by the maturing elastic modulus, and therefore provide essential information about the modulus development. As already mentioned in the introduction, the modulus is required to calculate the stress distribution in a complicated tooth-restoration system by means of the finite element method. As is seen in both the polymerization strain and stress experiments, thermal phenomena have an apparent influence on their dynamic behaviour. In the next chapter the temperature effects will be investigated in order to understand and to correct for them.

6 Temperature effects

6.1 Introduction

During polymerization of dental restorative composite materials, three physical external effects can be observed: hardening, shrinkage and temperature rise. While the first two effects are permanent, the third effect is temporary, and a result of the chemical process itself. The polymerization reaction starts when free radicals are formed by a photo initiator, which reacts on an intensive light source in a specific band width. During the polymerization reaction free radicals link monomer molecules, forming polymers. This chain and bridge (or cross link) forming causes the development of enhanced structural integrity of the composite, manifested in the development of stiffness. Another result of the creation of polymers is volumetric shrinkage, which is due to the higher density of the polymerized resin. Because the polymerization reaction is exothermic, heat will be generated. This temperature increase causes a temporarily volumetric expansion, which counteracts the polymerization shrinkage. During the first few seconds the thermal expansion is even higher than the polymerization contraction (see Chapter 4). The two parameters that control the amount of thermal expansion are (1) the temperature and (2) the coefficient of thermal expansion. In order to gain insight into and account for the effect of the temperature on the volumetric changes of composite materials during polymerization, these two parameters have to be determined.

Apart from a better understanding of the volumetric changes during the polymerization process, the evaluation of exotherm temperature rise also gives an impression of the character of the polymerization reaction for different resins. Therefore dynamic exothermic temperature measurements can show differences in polymerization properties between various composite materials.

Within the broad field of biomechanics, this study is focused on the origin and development of internal stresses in composite-tooth systems during the

polymerization reaction. However, thermal expansion due to frequent temperature changes in the oral environment are also a source of non functional internal stresses and will therefore also be considered briefly.

Several attempts have been undertaken to measure the *in vivo* temperature range. SPIERINGS *et al.* (1987) report a 14° to 56°C range, and PALMER *et al.* (1992) suggest a range of 0° to 67°C. In both publications the extreme temperatures are achieved by cold and hot drinks. Although the significance of the thermal expansion on the marginal integrity is questioned by ASMUSSEN AND JØRGENSEN (1978), the temperature induced volumetric change is generally associated to marginal leakage of composite restorations (POWERS *et al.*, 1979; MOMOI *et al.*, 1990), possibly leading to secondary caries and postoperative sensitivity. BULLARD *et al.* (1988) found a strong correlation between microleakage and the coefficient of thermal expansion, therefore they named this the leading factor in microleakage. Another effect of volumetric changes of composite restoration materials is the introduction of stresses in the tooth-composite bond and the surrounding tooth tissues. This attacks not only the tooth-restoration bonding, but it is also suggested that the thermal expansion is related to cracking of the tooth (HENCHANG *et al.*, 1989), chip fractures (LAMBRECHTS *et al.*, 1982) and wear (SODERHOLM, 1984). Therefore it is desirable that restorative composite materials exhibit thermal volumetric changes which are approximately the same as for the tooth material, in order to reduce the misfit. The amount of volumetric change is given by the coefficient of thermal expansion. For composite materials this coefficient ranges from 20-80 $10^{-6}/^{\circ}\text{C}$, for the tooth, it is about 17 $10^{-6}/^{\circ}\text{C}$ for enamel, and about 11 $10^{-6}/^{\circ}\text{C}$ for dentin (HENCHANG *et al.*, 1989).

The coefficient of thermal expansion has been determined using several test methods, such as a thermomechanical analyzer (POWERS *et al.*, 1979, VAIDYANATHAN *et al.*, 1992), a differential dilatometer (HASHINGER AND FAIRHURST, 1984), or a bimaterial strip (*e.g.* in the form of a split ring) (SCHERER, 1987). In this chapter a new test method, employing bonded strain

gages, is described for the determination of the coefficient of thermal expansion of some modern commercial composites.

Strain gages have been used previously in Chapter 4 for the determination of post-gel polymerization shrinkage. Strain gages are very accurate, they can measure sub-micron dimensional changes. In this chapter strain gages are used to measure the linear dimensional change along with temperature, following the same methodology as in the shrinkage measurements.

6.2 Materials and methods

The composite materials for which the exotherm temperature rise and the coefficient of thermal expansion is determined are commonly available restorative composites, and are shown in **Table XIV**. Ten composite resins are tested in the exotherm experiments, and seven for the evaluation of the thermal expansion. The sample size for each composite is five in both experiments.

The temperature during the tests is measured by means of a high response 0.5 mm (0.020") thin grounded copper-constantan sensor (TMTSS-020G-6, OMEGA).

- a. *Exotherm temperature determination* — The samples are 1.5 mm high, and the curing light probe (Visilux™2, 3M) is positioned 2 mm above the sample, and yields a light intensity output of 400 mw/cm². The tip of the sensor is immersed into the composite, at the bottom of the sample, **Figure 39**. The stage of immature light intensity is omitted by means of a shield, as is described in Chapter 4. The point at which the composite material is subjected to the curing light is registered by a light sensitive cell. The total-light curing time is 60 seconds. Because two heat sources exist during the polymerization reaction (exotherm and curing light), the curing procedure for every test run is repeated with the already cured composite sample in order to obtain by subtraction the temperature rise due to the curing light source only. (It is assumed that thermal properties of cured and uncured composites are the same.)
-

Table XIV. Materials investigated in this chapter.

Material	Manufacturer	Shade	Batch no.	Experiment
APH	Caulk	U	061289	ex [*] /th ^{**}
Conquest	Jeneric/	A2	2909921	ex
	Pentron	B1	2019511	ex/th
		Opaque	2019201	ex
Durafill	Kulzer	C	026	ex
Heliomolar	Vivadent	YB	466401	ex/th
Herculite XR	Kerr	U	9_2118	ex/th
P50	3M	Y	9CD4D	ex/th
Silux Plus	3M	DY	9CA1	ex/th
Z100	3M	P	2AA	ex/th

* ex = exotherm temperature development

** th = coefficient of thermal expansion

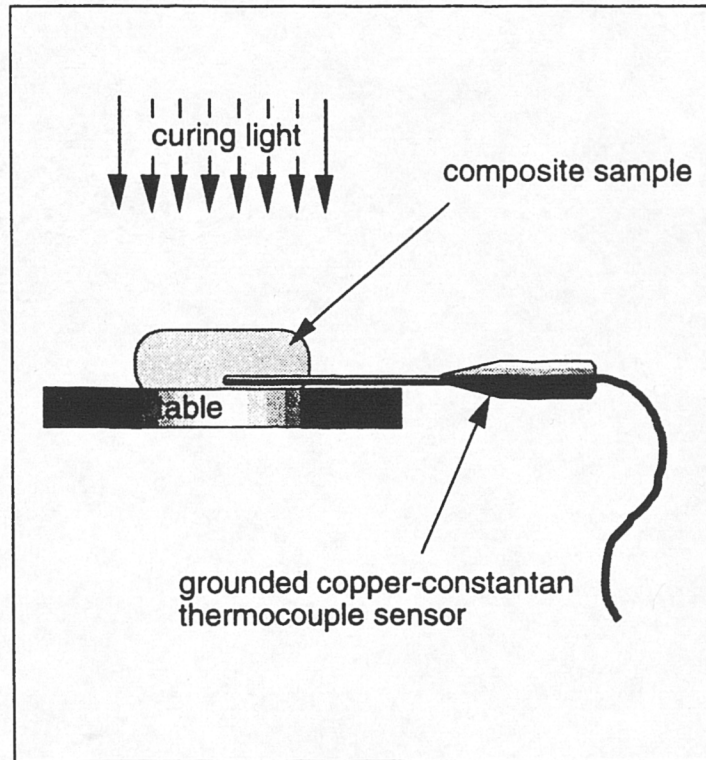


Figure 39. Positioning of the thermocouple sensor in the composite sample during the exotherm temperature measurements.

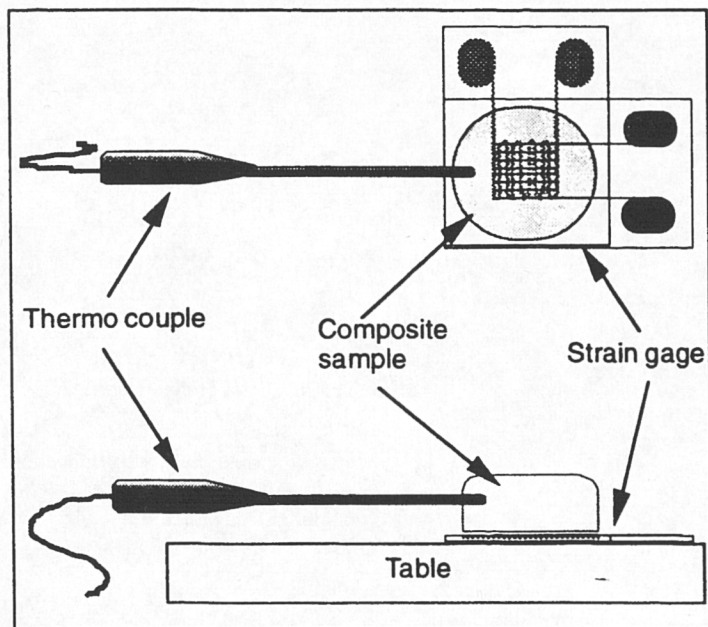


Figure 40. Positioning of the thermocouple tip in the composite, the composite on the strain gage, and the strain gage unrestrained on a table during the experimental determination of the coefficient of thermal expansion.

b. *Coefficient of thermal expansion* — The experiments are carried out in a mechanical convection oven (GCA Corporation). The temperature is controlled between approximately 26°C room temperature and 75°C. The thermocouple-tip is placed in composite sample, in order to read the actual temperature of the composite substance, **Figure 40**. The 2.5 mm thick composite samples are placed on top of a biaxial strain gage (CEA-06-032WT-120, Measurements Group Inc.) and the tip of a thermocouple is placed 1 mm into the composite at about 1.5 mm height, measured from the strain gage surface. In order to assure a high degree of polymerization, the composite samples are light cured for 2 minutes with a 500 mw/cm² curing light source (Visilux¹⁴², 3M), whereby the light probe is positioned about 1 mm above the sample. The strain gage with the composite sample on it is unrestricted in its movements, so that no other strains other than the thermal expansion are introduced during the temperature cycling. Each sample is thermo-cycled 3 to 7 times. The runs are numbered, starting with 0 for the first thermo-cycle run after light cure polymerization. Each run lasts 5 minutes. The data is collected only during the temperature increase. For the Z100 material five samples are bonded to the strain gage, according to the requirements of the strain gage manufacturer, with M-Bond 200 (Measurements Group Inc., Raleigh, USA), in order to compare the results with five samples which are naturally bonded. Natural bonding is established during the polymerization of the composite on top of the strain gage. The specimens bonded with M-bond showed higher standard deviation, and the difference between both methods was not significant (Scheffe's S-test, $p < 0.001$). Therefore all the other samples are naturally bonded to the strain gages.

All the readings (temperature, curing light detection, and/or strain output) are collected at 2-5 Hz, and stored on a desktop computer (Macintosh IICI, Apple), equipped with a 12-bit A/D-board. The output from the strain gage and the thermocouple is conditioned in a strain conditioner (Measurements Group Inc., Raleigh, USA). The analog thermocouple output is connected to the strain conditioner via an adapter (1611 Thermocouple Adapter, Measurements Group Inc.), an amplifier and a DC/DC converter (Model 1611-A25, Measurements Group Inc.).

6.3 Results and discussion

- a. *Exotherm temperature rise* — The results of the exotherm temperature rise measurements are listed in **Table XV**. The temperature values represent the peak values of the exotherm polymerization reaction and the time values give the time at which these peak values are reached after the start of the polymerization reaction. **Figure 41** is a typical temperature *versus* time plot, which shows the temperature changes during the first period of the polymerization, and the two different factors that are contributing to the temperature rise. Under the assumption that the total temperature can be regarded as a summation, the temperature change due to the curing light source is subtracted from the total temperature change during the polymerization reaction. The peak temperatures and the time they are reached after the start of the polymerization reaction, are graphically shown in **Figure 42**. The occurrence and magnitude of the peak temperature is a characterization for the polymerization reaction. Thus the development of polymerization *versus* time is determined in terms of temperature rise. High polymerization temperatures indicate a high amount of polymerization. A short time to reach these temperature peaks indicates a fast polymerization reaction. Materials such as Z100 (3M) and Herculite XR (Kerr) exhibit a faster and more intense polymerization reaction than for example Conquest. The peak temperature and the peak time results are analyzed using the Scheffe's S multiple comparison procedure ($p < 0.01$). The results are shown in **Tables XVI** and **XVII**. This comparison shows that Z100 and Herculite XR are snap-set type of composites, compared to Conquest which is at the other side of the balance.
 - b. *Coefficient of thermal expansion* — Because the apparent strain (no stress-free dummy gage can be installed for this setup) and the gage factor are temperature dependent, a correction has to be made for these errors on the strain output of the strain gage.
-

Table XV. Exotherm polymerization peak temperatures and time of the peak temperature after start of polymerization.

Material	Batch no.	Temperature (°C)	Time (sec)
APH	061289	5.1 ± 0.7	4.6 ± 0.7
Conquest	2909921	4.0 ± 1.1	11.1 ± 1.0
	2019511	5.2 ± 0.8	10.9 ± 1.0
	2019201	3.5 ± 0.3	9.1 ± 0.8
Durafill	026	4.1 ± 0.2	6.2 ± 1.4
Heliomolar	466401	4.0 ± 0.4	6.2 ± 1.4
Herculite XR	9_2118	7.4 ± 0.4	4.8 ± 0.3
P50	9CD4D	3.7 ± 0.6	6.3 ± 0.3
Silux Plus	9CA1	3.0 ± 0.6	7.2 ± 1.6
Z100	2AA	6.9 ± 0.4	3.8 ± 0.4

Note: curing light temperature is subtracted from total temperature,

$$\Delta T_{\text{polymerization}} = \Delta T_{\text{polymerization+curing light}} - \Delta T_{\text{curing light}}$$

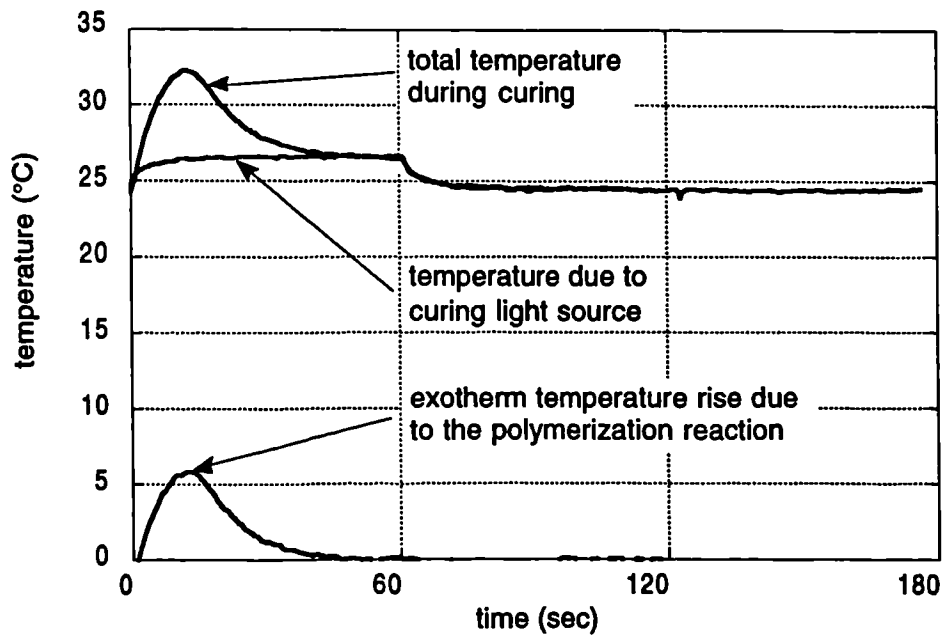


Figure 41. Temperature changes during the first 3 minutes of the polymerization process for a typical composite.

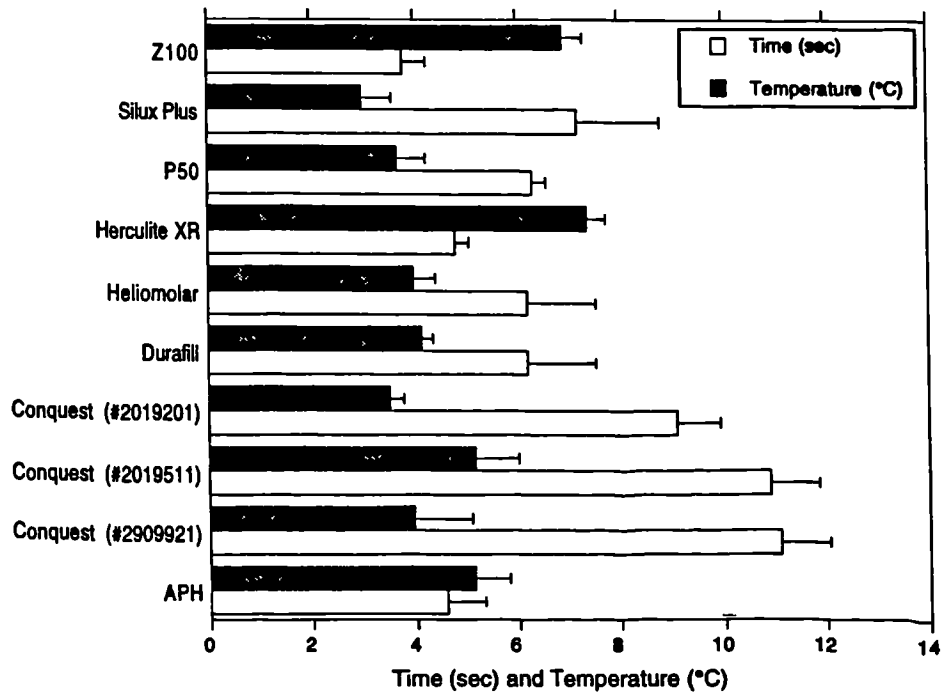


Figure 42. Peak values of the exotherm polymerization temperature (°C) and elapsed time (sec) after start of the reaction.

Table XVI. Scheffe's S multiple comparison test on the peak temperature data ($p < 0.01$).

Scheffe's S
Effect: material
Dependent: temperature ($^{\circ}\text{C}$)
Significance level: .01

	Count	Mean
Silux Plus	5	3.007
Conquest (#2019201)	5	3.519
P50	5	3.669
Conquest (#2909921)	5	3.973
Heliomolar	5	3.976
Durafill	5	4.137
APH	5	5.148
Conquest (#2019511)	5	5.164
Z100	5	6.926
Herculite XR	5	7.377

Table XVII. Scheffe's S multiple comparison test on the peak time data ($p < 0.01$).

Scheffe's S
Effect: material
Dependent: time (sec)
Significance level: .01

	Count	Mean
Z100	5	3.800
APH	5	4.600
Herculite XR	5	4.800
Heliomolar	5	6.200
Durafill	5	6.200
P50	5	6.300
Silux Plus	5	7.200
Conquest (#2019201)	5	9.100
Conquest (#2019511)	5	10.900
Conquest (#2909921)	5	11.100

The strain read-out can be corrected (Tech Note TN-504: Temperature-induced apparent strain and gage factor variation in strain gages. Measurements Group Inc., Raleigh, NC, USA, 1983) by use of the following relation:

$$\epsilon_1 = \left(\epsilon_{1_{ii}} - \epsilon_{APP}(T_1) \right) \frac{F^*}{F(T_1)}$$

where:

ϵ_1 is the strain magnitude corrected for both apparent strain and gage factor variation with temperature

$\epsilon_{1_{ii}}$ is the indicated strain, uncorrected for either apparent strain or gage factor variation with temperature

$\epsilon_{APP}(T_1)$ is the apparent strain at temperature T_1

T_1 is the test temperature

F^* is the gage factor setting

$F(T_1)$ is the gage factor at test temperature

$$F(T_1) = F_0 \left(1 + \frac{\Delta F(T_1)}{100\%} \right)$$

where:

F_0 is the room temperature gage factor

$\Delta F(T_1)$ is the deviation at test temperature from room temperature gage factor

The apparent strain $\epsilon_{APP}(T_1)$ at temperature T_1 is given in the Engineering Data Sheet which comes with the strain gages, **Figure 43**.

For a strain gage used here (CEA-06-032WT-120, Lot Number A38AD679) the polynomial representation is:

$$\epsilon_{APP}(T_1) = -24.0 + 2.33 T - 6.18 \times 10^{-2} T^2 + 3.44 \times 10^{-4} T^3 - 4.22 \times 10^{-7} T^4 \text{ (}^\circ\text{C)}$$

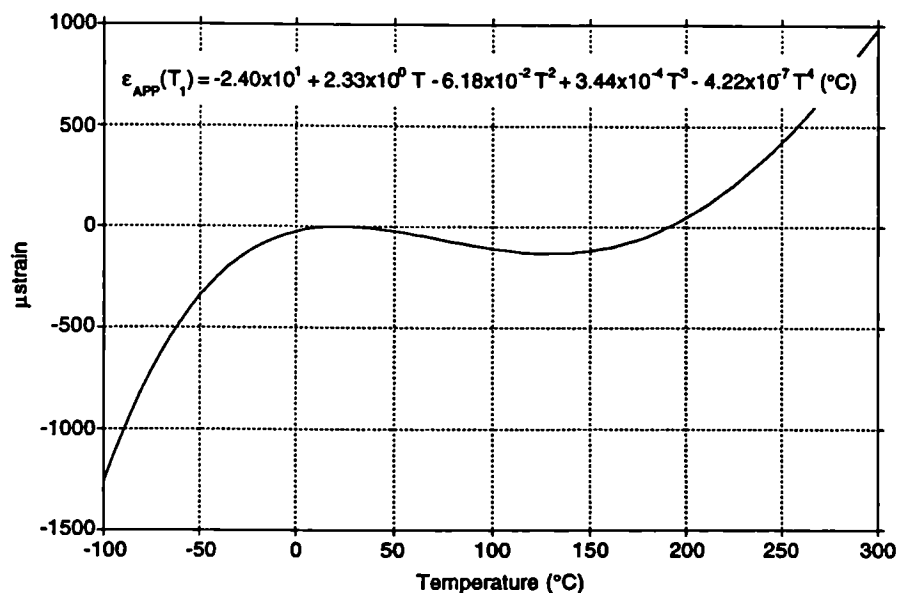


Figure 43. Apparent strain relation for CEA-06-032WT-120 (Lot Number A38AD679).

Table XVIII. Coefficient of thermal expansion for seven composite materials for the subsequent thermo-cycle runs (run 0 is the first run after light curing), obtained by Linear Least Squares Fitting ($R > 0.99$).

Material	Coefficient of thermal expansion ($10^{-6}/^{\circ}\text{C}$)					
	run 0	run 1	run 2	run 3	run 4	run 5
APH		34.1±1.8	32.4±1.7	31.5±1.2		
Conquest		35.4±1.4	33.9±1.2	32.1±1.0		
Heliomolar	45.4±1.8	44.7±1.2	42.9±1.3	42.3±1.1		
Herculite XR		32.6±1.6	30.9±1.1	30.0±0.8		
P50		23.5±1.4	22.1±1.0	21.4±0.6	19.8±0.7	19.3±0.6
Silux Plus	44.1±1.1	41.6±1.5	41.1±1.3	40.3±0.9		
Z100		22.5±1.4	21.7±1.1	20.7±0.8		

Also obtained from the Engineering Data Sheet are:

$$F_0 = 2.05, \text{ which is the gage factor at } 24^\circ\text{C}$$

$$\Delta F(T) = \frac{+0.7\% \pm 0.2\%}{100^\circ\text{C}} T - 0.168\% = 0.007\% * T - 0.168\%$$

The gage factor setting is: $F^* = 2.00$.

The thermal expansion coefficient α can be calculated from the temperature corrected thermal expansion strain by:

$$\alpha(T) = \frac{d\varepsilon}{dT} \left(\frac{1}{^\circ\text{C}} \right)$$

or, when the thermal expansion coefficient is constant with temperature:

$$\alpha = \frac{\varepsilon_2 - \varepsilon_1}{T_2 - T_1} = \frac{\Delta\varepsilon}{\Delta T} \left(\frac{1}{^\circ\text{C}} \right)$$

This last assumption is reasonable in the considered temperature range for the composites used in this study, considering the high degree of linearity of the temperature *versus* strain curve, obtained by the Linear Least Squares Fit ($R > 0.99$).

The results of the temperature and strain readings are shown in **Table XVIII**, which shows the mean values for the coefficient of thermal expansion ($10^{-6}/^\circ\text{C}$) and the standard deviation for each run.

In several publications it is reported that the determined coefficient of thermal expansion for the first and the subsequential thermo-cycling run changes (POWERS *et al.*, 1979; HASHINGER AND FAIRHURST, 1984; SODERHOLM, 1984; YAMAGUCHI *et al.*, 1989; VAIDYANATHAN *et al.*, 1992). This effect is attributed to postcure caused by the elevated temperature and to release of residual compressive stresses. POWERS *et al.* (1979) reported that upon reheating the values for the coefficient of thermal expansion tends to decrease by as much as 17%. In this study it is also found that the coefficient of thermal expansion tends to decrease for subsequent thermo-cycle runs, **Table XVIII**.

In the publications mentioned above, the coefficient of thermal expansion is also reported to be non-linear with the temperature. In this study the results show an almost perfect linearity, **Figure 44**, regarding the high R-values ($R > 0.99$) obtained by the Linear Least Squares Fit which is carried out on the data. Although, a slightly nonlinear trend can be observed, for which a slightly better fit can be achieved using a second order polynomial fit, this nonlinear effect however is so small that it seems to be justified to assume a linear relationship between expansion and temperature.

In **Figure 45** the determined values of the thermal expansion coefficient are graphically displayed in a bar diagram. This diagram shows the lowest coefficients for P50 and Z100, which are almost equal ($21 \cdot 10^{-6}/^{\circ}\text{C}$). This similarity in coefficients may be expected, because the resins are almost identical. The micro-filled composites Silux Plus and Heliomolar (high resin content) exhibit the highest coefficients of thermal expansion ($> 40 \cdot 10^{-6}/^{\circ}\text{C}$) compared with the other composites, which are heavily filled resins. The other three resins (APH, Conquest and Herculite XR) yield a coefficient of thermal expansion of about $32 \cdot 10^{-6}/^{\circ}\text{C}$. **Table XIX** shows a Scheffe's S multiple comparison test ($p < 0.01$) on the coefficient of thermal data for test run 1. Within the groups (indicated by a line at the right of the table) the difference is not significant. Note that these groups are similar to the groups distinguished above.

A strong inverse correlation is reported between filler content and the coefficient of thermal expansion (HASHINGER AND FAIRHURST, 1984; SODERHOLM, 1984; VAIDYANATHAN *et al.*, 1992). POWERS *et al.* (1979) report that compounds with glass fillers have lower values for the coefficient of thermal expansion than quartz filled. Silane treatment has no effect on the coefficient of thermal expansion (SODERHOLM, 1984).

In the oral environment a composite restoration undergoes temperature changes which ranges from, say, 10° to 60°C (SPIERINGS *et al.*, 1987; PALMER *et al.*, 1992). Consider that the temperature range is $\Delta T = 50$, then an APH restoration yields a volumetric change of $\Delta V = 50 \cdot 3 \cdot 33 \cdot 10^{-6} \cdot 100\% = 0.50\%$,

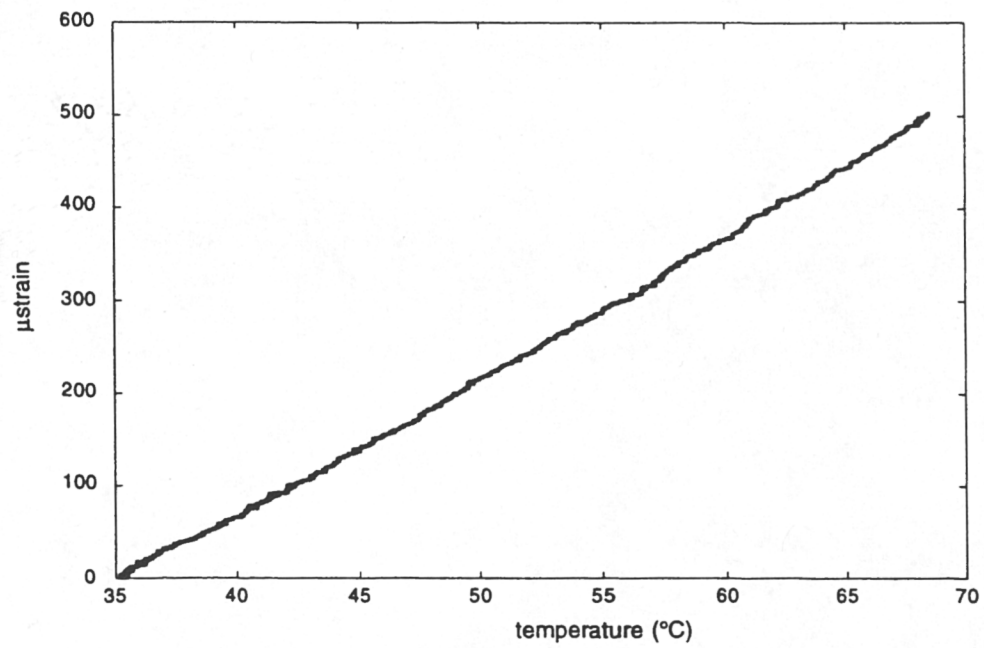


Figure 44. Temperature *versus* strain relation for a typical dental restorative composite.

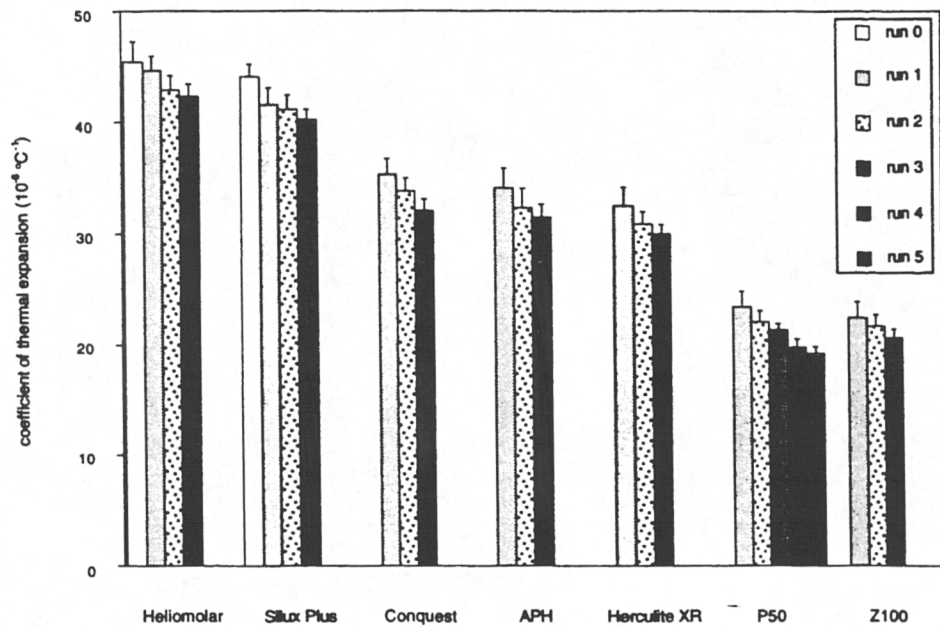



Figure 45. Coefficient of thermal expansion of seven composite materials for the subsequent thermo-cycle runs (run 0 is the first run after light curing), obtained by Linear Least Squares Fitting ($R > 0.99$).

Table XIX. Scheffe's S multiple comparison test on the coefficient of thermal expansion data for run 1 ($p < 0.01$).

Scheffe's S
Effect: Material
Dependent: run 1
Significance level: .01

	Count	Mean	
Z100	5	22.501	
P50	5	23.457	
Herculite XR	5	32.576	
APH	5	34.118	
Conquest	5	35.367	
Silux Plus	5	41.599	
Heliomolar	5	44.660	

which is higher than the post-gel polymerization shrinkage for this particular composite (see Chapter 4). Although this is an interesting calculation, it should be noted that fortunately the actual oral situation is far more complicated. Extreme temperatures last usually only for a short time and most likely will be confined to the surface. The extent of this effect will be controlled by the thermal diffusivity, and the fact that the dental pulp will act as a heat sink with a circulating blood supply at 37°C. Thermal equilibrium at extreme temperatures will likely seldom be obtained. Therefore the coefficient of thermal expansion is just one parameter in the complex of resulting thermal loads.

Compared with the thermal fluctuations in the oral environment, the exotherm temperature rise, and hence thermal expansion, during the setting of a composite restoration is likely to be clinically insignificant. However, it plays an important role in the complex of volumetric phenomena that take place during the polymerization reaction. In order to assess the development of polymerization stresses in tooth-composite systems, knowledge of all the volumetric processes is essential.

7 Determination of the elastic modulus

7.1 Introduction

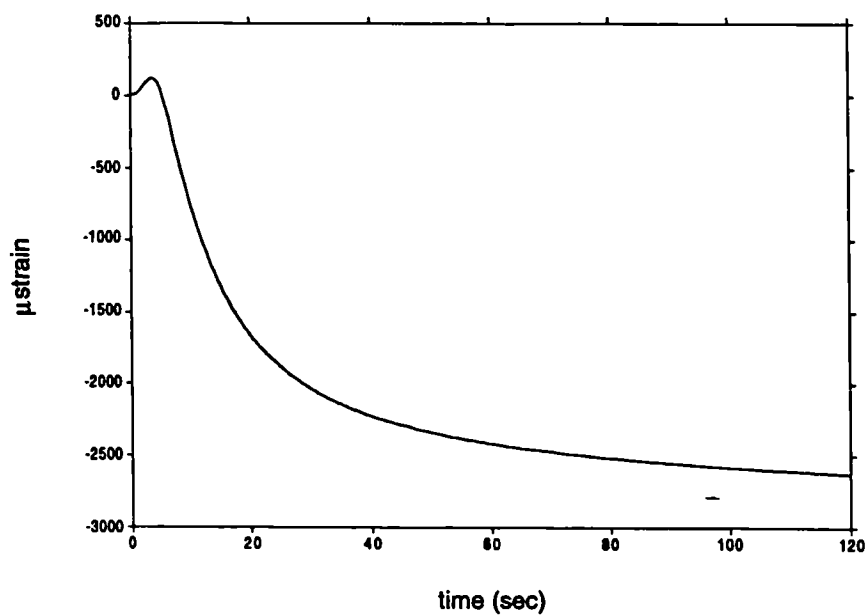
During polymerization several processes are taking place simultaneously. When the visual blue curing light shines at the composite, free radicals are produced and a chain of exotherm reactions starts. Monomeric chains are connected into a polymer network. The stiffness of the composite gel increases rapidly, along with the formation of the network. When the polymer network becomes denser, the initially gelly composite goes through a gel point, which can be defined as the onset of an elastic modulus for the solid composite. The transition from a paste with a monomeric matrix phase to a solid matrix polymeric material goes along with volumetric changes. The denser polymer network results in volumetric contraction during polymerization. During the polymerization reaction there is also an increase in temperature. Two sources for this temperature rise can be distinguished: the exotherm temperature release and temperature rise caused by the intense light of the curing light. Besides some possible thermal curing effect, these two thermal effects also temporarily influence the volumetric changes due to thermal expansion. The experimental measurements of the volumetric changes during polymerization comprises all three effects. To calculate the modulus of elasticity the effect of the thermal expansion due to the curing light and the exotherm have to be eliminated. That is not an easy exercise. The following section discusses the development of modulus with respect to the other phenomena that are going on.

7.2 Materials

In this section parameters, determined earlier in this study, are combined in an effort to gain insight into the processes that play a role in the development of an elastic modulus. In **Table XX** the materials and methods used in this section are given, with their reference to earlier chapters where they are described.

Table XX. Reference to experiments and materials used in Chapter 7.

Experiment	Material	Manufacturer/ Batch	Chapter
strain	Z100	3M/5702U(3BJ)	4
stress	Z100	3M/5702U(3BJ)	5
thermal expansion	Z100	3M/2AA	6
exotherm	Z100	3M/2AA	6

**Figure 46. Polymerization strain development.**

This discussion is an attempt to integrate the results from strain, stress, exotherm and thermal expansion experiments.

7.3 Discussion

The curing rate depends on several factors: the curing light intensity (*i.e.* the capacity of the light source and the distance of the light output probe), the size and shape of the composite sample, the translucency of the composite, the temperature of the composite and heat release rate of the test system, and the duration of the light curing. The dynamic mechanical parameters during polymerization are the modulus of elasticity, the volume or density, the coefficient of thermal expansion, and possibly also the heat transfer rate and translucency of the composite due to the density increase. The latter two parameters will not be considered further because it is assumed that these effects are small compared to the first three. Also the effect of the change in shape during polymerization is neglected.

The dynamic volumetric change is found with the strain gage method. The strain gage method measures the dynamic linear strain change, which can be transferred to volumetric change. Furthermore the strain gage method only measures the post-gel shrinkage, which is the significant part of the polymerization contraction in terms of stress development. Pre-gel shrinkage does not contribute to residual polymerization stresses, disregarding effects due to slight shape changes of the specimen. In **Figure 46** a linear polymerization curve is shown. For the determination of the pure polymerization shrinkage, first of all the thermal effect of the curing light source has to be eliminated. Therefore additional curing runs are performed for each sample and the thermal expansion curve is subtracted, as is shown earlier (Chapter 4). As can be observed, the curve still has some expansion at the begin of polymerization. This is attributed to the exotherm thermal expansion, which is an inherent property of the composite material. For the determination of the development of the pure modulus of elasticity, however, the effect of the exothermal expansion

has to be eliminated. The thermal expansion of the curing light is an external and alien influence, and therefore has to be omitted.

Two problems arise here with regard to the elimination of the thermal expansion and the exotherm contribution. First the effect of the exotherm temperature rise on the amount of thermal expansion depends on the heat release rate, and therefore on the shape of the composite sample, the heat conductivity, and the ambient temperature. Secondly the thermal expansion depends on the value of the coefficient of thermal expansion. This coefficient depends on the degree of cure (Chapter 6), and it is likely that the coefficient changes significantly during the transition from gel to solid. It is however extremely difficult to measure the development of the coefficient of thermal expansion dynamically during this transfer, because when the polymerization is started, it is hard to stop it. Although interrupting the application of the curing light will stop the production of free radicals, the existing free radicals keep the polymerization process going as long as there are any left. Furthermore thermal cycling of the composite for the determination of the coefficient causes thermal polymerization. If the degree of cure is unknown, it is hard to translate those intermittent coefficient of thermal expansion results to continuous polymerization experiments.

To illustrate the effect of a dynamic coefficient of thermal expansion on the polymerization strain curve, a time dependent function $f(t)$ is assumed:

$$\alpha(t) = \alpha_0 f(t)$$

where: $\alpha(t)$ time dependent coefficient of thermal expansion

α_0 coefficient of thermal expansion of solid

t time

Generally the thermal expansion coefficient is inverse related to the modulus of elasticity, but this rule cannot be used here, because the modulus starts at zero. That would mean that the coefficient at the start is infinite. A gel is supposed to

have a higher coefficient of thermal expansion than a solid, due to the more spacious and mobile nature of the molecular structure.

In a first assumption, the final value of the coefficient of thermal expansion is assumed to be reached at the peak of the polymerization process, just before the decline of the polymerization rate. This point is considered because the drop in activity rate indicates the establishment of a dense and rigid polymer network, where after additional networking becomes increasingly difficult due to the immobility of the remaining connectivity possibilities. Therefore the thermal expansion will also be restricted. The peak of the polymerization process can be determined from the exotherm temperature measurements, the stress or the strain development rates. An exponential relation is proposed:

$$f(t) = 1 + a e^{-2t}$$

where: a is a constant

A second possibility is to couple the development of coefficient of thermal expansion to the development of density, which is closely related to strain development. In that case the relation can be written as:

$$f(t) = b - c \frac{\epsilon}{\epsilon_F}$$

where: ϵ dynamic polymerization strain

ϵ_F final polymerization strain value

b and c constants

These two approaches are demonstrated in **Figure 47**. The coefficient of thermal expansion for the gel is assumed to be 2, 2.5, or 3 times the final solid value. This value can be taken from the experimentally determined coefficient (Chapter 6). However, it is not necessary to know the actual final value of the coefficient of thermal expansion. The linear polymerization strain ϵ_0 is (if ϵ includes the inherent exotherm strain component $\alpha \Delta T_{\text{exotherm}}$):

$$\epsilon_0 = \epsilon - \alpha \Delta T_{\text{curing light}}$$

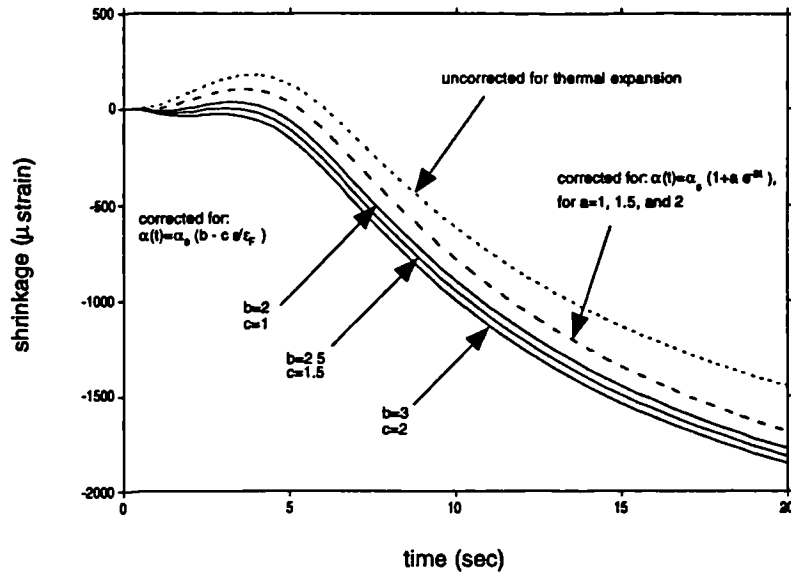


Figure 47. The time *versus* polymerization strain curve, corrected according to two assumptions for the time dependent behaviour of the coefficient of thermal expansion (due to the curing light).

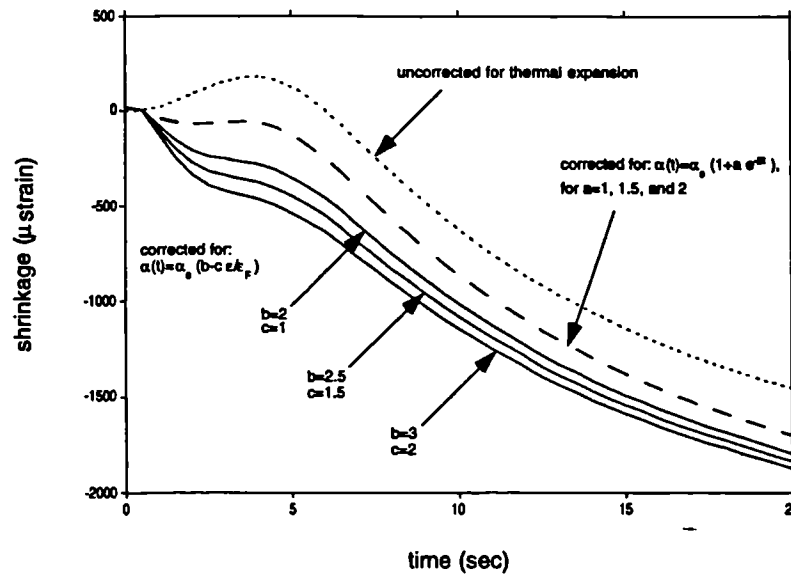


Figure 48. The time *versus* polymerization strain curve, corrected according to two assumptions for the time dependent behaviour of the coefficient of thermal expansion (due to the curing light *and* exotherm).

The post curing strain ε_1 is:

$$\varepsilon_1 = \alpha_0 \Delta T_{\text{curing light}}$$

\Rightarrow

$$\Delta T_{\text{curing light}} = \frac{\varepsilon_1}{\alpha_0}$$

Therefore:

$$\varepsilon = \varepsilon_0 + \alpha_0 f(t) \Delta T_{\text{curing light}}$$

\Rightarrow

$$\varepsilon = \varepsilon_0 + f(t) \varepsilon_1$$

The corrected polymerization strains for the two assumed time-dependent functions for the coefficient of thermal expansion become respectively:

$$\varepsilon = \varepsilon_0 + (1 + a e^{-2t}) \varepsilon_1$$

and:

$$\varepsilon = \frac{\varepsilon_0 + b \varepsilon_1}{1 + c \frac{\varepsilon_1}{\varepsilon_F}}$$

Figure 47 shows no difference between the three cases of $f(t) = 1 + a e^{-2t}$. The time-dependent change is over a very short period (2 seconds), the temperature rise is still starting at that time. The three cases of $f(t) = b - c \varepsilon/\varepsilon_F$, however, show a shift of the curve to the left, *i.e.* the polymerization shrinkage starts earlier.

The exotherm thermal expansion can also be eliminated from the polymerization shrinkage, assuming that the total thermal effect is a sum of both thermal effects:

$$\varepsilon_0 = \varepsilon - \alpha(t) (\Delta T_{\text{exotherm}} + \Delta T_{\text{curing light}})$$

with $\Delta T_{\text{curing light}} = \varepsilon_1/\alpha_0$ this expression can be rewritten as:

$$\varepsilon = \varepsilon_0 + f(t) (\alpha_0 \Delta T_{\text{exotherm}} + \varepsilon_1)$$

The exotherm and curing light temperature corrected polymerization strains for the two assumed time-dependent functions for the coefficient of thermal expansion become respectively:

$$\varepsilon = \varepsilon_0 + (1 + a e^{-2t}) (\alpha_0 \Delta T_{\text{exotherm}} + \varepsilon_1)$$

and:

$$\varepsilon = \frac{\varepsilon_0 + b (\alpha_0 \Delta T_{\text{exotherm}} + \varepsilon_1)}{1 + \frac{c}{\varepsilon_F} (\alpha_0 \Delta T_{\text{exotherm}} + \varepsilon_1)}$$

The exotherm temperature development data is determined from the exotherm temperature measurements (Chapter 6). The results are shown in **Figure 48**. The correction for exotherm temperature effects on the strain are significant in this example, although it should be noted that the exotherm temperature development data depend on the specimen size and test setup. Therefore the applicability of the exotherm temperatures used is open to dispute.

A polymerization stress development curve is shown in **Figure 49**. The stress development curve does not show any thermal expansion. This may be caused by a relatively less sensitive load cell method; by comparison the strain gage method is very sensitive. Furthermore the free surfaces of the cylindrical specimen in the axial stress development experiments, can release the compressive stresses especially during the early post-gel phase. On the other hand, at the strain gage surface, where the strain is measured, the expansion is restricted.

The determination of the elastic modulus (Young's modulus) is based on the general equation:

$$\sigma = \varepsilon E$$

where: σ stress

ε strain

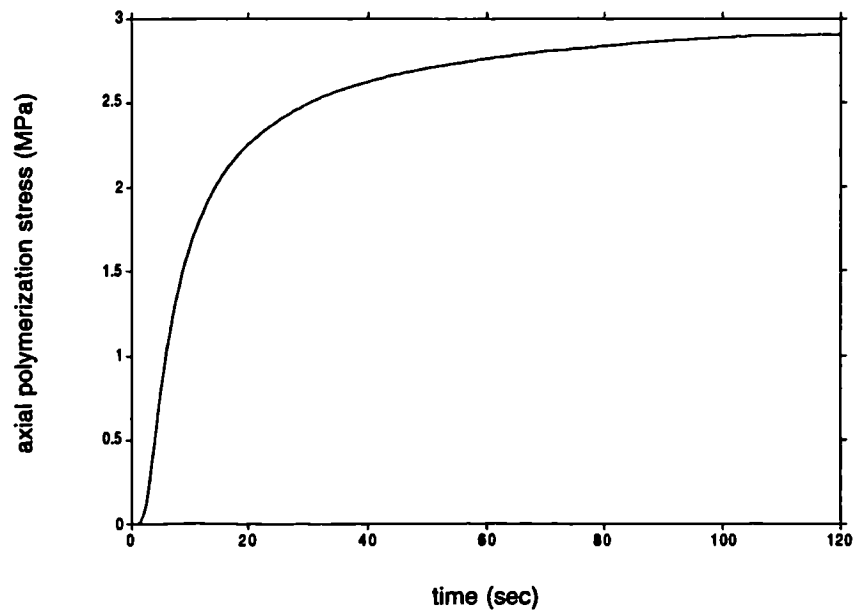


Figure 49. Axial polymerization stress development.

Table XXI. Overview of the parameters defined in the curing and post-curing runs of polymerization stress and strain experiments (ϵ is strain, F is axial force, and δ is axial load cell displacement).

experiment		run	obtained parameters
shrinkage	curing	0	ϵ_0
strain	post-curing	1	ϵ_1
shrinkage	curing	0	F_0, δ_0
stress	post-curing	1	F_1, δ_1

E elastic modulus

The stress developed during the experiment depends on the measured load F and the cross-sectional surface A of the cylindrical specimen. The resulting strain consists of the dimensional change of the composite (polymerization contraction and thermal expansion) and the deflection of the load cell δ . Because the finite dimensions, a geometry correction factor K has to be applied to take into account the dimensional constraints. The expression can be rewritten as:

$$F = K E A \left(\epsilon - \alpha \Delta T - \frac{\delta}{L} \right)$$

where: F axial load

K geometry constraint factor

E elastic modulus

$A = \pi D^2/4$ cross-sectional surface (D diameter)

ϵ polymerization shrinkage, exotherm thermal expansion

$\alpha \Delta T$ thermal expansion due to curing light source

δ deformation of the load cell

L length of the specimen

The results of two different experiments are used for the determination of the development of the modulus of elasticity: axial polymerization stress and polymerization strain experiments. As described before, in both experimental setups two subsequent runs are carried out for each specimen. The results that are obtained out of each of these experiments are listed in **Table XXI**, where ϵ is strain, F is axial force, and δ is the displacement of the load cell.

If it is assumed that the degree of curing is identical in both type of experiments, for strain and the stress, the following procedure (4 steps) can be followed to calculate the development of the elastic modulus:

1. The linear shrinkage stress ε , which contains only the polymerization contraction and the exotherm thermal expansion components, is obtained by subtracting the strain value of the second run ε_1 from the first run ε_0 , eliminating the thermal expansion component due to the curing light (Chapter 4):

$$\varepsilon = \varepsilon_0 - \varepsilon_1$$

2. The curing light is shut off after 2 minutes of light curing. The parameters obtained long enough after shut down do not contain the thermal effect of the curing light. The elastic modulus at time $t=600$ seconds $E_{0;t=600}$ can be calculated from ε , F_0 and δ_0 (Table XXII):

$$E_{0;t=600} = \frac{F_{0;t=600}}{KA \left(\varepsilon_{t=600} - \frac{\delta_{0;t=600}}{L} \right)}$$

3. Using the elastic modulus determined in step 2, the thermal expansion $\alpha_{t=600} \Delta T$ due to the curing light sources can be determined out of the second run of the shrinkage stress experiments and the results for α in the thermal expansion experiments (Chapter 6):

$$\Delta T = \frac{1}{\alpha_{\text{solid}}} \left(\frac{F_1}{KA E_{0;t=600}} + \frac{\delta_1}{L} \right)$$

4. Finally the development of the elastic modulus during polymerization can be calculated:

$$E_0 = \frac{F_0}{KA \left(\varepsilon - \alpha \Delta T - \frac{\delta_0}{L} \right)}$$

The values for the elastic modulus calculated in step 2-(Table XXII) are about 1/10 of the values reported from quasi-static modulus determinations. This can point to too much compliance in this experimental setup, possibly due to the composite mounting heads because that compliance is not measured and thus not corrected for.

Table XXII. Elastic moduli calculated 600 seconds after the start of the polymerization reaction from corresponding stress and strain values.

material	t = 600 seconds					
	polymerization		polymerization		modulus of	
	stress	n	shrinkage	n	elasticity	n
	(MPa)		(μ strain)		(GPa)	
Herculite XR	3.54 ± 0.30	7	1754 ± 74	5	2.02 ± 0.17	7
Silux Plus	3.73 ± 0.39	10	2669 ± 55	5	1.40 ± 0.15	10
Z100	4.15 ± 0.26	9	2845 ± 49	5	1.46 ± 0.09	9

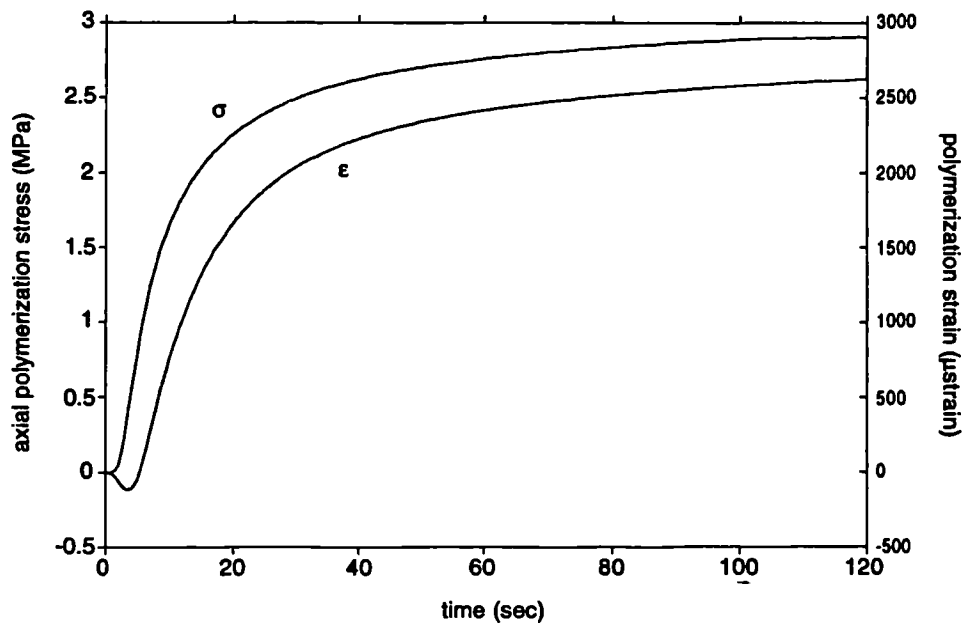


Figure 50. Comparison of the development rate of the polymerization stress σ and strain ϵ experiments.

As discussed earlier in this section, the coefficient of thermal expansion changes during the transition of the composite from a gel phase to a solid material. Therefore instead of a constant α , a time dependent function $\alpha(t)$ has to be used. However, the actual expression for this function is unknown.

To calculate the development of the elastic modulus, the key assumption is made that the polymerization process is identical for the strain and the stress measurements. This assumption turns out to be false, as illustrated in **Figure 50**. In this figure the stress and strain development are plotted in the same plot. It turns out that the peak rate of the polymerization of the axial stress experiments is earlier than in the strain experiments, **Figure 51**. If the strain is corrected according to one of the assumed coefficient of thermal expansion time-dependent functions ($f(t)=b-c \epsilon/\epsilon_F$, $b=3$, $c=2$), **Figure 52**, the strain curve shifts to the left, but not enough to match the curing rate of the axial stress experiments.

Assume that the polymerization rates and materials of stress, strain, exotherm and thermal expansion experiments are identical. In that case the resulting strain ($\epsilon_0=\sigma_0/E_0$) can be calculated:

$$\epsilon_0 = \epsilon - f(t) \left(\frac{\sigma_1}{E_1} + \frac{\delta_1}{L} \right) - \frac{\delta_0}{L}$$

where: $f(t) = 1 + a e^{-2t}$

or

$$f(t) = b - c \epsilon/\epsilon_F$$

The resulting strain development for both $\alpha(t)$ -functions (for $a=1$; and $b=4$, $c=3$) is illustrated with **Figure 53** for several steps:

$$\begin{aligned} &\epsilon \\ &\frac{\delta_0}{L} \\ &\epsilon - \alpha(t)\Delta T \end{aligned}$$

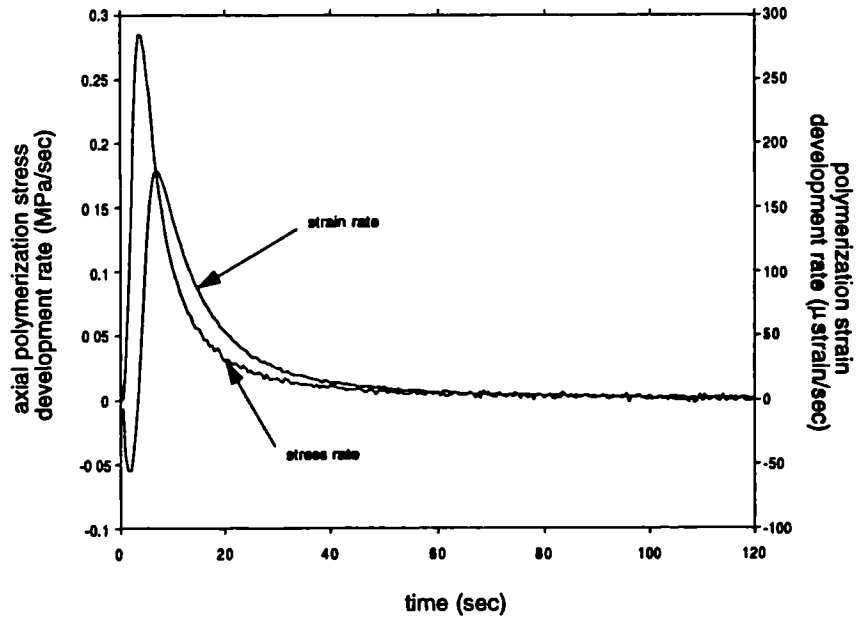


Figure 51. Comparison of the polymerization rate for the axial stress and the strain development experiments.

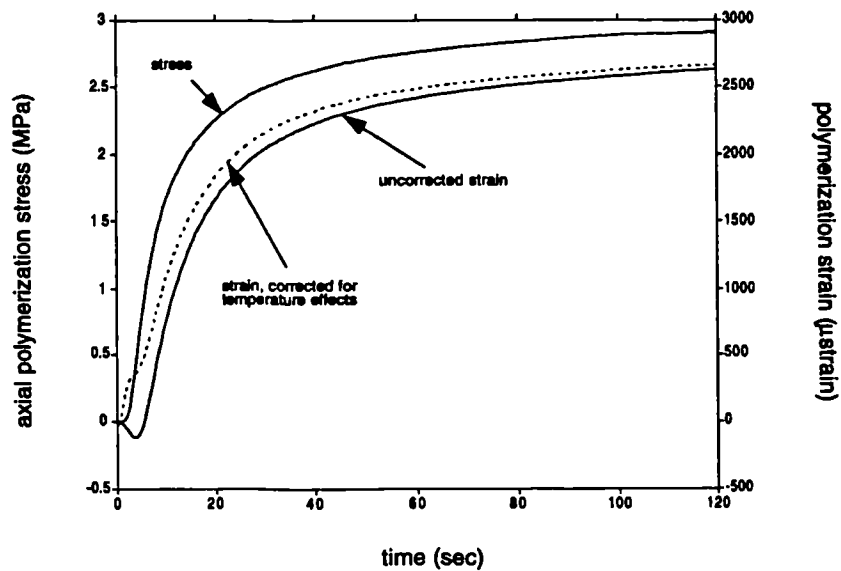


Figure 52. Comparison of the development rate of the polymerization stress and strain experiments. The strain results are corrected for the thermal effect of the exotherm and curing light, using an assumed time-dependent function of the coefficient of thermal expansion $\alpha(t)$.

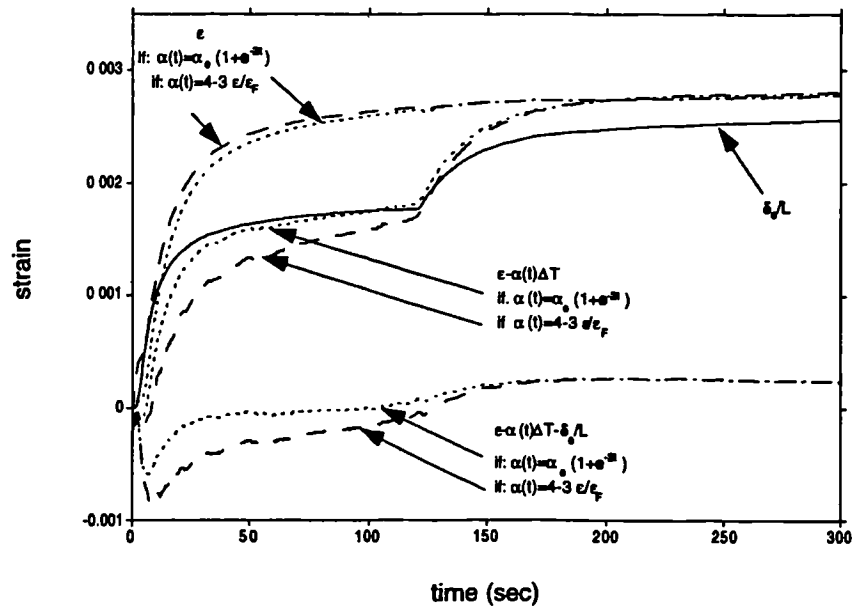


Figure 53. Development of resulting strain in stress experiment, calculated under assumption of identical polymerization rate and materials and two different functions of the coefficient of thermal expansion $\alpha(t)$.

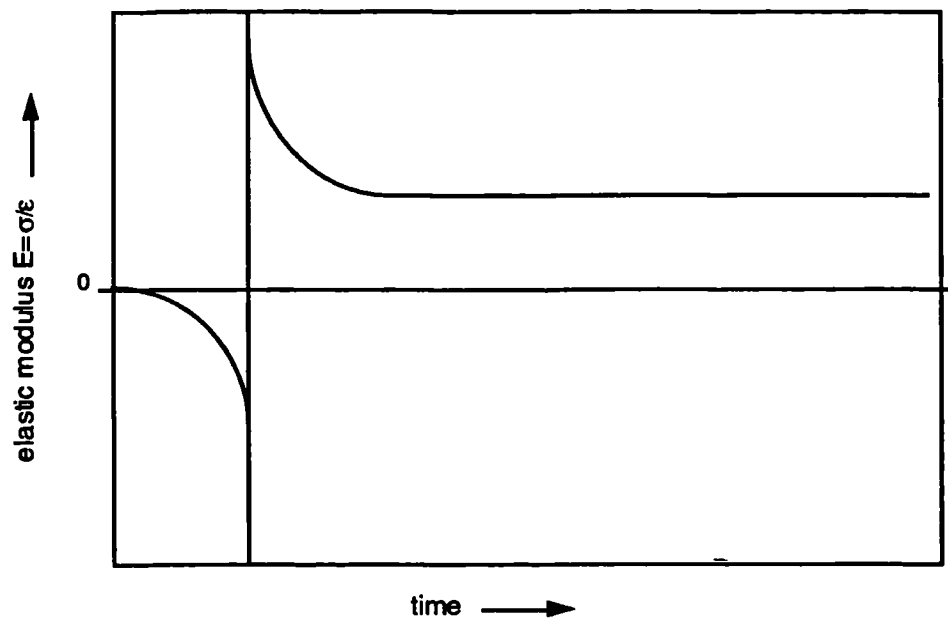


Figure 54. Behaviour of the calculated elastic modulus curve if data from different experimental setups (strain, stress, temperature effects) are used, due to a difference in curing rate.

and

$$\epsilon - \alpha(t)\Delta T - \frac{\delta_0}{L}$$

As can be seen in **Figure 53**, the $(\epsilon - \alpha(t)\Delta T)$ -component develops too slowly, and therefore the term $(\epsilon - \alpha(t)\Delta T - \delta_0/L)$ initially becomes negative. As a result the modulus of elasticity calculated from these data starts with negative values, jumps from negative to positive infinite when the $(\epsilon - \alpha(t)\Delta T - \delta_0/L)$ -term goes through zero, and finally levels out (**Figure 54**). The elastic modulus at these final levels have been calculated and applied earlier in this section (**Table XXII**). This figure shows that the calculation of elastic modulus development out of the results of several experiments is a very delicate exercise. Obviously the rate of change in the stress and strain experiments is not identical. It is possible to increase the rate of polymerization by means of a higher curing light intensity, but the real issue here is the difference in degree of cure. The development of degree of cure for both stress and strain tests has to be identical. Only in that case it is allowed to combine both polymerization results for the determination of the development of the modulus of elasticity.

7.4 Conclusion

In conclusion it can be stated that the development of mechanical parameters during polymerization of restorative composites is an extremely complicated process. A variety of mechanical parameters are being developed, and do affect each other. The development of the different parameters depend heavily on the rate of curing, which is influenced by the curing light intensity, translucency, heat transfer, specimen shape, and temperature. This section showed the significant influence of the degree of cure and polymerization rate in the development of the mechanical parameters and outlined an approach for the determination of several parameters involved. If strain and stress can be obtained simultaneously out of the same experiment, the difference in polymerization rate between both parameters can be eliminated – provided that the polymerization is homogeneous throughout the sample. Strain can be

measured by means of a strain gage, attached to the composite sample. The output of the strain gage will be:

$$\epsilon_{\text{strain gage}} = \epsilon - \frac{\delta}{L}$$

where: ϵ is the linear post-gel polymerization shrinkage

δ is the displacement of the load cell

L is the length of the sample

Because δ/L is determined by the capacitance probe, the shrinkage ϵ can be calculated. However, practically it is difficult to attach a strain gage to a composite paste. Apparently it is extremely hard to determine the time-dependent modulus during the polymerization process. There are, however, a variety of less complicated methods to determine the quasi-static modulus of elasticity after the polymerization reaction has ended. As is outlined before, the elastic modulus is required for a finite element analysis of the shrinkage stress fields. Fortunately the exact quantitative development of the elastic modulus appears not to be crucial for further determination of the polymerization stresses, as will be shown in the next chapter. Values settled by those quasi-static experimental methods can also be used in the numerical stress analysis of residual stress states of tooth-restoration complexes. Nevertheless, stress development experiments as performed in Chapter 5 have proved to be very helpful in a better understanding of the complexity of the polymerization phenomena and modulus development.

8 Numerical simulation

8.1 Introduction

During the polymerization reaction, after the gel-point, the composite material develops an elastic modulus. Along with the volumetric polymerization contraction this results in shrinkage stresses if the composite is restricted by the surrounding tooth structure. These conditions often result in heavily pre-stressed restorations which frequently leads to deformation and even fracture. These internal polymerization stresses have clinical significance, as is already outlined in the general introduction.

The clinical significance of shrinkage stresses in a restoration is the potential to initiate failure of the composite-tooth bond (adhesive failure), which may cause micro leakage and secondary caries (JENSEN AND CHAN, 1985) or to initiate micro-cracking of the restorative material (cohesive failure) (LAI AND JOHNSON, 1993). Polymerization contraction stresses transferred to the tooth structure cause deformation of the tooth. The resulting coronal deformation may result in postoperative sensitivity and micro cracks in the cervical enamel (JENSEN AND CHAN, 1985). Careful composite placement through incremental layering and directing of polymerization shrinkage vectors by means of light reflecting wedges (LUTZ *et al.*, 1986) is believed to minimize the effects of the polymerization contraction. Furthermore polymerization stress transfer into the tooth structure can be reduced by the use of base materials (MCCULLOCK AND SMITH, 1986). Stress relaxation through composite hydration is evident in mature composites (FEILZER *et al.*, 1990; SEGURA AND DONLY, 1993) but this occurs over a long period of time, well after post-gel polymerization is complete. Shrinkage induced enamel fracture reportedly occurs immediately after polymerization (JENSEN AND CHAN, 1985). Therefore the tooth-restoration complex is in a pre-stressed state even before occlusal stresses result in further

coronal deformation (SAKAGUCHI *et al.*, 1991). Obviously, the whole tooth-restoration system remains pre-stressed after the composite is polymerized.

The geometry of a tooth-restoration is complex, and therefore it is hard to get a good insight into the actual stress distribution throughout the system. There have been few attempts to relate the polymerization stress to actual restorations. FEILZER *et al.* (1987) assume a linear relation between the ratio of the free and restrained composite surface area of a cylindrical test sample (the so-called C-factor) and a dental restoration. This simplification allows them to perform polymerization stress development experiments on cylindrical shaped specimens, and generalize the results to restorations with similar ratios. However, the meaning of this C-factor approach is questionable, because it does not take the considerable shape and size functions into account, nor does it give any information about the stress distribution in the restoration-tooth complex.

In the hybrid experimental-numerical approach suggested in this study, however, it is possible to use experimental data obtained from different specimen shapes and sizes for the calculation of stress distributions in tooth-composite systems. Experimentally determined basic material parameters for a composite during polymerization can be used for the numerical calculation of internal non functional stresses that are a result of the polymerization contraction. In this section the effect of different filling techniques on the shrinkage stresses along the tooth-restoration interface and along the coronal tooth surface are numerically analyzed.

8.2 Materials and methods

Finite element stress analysis methods are powerful numerical techniques for the evaluation of complex physical processes (ZIENKIEWICZ AND TAYLOR, 1989; REDDY, 1993). The most distinctive feature of the finite element method is the division of a given domain into a set of simple subdomains, called finite elements. A finite element comprises of a geometric shape that allows computation of the solution (or its approximation), or it provides necessary

relations among the values of the solution at selected points (nodes). Other features of a finite element method include seeking continuous approximations of element equations by imposing the interelement continuity of the solution and balance of the interelement forces.

In a numerical computation a computer is employed to evaluate a mathematical model of the process. The way a finite element method solves this physical process is characterized by three features:

1. The domain of the problem is represented by a collection of simple subdomains (finite elements). The collection of finite elements is called the finite element mesh.
2. Over each finite element the physical process is approximated by functions of desired type and algebraic equations, relating physical quantities at selective points (nodes) of the element, are developed.
3. The element equations are assembled using continuity and/or balance of physical quantities.

In the finite element method, in general, an approximate solution u is sought for a differential equation in the form:

$$u \approx \sum_{j=1}^n u_j \psi_j + \sum_{j=1}^m c_j \phi_j$$

where u_j are the values of u at the element nodes, ψ_j are the interpolation functions, c_j are the nodeless coefficients, ϕ_j are the associated approximation functions. Direct substitutions of such approximations into the governing differential equations does not always result in necessary and sufficient number of equations for the undetermined coefficients u_j and c_j . The necessary and sufficient number of equations for the undetermined coefficients over an element can be obtained by different procedures, one of such is provided by a weighted-integral form of the governing differential equation.

The finite element stress analysis for this study is carried out using the MARC Analysis solver (MARC K5.2, MARC Analysis, Palo Alto, CA). **Figure 55** is a diagram showing the flow sequence of the MARC program. This diagram shows the input phase, equivalent nodal load vector calculation, matrix assembly, matrix solution, stress recovery, load incrementation and iteration within a load increment, and output phase. A numerical problem can generate a considerable amount of numbers. To make an efficient use of this computational analysis, it is wise to make proper reductions if possible in the modeling of the finite element mesh, *e.g.* by employing 2-dimensional features and/or symmetry if applicable. This will not only decrease the computation time, but will also enhance the postprocessing of the results.

To demonstrate the stress development caused by polymerization contraction and modulus development, a bucco-lingual cross-section of a molar with a MOD-cavity (Mesio-Occluso-Distal) is modeled in a two-dimensional finite element mesh (**Figure 56A**). The pulp is not considered in this figure. Symmetry is used to justify the modeling of only one half of the cross sectional area, reducing the total number of elements. The root of the tooth is not modeled, assuming that it will not affect the overall stress distribution around the restoration. The root is important for the functional stress transfer into the jaw, but the residual non functional stresses due to the polymerization contraction of a restoration remain localized in the crown of the tooth. Therefore a simplified boundary condition is assumed at the place where the root is cut (**Figure 56C**). This simplified boundary condition consists of fixed displacements in horizontal direction (x-axis) along the dentin edge because the root restricts horizontal movements, and one vertically (y-axis) fixed point at the symmetry-axis to anchor the whole mesh. Vertical displacement is not restricted along the dentin-edge because vertical displacement is less restricted by the root. Note that the enamel edge is left unrestrained. Along the symmetry-axis the displacement is fixed in x-direction, due to the symmetry. The three boundary conditions (indicated in **Figure 56C**) are applied throughout this simulation, unless otherwise noted. The dimensions are given in **Figure 56B**. Because this two-dimensional model represents a slice mid

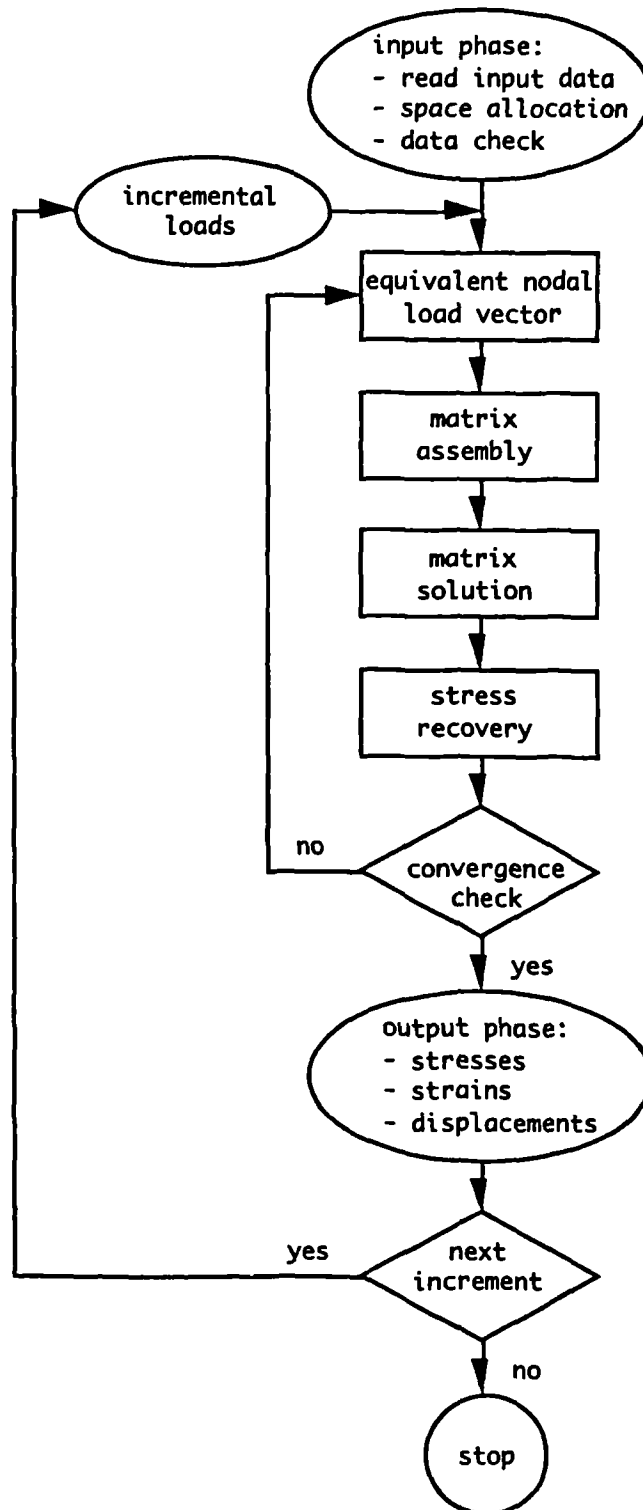


Figure 55. Flow diagram of the MARC finite element program.

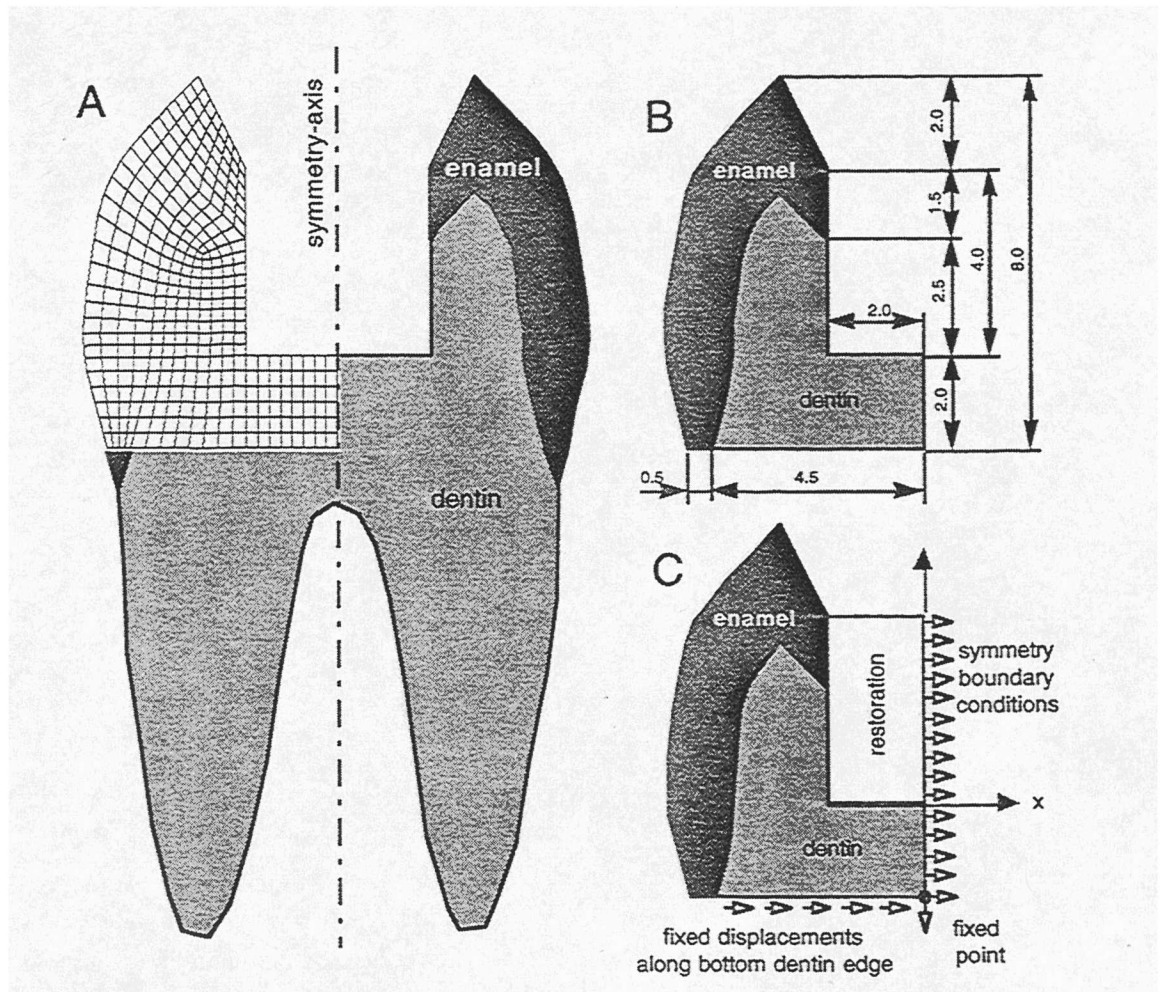


Figure 56.

A. Simplified cross section of a molar, containing a MOD-cavity

B. Dimensions (mm)

C. Coordinate system and boundary conditions

through the tooth, a plane strain condition may be considered. Hence the elements used in this model are plane strain elements (isoparametric quadrilateral, 4-noded).

The size of a restoration affects the amount of the polymerization shrinkage stresses. This will be illustrated by varying the width and the depth of the composite restoration, **Figure 57** and **58**. The composite restoration in this analysis is modeled as a simple straight box, and the geometry of the occlusal enamel is also simplified. Three different incremental filling techniques are simulated:

- Gingivo-occlusal increments (horizontal, **Figure 59**)
- Bucco-lingual increments (vertical, **Figure 60**)
- Diagonal increments (v-shape, **Figure 61**)

To enable the modeling of the three different filling techniques, two meshes are used for the composite restoration (**Figure 62A** and **62B**). The incremental filling procedure is simulated during the course of the calculation by activating subsequent element layers of the composite restoration in succeeding numerical increments, that were deactivated at the start of the computation. The effect of an underfilled and overfilled restoration is calculated with the finite element meshes shown in **Figures 62C** and **62D** respectively.

To perform the finite element simulation of polymerization shrinkage and modulus development, three mechanical material parameters are required:

- the linear shrinkage coefficient α
- the Poisson's ratio ν
- the modulus of elasticity E .

The material properties applied in this study are listed in **Table XXIII**.

The material properties for the composite material simulated in this analysis are for P-50 (3M, St Paul, MN, USA), because the values determined in Chapter

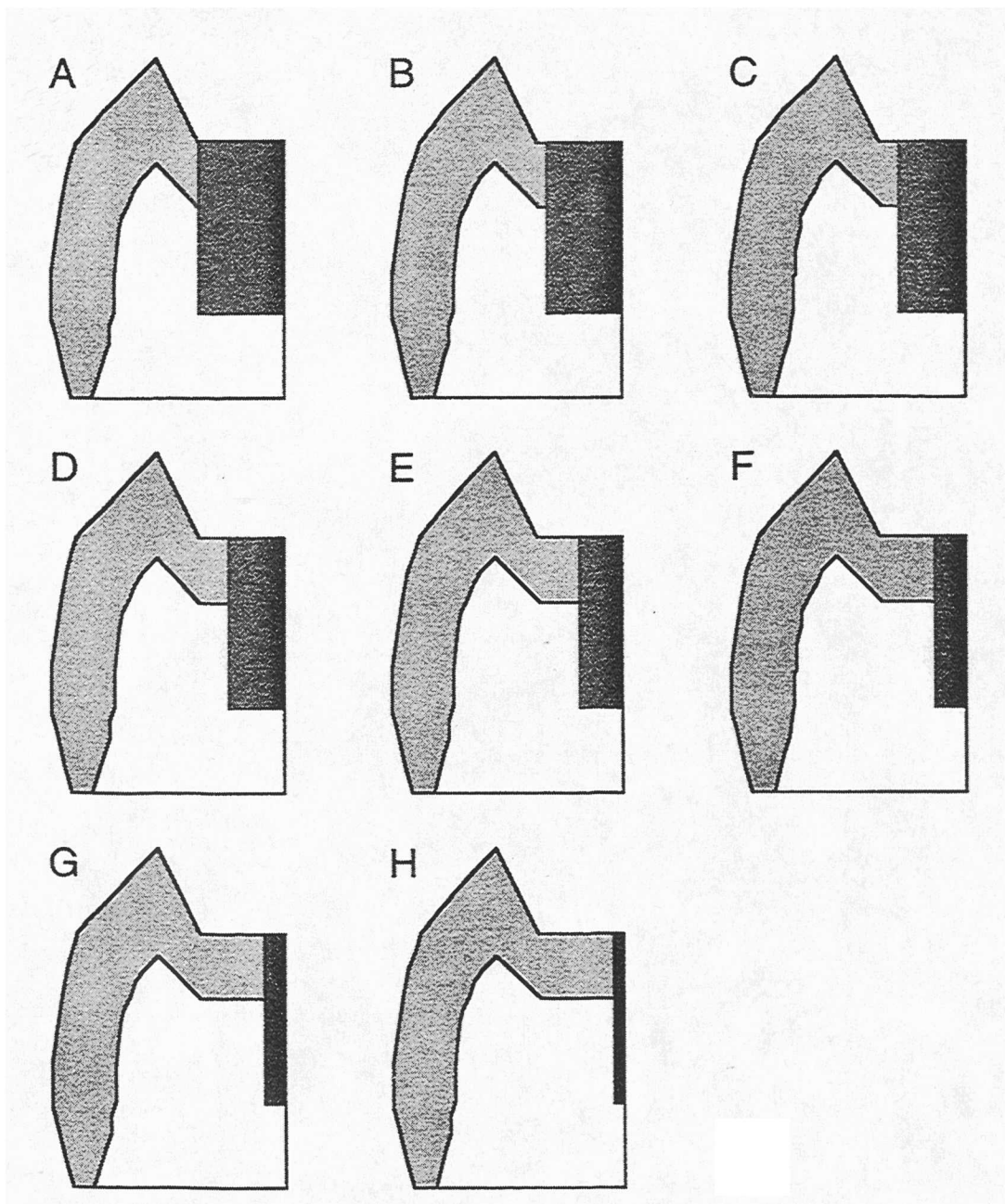


Figure 57. Simplified geometry of tooth-restoration complex, for eight restoration widths (A-H): 4.0, 3.5, 3.0, 2.5, 2.0, 1.5, 1.0, and 0.5 mm.

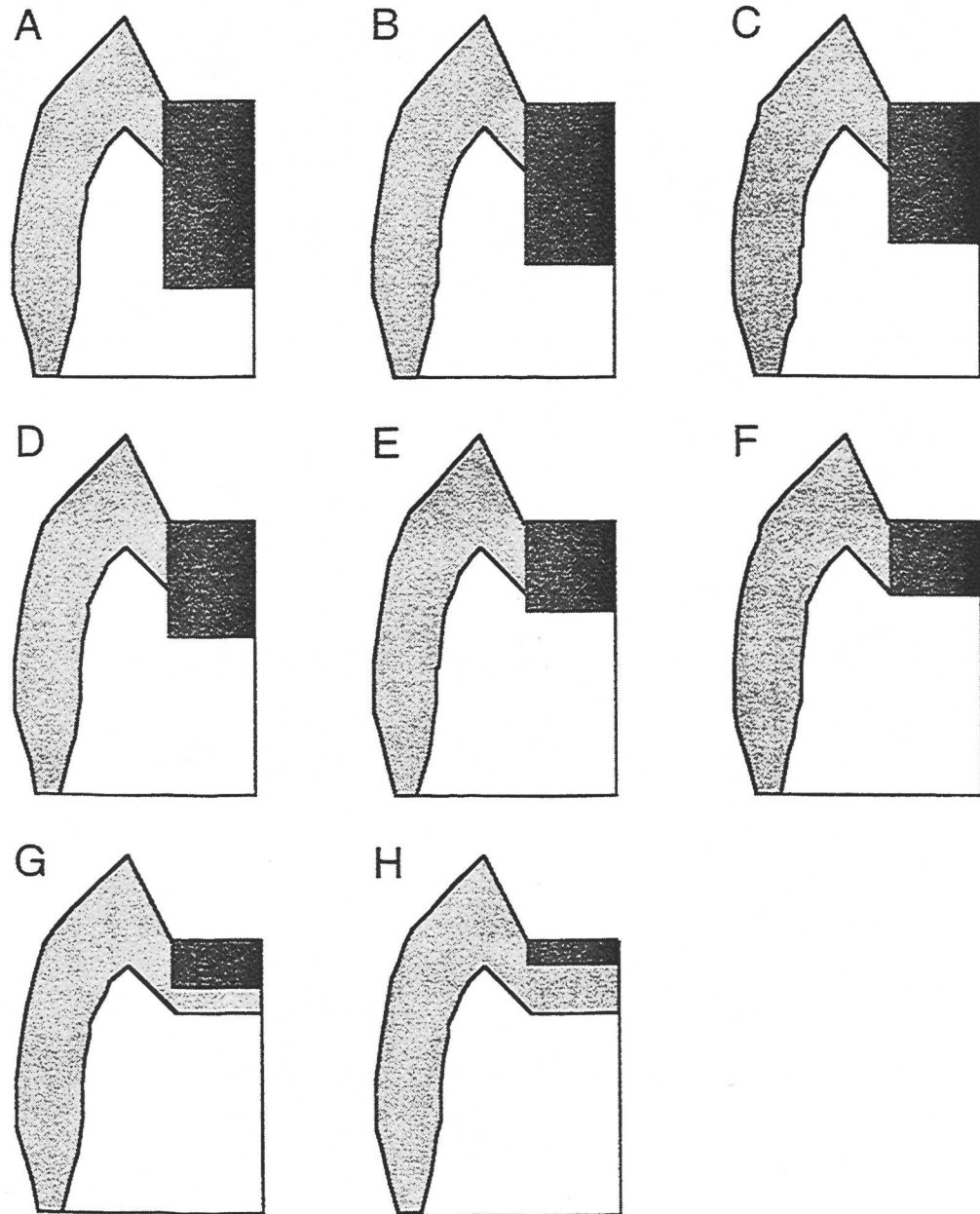


Figure 58. Simplified geometry of tooth-restoration complex, for eight restoration depths (A-H): 4.0, 3.5, 3.0, 2.5, 2.0, 1.5, 1.0, and 0.5 mm.

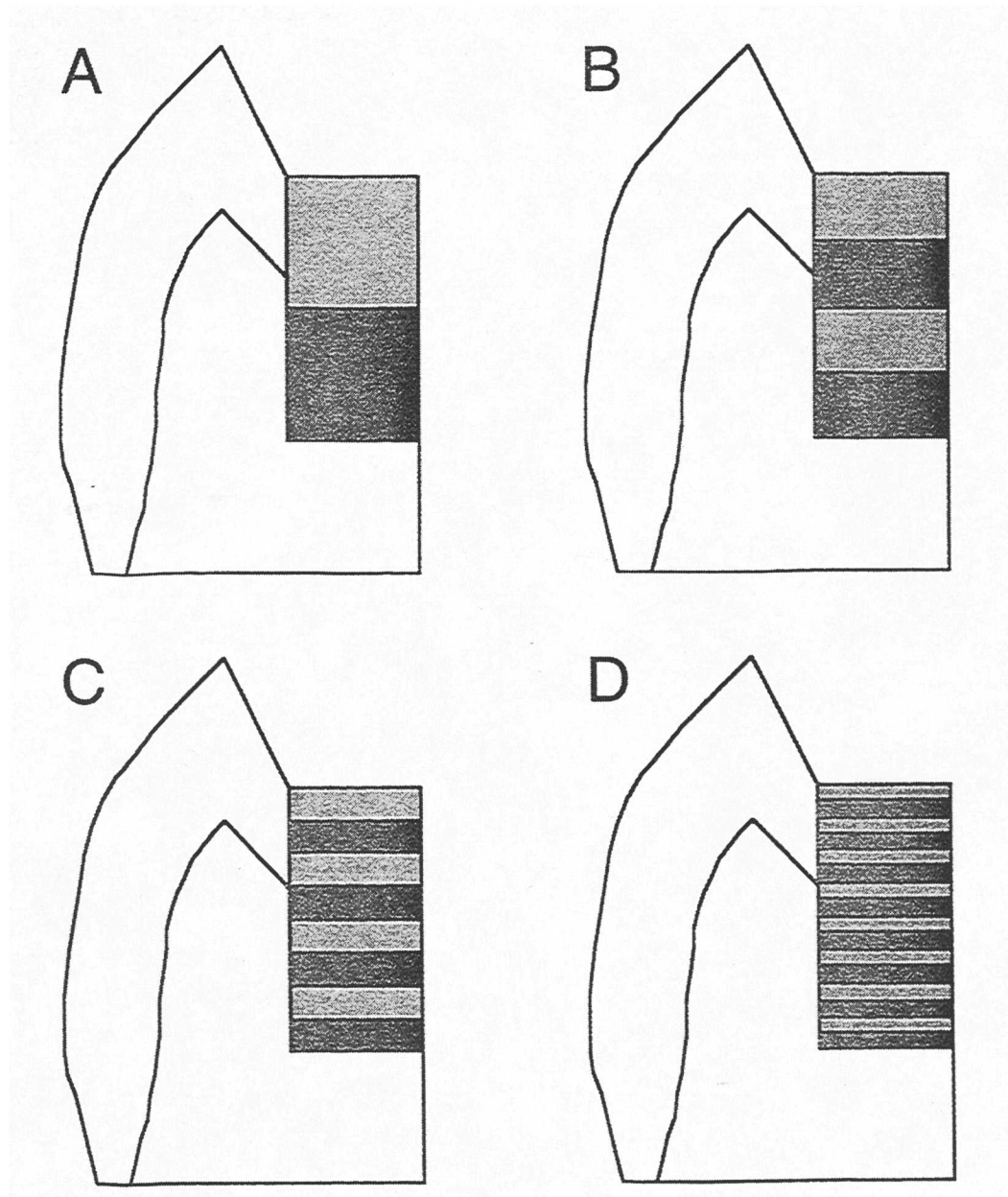


Figure 59. Gingivo-occlusal (horizontal) incremental filling technique, for 2, 4, 8, and 16 increments (A-D).

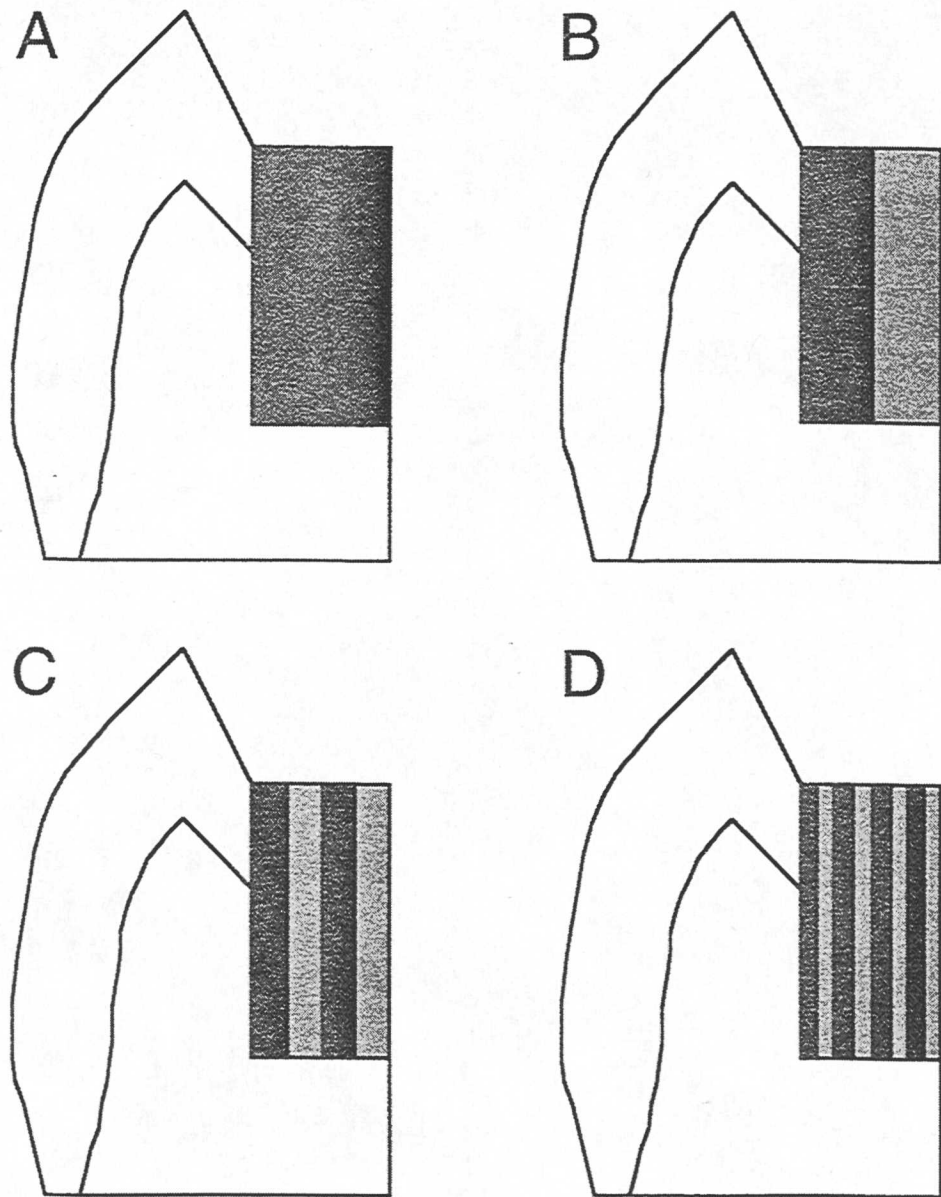


Figure 60. Single step (A) and bucco-lingual (vertical) incremental filling technique, for 2, 4, and 8 increments (B-D).

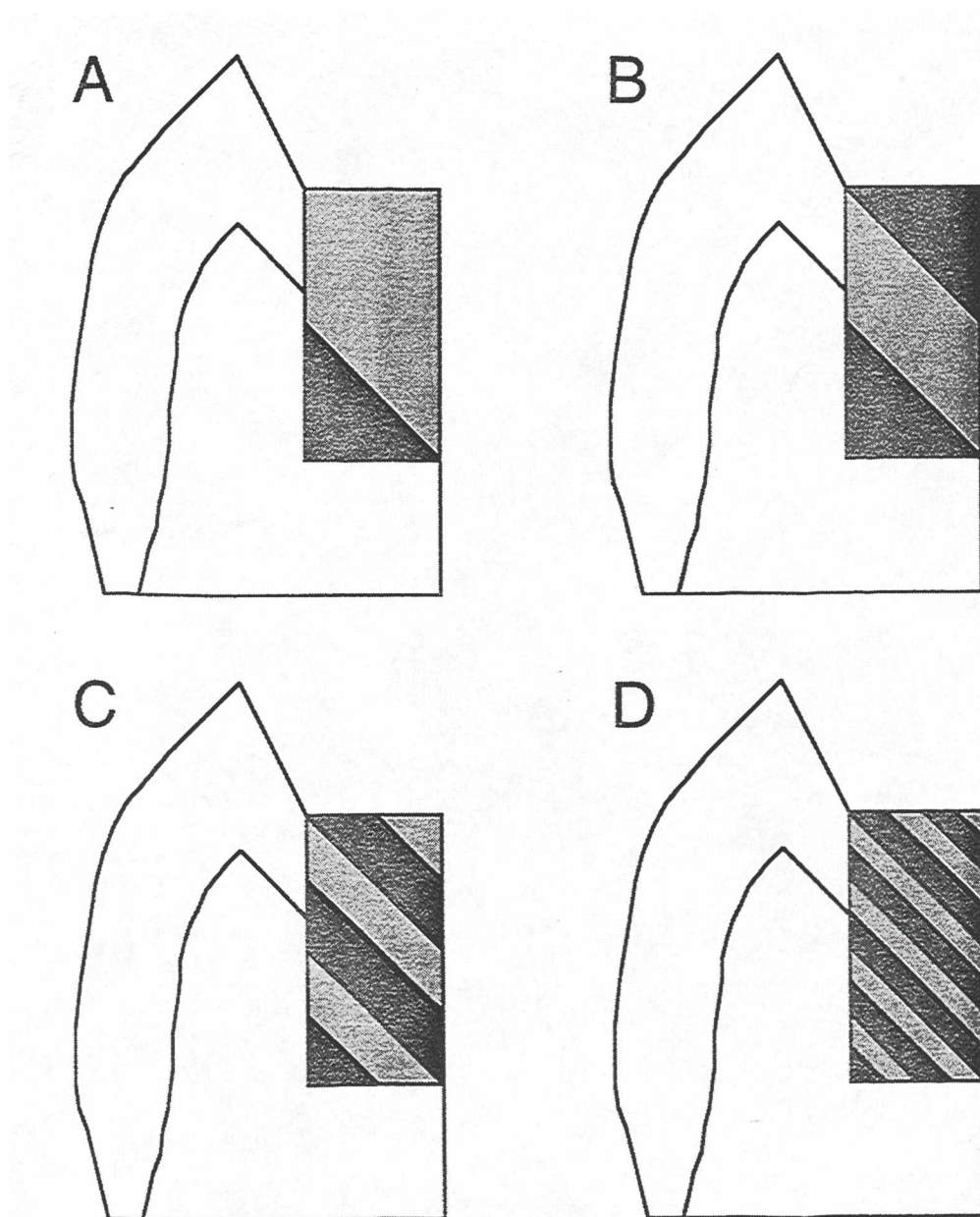


Figure 61. Diagonal (v-shape) incremental filling technique, for 2, 3, 6, and 12 increments (A-D). The 24-increment filling is not depicted.

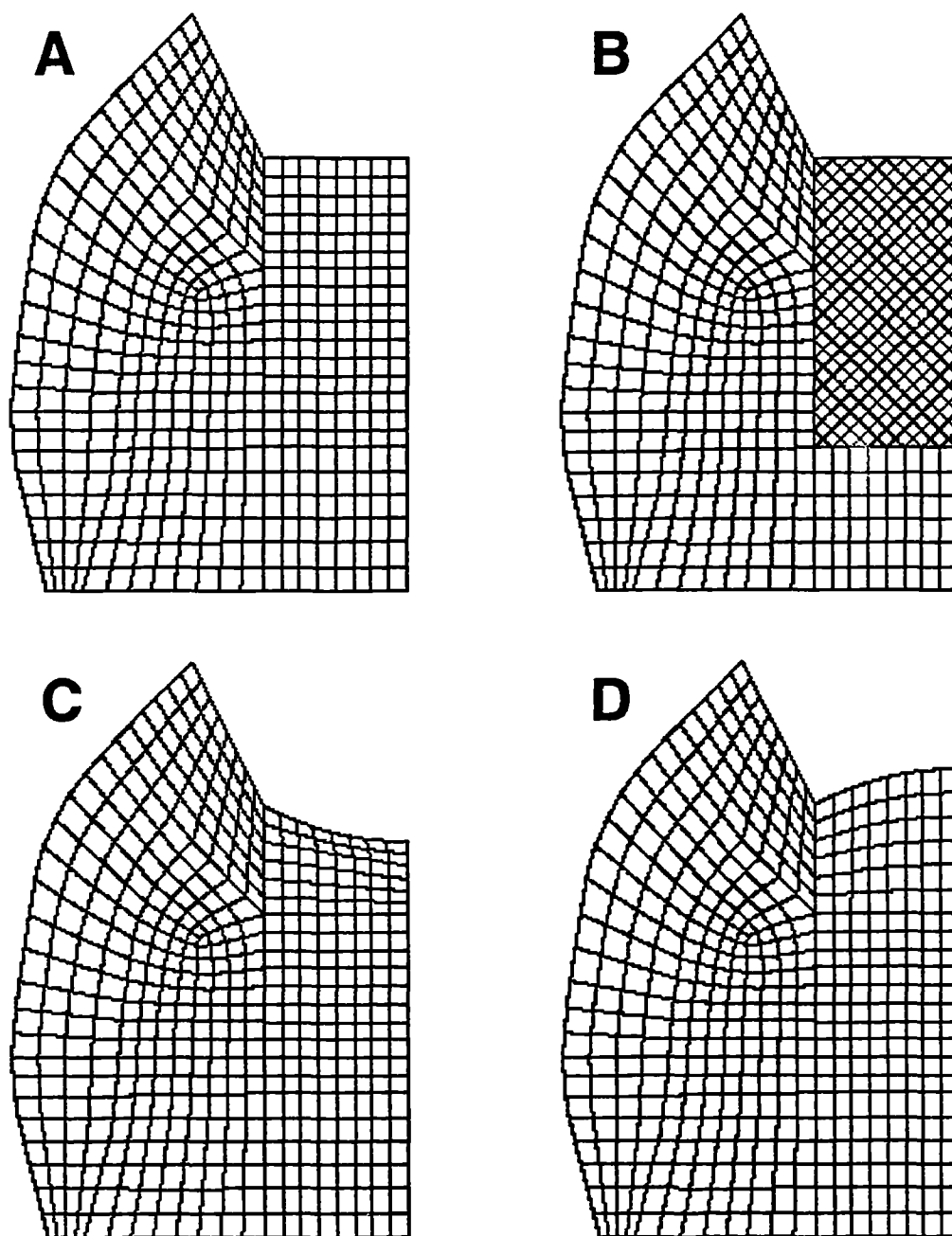


Figure 62. Four finite element meshes used for the analysis of polymerization shrinkage stresses in the tooth-restoration complex for three different filling techniques - gingivo-occlusal (A), bucco-lingual (A), and diagonal (B) - , an underfilled (C) and an overfilled (D) restoration.

Table XXIII. Mechanical properties.

Material	Elastic modulus (GPa)	Poisson's ratio	Linear shrinkage
Composite	20	0.24	0.0022
Enamel	50	0.30	
Dentin	12	0.10	

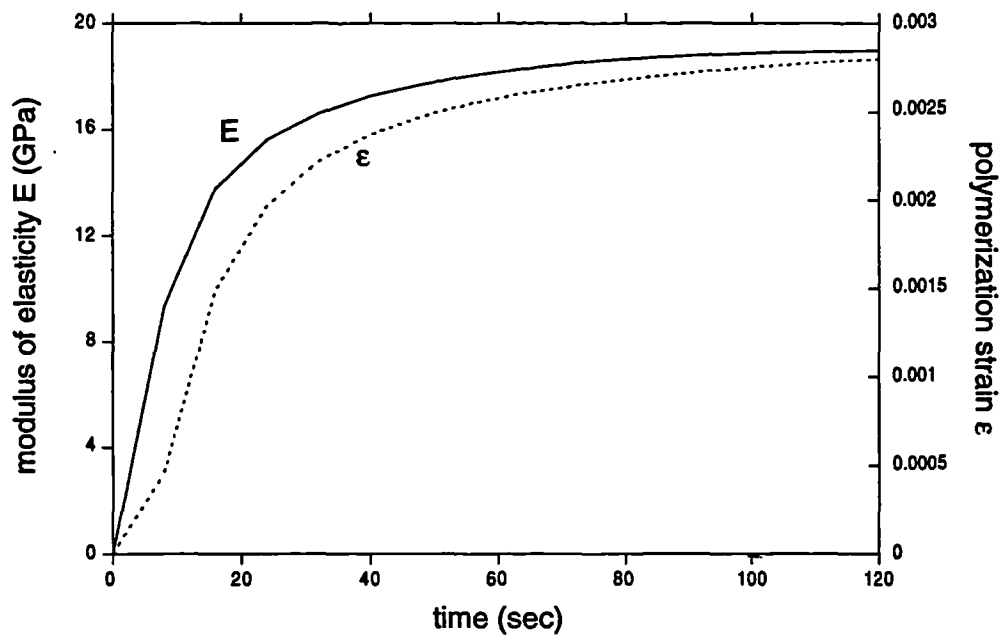


Figure 63. Assumed time-dependent behaviour of modulus of elasticity (E) and polymerization shrinkage strain (ϵ).

7 (Table XXII) are believed to be too low (as is discussed in that section). The modulus of elasticity applied for P-50 is $E=20$ GPa (LIN, 1993), and the Poisson's ratio $\nu=0.24$ (CRAIG (1985)). The linear shrinkage coefficient $\alpha=0.0022$ is determined earlier in this study (Chapter 4).

A variety of values are reported in literature for the elastic modulus of enamel, ranging from 11 to 84 GPa (BRADEN, 1976). Varying not only for different references, but also as a function of the location of the enamel (cusp, occlusal, side, etc.). For dentin the reported elastic moduli are more consistent, ranging between 11 and 19 GPa (BRADEN, 1976). The finite element calculations performed in this study are basically linear elastic. Therefore only the correct ratio of moduli is important for a qualitative analysis. CRAIG (1985) reports elastic moduli of 84.1 and 18.3 GPa for enamel (molar, cusp) and dentin respectively, and STANFORD *et al.* (1958, 1960) established about 46.2 and 11.7 GPa respectively. In both references the results were obtained by means of a compression method. As a result Craig's enamel/dentin ratio of the elastic moduli is 4.6, and for Stanford *et al.* the ratio is 4.0. For use in this finite element analysis moduli of 50 and 12 GPa are chosen for enamel and dentin respectively, obtaining an enamel/dentin ratio of 4.2.

The Poisson's ratios compiled in BRADEN (1976) range from -0.16 to 0.07, depending on tooth type, location and subject. In this model, the Poisson's ratio for dentin is set at $\nu=0.10$, while for enamel a Poisson's ratio $\nu=0.30$ (CRAIG, 1985) is used.

For this finite element simulation several assumptions have to be made for the material behaviour, concerning:

- a. homogeneous isotropic material properties
 - b. constant Poisson's ratio
 - c. homogeneous polymerization
 - c. solid material behaviour
-

e. time-dependent polymerization contraction and elastic modulus

- a. *Homogeneous isotropic material properties* — The material properties of composite, enamel and dentin are assumed to be homogeneous and isotropic. Considered at macro scale, this assumption is widely accepted for restorative composites. For enamel and dentin, however, this assumption is clearly of doubtful validity, though can be justified for this occasion because the goal of this analysis is not to properly model the biological materials but to illustrate the stress distribution due to the development of some mechanical properties during polymerization.
- b. *Constant Poisson's ratio* — The Poisson's ratio ν for the composite is assumed to remain constant during the polymerization reaction, even during the gel-transition. This assumption has to be made because the time dependent behaviour for ν is unknown. It is likely that the Poisson's ratio is higher than 0.24 when the composite is uncured (paste phase), possibly approaching the upper limit ratio $\nu=0.5$ for incompressible fluids. However, this presumably higher ratio exists only during the pre-gel phase, when the modulus is not yet developed. For that reason it has no effect for the instantaneous polymerization stresses. The post-gel variation of the Poisson's ratio is likely small and insignificant for the stress distribution.
- c. *Solid material behaviour* — Flow of composite material before the gel-point is assumed to be negligible, and hence mass transport is not considered. Consequently no shift in density values of the bulk of the composite restoration will occur during polymerization.
- d. *Homogeneous polymerization* — The polymerization of the composite is assumed to be isotropic and homogeneous, and only time-dependent. This assumed homogeneity of the polymerization process is questionable, because it is concluded from experimental observations in previous sections, that different curing light intensities result in different polymerization shrinkage values and rates. However, modeling non homogeneous polymerization is beyond the scope of this numerical simulation. Stress distribution is not expected to be much
-

influenced by the gradient of the polymerization reaction. Therefore the shrinkage phenomenon can be simulated for the whole composite restoration using homogeneous time-dependent material properties.

- e. *Time-dependent polymerization contraction and elastic modulus* — The volumetric polymerization shrinkage can be simulated in MARC by the linear coefficient of thermal expansion α . This factor α provides a homogeneous volumetric shrinkage if the temperature decreases. Since α is related to the temperature, in the used MARC finite element program, polymerization time has to be simulated by temperature changes, which will be referred to as the equivalent time. Therefore the time-dependent modulus of elasticity will also be modeled as a temperature dependent property. During the polymerization period the temperature is lowered linearly.

The time-dependent shrinkage strain $\epsilon(t)$ is determined earlier in this study (Chapter 4), and is assumed to be valid for the composite restoration material in this finite element model. Although it is discussed previously that the curing conditions have a significant influence on the polymerization contraction, the use of these shrinkage data can be justified because of the qualitative character of this numerical analysis. The MARC Analysis program uses an instantaneous coefficient of thermal expansion:

$$d\epsilon = \alpha dT$$

where: ϵ strain

α thermal expansion coefficient

T temperature (equivalent time)

which can be determined as:

$$\epsilon_2 = \int_1^2 \alpha(T)dT + \epsilon_1 = \int_1^2 \frac{(\alpha_2 - \alpha_1) T + \alpha_1 T_2 - \alpha_2 T_1}{T_2 - T_1} dT + \epsilon_1$$

⇒

$$\alpha_2 = \frac{2(\epsilon_2 - \epsilon_1)}{T_2 - T_1} - \alpha_1$$

As is also discussed in a previous section (Chapter 7), the elastic modulus development is hard to determine out of the current experimental data due to the difference in polymerization rate of the diverse test setups. Therefore an assumption for the time-dependency of the elastic modulus is made for this numerical analysis. It is assumed that the development of the modulus is similar to the development of the polymerization stress $\sigma(t)$. A final value is assumed after 120 seconds for the elastic modulus $E(t)$, which is set at 20 GPa. The time-dependent elastic modulus can be derived from:

$$E(t) = \frac{\sigma(t)}{\sigma_0} E_0$$

where: $E(t)$ is the time-dependent elastic modulus

E_0 is the elastic modulus after 120 seconds

$\sigma(t)$ is the time-dependent polymerization stress

σ_0 is the polymerization stress after 120 seconds

In **Figure 63** both the assumed elastic modulus and the polymerization strain development functions used in this analysis are shown.

8.3 Results and discussion

The clinical problems associated with polymerization shrinkage are discussed earlier. The possible causes of two of those problems are analyzed numerically:

1. Coronal deformation, resulting in post-operative sensitivity and possible enamel fracture.
 2. Microleakage due to failing of the tooth-composite bonding because of the high shrinkage stresses at the interface.
-

Because it is widely accepted that an incremental filling technique reduces shrinkage stresses, three different incremental techniques are simulated and compared with a single step placement of the composite restoration. Furthermore the effect of the restoration size on the occurring shrinkage stresses is shown. The results of the finite element calculations are discussed under the next four headings:

- Effect of the restoration size
- Filling techniques
- Coronal surface stresses
- Stresses at the tooth-restoration interface

8.3.1 Effect of the restoration size

The amount of polymerization shrinkage stresses depends on the size of the restoration (SULIMAN *et al.*, 1993A and B). The intercusp distance change of the tooth cusps is commonly used as a measure for the polymerization shrinkage effect of a restored tooth (JENSEN AND CHAN, 1985; LUTZ *et al.*, 1991; SEGURA AND DONLY, 1993). Therefore this inward displacement, *i.e.* displacement in x-direction, will also be considered here to investigate the effect of the width of a restoration on the shrinkage stresses.

In **Figure 64** the cusp displacement is given for eight different restoration widths: 0.5, 1.0, 1.5, 2.0, 2.5, 3.0, 3.5, and 4.0 mm. The depth of all restorations is 4.0 mm (**Figure 57**); and in **Figure 65** for eight different restoration depths: 0.5, 1.0, 1.5, 2.0, 2.5, 3.0, 3.5, and 4.0 mm. The width of all restorations is 4.0 mm (**Figure 58**). The composite is placed in a single step. **Figure 64** shows an almost linear relation of the restoration width and the horizontal cusp displacement, while **Figure 65** also shows an increasing cusp displacement for increasing restoration depths.

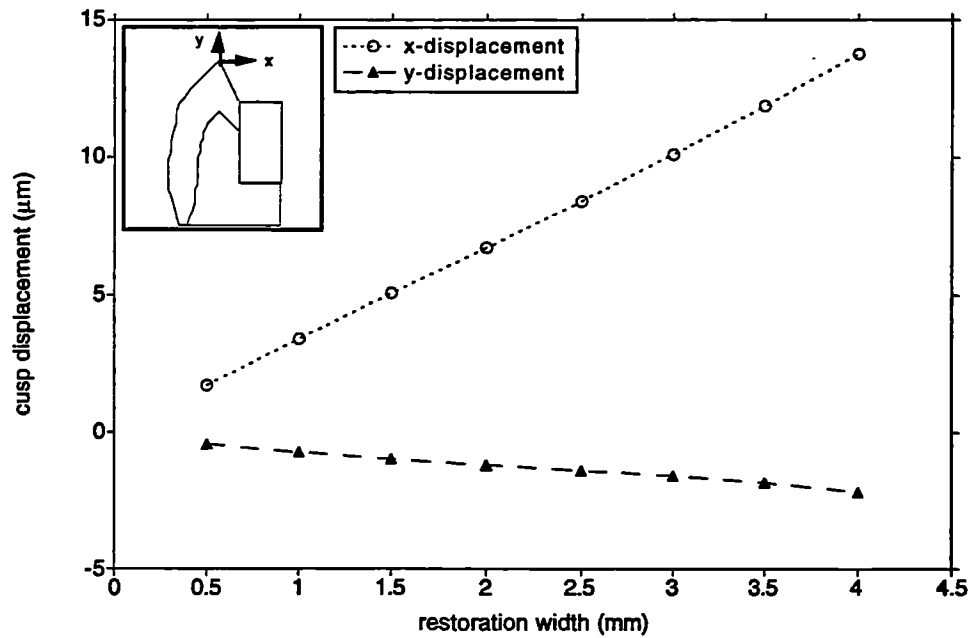


Figure 64. Numerically calculated cusp displacement (μm) due to polymerization contraction in x- and y-direction for eight restoration widths: 4.0, 3.5, 3.0, 2.5, 2.0, 1.5, 1.0, and 0.5 mm.

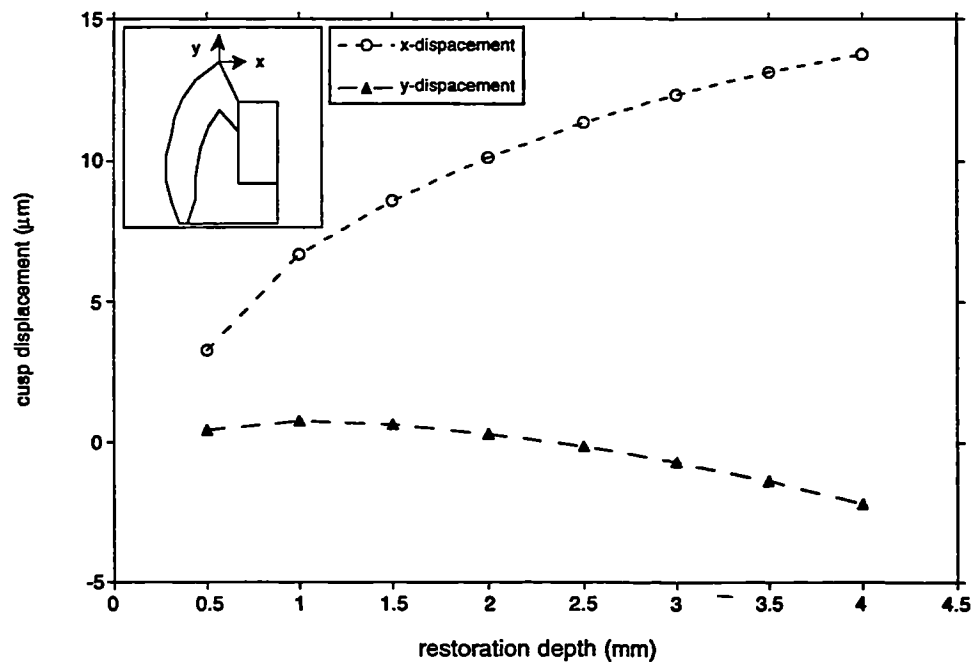


Figure 65. Numerically calculated cusp displacement (μm) due to polymerization contraction in x- and y-direction for eight restoration depths: 4.0, 3.5, 3.0, 2.5, 2.0, 1.5, 1.0, and 0.5 mm.

Furthermore the effect of underfilling and overfilling of a composite restoration is compared with an exactly filled cavity in **Table XXIV**. The cusp displacement in x-direction appears to be larger for the underfilled cavity, although the displacement in y-direction is lower. It seems that an underfilled restoration provides less constraint against the inward bending of the walls, while the down-pulling effect of the shrinking filling on the tooth walls depends on the amount of the composite.

8.3.2 Filling techniques

The filling technique of a composite restoration can have a significant effect on the resulting polymerization shrinkage stresses in the tooth-restoration complex. The inward displacement, *i.e.* displacement in x-direction, will be used here to compare the overall effect of incremental filling techniques.

In **Table XXV** and **Figure 66** the finite element analysis results are shown for the cusp displacement in x-direction for a bucco-lingual incremental filling technique (4 increments), if the time-delays between the subsequent increments are varied.

Note that a time-delay of 0 seconds compares to a single step placement technique, while a 120 seconds time-delay equals an incremental composite placement on top of fully cured former increments. Apparently the curing time-delay between sequential increments affect the cusp displacement, shorter time-delays decrease the horizontal cusp displacement. The cause will be discussed below, where different methods of incremental techniques for different orientation and count of layers are analyzed. In the following the worst case, *i.e.* the 120 seconds time-delay between successive curings, is considered.

In **Table XXVI** the results of the numerically calculated cusp displacements are listed for the three types of filling techniques for a various number of increments, and they are graphically displayed in **Figure 67**. In **Table XXVII** the results for the cusp displacements are listed in case of different boundary conditions: the mesh is only restrained by the symmetry assumption (symmetry

Table XXIV. Numerically calculated cusp displacement (μm), due to polymerization shrinkage for an underfilled, an exactfilled, and an overfilled restoration.

	cusp displacement	
	x (μm)	y (μm)
underfill	15.1	-1.7
exactfill	13.8	-2.2
overfill	12.9	-2.6

Table XXV. Numerically calculated cusp displacement in x-direction (μm) for a bucco-lingual incremental filling technique (4 increments) with different time-delays between the curing of the successive layers.

time-delay between increments (sec)	cusp displacement in x-direction (μm)
0	14
15	17
30	20
60	23
120	23

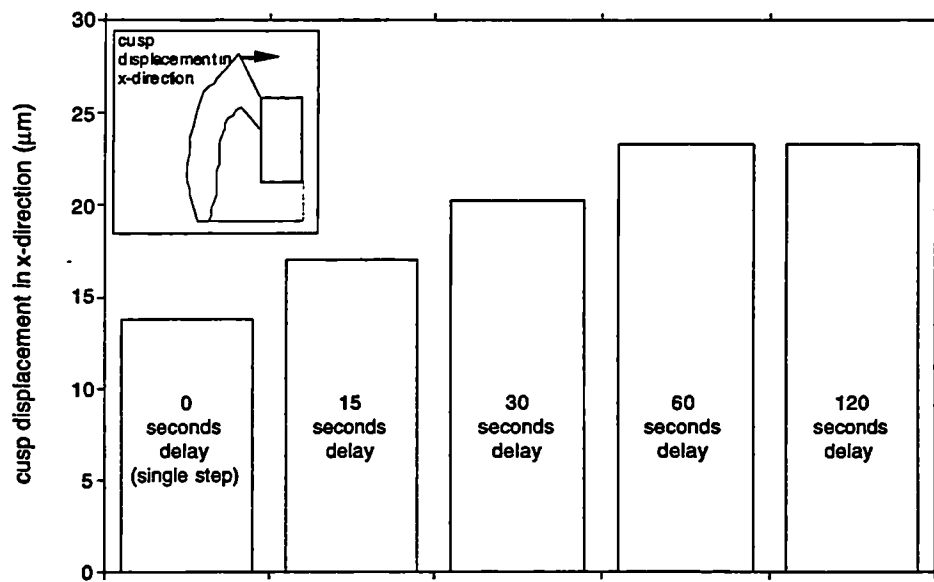


Figure 66. Numerically calculated cusp displacements in x-direction (μm) for an incremental filling technique (bucco-lingual layers, 4 increments) with different time-delays between the curing of the layers: 0 (single step), 15, 30, 60, and 120 seconds.

Table XXVI. Numerically calculated displacement of one cusp (x- and y-direction), due to polymerization shrinkage in a MOD-restoration, for three incremental filling techniques. Boundary conditions: symmetry, fixed point, and dentin bottom edge fixed in x-direction.

increments	gingivo-occlusal		bucco-lingual		diagonal	
	(horizontal)		(vertical)		(v-shape)	
	x (μm)	y (μm)	x (μm)	y (μm)	x (μm)	y (μm)
1	13.8	-2.2	13.8	-2.2	13.8	-2.2
2	26.5	1.7	19.3	-3.3	27.7	0.2
3					35.9	2.1
4	39.9	6.4	22.9	-4.9		
5						
6					46.0	3.1
7						
8	50.9	10.6	24.5	-6.4		
12					53.3	3.3
16	58.6	13.7				
24					58.0	3.1

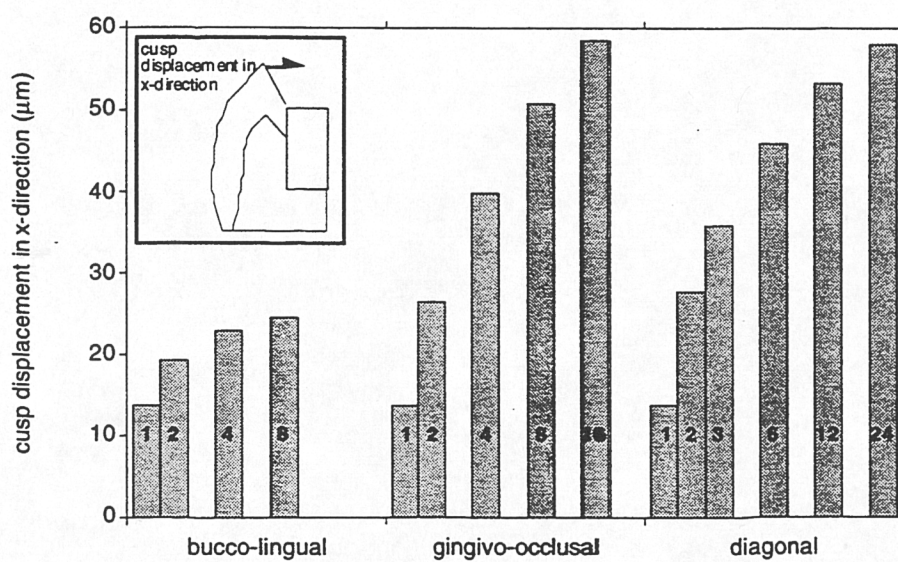


Figure 67. Numerically calculated cusp displacement in x-direction (μm) due to polymerization contraction for three incremental filling techniques: bucco-lingual (1, 2, 4, and 8 increments), gingivo-occlusal (1, 2, 4, 8, and 16 increments), and diagonal (1, 2, 3, 6, 12, and 24 increments).

Table XXVII. Numerically calculated displacement of one cusp (x- and y-direction), due to polymerization shrinkage in a MOD-restoration, for three incremental filling techniques. Boundary conditions: symmetry and fixed point.

increments	gingivo-occlusal		bucco-lingual		diagonal	
	(horizontal)		(vertical)		(v-shape)	
	x (μm)	y (μm)	x (μm)	y (μm)	x (μm)	y (μm)
1	12.9	-2.9	12.9	-2.9	12.9	-2.9
2	29.2	2.9	22.5	-2.9	33.4	2.0
3					44.6	5.4
4	51.4	10.6	30.5	-3.3		
6					61.8	8.7
8	72.1	17.8	35.0	-4.0		
12					75.6	10.7
16	87.5	23.2				
24					84.8	11.7

boundary conditions and fixed point, **Figure 56**). Because these results in **Table XXVII** show the same trend as the results in **Table XXVI**, **Table XXVII** will not be discussed further.

The finite element calculations show that incremental composite restoration filling techniques result in higher polymerization shrinkage stresses than bulk filling (single step). This is clearly contrasting with the widely accepted opinion (JENSEN AND CHAN, 1985; LUTZ *et al.*, 1986; MCCULLOCK AND SMITH, 1986; SEGURA AND DONLY, 1993; SULIMAN *et al.*, 1993A) that an incremental filling technique should be used to decrease the polymerization stresses. There are several publications in which the effect of incremental filling techniques are determined experimentally. **Table XXVIII** shows some results.

The experimental results shown in **Table XXVIII** point to a conclusion opposite to that drawn from the finite element results in **Table XXVI**. They indicate that incremental filling techniques decrease the polymerization stresses. The general argument behind the broad acceptance that incremental filling decreases shrinkage stresses, is that this decrease is due to minimal contact across the cavity during polymerization as well as the reduced shrinkage produced by a small volume of material (MCCULLOCK AND SMITH, 1986). Although this is correct for each individual increment, the final shrinkage stress field is a result of all the subsequent layers, when the whole cavity is in full contact and the total shrinkage is the sum of all the increments together. The total amount of composite material applied to fill the restoration cavity is lower in case of an incremental filling technique compared with a single increment filling. This is because the polymerization contraction of each individual filling increment will cause some deformation of the cavity, forcing the cavity walls to bend in- and downward and consequently decreasing the cavity volume. A decreased cavity volume means that less composite can be placed for the next filling increment, in the end resulting in a cavity which is volumetrically filled with less composite material (volume of the paste) than the original volume of the cavity. Evidently this must result in higher shrinkage stresses in the tooth-restoration complex, as is illustrated by the numerical

Table XXVIII. Compilation of some published intercuspal distance changes (x-direction), due to polymerization shrinkage of a MOD-restoration for different filling techniques.

References	Intercuspal distance change \pm sd (μm)			
	single increment	gingivo- occlusal	bucco- lingual	diagonal
JENSEN AND CHAN (1985)	45 \pm 6	37 \pm 4 (3/4 incr)		33 \pm 4 (3/4 incr)
MCCULLOCK AND SMITH (1986)	13.0 \pm 1.0			5.3 \pm 4.0 (2 incr)
SEGURA AND DONLY (1993)	22.4 \pm 22.9	12.4 \pm 9.2 (2 incr)	9.8 \pm 16.9 (2 incr)	

results (**Figure 66** and **67**), where the cusp displacement increases with the number of increments and the time-delay between these increments (causing a higher degree of curing, hence higher contraction and modulus before a next layer is cured on top of it). The numerical results show that the type of incremental technique clearly affects the amount of cusp displacement.

In **Table XXIX** and in **Figure 68** the applied composite volume fraction per unit thickness is given before the polymerization as a result of different filling techniques. The fraction f is defined as:

$$f = \frac{V_{\text{cavity}} - V_{\text{composite}}}{V_{\text{cavity}}}$$

where: V_{cavity} is the volume of the cavity

$V_{\text{composite}}$ is the volume of the composite

The volume of the restoration after curing is determined by the sum of two effects: the volumetric shrinkage and the deformation of the cavity. The sign of both effects is usually opposite. **Table XXIX** indicates that the effect of the cavity deformation is larger than the gain of volume due to polymerization shrinkage since the applied composite volume decreases if an incremental filling technique is performed. The difference between the cavity volume, the applied composite volume and the resulting deformed cavity volume gives an indication of the shrinkage forces involved, because of the following relation:

$$p = B \frac{V_0 - V_1}{V_0} = B \frac{\Delta V}{V_0}$$

where: p is a measure for internal stresses

V_0 is the original volume

V_1 is the resulting volume

B is the bulk modulus ($B = E / (3(1 - 2\nu))$)

Comparing **Figures 67** and **68** shows that the difference in magnitude for both means of measurement (cusp displacement and applied filling volume) are not

Table XXIX. Volume fractions ($10^{-3} \Delta V/V$) per unit thickness of the uncured filling material as a result of different filling techniques.

increments	gingivo-occlusal	buccolingual	diagonal
1	0	0	0
2	2.58	0.57	2.30
3			2.40
4	3.70	0.67	
6			4.09
8	6.05	0.50	
12			5.36
16	7.83		
24			6.19

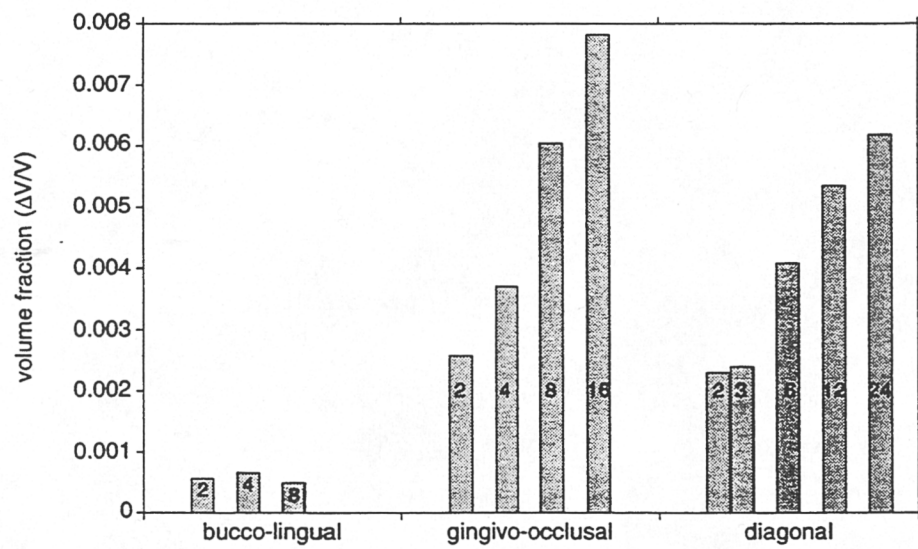


Figure 68. Applied composite volume fraction from the original cavity volume ($\Delta V/V$) as a result of incremental filling techniques.

totally corresponding. The difference between the bucco-lingual and the other two filling methods is larger for the volume fraction compared with the cusp displacement. Furthermore the used composite volume in an eight incremental bucco-lingual filling is lower than for four increments, while the cusp displacement is larger. Apparently the total amount of applied composite is not the only determinant for the resulting deformation pattern, the form in which each increment is applied also has a significant effect.

A bucco-lingual incremental technique affects the final cusp displacement less than a gingivo-occlusal or a diagonal incremental technique. This can be explained by the bridging of the incremental layers of the two latter techniques. They connect the two cavity walls, forcing them to bend more inward than in case of a bucco-lingual technique. A bucco-lingual filling technique also exhibits a larger surface area capable of free shrinkage than the other two techniques, which results in less cavity volume occupation after curing, and therefore more composite can be applied in the next increment. The experimental data in **Table XXVIII** show the same trend for the different multiple-increment filling techniques (JENSEN AND CHAN, 1985; SEGURA AND DONLY, 1993).

It is not clear why the numerical results and these cited experimental data yield opposite conclusions concerning the benefits of an incremental filling technique. There are many parameters involved, that may affect the occurring shrinkage stresses. The following parameters will be discussed briefly:

- a. Tooth-composite interface
- b. Bonding between incremental layers
- c. Stress relaxation and hygroscopic recovery
- d. Homogeneity of the polymerization reaction

- a. *Tooth-composite interface* — The use of an underlayer (cermet, glass-ionomer cement) reportedly reduces the cusp movement significantly, while a dentin bonding increases the displacement (LUTZ *et al.*, 1986; MCCULLOCK AND SMITH, 1986). The cited values in **Table XXVIII** from MCCULLOCK AND SMITH (1986)
-

are obtained without any bonding or under layers. JENSEN AND CHAN (1985) applied a dentin bonding agent, as did SEGURA AND DONLY (1993). In the numerical simulation the bonding is perfect. However, whether it is a perfect bonding or not, the fact remains that incremental filling techniques reduce the total amount of composite placed in a cavity.

- b. *Bonding between incremental layers* — If the bonding between subsequent incremental layers is weaker than the bulk material, more incremental layers decrease the stiffness of the total restoration. This results in less deformation of the tooth, and therefore less displacement of the cusps. In the numerical simulation the bonding between the incremental layers is perfect. This effect of a reduced stiffness due to a weakened composite-composite bond might be a possible reason for lower cusp displacements found experimentally for incremental filling techniques.
 - c. *Stress relaxation and hygroscopic recovery* — It is known that a composite restoration exhibits some stress relaxation due to water absorption, which has a softening and expanding effect on the composite material (HANSEN, 1982; FEILZER *et al.*, 1990; SEGURA AND DONLY, 1993; SULIMAN *et al.*, 1993A). If this relaxation/expansion takes place between each incremental placement, the negative effect of an incremental filling technique may be eliminated. However, SULIMAN *et al.* (1993A) show that in a wet environment recovery of the cusp movement starts approximately 10 minutes after the start of polymerization reaction, while if there is any recovery in a dry environment, this does not happen before 20 hours after the polymerization reaction (P-50). The data cited in **Table XXVIII** are obtained under dry conditions. Therefore stress relaxation or water absorption cannot explain the lower cusp displacements in the experimental situations. Moreover, stress relaxation is unlikely to change the ranking among the different filling techniques.
 - d. *Homogeneity of the polymerization reaction* — Homogeneous polymerization is an assumption made in the numerical determination of the shrinkage stresses. In light of the conclusions of previous chapters, it may be expected that this assumption is not fully correct. Which means that polymerization, and therefore
-

shrinkage, reduces if it is farther located inside the restoration, away from the light cured surface. This effect of inhomogeneous shrinkage is more likely for thicker layers. More and thinner layers in an incremental filling technique would have diminished the inhomogeneity effect, and therefore increased the cusp displacement compared with a single increment technique. Homogeneity assumption for the polymerization reaction cannot explain the discrepancy between the numerical results and some experimental data as cited in **Table XXVIII**.

Other factors that may play a role are the quality of the restoration and the degree of curing throughout the composite filling. Although an incremental filling technique is widely promoted as a method to reduce polymerization shrinkage stresses, there are some observations that point to less successful applications. JENSEN AND CHAN (1985) report that in spite of the usage of an incremental placement post-operative sensitivity still occurs, assuming that there is a relation between polymerization shrinkage and post-operative sensitivity. Furthermore ZIDAN *et al.* (1985) and GRIM AND CHAPMAN (1986) found that the (incremental) technique to place the composite materials did not alter the occurrence of marginal leakage.

8.3.3 Coronal surface stresses

Polymerization shrinkage has reportedly caused coronal enamel fractures (JENSEN AND CHAN, 1985). Here the occurring coronal stresses in y-direction (σ_y) are examined, which are the stresses almost parallel to the coronal surface. These y-stresses may be responsible for the observed enamel fractures. The fractures are typically horizontal in nature and occurring both on buccal and lingual sides, characteristically at the juncture of the middle and gingival third of the tooth (JENSEN AND CHAN, 1985). In **Figure 69** the coronal stresses in y-direction are plotted for eight different cavity widths: 0.5, 1.0, 1.5, 2.0, 2.5, 3.0, 3.5, and 4.0 mm. The composite restoration is placed in a single step. The figure shows that the highest σ_y is located at the middle of the coronal surface and appears independent of the restoration width. In **Figure 70** the coronal stresses

in y-direction are plotted for eight different cavity depths: 0.5, 1.0, 1.5, 2.0, 2.5, 3.0, 3.5, and 4.0 mm. The restoration is also applied in a single step. **Figure 70** shows that the coronal stress level does not change much anymore if the cavity is through the occlusal enamel (depth \geq 1.5 mm). The figure also shows that the highest σ_y is located at the middle of the coronal surface and almost independent of the restoration depth. If the cavity is filled in bucco-lingual (vertical) increments (**Figure 71**) or diagonal (**Figure 72**), the location of the highest coronal stresses remain at the same place, but the maximum stress value increases dramatically with the number of increments. If the cavity is filled employing a gingivo-occlusal (horizontal) incremental filling technique, the y-stresses increase too (**Figure 73**), although less dramatically, but the location of the peak stresses shifts in the negative y-direction (gingival). Interestingly, the gingivo-occlusal incremental filling technique yielded a higher cusp displacement in x-direction than the bucco-lingual technique, while the coronal stresses are lower. The y-stresses along the coronal surface are a result of a combination of bending and compression of the outer tooth structure. Inward bending yields tensile stresses, pressure downwards yields compressive stresses. The higher y-stresses in the bucco-lingual and diagonal incremental fillings suggest relatively higher bending. This can be explained by the larger coverage of the cavity walls earlier in the incremental filling procedure, which will cause more bending than the initially lower applied gingivo-occlusal incremental layers. Note the negative y-stresses, *i.e.* compression, for higher number of increments just under cusp, the top of the tooth (occlusal).

Two observations can be made from the obtained coronal stress distributions for future shrinkage stress research. First, the technique of measuring intercusp distance change is not uncontroversial, because a high-horizontal displacement of the cusps does not necessarily express higher (coronal) stresses. If strain gages are used to measure the effect of polymerization shrinkage on the coronal stresses, the strain gages should be placed on the coronal surface, corresponding in height just below halfway the restoration.

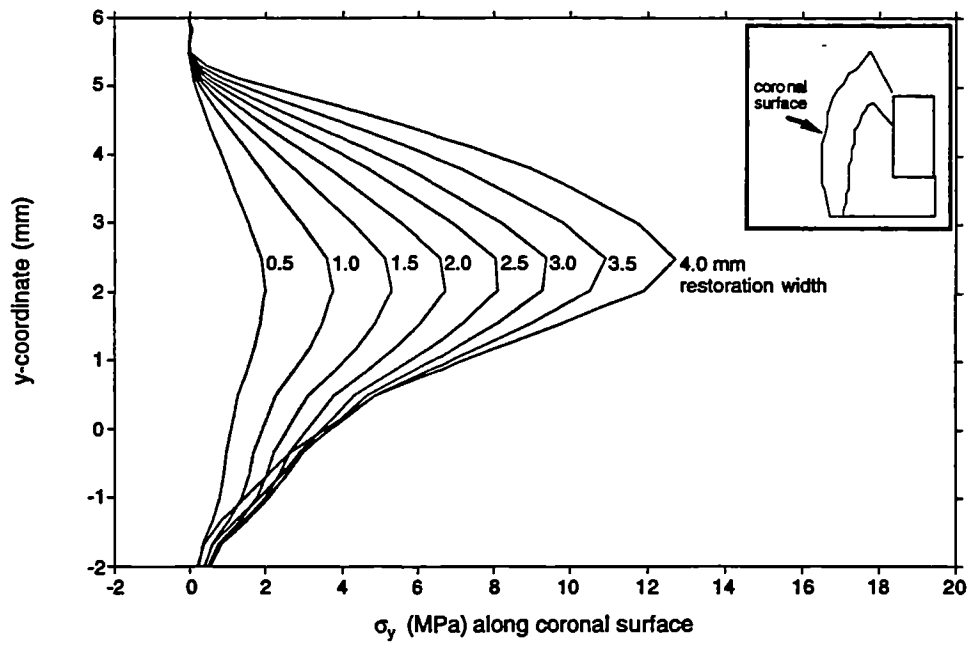


Figure 69. Stresses in y-direction along the coronal surface for eight restoration widths: 4.0, 3.5, 3.0, 2.5, 2.0, 1.5, 1.0, and 0.5 mm.

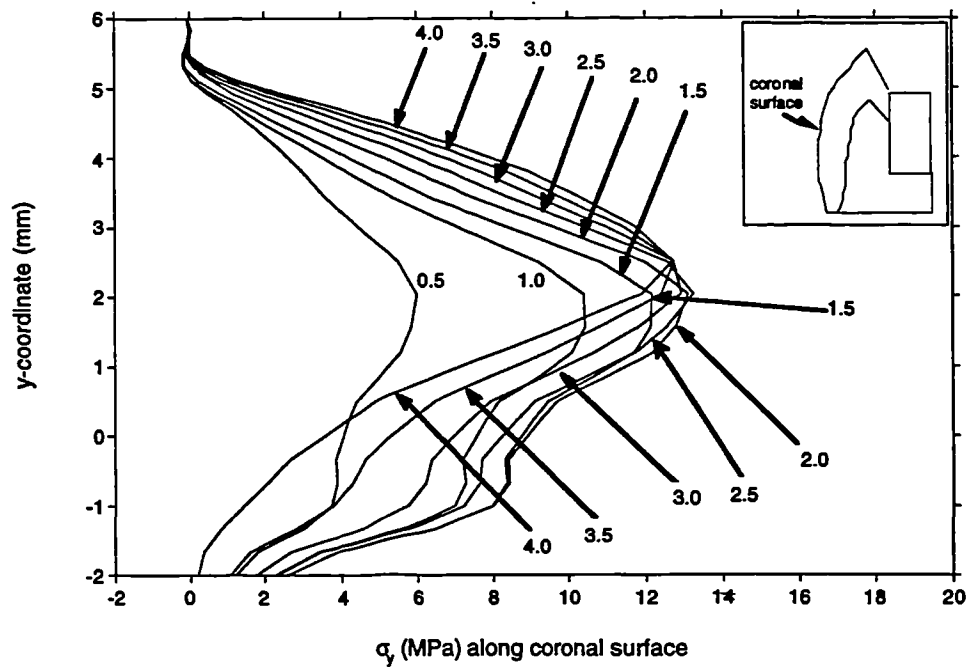


Figure 70. Stresses in y-direction along the coronal surface for eight restoration depths: 4.0, 3.5, 3.0, 2.5, 2.0, 1.5, 1.0, and 0.5 mm.

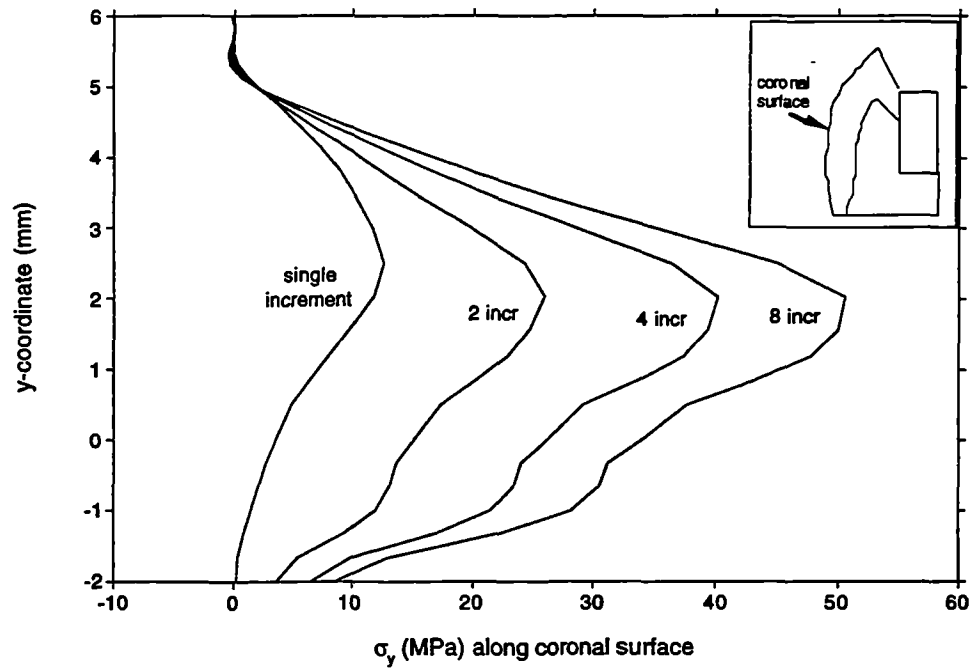


Figure 71. Stresses in y-direction along the coronal surface for a bucco-lingual filling technique for 1, 2, 4, and 8 increments.

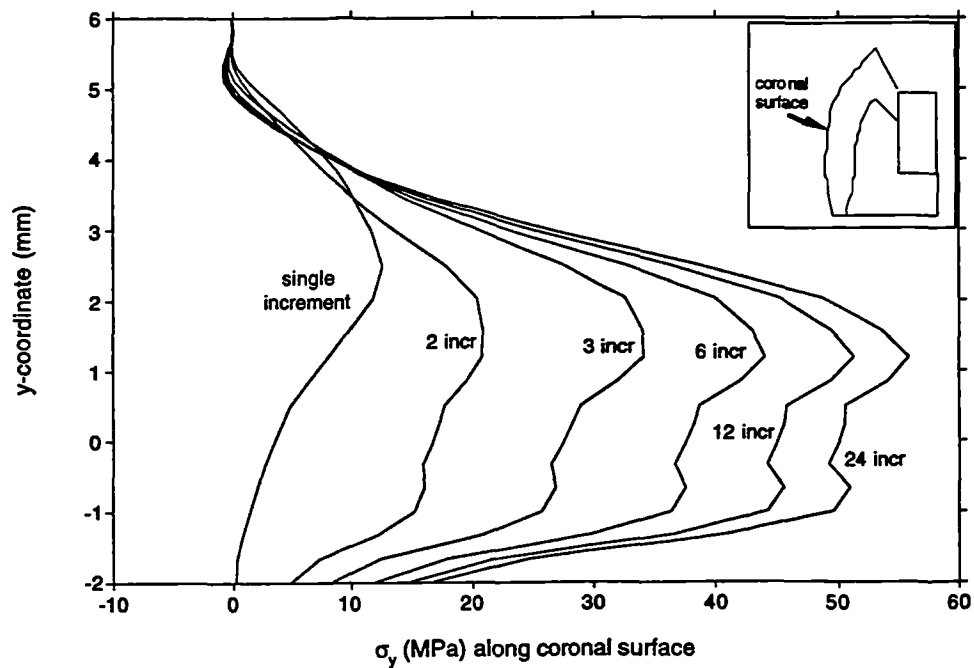


Figure 72. Stresses in y-direction along the coronal surface for a diagonal filling technique for 1, 2, 3, 6, 12, and 24 increments.

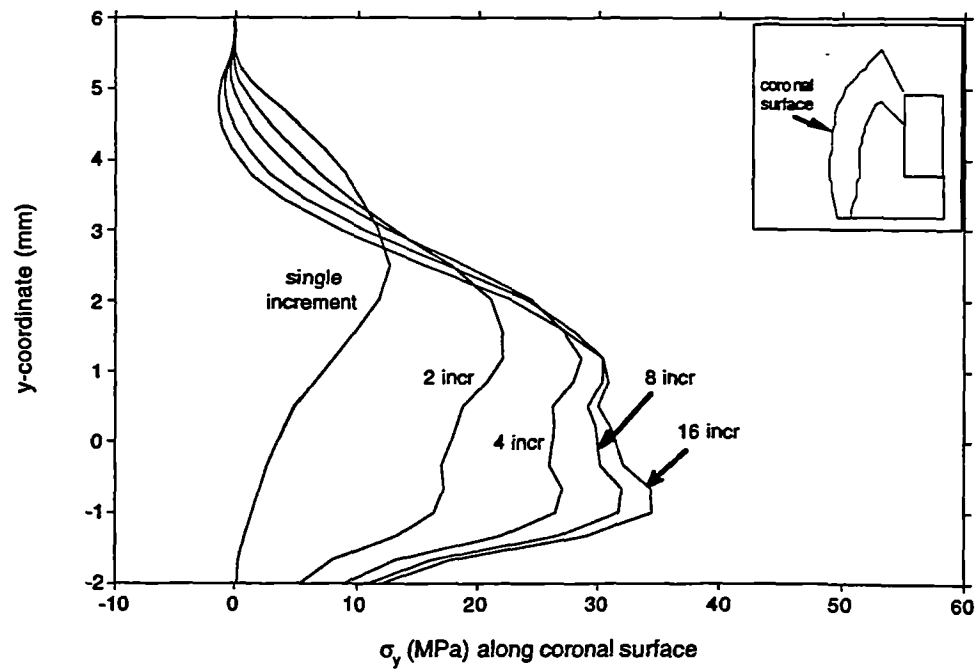


Figure 73. Stresses in y-direction along the coronal surface for a gingivo-occlusal filling technique for 1, 2, 4, 8, and 16 increments.

8.3.4 Stresses at the tooth-restoration interface

Polymerization shrinkage stresses at the tooth-composite interface are considered to play an important role in the process of debonding and hence micro leakage, which leads to secondary caries. In this paragraph the x-stresses (σ_x) in the dentin and enamel, directly adjacent to the composite restoration are determined. Failure of the interface bonding is believed to be mainly a result of separation forces, perpendicular to the interface. In **Figures 74-76** the x-stresses for the three different incremental filling techniques are shown for a bucco-lingual (1, 2, and 8 increments), a gingivo-occlusal (1, 2, and 8 increments), and a diagonal (1, 2, and 12 increments) technique respectively. The saw-tooth appearance of the gingivo-occlusal and diagonal stress curves (**Figures 75 and 76**) is a result of the layered polymerization techniques. This shape is not observed in the stress curve of the bucco-lingual technique (**Figure 74**), because the first layer covers the entire cavity wall. Furthermore the effect of the difference in elastic modulus of dentin and enamel is revealed in the stress curve by a discontinuity near y-coordinate 2.5. Apparently the stresses in the lower part of the enamel interface are in compression, as well as the dentin interface for multi-incremental fillings (gingivo-occlusal and diagonal). The x-stresses at the upper part (occlusal) of the enamel are in tension, and sharply peaking at the occlusal surface. The stress distribution is a result of a combination of inward bending and downward pressure to which the tooth structure is subjected by the contracting composite filling. In **Figure 77** four deformed shapes are shown, for a single step (A), a bucco-lingual (4 increments, B), a gingivo-occlusal (4 increments, C), and a diagonal (3 increments, D) placement technique. Subsequently applied increments, which are higher located (higher y-coordinates), tend to compress earlier layers which result in compressive stresses. This can be observed for the gingivo-occlusal and diagonal techniques (**Figures 75 and 76**), and is obviously less pronounced for the vertical oriented bucco-lingual technique (**Figure 74**). The high tensile x-stresses are a result of the end effect of the last polymerized incremental layer and the free surface. Although the absolute value of the tensile peak stress at

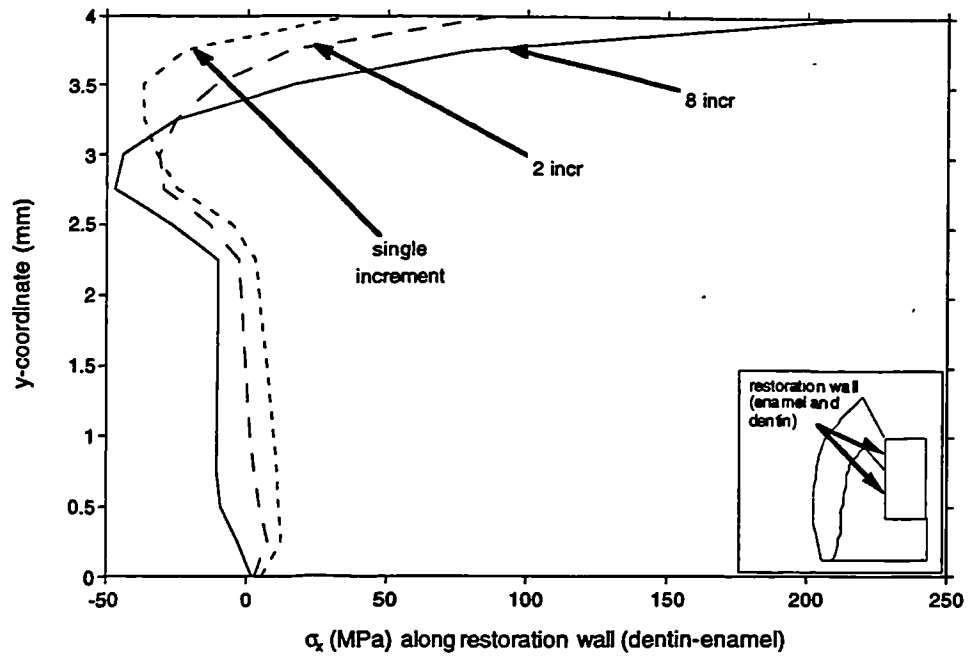


Figure 74. Stresses in x -direction along the tooth-enamel restoration wall (in the dentín-enamel) for a bucco-lingual filling technique for 1, 2, and 8 increments.

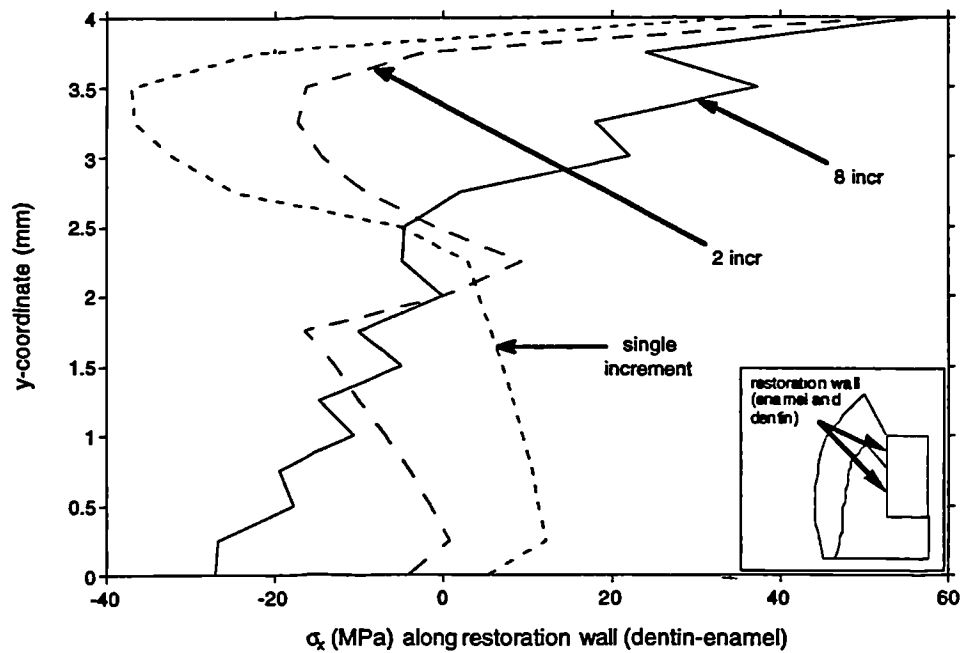


Figure 75. Stresses in x -direction along the tooth-enamel restoration wall (in the dentín-enamel) for a gingivo-occlusal filling technique for 1, 2, and 8 increments.

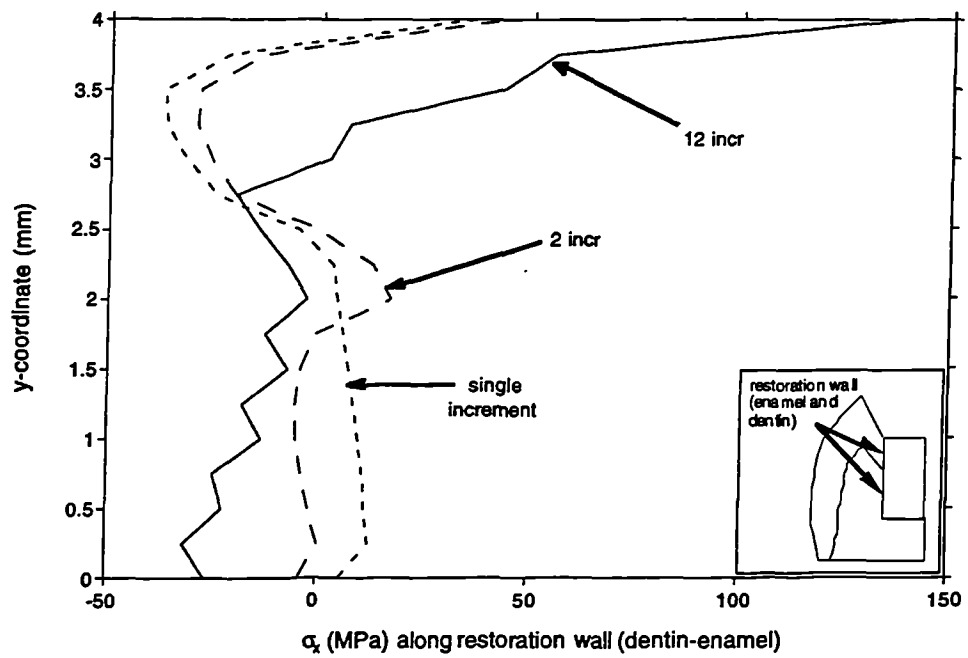


Figure 76. Stresses in x-direction along the tooth-enamel restoration wall (in the dentin-enamel) for a diagonal filling technique for 1, 2, and 12 increments.

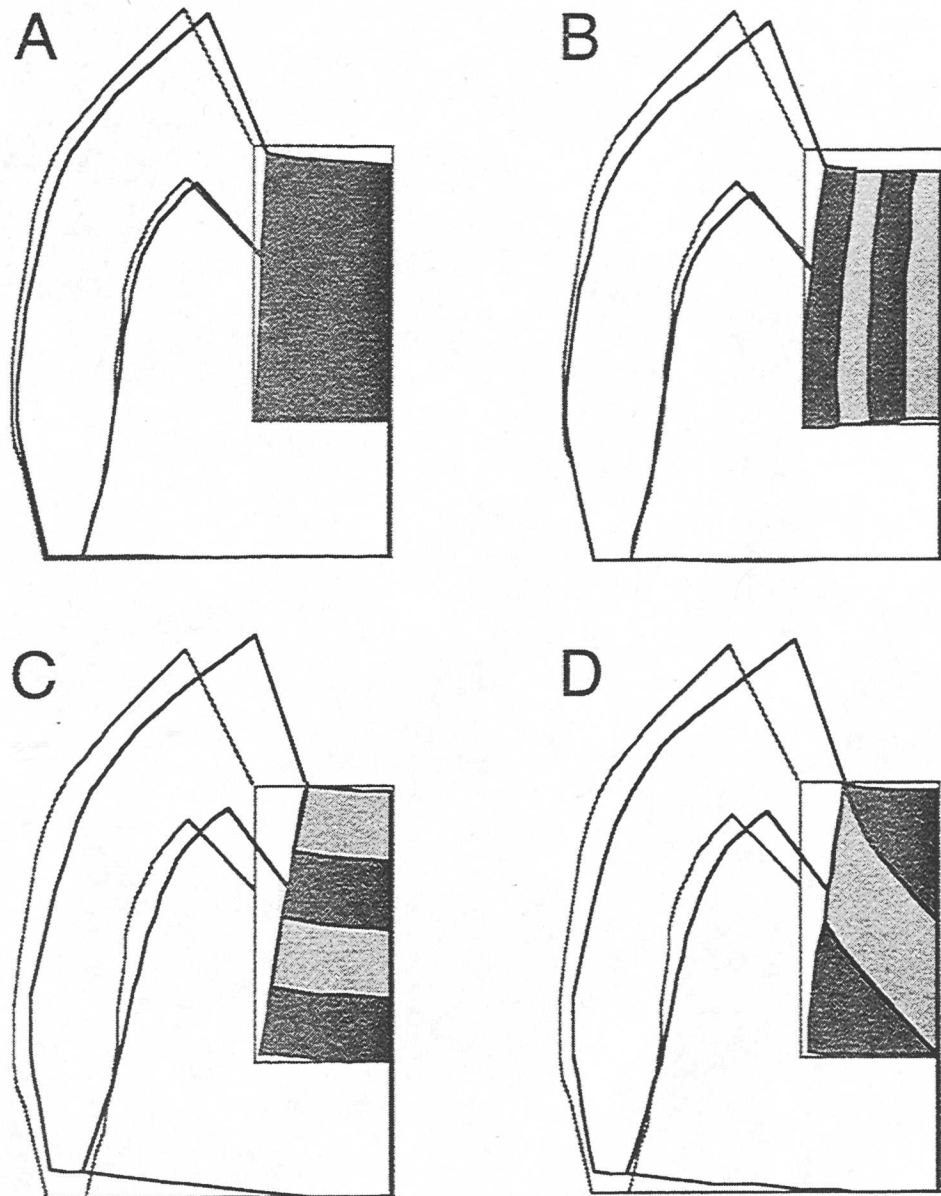


Figure 77. Deformed shapes (magnification 100 times) for four filling techniques:

A. single step

B. bucco-lingual (4 increments)

C. gingivo-occlusal (4 increments)

D. diagonal (3 increments)

the occlusal surface is likely to be flattened in the real situation due to yielding, the high tensile stress condition is not an artifact. These high tensile stresses at the surface will challenge the tooth-composite bond, and therefore failure of the bonding is likely to take place at the occlusal surface. These stresses are likely the inhibitors of the marginal gap occurrence. The compressive stresses under the surface suggest that the subsurface bond strength is not too challenged yet. However, the point of tensile peak stresses will move down along the interface in case this interface fails and gap formation happens. Note that stress curves do not change dramatically for a moderate number of increments. However, if the number of increments increases, the tensile surface stresses (supposedly responsible for marginal gap formation) tend to increase considerably in case of bucco-lingual and diagonal filling techniques (**Figures 74 and 76**).

8.4 Conclusions

A tooth-restoration system is a complicated structure, due to its geometry, materials, and boundary conditions. Finite element analysis of this complex can only be as accurate as the parameters for the geometry, material properties, and boundary conditions used in the analysis. Especially the latter two parameters are still largely unpredictable, and therefore a quantitative use of the finite element method for the tooth-restoration complex is not applicable yet. However, the finite element method is a strong tool for a qualitative analysis, providing a better understanding of qualitative stress and strain distributions. In this context it is a powerful conceptual tool.

In this chapter the effect of the polymerization contraction in a tooth-composite complex was analyzed. The numerical results suggest that incremental filling techniques do not reduce the residual shrinkage stresses, as is widely assumed, but in fact increase these stresses. This result is not surprising, because an incremental filling technique effectively decreases the total amount of composite applied to fill a cavity, which must lead a higher stressed tooth-composite structure. The polymerization shrinkage stresses in the tooth-composite complex increase with the number of increments and with the time-delay

between the curing of the layers. Residual shrinkage stresses in the tooth depend on the restoration size, and thus on the size of the cavity. Incremental filling techniques increase the coronal surface stresses, responsible for coronal enamel fracture, and they increase the tensile stresses at the occlusal surface, responsible for marginal gap formation. In terms of intercuspal distance measurements, the bucco-lingual incremental technique yields less displacement than the gingivo-occlusal and diagonal incremental techniques. In terms of coronal stresses and occlusal stresses a gingivo-occlusal incremental technique yields less high stresses than the other two incremental techniques. The assessment of intercuspal distance measurements is therefore insufficient to characterize the effect of polymerization shrinkage on a tooth-restoration complex.

9 General conclusions

In Chapter 1 of this thesis the central problem (1.6) of the work was defined, namely, the development and distribution of internal stress in the tooth-restoration complex, with special reference to composite resins. In the approach to the problem (1.7) a review of failure mechanisms was reported. It was clear from the work of many authors that micro structure in terms of filler-matrix relationships had a profound effect on fracture properties (Chapter 2). The same relationships affect directly the shrinkage and modulus development, and hence the internal stress development that could shorten the life of a restoration by elevating the general stress level, accelerating crack propagation and fracture.

Material properties often get much attention at the expense of other criteria. In Chapter 3 a critical review of yield stress criteria was reported, which pointed to the significance of these criteria in evaluation of cavity design with respect to external anatomic features as locations for the stress concentrations.

The techniques of measurement of post-gel shrinkage were optimized in Chapter 4. It is possible to improve overall composite shrinkage by reducing pre-gel shrinkage. Indirectly this chapter emphasized that only improvement in post-gel shrinkage will lead to substantial benefits, a fact that the scientific community may not be fully aware of. This chapter also showed that temporarily expansion was experienced during the post-gel phase, and the technique may have real-time value in the study of the kinetics of the polymerization process itself. The technique of measurement was shown to be discriminating in the evaluation of generically different composites, and the numeric values would prove useful in the planned finite element studies.

It should be noted that although the implication of polymerization shrinkage is bad, it is a consequence of degree of polymerization. One easy, trivial and unacceptable way of reducing shrinkage would be simply to reduce the amount of polymerization. This would disastrously compromise other physical and mechanical properties. The development of stress which accompanies shrinkage

strain should be interpreted in this light. Chapter 5 shows that the peak exotherm (Chapter 6) is closely associated with the peak stress development, suggesting the close relationship between the polymerization rate and shrinkage stress development. This approach discriminates nicely between those composites which have a snap set (*e.g.* Z100). The computation of stress in association with shrinkage strain will be important in the study of modulus development which lies at the heart of importance of post-gel shrinkage.

Temperature effects (Chapter 6) appear in the study of internal stress development in two ways: the chemical exotherm, and the dietary thermal cycling which food of different temperature may mediate to the composite intraorally. These temperature effects are expressed as a volume change via the coefficient of thermal expansion. A modification of the strain gauge method gave an elegant method of measuring the coefficient of thermal expansion. The generically different composites could be differentiated based on this property. The exotherm itself strictly belongs to the area of thermochemistry, and probably does not have a direct long term effect on the internal stress. The thermal cycling consideration should probably be considered as a surface effect, which does not involve the whole restoration.

As noted, almost by definition the characterizing feature of the post-gel period is the development of a modulus of elasticity (Chapter 7). This controls the relationship between the shrinkage strain and the resulting unfavorable internal stress distribution. It is expressed as a change in density, due to the same mass being constrained into a small volume. Further, the modulus is not a constant or even a near constant, but rises from close to zero at the beginning of the post-gel period to the approximately maximum value at the end of the period. The experimental measurement of the modulus in the early post-gel period when the chemical reaction is fast, proved to be very difficult. A part of the reason was due to different stress and strain experiments, which were slightly asynchronous. This is an area which can be fairly described as requiring further study and will present special experimental difficulties.

However the greatest challenge to the restoration-tooth complex is when the full shrinkage and full modulus have been developed.

The work so far enabled certain experimental techniques to be optimized and validated and produced experimental data which was of interest in its own right. However such data is raised to another level of usefulness when fed into a sophisticated finite element program (Chapter 8). Such a model can be examined at any location to identify stress and strain conditions and in addition may offer general insight into the significance of the development of internal stresses. The numerical model did not support the widely held belief that incremental filling of a cavity with a composite results in less overall shrinkage than single bulk filling of the same cavity. In fact the incremental method of filling yielded more shrinkage stresses. The basic reason was that incremental filling resulted in the use of less composite than a single filling, since each increment cured in the cavity decreased the total cavity volume due to deformation by the incremental shrinkage stresses. Although the extent of this effect depended on the exact incremental filling method, it was never overridden. The experimental data on this point is mixed as reviewed in Chapter 8. It turned out that bucco-lingual incrementalization produced the least shrinkage of all the incrementalization methods. In general, from the present work it is difficult to justify incremental filling on the grounds of reduced shrinkage. It was also shown that the assessment of intercuspal distance measurements is insufficient to characterize the effect of polymerization shrinkage on a tooth-restoration complex.

The other surprising result, unforeseen by intuition, was the presence of compressive stresses at the hard tissue interface about 500 microns below the surface. These stresses were in the x-direction and forced the composite down onto the interface. Intuition would tell us to expect tensile forces here due to the shrinkage: such was not the case. Large tensile forces were found close to the occlusal surface. Once again these increased by incremental filling. Much deeper in the cavity the forces in the x direction at the interface were quite low in most cases.

Although the last word on incremental filling has not been written, and there is much further work to do, these examples make an important point about the relationship between intuition, experimentation and numerical modeling. Probably all three are needed in the final judgment of clinical technique. Numerical modeling can evaluate commonly held clinical belief, by examining the solution at points where experimental assessment is impossible (*e.g.* 500 microns below the surface of a composite). This has more value if certain numerical points are validated by experimental measurement. But no doubt clinical judgment and practical knowledge also play a part. For instance, there may be other reasons for incremental filling, such as more complete cure of thin composite layers and the desire to form an adhesive bond on dentine before the enamel bond is formed. However it is the judgment of this thesis, at the present state of development that reduced overall shrinkage and hence deformation of the remaining hard tissue walls is not a reason to prefer incremental filling over single bulk filling. The further work in this field will depend on highly precise, well controlled experimentation on the tooth-restoration complex, capable of micron or submicron measurement.

References

ANUSAVICE KJ AND DE RIJK WG (1990): Performance of dental biomaterials: Conference report. *Dent Mater* 6: 69-72.

ARCHARD JF (1953): Contact and rubbing of flat surfaces. *J Appl Phys* 24: 981-988.

ASMUSSEN E AND JØRGENSEN KD (1978): Restorative resins: Coefficient of thermal expansion — a factor of clinical significance? *Quintessence Int* 9: 79-82.

ASMUSSEN E AND JØRGENSEN KD (1982): Fatigue strength of some resinous materials. *Scand J Dent Res* 90: 76-79.

ASMUSSEN E AND MUNKSGAARD EC (1985): Adhesion of restorative resins to dentinal tissues. In: Vanherle G and Smith DC (Eds). Posterior composite resin dental restorative materials. Peter Szulc Publishing Co., The Netherlands: 217-230.

BARKER LM (1984): Specimen size effects in short-rod fracture toughness measurements. In: Underwood JH, Freiman SW, and Baratta FI (Eds). Chevron-notched specimens: testing and stress analysis. ASTM STP 855, Philadelphia: 117-133.

BENKESER G AND SOLTÉSZ U (1988): Wechsellastverhalten von Füllungsmaterialien — eine vergleichende Untersuchung ausgewählter Materialien. Fraunhofer-Institut für Werkstoffmechanik, Freiburg, Wiss Ber W1/88.

BERGLUND A (1993): An *in vitro* and *in vivo* study of the release of mercury vapor from different types of amalgam alloys. *J Dent Res* 72: 939-946.

BILLINGTON EW (1986): Introduction to the mechanics and physics of solids. Adam Hilger Ltd, Bristol, England: 177.

- BOWEN RL (1967): Adhesive bonding of various materials to hard tooth tissues. VI. Forces developing in direct-filling materials during hardening. *J Amer Dent Assoc* 74: 439-445.
- BOWEN RL, MENIS DL, SETZ LE, AND JENNINGS KA (1985): Theory of polymer composites. In: Vanherle G and Smith DC (Eds). Posterior composite resin dental restorative materials. Peter Szulc Publishing Co., The Netherlands: 95-105.
- BOWEN RL, NEMOTO K, AND RAPSON JE (1983): Adhesive bonding of various materials to hard tooth tissues: forces developing in composite materials during hardening. *J Amer Dent Assoc* 106: 475-477.
- BRADEN M (1976): Biophysics of the tooth. *Front Oral Physiol*, Karger, Basel, Vol 2: 1-37.
- BRAEM M, LAMBRECHTS P, VANHERLE G, AND DAVIDSON CL (1988): *In-vitro* flexural fatigue testing of dental composites. *J Dent Res* 67, Special Issue, Abstract #1187.
- BROEK D (1986): Elementary engineering fracture mechanics. 4th revised edition, Martinus Nijhoff Publishers, Dordrecht.
- BROUTMAN LJ AND SAHU S (1971): The effect of interfacial bonding on the toughness of glass filled polymers. *Materials Science and Engineering* 8: 98.
- BULLARD RH, LEINFELDER KF, AND RUSSELL CM (1988): Effect of coefficient of thermal expansion on microleakage. *J Am Dent Assoc* 116: 871-874.
- COOK WD AND JOHANNSON M (1987): The influence of postcuring on the fracture properties of photocured dimethacrylate based dental composite resin. *J Biomed Mater Res* 21: 979-989.
- CRAIG RG (1985): Restorative dental materials. The C.V. Mosby Company, St Louis, Missouri.
-

DAVIDSON CL AND DE GEE AJ (1984): Relaxation of polymerization contraction stresses by flow in dental composites. *J Dent Res* 63: 146-148.

DAVIDSON CL, DE GEE AJ, AND FEILZER AJ (1984): The competition between the composite-dentin bond strength and the polymerization contraction stress. *J Dent Res* 63: 1396-1399.

DAVIS DM AND WATERS NE (1987): An investigation into the fracture behavior of a particulate-filled Bis-GMA resin. *J Dent Res* 66: 1128-1133.

DE GEE AJ, DAVIDSON CL, AND SMITH A (1981): A modified dilatometer for continuous recording of volumetric polymerization shrinkage of composite restorative materials. *J Dent* 9: 36-42.

DE GROOT R (1986): Failure characteristics of tooth-composite structures. PhD Thesis, University of Nijmegen, The Netherlands.

DE GROOT R, PETERS MCRB, DE HAAN YM, DOP GJ, AND PLASSCHAERT AJM (1987): Stress criteria for failure of dental composite. *J Dent Res* 66: 1748-1752.

DE GROOT R, VAN ELST HC, AND PETERS MCRB (1988): Fracture mechanics parameters for failure prediction of composite resins. *J Dent Res* 67: 919-924.

DE VREE JHP, PETERS MCRB, AND PLASSCHAERT AJM (1984): The influence of modification of cavity design on distribution of stresses in a restored molar. *J Dent Res* 63: 1217-1220.

DELONG R AND DOUGLAS WH (1991): An artificial oral environment for testing dental materials. *IEEE Trans Biomed Eng* 38: 339-345.

DELONG R, SAKAGUCHI RL, DOUGLAS WH, AND PINTADO MR (1985): The wear of dental amalgam in an artificial mouth: a clinical correlation. *Dent Mater* 1: 238-242.

DEVRIES KL, KNUTSON M, DRAUGHN RA, REICHART JL, AND KOBLITZ FF (1981): Friction and wear of dental polymeric composite restoratives. In: Gebelein CG and Koblitz FF (Eds). Biomedical and dental applications of polymers. Polymer Science and Technology 14, Plenum Press, New York: 459-482.

DHURU VB AND LLOYD CH (1986): The fracture toughness of repaired composite. *J Oral Rehabil* 13: 413-421.

DOGON IL (1985): Current status of posterior composite resins in North America. In: Vanherle G and Smith DC (Eds). Posterior composite resin dental restorative materials. Peter Szulc Publishing Co., The Netherlands: 163-172.

DONLY KJ, JENSEN ME, REINHARDT J, AND WALKER JD (1987): Posterior composite polymerization shrinkage in primary teeth: an *in vivo* comparison of three restorative techniques. *Pediatr Dent* 9: 22-25.

DOUGLAS WH (1985): Methods to improve fracture resistance of teeth. In: Vanherle G and Smith DC (Eds). Posterior composite resin dental restorative materials. Peter Szulc Publishing Co., The Netherlands: 433-441.

DRAUGHN RA (1979): Compressive fatigue limits of composite restorative materials. *J Dent Res* 58: 1093-1096.

DRAUGHN RA (1981): Effect of micro structure on compressive fatigue of composite restorative materials. In: Gebelein CG and Koblitz FF (Eds). Biomedical and dental applications of polymers. Polymer Science and Technology 14, Plenum Press, New York: 441-451.

DRAUGHN RA (1985): Fatigue and fracture mechanics of composite resins. In: Vanherle G and Smith DC (Eds). Posterior composite resin dental restorative materials. Peter Szulc Publishing Co., The Netherlands: 299-307.

DRÜCKER DC (1951): A more fundamental approach to plastic stress-strain relations. Proc 1st US Nat Congr Appl Mech, New York, ASME: 487-491.

DRUCKER DC AND PRAGER W (1952): Soil mechanics and plastic analysis or limit design. *Quarterly of Applied Mathematics* 10: 157-165.

EICK JD AND WELCH FH (1986): Polymerization shrinkage of posterior composites and its possible influence on postoperative sensitivity. *Quintessence Int* 17: 103-111.

ELEY BM AND COX SW (1993): The release, absorption and possible health effects of mercury from dental amalgam: a review of recent findings. *Br Dent J* 175: 355-362

EWALDS HL AND WANHILL RJH (1985): Fracture mechanics. Delftse Uitgevers Maatschappij b.v., Delft.

FEILZER AJ, DE GEE AJ, AND DAVIDSON CL (1987): Setting stress in composite resin in relation to configuration of the restoration. *J Dent Res* 66: 1636-1639.

FEILZER AJ, DE GEE AJ, AND DAVIDSON CL (1990): Relaxation of polymerization contraction shear stress by hygroscopic expansion. *J Dent Res* 69: 36-39.

FEILZER AJ, DE GEE AJ, AND DAVIDSON CL (1993): Setting stresses in composites for two different curing modes. *Dent Mater* 9: 2-5.

FERRACANE JL AND ANTONIO RC (1988): Fracture toughness and compressive yield of aged experimental dental composites. *J Dent Res* 67, Special Issue, Abstract #1183.

FERRACANE JL, ANTONIO RC, AND MATSUMOTO H (1987): Variables affecting the fracture toughness of dental composites. *J Dent Res* 66: 1140-1145.

GERE JM AND TIMOSHENKO SP (1990): Mechanics of materials. 3rd Edition, PWS-Kent Publishing Company, Boston.

GIECK K AND GIECK R (1990): Engineering formulas. 6th edition, McGraw-Hill, New York.

GOLDMAN M (1985): Fracture properties of composite and glass ionomer dental restorative materials. *J Biomed Mater Res* 19: 771-783.

GREEN GE AND BISHOP AW (1969): A note on the drained strength of sand under generalized strain conditions. *Geotechnique* 19: 144-149.

GREENWOOD JA AND WILLIAMSON JB (1966): Contact of nominally flat surfaces. *Proceedings of the Royal Society (London) A* 295: 300.

GRIM GA AND CHAPMAN KW (1986): Prevention of marginal leakage by four dentinal adhesives. *Gen Dent* 3:235-236.

GUDEHUS G (1973): Elastoplastische Stoffgleichungen für trockenen Sand. *Ingenieur Archiv*, B42, H3: 151-169.

GUENNOUNI T (1987): Yield criteria of heterogeneous materials with rigid-plastic constituents. Case of porous or cracked materials. *J Mec Theor Appl* 6: 571-615.

HAHNEL L, SOLTÉSZ U, AND KLAIBER B (1986): Festigkeitsverhalten von Kompositen unter Wechsellast - Einfluß von Prüfverfahren, Frequenz und Umgebung. Fraunhofer-Institut für Werkstoffmechanik, Wiss Ber W4/86, Freiburg.

HANSEN EK (1982): Visible light-cured composite resin: polymerization contraction, contraction pattern and hygroscopic expansion. *Scand J Dent Res* 90: 329-335.

HASHIN Z (1983): Analysis of composite materials — a survey. *Journal of Applied Mechanics* 50: 481-505.

HASHINGER DT AND FAIRHURST CW (1984): Thermal expansion and filler content of composite resins. *J Prosthet Dent* 52: 506-510.

HEGDAHL T AND GJERDET NR (1977): Contraction stresses of composite resin filling materials. *Acta Odont Scand* 35: 191-195.

HENCHANG X, WENYI L, AND TONG W (1989): Measurement of thermal expansion coefficient of human teeth. *Australian Dent J* 34: 530-535.

- HILL R (1948): A theory of yielding and plastic flow of anisotropic metals. *Proceedings of the Royal Society (London) A* 193: 281-297.
- IRWIN GR (1958): Fracture. In: Flüge S (Ed). *Encyclopaedia of physics*. Vol VI. Springer Verlag, Berlin: 551-590.
- JAEGER JC (1967): Brittle fracture of rocks. In: Fairhurst C (Ed). *Failure and breakage of rock*. The American Institute of Mining, Metallurgical and Petroleum Engineers Inc, New York: 3-57.
- JENDRESEN MD (1985): Overview of the clinical requirements for posterior composites. In: Vanherle G and Smith DC (Eds). *Posterior composite resin dental restorative materials*. Peter Szulc Publishing Co., The Netherlands: 41-43.
- JENKINS GN (1978): *The physiology and biochemistry of the mouth*. 4th edition, Blackwell Scientific Publications.
- JENSEN ME AND CHAN DCN (1985): Polymerization shrinkage and microleakage. In: Vanherle G and Smith DC (Eds). *Posterior composite resin dental restorative materials*. Peter Szulc Publishing Co., The Netherlands: 243-262.
- KUMADA K, SAWA N, HANAOKA K, TERANAKA T, IWAMOTO T, ODA Y, HIGO Y, AND NUNOMURA N (1991): Fracture toughness determination of composite resins using a ring specimen. *J Dent Res* 70, D.M.G. Microfilm: #1714.
- KYDD WL AND DALY C (1985): Duration of nocturnal tooth contacts during bruxing. *J Prosthet Dent* 53: 717-721.
- LADE PV (1982): Three-parameter failure criterion for concrete. *Journal of the Engineering Mechanics Division*, ASCE, Vol 108, No EM5: 850-863.
- LAI JH AND JOHNSON AE (1993): Measuring polymerization shrinkage of photo-activated restorative materials by a water-filled dilatometer. *Dent Mater* 9: 139-143.
-

LAMBRECHTS P (1983): Basic properties of dental composites and their impact on clinical performance. PhD Thesis, Katholieke Universiteit Leuven, Belgium.

LAMBRECHTS P, AMEYE C, AND VANHERLE G (1982): Conventional and microfilled composite resins. Part II: Chip fractures. *J Prosthet Dent* 48: 527-538.

LAMBRECHTS P, BRAEM M, AND VANHERLE G (1985): Accomplishments and expectations with posterior composite resins. In: Vanherle G and Smith DC (Eds). Posterior composite resin dental restorative materials. Peter Szulc Publishing Co., The Netherlands: 521-540.

LANGE FF AND RADFORD KC (1971): Fracture energy of an epoxy composite system. *Journal of Materials Science* 6: 1197-1203.

LEINFELDER KF (1981): Composite resins in posterior teeth. *Dent Clin N Amer* 25: 357-364.

LEINFELDER KF AND LEMONS JE (1988): Clinical restorative materials and techniques. Lea&Febiger, Philadelphia.

LIN C-P (1993): Structure-property-function relationships in the dentin-enamel complex and tooth-restoration interface. PhD Thesis, University of Minnesota.

LLOYD CH (1982): The fracture toughness of dental composites: II. The environmental and temperature dependence of the stress intensification factor (K_{Ic}). *J Oral Rehabil* 9: 133-138.

LLOYD CH (1983): Resistance to fracture in posterior composites. *Br Dent J* 155: 411-414.

LLOYD CH (1984): The fracture toughness of dental composites: III. The effect of environment upon the stress intensification factor (K_{Ic}) after extended storage. *J Oral Rehabil* 11: 393-398.

LLOYD CH (1988): The fracture toughness (K_{Ic}) of composite filling materials and crack-tip radius (letter). *J Dent Res* 67: 883-884.

LLOYD CH AND ADAMSON M (1987): The Development of Fracture Toughness and Fracture Strength in Posterior Restorative Materials. *Dent Mater* 3: 225-231.

LLOYD CH AND BUTCHART DGM (1990): The retention of core composites, glass ionomers, and cermets by a self-threading dentin pin: the influence of fracture toughness upon failure, *Dent Mater* 6: 185-188.

LLOYD CH AND DHURU VB (1985): Effect of a commercial bonding agent upon the fracture toughness (K'_{Ic}) of repaired heavily filled composite. *Dent Mater* 1: 83-85.

LLOYD CH AND IANNETTA RV (1982): The fracture toughness of dental composites: I. The development of strength and fracture toughness. *J Oral Rehabil* 9: 55-66.

LLOYD CH AND MITCHELL L (1984): The fracture toughness of tooth coloured restorative materials. *J Oral Rehabil* 11: 257-272.

LUTZ F AND KREJCI I (1991): Quality and durability of marginal adaptation in bonded composite restorations. *Dent Mater* 7: 107-113.

LUTZ F AND PHILLIPS RW (1983): A classification and evaluation of composite resin systems. *J Prosthet Dent* 50: 480-488.

LUTZ F, KREJCI I, AND OLDENBURG TR (1986): Elimination of polymerization stresses at the margins of posterior composite resin restorations: a new restorative technique. *Quintessence Int* 7: 777-784.

MANDEL ID (1980): Sialochemistry in disease and clinical situations affecting salivary glands. *CRC Crit Rev Clin Lab Sci* 12: 321-366.

MARIN J (1957): Theories for strength for combined stresses and nonisotropic materials. *J Aeronautical Sciences*: 265-268 and 274.

- MCCABE JF AND OGDEN AR (1987): The relationship between porosity, compressive fatigue limit and wear in composite resin restorative materials. *Dent Mater* 3: 9-12.
- MCCABE JF, CARRICK TE, CHADWICK RG, AND WALLS AWG (1990): Alternative approaches to evaluating the fatigue characteristics of materials. *Dent Mater* 6: 24-28.
- MCCULLOCK AJ AND SMITH BGN (1986): *In vitro* studies of cuspal movement produced by adhesive restorative materials. *Br Dent J* 161: 405-409.
- MEILDAHL A (1944): A new graphical method of representing strength characteristics. *Brown Boveri Review* 31: 260-267.
- MILLS LL AND ZIMMERMAN RM (1970): Compressive strength of plain concrete under multiaxial loading conditions. *ACI Journal*: 802-807.
- MODEER M (1979): A fracture mechanics approach to failure analyses of concrete materials. PhD Thesis, Lund, Sweden.
- MOMOI Y, IWASE H, NAKANO Y, KOHNO A, ASANUMA A, AND YANAGISAWA K (1990): Gradual increase in marginal leakage of resin composite restorations with thermal stress. *J Dent Res* 69: 1659-1663.
- MONTES-G GM AND DRAUGHN RA (1987): Slow crack propagation in composite restorative materials. *J Biomed Mat Res* 21: 629-642.
- MORIN DL, DOUGLAS WH, CROSS M, AND DELONG R (1988): Biophysical stress analysis of restored teeth: experimental strain measurement. *Dent Mater* 4: 41-48.
- NADAI A (1950): Theory of flow and fracture of solids. McGraw-Hill Book Co, New York.
- NEWMAN JR JC (1984): A review of chevron-notched fracture specimens. In: Underwood JH, Freiman SW, and Baratta FI (Eds). Chevron-notched specimens: Testing and stress analysis. ASTM STP 855, Philadelphia: 5-31.
-

- NEWMAN K (1965): The structure and engineering properties of concrete. In: Rydzewski, JR (Ed). Theory of arch dams. Pergamon Press, Oxford: 683-712.
- NEWMAN K AND NEWMAN JB (1971): Failure theories and design criteria for plain concrete. In: Te'eni M (Ed). Structure, solid mechanics and engineering design. Wiley-Interscience, London, England: 963-995.
- OKESON JP, PHILLIPS BA, BERRY DTR, COOK Y, PAESANI D, AND GALANTE J (1990): Nocturnal bruxing events in healthy geriatric subjects. *J Oral Rehabil* 17: 411-418.
- OTTOSEN NS (1977): A failure criterion for concrete. *Journal of the Engineering Mechanics Division*, ASCE, Vol 103, No EM4: 527-535.
- OUTWATER JO, MURPHY MC, KUMBLE RG, AND BERRY JT (1974): Double torsion technique as a universal fracture toughness test method. In: Fracture toughness and slow-stable cracking. ASTM STP 559: 127-138.
- PALMER DS, BARCO MT, AND BILLY EJ (1992): Temperature extremes produced orally by hot and cold liquids. *J Prosthet Dent* 67: 325-327.
- PENN RW (1986): A recording dilatometer for measuring polymerization shrinkage. *Dent Mater* 2: 78-79.
- PHILLIPS RW (1982): Science of dental materials. Skinner's, 8th edition, WB Saunders Company.
- PILLIAR RM, SMITH DC, AND MARIC B (1986): Fracture toughness of dental composites determined using the short-rod fracture toughness test. *J Dent Res* 65: 1308-1314.
- PILLIAR RM, VOWLES R, AND WILLIAMS DF (1987A): Note: Fracture toughness testing of biomaterials using a mini-short rod specimen design. *J Biomed Mater Res* 21: 145-154.
- PILLIAR RM, VOWLES R, AND WILLIAMS DF (1987B): The effect of environmental aging on the fracture toughness of dental composites. *J Dent Res* 66: 722-726.
-

- PODGÓRSKI J (1985): General failure criterion for isotropic media. *Journal of Engineering Mechanics* 11: 188-201.
- POWERS JM, HOSTETLER RW, AND DENNISON JB (1979): Thermal expansion of composite resins and sealants. *J Dent Res* 58: 584-587.
- PUCKETT AD AND SMITH R (1992): Method to measure the polymerization shrinkage of light-cured composites. *J Prosthet Dent* 68: 56-58.
- RAGHAVA R, CADDELL RM, AND YEH GSY (1973): The macroscopic yield behaviour of polymers. *Journal of Materials Science* 8: 225-232.
- REDDY JN (1993): An introduction to the finite element method. 2nd edition, McGraw-Hill, New York.
- REEH ES (1993): Salivary defense against friction and wear of dental enamel. PhD Thesis, University of Minnesota.
- ROBERTS JC, POWERS JM, AND CRAIG RG (1977): Fracture toughness of composite and unfilled restorative resins. *J Dent Res* 56: 748-753.
- ROBERTS JC, POWERS JM, AND CRAIG RG (1978): An empirical equation including fracture toughness and describing friction of dental restorative materials. *Wear* 47: 139-146.
- ROSENFELD AR (1981): Wear and fracture mechanics. In: Rigney DA (Ed). *Fundamentals of friction and wear of materials*. American Society for Metals, Metals Park: 221-234.
- RUYTER IE (1985): Monomer systems and polymerization. In: Vanherle G and Smith DC (Eds). *Posterior composite resin dental restorative materials*. Peter Szulc Publishing Co., The Netherlands: 109-135.
- SAKAGUCHI RL AND DOUGLAS WH (1989): Strain gauge measurement of polymerization shrinkage. *J Dent Res* 68: 977 (abstr #885).
-

- SAKAGUCHI RL, PETERS MCRB, NELSON SR, DOUGLAS WH, AND POORT HW (1992): Effects of polymerization contraction in composite restorations. *J Dent* 20: 178-182.
- SAKAGUCHI RL, SASIK CT, BUNCZAK MA, AND DOUGLAS WH (1991): Strain gauge method for measuring polymerization contraction of composite resins. *J Dent* 19: 312-316.
- SANDS MP, MORENA R, AND FAIRHURST CW (1988): Fracture toughness of posterior composite resins. *J Dent Res* 67, Special Issue, Abstract #857.
- SCHERER GW (1987): Use of a biomaterial strip to predict expansion compatibility. *J Dent Res* 66: 1340.
- SCHLEICHER F (1925): Die Energiegrenze der Elastizität (Plastizitätsbedingung). *Zeitschrift für angewandte Mathematik und Mechanik*, Band 5, Heft 6: 478-479.
- SEGURA A AND DONLY KJ (1993): *In vitro* posterior composite polymerization recovery following hygroscopic expansion. *J Oral Rehab* 20: 495-499.
- SHEOREY PR, BISWAS AK AND CHOUBEY, VD (1989): An empirical failure criterion for rocks and jointed rock masses. *Engineering Geology* 26: 141-159.
- SHETH JJ, FULLER JL, AND JENSEN ME (1988): Cuspal deformation and fracture resistance of teeth with dentin adhesives and composites. *J Prosthet Dent* 60: 560-569.
- SMITH DC (1982): A milestone in dentistry. *Oper Dent* 7: 14-25.
- SMITH DC (1985): Posterior composite dental restorative materials: materials development. In: Vanherle G and Smith DC (Eds). Posterior composite resin dental restorative materials. Peter Szulc Publishing Co., The Netherlands: 47-60.
- SODERHOLM K-JM (1984): Influence of silane treatment and filler fraction on thermal expansion of composite resins. *J Dent Res* 63: 1321-1326.
-

SODERHOLM K-JM (1985): Filler systems and resin interface. In: Vanherle G and Smith DC (Eds). Posterior composite resin dental restorative materials. Peter Szulc Publishing Co., The Netherlands: 139-159.

SOLTÉSZ U, KLAIBER B, AND HÄHNEL L (1985): Strength behaviour of two composite dental filling materials under cyclic loading conditions. In: Perren SM and Schneider E (Eds). Biomechanics: Current interdisciplinary research. Martinus Nijhoff Publishers, Dordrecht: 277-282.

SPIERINGS TAM, MCRB PETERS, BOSMAN F, AND PLASSCHAERT AJM (1987): Verification of theoretical modeling of heat transmission in teeth by *in vivo* experiments. *J Dent Res* 66: 1336-1339.

STANFORD JW, PAFFENBARGER GL, KAMPULA JW, AND SWEENEY WT (1958): Determination of some compressive properties of human enamel and dentin. *J Amer Dent Assoc* 57: 487-495.

STANFORD JW, WEIGEL KV, PAFFENBARGER GL, AND SWEENEY WT (1960): Compressive properties of hard tooth structure and some restorative materials. *J Amer Dent Assoc* 60: 746-756.

STASSI-D'ALIA F (1967): Flow and fracture of materials according to a new limiting condition of yielding. *Meccanica* 3: 178-195.

SULIMAN AA, BOYER DB, AND LAKES RS (1993A): Cusp movement in premolars resulting from composite polymerization shrinkage. *Dent Mater* 9: 6-10.

SULIMAN AA, BOYER DB, AND LAKES RS (1993B): Interferometric measurements of cusp deformation of teeth restored with composites. *J Dent Res* 72: 1532-1536.

SUZUKI M, JORDAN RE, AND BOKSMAN L (1985): Posterior composite resin restoration — clinical considerations. In: Vanherle G and Smith DC (Eds). Posterior composite resin dental restorative materials. Peter Szulc Publishing Co., The Netherlands: 455-464.

THEOCARIS PS (1986): Yield criteria based on void coalescence mechanisms. *Int J Solids Structures* 22: 445-466.

THEOCARIS PS (1988): The independence of the T-criterion from the strength anisotropy of the materials. *Engineering Fracture Mechanics* 31: 39-53.

THEOCARIS PS AND PHILIPPIDIS, TP (1987): The paraboloidal failure surface of initially anisotropic elastic solids. *Journal of Reinforced Plastics and Composites* 6: 378-395.

TRUONG VT AND TYAS MJ (1988): Prediction of *in vivo* wear in posterior composite resins: a fracture mechanics approach. *Dent Mater* 4: 318-327.

TSAI SW AND WU EM (1971): A general theory of strength for anisotropic materials. *J Composite Materials* 5: 58-80.

TSCHOEGL NW (1971): Failure surfaces in principal stress space. *J Polymer Sci Part C, Polymer Symposia* 32: 239-267.

TYAS MJ (1990): Correlation between fracture properties and clinical performance of composite resins in class IV cavities. *Australian Dent J* 35: 46-49.

VAIDYANATHAN J, VAIDYANATHAN TK, WANG Y, AND VISWANADHAN T (1992): Thermoanalytical characterization of visible light cure dental composites. *J Oral Rehabil* 19: 49-64.

VANHERLE G, LAMBRECHTS P, AND BRAEM M (1985): Overview of the clinical requirements for posterior composites. In: Vanherle G and Smith DC (Eds). *Posterior composite resin dental restorative materials*. Peter Szulc Publishing Co., The Netherlands: 21-40.

VON MISES R (1928): Mechanik der plastischen Foränderung von Kristallen. *Zeitschrift für angewandte Mathematik und Mechanik*, Band 8, Heft 3: 11-185.

- WATTS DC AND CASH AJ (1991): Determination of polymerization shrinkage kinetics in visible-light-cured materials: methods development. *Dent Mater* 7: 281-287.
- WILLIAMS JG (1973): *Stress analysis of polymers*. Longman Group Limited, London.
- WU EM (1974): Phenomenological anisotropic failure criterion. In: Sendekyj GP (Ed). *Mechanics of composite materials*. In: Broutman LJ and Krock RH (Ed). *Composite materials*. Volume 2. Academic Press Inc, New York: 353-431.
- YAMAGUCHI R, POWERS JM, AND DENNISON JB (1989): Thermal expansion of visible-light-cured composite resins. *Oper Dent* 14: 64-67.
- ZIDAN O, GOMEZ-MARIN O, AND TSUCHIYA T (1987): A comparative study of the effects of dentinal bonding agents and application techniques on marginal gaps in class V cavities. *J Dent Res* 66: 716-721.
- ZIENKIEWICZ OC AND TAYLOR RL (1989): *The finite element method*, McGraw-Hill, London.
-